Dynamic Modelling and Intelligent Control of A Single Screw Extrusion Process

A thesis submitted in partial fulfilment of the requirements of the Nottingham Trent University for the degree of Doctor of Philosophy

Leong Ping Tan

September 2004

College of Science & Technology
The Nottingham Trent University
Burton Street, Nottingham NG1 4BU, UK
leong.tan@ntu.ac.uk
Tel: +44-115-8484131; Fax: +44-115-8484749

Dynamic Modelling and Intelligent Control of A Single Screw Extrusion Process

Leong Ping TAN
September 2004

A thesis submitted to The Nottingham Trent University
in partial fulfilment of the requirements for the degree of
Doctor of Philosophy

Abstract

In the plastics industry, single screw extruders are widely used to melt the solid polymer. The extruder contains a helical screw with a varying channel depth along the barrel. It is designed to optimise the efficiency of energy conversion, and the consistency of the molten polymer during the operation. The relative motion between the rotating screw and the stationary barrel continuously shears, melts and pumps the molten polymer out of the extruder die. The extrusion process is generally steady, but it is very difficult to maintain constant operating conditions. This is mainly because the process is subjected to various sources of process disturbances including variations in the quality and quantity of the feed polymer, which can result in poor quality product. Therefore, an effective extrusion controller needs to be developed.

The present extrusion controllers have been mostly concentrated on Proportional-Integral (PI) controllers and Self Tuning Regulators (STR). Generally, the resulting control systems are in Single-Input-Single-Output (SISO) structure. The SISO control systems exhibit a major shortcoming that only one process output could be regulated at each control cycle. Past experience suggests that strong interactions exist between the process parameters. This implies that an encouraging control performance could only be attained if the parameter interactions are taken into consideration while calculating a control action.

In this thesis, an intelligent control system namely Fuzzy supervisory indirect Learning Predictive Control (FsiLPC) system is proposed. The system is designed based on Model Based Predictive Control (MBPC), Controller Output Error Method (COEM) and Fuzzy Rule Based System (FRBS). The basic operating mechanism of the FsiLPC system is similar to the MBPC system, with one distinctive operating strategy. A control action in the FsiLPC system is calculated by a fuzzy supervisory unit, rather than using a control law as in a MBPC system. To improve the control action, the COEM is employed to tune the parameters of the fuzzy supervisory unit. This strategy allows the system to accept a predictive model of any structure.

The predictive model in the FsiLPC system needs to predict the behaviour of the extrusion process, and also be adaptive to the varying operating conditions. A semi-

physical dynamic extrusion model is developed for the needs. The model is governed by a set of partial differential equations, algebraic equations and FRBS sub-models. A hybrid GA-Fuzzy algorithm is implemented to produce an optimal structure for each FBRS sub-model. The sub-models thus obtained show advantages including simpler rule-base and fewer membership functions. These help to improve their interpretability and adaptive ability.

The implementation of the FsiLPC system for the extrusion process has been evaluated by means of simulation studies. The simulation studies include a parametric study and a comparative study. In the parametric study, the characteristics of the FsiLPC system are examined. The results of the study also help in finding suitable settings of the system parameters. The FsiLPC system is then compared with the PI and STR systems in the comparative study. These three control systems are evaluated based on the performance in tracking the changes of desired process output and minimising the impact of process disturbances. The performance of the FsiLPC system is relatively encouraging.

The work described in this Thesis is the Author's own, unless otherwise stated, and it is, as far as he is aware, original.

Acknowledgements

First of all, I would like to express my sincere gratitude to my supervisors Dr. Ahmad Lotfi and Dr. Eugene Lai for their dedicated help and support during my years at Nottingham Trent University. Ahmad has offered me the opportunity to carry out this research programme. His readiness to sit down and share his knowledge on intelligent control theory has been an important stimulant for the research work. Eugene always provided me with interesting discussions, which helped strengthening my research work. His willingness to share his experience in different aspects of life is very much appreciated. Thanks again to Ahmad and Eugene for their time and effort spent on editing this thesis.

I am also grateful to the staffs in the university for their support and advices. I am particularly thankful to Judith Kipling for her patience to explain the basics of the polymer materials and her kindness to proofreading my publications. I would like to thank Doreen Corlett for her professional administrative support and always offers a warm welcome whenever I need her help.

To my friends, too numerous to mention individually, I appreciated many enjoyable hours that we have spent together. I would take this opportunity to thank Jer Wang, Chee Khoon and Wing Seong, who have not only been wonderful housemates, but also a source of 'inspiration'.

A very special thank to my wife, JooKia, for maintaining her patience, understanding, support and encouragement. I love you very much!

Finally, my deepest gratitude goes to my parents back in Malaysia for sharing with me, not only their genes, but also their worldly wisdom. The research has been a long and challenging experience, there is a little doubt that I would not able to accomplish the work without their innate support.

I hope that I won't miss to acknowledge any person that has contributed to the preparation of this thesis, but this is impossible for the limiting space. If this does indeed happen, I will have you know that it is not intentional.

Table of Contents

List of Figures

List of Tables

Nomenclature

Terms:

Chromosome	A string in GA with complete information of system.
Controlled parameter	Output parameter of process.
Data Base (DB)	A collection of linguistic terms and membership functions.
Down channel direction	Helical direction of screw channel.
Extrudate	Molten polymer at the die exit.
Flight noise	Signal distorted by screw flight passing pressure transducer.
Implicit scheme	A strategy to calculate a representative point at the new time level with the information of neighbouring representative points at the new time level.
Initial Euclidean distance	Difference between the outputs of the best possible fuzzy supervisory unit and current imaginary supervisory unit.
Knowledge Base (KB)	A complete system containing information (data base) of process in the form of fuzzy rule (rule base).
Manipulating parameter	Input parameter of process.
Melt Temperature Profile (MTP)	Variation of melt temperature along helical screw channel.
Prediction horizon	A period when the future controlled signal is predicted.
Pressure Profile (PP)	Pressure variation along helical screw channel.
Semi-physical	A combination of theoretical and empirical.
Slow response barrel temperature	Barrel temperature with response of 2000 seconds time constant and 70 seconds transport delay.
Solid Bed Profile (SBP)	Variation of solid bed width along helical screw channel.
Reference signal	Desired output of process.
Rheological	A branch of physics that concerns itself with mechanism of deformable bodies
Rheometer	A device to estimate the viscosity of the molten polymer.
Rule Base (RB)	A collection of linguistic rules associating data base.
Transient	Time before the process reaches the steady state condition.
Viscous dissipation	Energy generated when molten polymer being sheared by relative motion of rotating screw and stationary barrel.

Abbreviations:

ARX	Autoregressive Exogenous Input
COEM	Controller Output Error Method
CP	Control Phase
DC	Direct Current
FFT	Fast Fourier Transformation
FRBS	Fuzzy Rule Based System
FsiLPC	Fuzzy supervisory indirect Learning Predictive Control
FVM	Finite Volume Method
HDPE	High Density Polyethylene
I/O	Input-Output
LDPE	Low Density Polyethylene
LLDPE	Linear Low Density Polyethylene
MAP	Model Adaptation Phase
MBPC	Model Based Predictive Control
MDPE	Medium Density Polyethylene
MF	Membership Function
MIMO	Multi-Input-Multi-Output
MISO	Multi-Input-Single-Output
MSE	Mean Square Error
MSOP	Manipulating Signal Optimisation Phase
PB	Pressure transducer
PDE	Partial Differential Equation
PID	Proportional-Integral-Derivative
PSD	Power Spectrum Density
SISO	Single-Input-Single-Output
TB	Thermocouple at barrel
TDMA	Tri-Diagonal Matrix Algorithm
TS	Thermocouple at screw

Symbols:

Chapter 2:

δ	process output polynomial
ω	process input polynomial
e_u	manipulating error
e_y	controlled error
f	number of delay
r	reference signal
u	manipulating signal
y	controlled signal
N_t	noise model
P_t	process output parameter
U_t	input parameter
z^{-1}	backward shift operator

Chapter 3:

b	basis function for FFT
f	frequency component
$H(z)$	digital filter function
$H_m(z)$	function of second-order filters
t	time component
T_{bar}	barrel temperature
T_{scr}	screw temperature
$x[n]$	filter input
$y[n]$	filter output

Chapter 4:

$\overline{T}_c$	average melt temperature
$\overline{D}$	average diameter
$\overline{\theta}$	average helix angle
$F^{I/O}$	fitness index for accuracy
$\hat{o}$	predicted plant output
$\dot{\gamma}$	shear rate
λ	heat of fusion
ϕ	melting rate
∂	partial differential
ω	screw speed
η	viscosity
ψ	weight of never activated criterion
ν	weight of similarity criterion
χ, ς	weights of entropy criterion
Δl	small increment in axial distance
ρ_m	mean density of molten polymer
ΔP_{die}	Pressure drop at die head
ρ_s	mean density of solid polymer
a	power law model coefficients
A	channel taper at compression zone
b	source vector
c	flight clearance
C_m	heat capacity of molten polymer
C_s	heat capacity of solid polymer
d	coefficient of tri-diagonal matrix
E	tri-diagonal matrix
e	flight width
F^A	collective fitness index
F_{dr}	'shape factors' for the drag flow
F^E	fitness index for entropy
$f_{fz(.)}$	fuzzy function of sub-model
F_{pr}	'shape factors' for pressure flow
F^S	fitness index for similar MF
F^Z	fitness index for rule activation
g	membership function parameters
G_m	melt flow rate
H	channel depth
h	space step
i	sub-model index
J	cost function
J_{max}	maximum limit of tolerance
k	discrete time instant
K_{die}	constant for die
K_m	polymer melt thermal conductivity
L	length of chromosome
m	number of input
n	number of output
o	desired plant output
p	number of channel in parallel
P	pressure
q	number of membership function
Q	volumetric flow rate
Q_{dr}	volumetric drag flow rate
Q_{pr}	volumetric pressure drag flow
q_{tr}	heat transfer rate
q_{vc}	viscous dissipation rate

r	number of rule
s	number of bit
S	number of similarity MF
T	temperature
t	time
t_0	initial time
T_b	barrel temperature
T_f	film temperature
T_m	melting point
T_s	temperature of solid polymer
V	number of data pairs
v_b	relative barrel velocity
v_{bx}	barrel velocity in x direction
v_{bz}	barrel velocity in z direction
v_j	velocity difference between barrel
v_{mz}	relative melt velocity in z direction
v_{sz}	relative solid velocity in z direction
W	channel width
w	fuzzy inferred membership grade
X	solid bed width
x	cross sectional distance
z	down channel helical distance
Z	number of never activated rule

Chapter 5:

U'	imaginary manipulating signal vector
φ	label of fuzzy supervisory unit
η	learning rate
λ	prediction horizon
δ	deadzone radius
α, β	coefficients of trajectory planner
$\hat{E}, \hat{F}$	coefficients from $\hat{A}$ and $\hat{B}$
χ, γ	coefficients from α and β
$\hat{A}, \hat{B}$	coefficients of predictive model
$\hat{m}, \hat{n}$	predicted process behaviour order
A, B	coefficients of ideal model
E	prediction error vector
E_u	supervisory output error vector
$\hat{G}$	function of predictive model
G	process function
$\hat{G}_c$	function of fuzzy supervisory unit
h	unit of manipulating parameters
$\hat{J}$	cost function for control law
J	cost function for model adaptation
j	predictive step
J_u	manipulating signal cost function
k	discrete time instant
m, n	order of the process behaviour
p, q	order of the trajectory
$\hat{U}$	predicted manipulating signal vector
u	actual manipulating signal
U	actual manipulating signal vector
u'	imaginary manipulating signal
V	Lyapunov function for the system
$\hat{w}$	parameter set of supervisory unit
$\hat{W}$	parameter vector of supervisory unit
$\hat{Y}$	predicted controlled signal vector
y	controlled signal
Y	controlled signal vector
Y_d	desired controlled signal vector
Y_r	reference controlled signal vector

Chapter 6:

α	forgetting factor
Δ	increment
τ_i	integration constant
θ	model parameter set
a	newly measured data
e	error signal
k	discrete time instant
K_c	critical gain
K_p	proportional gain
M	matrix of old data pairs
P	melt pressure
P_r	reference pressure
Q	weight of controlled parameters
y_r	reference signal
R	weight of manipulating parameters
T_b'	imaginary barrel temperature
T	melt temperature
T_b	barrel temperature
T_c	critical time
T_r	reference melt temperature
t_s	sampling interval
u	manipulating signal
$\hat{u}$	predicted manipulating signal
$\hat{y}$	predicted controlled signal
ω	screw speed
ω'	imaginary screw speed

Chapter 1
Introduction

1.1 Background

Polymers are products extracted from crude oil and natural gas. Unlike other traditional materials such as metal, the polymer properties are highly amendable. This provides designers and industries with a great range of innovative and cost-effective solutions when it comes to meeting specific performance requirements. For example, carbon fibres are added to improve the thermal and electrical conductivities, colour pigments are used to modify the appearances, and polymer structure is altered for better elasticity of the product. Consequently, polymers always appear to be the material of choice for numerous applications, from cars to buildings, medical equipment to components of mobile phones (Corporation, 1986; Strong, 1996).

The increasing demands of polymer products have led to continuous growth in three sectors of the plastics industry, which are material and additive manufacture, polymer processing, and machinery manufacture. In the year 2000, the plastics industry in Western Europe accounted for a turnover of 135700 million euros (APME, 2001 [Online]). The polymer processing sector was a major contributor that shared approximately 74% of the turnover. A number of processing operations are designed to support this enormous polymer processing business. Among the operations are screw extrusion, injection moulding, film blowing, calendaring, and coating. About 60% of polymers pass through screw extruders in the process of converting polymers into products (Levy, 1981; Rosato, 1997).

A screw extruder is an efficient polymer processing device. It provides ideal processing conditions including large surface area of contact between the polymers and the extruder, uniform shear action and homogeneous mixing of additives. Carbon fibres and colour pigments are examples of additives. An extruder continuously compounds, melts, and pumps molten polymer out of the extruder die. The melt leaving the die solidifies and forms into the polymer product.

The polymer processing business is very competitive. There is a constant need for improving the extruder performance to cope with a rising pressure in aspects of production cost, product quality, and environmental issue due to plastics waste. The latter receives considerable attention as the growth in plastics consumption has been accompanied by a parallel growth in plastics waste. It was reported that each European on average consumed 91 kg of plastics in year 2000, and only 3.6% of the plastics waste was being recycled in the plastics production line (Hannequart, 2004 [Online]). Efforts have been made to stimulate the practice of plastics recycling. Apart from raising public awareness, legislation has been introduced to reduce the plastics waste in the industrial sector. In-house scraps produced during start-up and end of operations, samples for quality control and defective polymer products are reground to mix with the fresh polymers during the extrusion process. This practice also offers savings in term of material cost, but the product quality may be affected by the contaminated or degraded plastics mixture. Maintaining the product quality requires the design and the operation of the extruder to be optimal.

The extruder screw is the main element that determines the melting performance of an extruder. The geometric design of the screw defines the amount of shear experienced by the polymer, the residence time of the melt inside the extruder, and the amount of energy consumed during extrusion (Prentice, 1995). The majority of extruders in the industry are single screw extruders (Todd, 1998). In the past, the screws for single screw extruders were designed on the basis of trail-and-error by experts. This approach is expensive and time consuming. In recent years, the numerical optimisation of extruder screw geometry emerged to be a popular method. Several research works have been undertaken towards this direction (Potente and Hanhart, 1994; Gen and Cheng, 1996; Yu, 2000). Optimal screw geometry is normally calculated based on a process model with respect to the input operating conditions including the polymer properties.

The screw design alone is insufficient to ensure that the polymer products are of good quality, as the operating conditions are inconsistent in practice. In line with legislative requirements on recycling, an increasing percentage of regrind polymers are mixed with the fresh polymers during extrusion. The properties of the compounded polymers inside the extruder are subsequently different from the properties of the fresh polymers. Moreover, the extrusion operation is subjected to various sources of process

disturbances including variations in room temperature and humidity. These would affect the performance of an extruder even with an optimally designed screw. To cope with these variations, an adequate control system is required.

Control of the single screw extrusion process does not receive the same level of attention as the screw design. The standard Single-Input-Single-Output three-term controller (PID) is still a popular method of regulating the extrusion process. As the principal goal of a PID control is to stabilise an operation while achieving the target outcome as closely as possible, the method has two drawbacks. It cannot cope with Multi-Input-Multi-Output (MIMO) problems and there is no means of ensuring that the control function is optimum. Inevitably, these limitations have an impact on the quality and quantity of the final product. Little or no detailed work has been conducted on the MIMO control of the extrusion process. Gawthrop (1998) considered the viability of applying MIMO Continuous-time Generalised Predictive Control to extruders, but the work was not of a sufficient depth to enable a proper evaluation to be made.

Attempts have also been made to improve the control of extrusion process by means of soft computing techniques. Chiu and Pong (1999) introduced a fuzzy gain scheduled PID controller for the extrusion operation. McKay *et al* (1996) developed inferential models using Multi-Layered Perceptron Neural Networks and Genetic algorithms for the polymer viscosity control. The published results have shown that the soft computing techniques could be used to enhance the predictive capability of a control system and to achieve a near optimum control solution.

Inspired by their apparent success elsewhere, soft computing techniques are incorporated as part of the control and optimisation strategy. It is remarked that the extrusion of compounded polymers is a highly non-linear process. Some of the process parameters, namely operational-sensitive parameters, might not be appropriate to express in a deterministic manner. Past experience suggests that by defining these parameters as fuzzy parameters, reasonable approximations of their functional relationships could be obtained. In addition, the control of extrusion process is essentially a MIMO optimisation problem. Hence soft computing techniques might also be the solution of choice.

The present work represents the third phase of the University research programme on the single screw extruder. In Phase 1, an experimental study on an in-house single screw extruder was carried out (Qiu, 1998). The work investigated the compounding performance of the extruder operated under different operating conditions including different extruder screw geometries. In Phase 2, an intelligent tool was developed to facilitate the design and optimisation of extruder screws for single screw extruders (Yu, 2000). The tool generates an optimal screw design with respect to the relevant data and operating conditions provided by the user. The present phase, Phase 3, proposes a dynamic model and an intelligent MIMO control system for the single screw extruder. The experimental results obtained in Phase 1 will be used as an aid to understanding the extruder behaviour and process disturbances of melt temperature and melt pressure. Being aware of a diverse range of screw designs available, the work is restricted to a screw with a standard geometry.

1.2 Aims and Objectives

Aims:

- To develop an adaptive dynamic model for the single screw polymer extrusion process.
- To design an intelligent MIMO control system to improve the quality of the polymer product by means of regulating the melt temperature and pressure.
- To evaluate the implementation of the proposed extrusion control system.

Objectives:

- Review previous findings on modelling and control of the single screw extrusion process. Identify the process parameters that are important to the extrusion control system.
- Study the specifications of the in-house extrusion system. Review the experimental data to understand the behaviour of extrusion process including the disturbances on the melt temperature and the melt pressure.
- Develop a semi-physical dynamic extrusion model. Identify and approximate those operational-sensitive parameters by empirical sub-models.
- Evaluate the predictions of the semi-physical dynamic extrusion model with respect to published results.

- Integrate the concepts of model based predictive control, fuzzy rule base system and controller output error method to design an intelligent MIMO extrusion control system.
- Evaluate the characteristics of the proposed control system by means of a parametric study.
- Compare the performance of the proposed control system with other control systems.

1.3 Scope of Report

This thesis presents the research work on dynamic modelling and intelligent control of the polymer extrusion process. The contents consist of background study, literature review, data review, semi-physical dynamic extrusion modelling, extrusion control design, simulation studies, discussion, conclusion and future work. Previous publications on the modelling and control of single screw extrusion are reviewed in Chapter 2. The physics of the extrusion process is also briefly described.

In Chapter 3, the in-house extruder is studied to acquire basic knowledge of the machine especially in terms of its instrumentation. Melt temperature and pressure were two process output parameters measured in the Phase 1 programme to indicate the performance of the extruder with respect to the screw design. The data is now reviewed to analyse the extrusion process behaviour including the process disturbances. The analysis is important for the understanding of the control problems. In the chapter, a signal conditioning approach is also presented to filter measurement noises and a technique to deduce a true melt temperature is given.

The development of the semi-physical dynamic extrusion model is described in Chapter 4. The semi-physical model is derived from the theoretical model with the operational-sensitive parameters approximated by empirical sub-models. The sub-models are developed in a form of fuzzy rule based system and identified using a GA-fuzzy optimisation algorithm. The semi-physical model is then simulated and evaluated by comparing the consistency of the model predictions with the experimental observations. The usefulness of the adaptive ability of the model is also discussed.

A new intelligent control system, namely Fuzzy supervisory indirect Learning Predictive Control (FsiLPC) system is proposed in Chapter 5. Since the FsiLPC system is developed based on the Model Based Predictive Control (MBPC), the operating procedure of a MBPC system is described to serve as background knowledge. Then, the operating procedure and the detailed operating mechanisms of the FsiLPC system are presented. A simple example is employed to illustrate the development of the FsiLPC system. Its performance is compared with the MBPC system.

Chapter 6 presents the development of a FsiLPC system for the extrusion process. The screw speed and the barrel temperature are used to control the melt pressure and the melt temperature simultaneously. The characteristics of the FsiLPC system in controlling the extrusion process are investigated using a parametric study. The performance of the FsiLPC system is then compared with other control systems, when step-changes of reference signal and process disturbances are imposed. The present research work is discussed in Chapter 7. In Chapter 8, the contributions towards the research aims are highlighted and directions for future work are given.

Chapter 2
Literature Review

2.1 Introduction

Control of single screw extrusion process is an appropriate approach to maintain the consistency of polymer melt conditions, hence produces high quality products. In this chapter, the background study on designing the extrusion control system is presented. The study comprises an overview of a complete extrusion system, melting mechanisms of a single screw extrusion process, previous publications of dynamic extrusion models, control system designs and learning methods of intelligent control systems.

2.2 A Complete Single Screw Extrusion System

A complete single screw extrusion system comprises three basic components: a single screw extruder that compounds the feed polymers, a die that defines the shape of the melt, and downstream equipment that transforms the melt into the final product. These components are described below with respect to the polymer flow direction:

1. The single screw extruder is the primary component of the complete extrusion system. It provides mechanical and heat energies to efficiently melt the solid polymers and deliver the molten polymers with very high viscosity to the extruder die. In this thesis, the state conversion of polymers from solid to melt using the single screw extruder is referred to as "extrusion process". The melting mechanisms of the extrusion process will be detailed in the next section.

2. The extruder die, which is mounted to the extruder end, provides a cavity to improve homogeneity of the melt conditions. As the pressure in the die is developed, the melt is pumped off from the die continuously. The melt leaving the die exit is called "extrudate". A properly designed die will provide the extrudate with a correct velocity profile and temperature distribution during the

extrusion. The design should take into considerations of physical, rheological and thermodynamics of the melt when flowing through the die (Huang, 1999).

3. The downstream equipment consists of a conveyer system, a cooling bath, and a set of rollers for instance. The function of the downstream equipment is to modify the shape of extrudate so that the desired form of the final product is acquired. This shaping process is called "orienting". With the proper configurations on the die and the downstream equipment, many orienting processes are possible. Some examples are given in Table 2-1.

The combination of the extruder, the die and the downstream equipment needs calibration to attain a good quality product. The calibration in practice is time consuming. Therefore, the single screw extruder is generally designed to operate under steady state conditions. It is very important that the output polymer melt of the extruder is of consistent conditions, as it represents the quality of material supply to the downstream equipment. An extrusion control system is normally applied to minimise the variations of the melt conditions.

Table 2-1: Examples of orienting (Rosato, 1997).

Orienting	Descriptions/ product examples
Film extrusion	Flat shape extrudate is passed through a set of chilled rolls, which calibrate, cool and form a product such as a food wrapping film.
Film blowing	Extrudate in tubular shape is blown by air, causing it to expand in the radial direction to form a thin bubble-like film. The extension of the film stops when it is cooled and nip rolls are used to collect the film. A typical product is a refuse sack.
Blow moulding	Tubular shape extrudate enters a split mould. Air pressure is injected into the extrudate after the mould is closed. The extrudate expands against the mould wall. A product is obtained when the expanded extrudate is cooled. An example of the product is a plastic bottle.
Coating	Extrudate is forced to adhere to a moving substrate. The substrate can be in different form and shape, such as copper wire, wooden rod and paper film. The coated surface may provide several desired properties including electric insulation and water resistance.

2.3 Melting mechanisms of Extrusion Process

The schematic diagram of a single screw extruder is illustrated in Fig. 2-1. The extruder consists of a barrel, which is heated by a series of wall-mounted heaters and a rotating screw; the latter is linked to a gear system and a motor. Polymer particles are fed in through the hopper, by gravity, into the helical screw channel. The screw has a varying channel depth along its axial direction. The designs of screw geometry could vary to meet different processing conditions of the extrusion; for example standard, rapid, compression and barrier. In this work, only the standard screw is considered.

The geometry of the standard screw is classified according to the channel depth into three sections, which are the feed, the compression and the metering sections. In the feed section, the channel depth is relatively deep. This ensures that the solid polymer particles are loaded and conveyed efficiently to the compression section. The moving particles in the feed section are heated by two sources of energy, namely frictional heat and conductive heat. The frictional heat is generated when the particles shear against the barrel, the screw, and each other, while the conductive heat is obtained from the hot barrel wall near the compression section. The surfaces of the particles begin to melt when the temperature of the polymer reaches its melting point. The particles moving towards the compression section in the screw channel are compacted to form a solid bed (shown in Fig. 2-2).

The channel depth in the compression section decreases constantly to develop the delivery pressure. A thin melted film is normally formed at the interface of the solid bed and the barrel wall upon entering the compression section. As the relative motion exists when the screw is rotating, the film adhered to the stationary barrel surface is dragged towards the advancing flight. The film meeting the flight is then 'scraped off' and mixed with previously melted polymer, forming a melt pool (shown in Fig. 2-2). Started from this stage, the energy for the melting mechanism is mainly attributed to viscous dissipation. Viscous dissipation is the heat generated when the melt is being sheared.

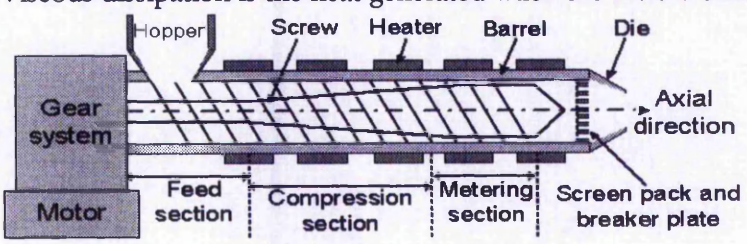

Fig. 2-1: Single screw extruder.

The content of a typical helical cross section of the screw channel in the compression section is illustrated in Fig. 2-2, which encloses the solid bed and the melt pool. The solid bed diminishes, as the melting process proceeds in the axial direction along the screw. The melting process ends when the solid bed completely disappears. The variation of the width of solid bed along the screw channel in helical direction is referred to as the "Solid Bed Profile" (SBP). Likewise, the variations of the temperature and the pressure of the melt pool are termed as the "Melt Temperature Profile" (MTP) and the "Pressure Profile" (PP) respectively. These profiles are the indications to the efficiency of an extruder performance.

The depth of the screw channel at the metering section is relatively shallow. This helps to improve the homogeneities of the melt temperature and the pressure, because of a better melt circulation. At the end of the extruder, the melt is continuously pumped off from the die through a set of screen pack and breaker plate. The latter equipment set is needed to filter the melt and create a backpressure. The melt flowing through the die is delivered to the downstream equipment and formed into the product.

In short, the polymers experience a complicated and continuous state conversion from solid to melt during the operation. The flow of the polymer melt inside the extruder (flow history) could have significant influence on the end product quality. A number of scientific analyses were conducted during the past decades when attempting to model the flow history, as this information is a prerequisite for a screw design. The previously described melting mechanisms are acquired from the analysis proposed in Tadmor (1966), which was developed based on the Maddock observation as illustrated in Fig. 2-2 (Maddock, 1959). The analysis is a basic reference for many technical studies on the extrusion process (Donovan *et al*, 1971; Brukek and Balch, 1989; Amellal and Lafleur, 1993; Wilczynski, 2001).

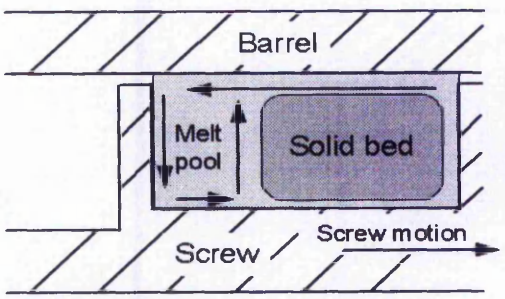

Fig. 2-2: Melting of solid bed.

Lindt (1976) noted a different melting behaviour of solid polymers when operating a large extruder without the barrel heat supply. The observation is depicted in Fig. 2-3. The molten polymer was found surrounding the solid bed instead of accumulated in the melt pool. Based on this observation, a theoretical model was developed using the momentum and energy balances between the melt and the solid bed. The predicted pressure profile and solid bed profile were validated with the experimental data. The analysis, however, was incomplete and yet to be comprehended.

In a survey paper, Lindt (1985) concluded that the models available at that time were fairly useful for the screw design. The required length to completely melt the polymer could be predicted. However, prediction of pressure profile in the compression section required refining, in which the effect of cross-channel melt circulation should be considered. Lindt commented that the developments of melting models based on Maddock observation (Fig. 2-2) were virtually completed. Further progress was suggested to analyse the melting process derived from powder mechanics principles to govern the behaviour of solid bed.

Subsequent to the development of numerical methods, numerical analysis emerges to be a popular approach to analyse the extrusion process. Essentially, there are three types of the numerical methods, namely Finite Difference Method, Finite Element Method and Finite Volume Method. These methods are used to solve the process governing equations that can no longer be solved by analytical methods. Chiruvella *et al* (1995) analysed the fluid flow and heat transfer in the metering section of an extruder. A Finite Different Method was used to solve the equations of momentum and energy to obtain the velocity and temperature profiles in the screw channel. By simulating the fluid flow and heat transfer phenomena in the screw channel, the performance of the extruder could be predicted for the chosen thermal boundary conditions, screw geometries, die geometries, polymers material and operating conditions.

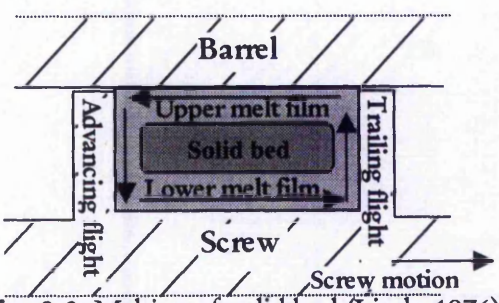

Fig. 2-3: Melting of solid bed (Lindt, 1976).

Syrjala (1999) simulated the non-isothermal flow of molten polymer in the metering section. A Finite Element Method was employed to solve the governing equations of a cross-sectional plane. Then, the calculation proceeded to the following cross-sectional planes until the end of the extruder by using a marching-type technique. The calculated pressure and temperature profiles were validated against experimental data but indicated some discrepancies (Syrjala, 2000). Kwag *et al* (2002) commented that the marching-type technique was unable to calculate the precise pressure flow, since the velocity deviations along the down-channel direction were neglected during the calculation. A Finite Volume Method was used to calculate the three-dimensional velocity, temperature, viscosity, and pressure profiles in the metering section, without simplification of flow fields for incompressible non-Newtonian fluid. The results were compared to those marching-type solutions and the improvement was justified theoretically.

Lai and Yu (2000) proposed a different approach to analyse the entire extrusion process. The continuous domain of screw extruder was discretised into a finite number of tiny segments, with each segment formed a control volume. A cross-sectional diagram of a control volume is illustrated in Fig. 2-4a. The content was mapped to Fig. 2-4b by means of a concept known as "equivalent radius". The continuity of mass flow, heat energy and force balances were solved to predict the state of the control volume, namely the solid bed, temperature and pressure. The developed model was effective in providing a rapid and accurate analysis of the steady state extrusion process.

The described analyses represent different means of understanding the melting behaviour and flow history of polymers under the steady state extrusion operation. The analyses are useful for designing single screw extruders. In light of designing a control system, the dynamic behaviour of extrusion process is more meaningful. A number of dynamic extrusion models have been proposed for this purpose.

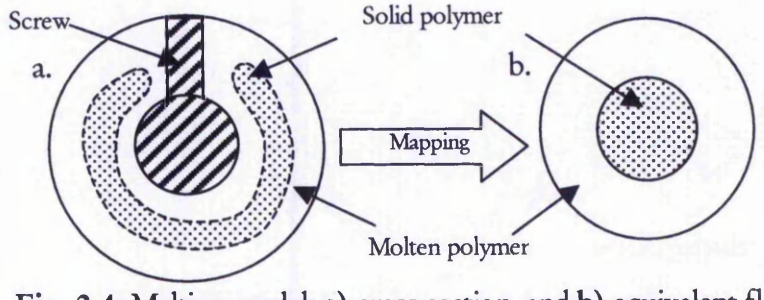

Fig. 2-4: Melting model: **a)** cross section, and **b)** equivalent flow.

2.4 Dynamic Modelling of Single Screw Extrusion

The dynamics of the extrusion process often necessitates changes in the state of the process, brought about by process disturbances including variations in properties of the polymer materials. Attempts have been made to study the dynamic extrusion behaviour both theoretically and empirically. The published models are reviewed here.

Relatively little attention has been paid to the theoretical analysis of dynamic extrusion behaviour. Tadmor *et al* (1974) proposed a theoretical dynamic extrusion model by assuming that the dynamic conditions exist only when the polymers start melting. The transport equations to describe the transport processes in the melting mechanism were derived. The results shown in Table 2-2 represented the orders of magnitude for the fictitious time constants of the transport processes calculated from the equations under typical operating conditions. The heat and momentum transport processes at a point in the thin melt film and the melt pool, which occur perpendicularly to the down channel direction, are fast and diffusive in nature. Comparatively, the bulk flow (solid and melt convection) at a point, which occurs tangentially to the down channel direction, is in several orders of magnitude slower. This implied that the rate of the bulk flow could be sensibly chosen as the rate of dynamic calculation. Meanwhile, the responses of the parameters in the heat and momentum transport processes were assumed to reach their steady state conditions before any bulk flow has taken place. Hence, the parameters could be calculated using steady state equations according to local instantaneous conditions.

The model simulated the transient[1] responses of SBP, MTP, PP and flow rate in response to changes in operating conditions. The results were verified qualitatively based on step tests and experimental observations. This dynamic model serves as the foundation for the development of a semi-physical dynamic extrusion in Chapter 4.

Table 2-2: Order of magnitude of transport processes (Tadmor *et al*, 1974)

Transport processes	Heat transport		Momentum transport		Bulk flow
	Melt film	Melt channel	Melt film	Melt channel	
Order of magnitude	1 second	1 second	10^{-7} second	10^{-4} second	>10 seconds

[1] The time before the process reaches the steady state condition

Brauner *et al* (1977) extended Tadmor's work (1974) to examine the transient responses when the extrusion process was subjected to changes in polymer materials. The simulation results showed that the pressure waves were created in the metering section in response to the material changes. This adversely disturbed the flow rate when the pressure waves reached the die. Brauner *et al* proposed an approximate model for the control application. It was obtained by means of equation linearisation with respect to the localised conditions. Therefore, the validity was confined to the observed operating region. Evaluation of the approximate model was not presented.

Kochhar and Parnaby (1977) commented on the development of a theoretical dynamic extrusion model as unrealistic. The complex interactions between the polymer properties and the operating conditions were described as a main restriction. Further complication includes the limited accessibility of the distributed process parameters. Some important process parameters including the velocity and the properties of molten polymer could not be measured along the extruder during the dynamic conditions. Time series modelling technique was recommended to develop empirical dynamic extrusion models for the control application.

An empirical linear model is obtained by relating the Input-Output (I/O) process parameters, through a model structure that is known to have 'good flexibility' (Ljung, 1999). The empirical modelling techniques for the extrusion process have been categorised into classical technique and modern technique (Costin *et al* , 1982a). In the case where the classical technique is employed, the dynamic model is expressed in terms of Laplace transform structure. This technique has been applied in several works (White and Schott, 1972; Dormeier, 1979). The dynamic extrusion models could be one or a combination of the first order, second order and lead-lag transfer functions.

The modern technique was referred to as the time series modelling technique. An early work using the time series modelling technique was described in Kochhar and Parnaby (1977). A general structure for empirical extrusion models identified is given in Equation (2-1):

$$P_t = \frac{\omega(z^{-1})}{\delta(z^{-1})} z^{-f-1} U_t + N_t \qquad \textbf{(2-1)}$$

where Equation (2-1) represents a discrete time transfer function, P_t is the process output parameter, U_t is the input parameter, f is the number of sampling periods of delay, $\delta(z^{-1})$ is the characteristic polynomial of the process, $\omega(z^{-1})$ is the polynomial corresponding to the process input, and N_t is the noise model. The polynomial could be estimated using the least mean square analysis.

The survey of Costin *et al* (1982a) indicated that most of the empirical dynamic extrusion models available at that time were in a Single-Input-Single-Output (SISO) structure. The common output parameters of the models were the melt temperature, melt pressure, and extrudate thickness. In aspects of input parameters, the screw speed, backpressure, and barrel temperature were widely used. Nelson *et al* (1986) investigated the transient responses of barrel pressure, die pressure, melt temperature and extrudate thickness in response to the step-changes in screw speed, pulling speed, backpressure and polymer materials through a series of experiments. They found that when the backpressure was changed, cyclic fluctuations in the output flow rate were resulted. These fluctuations were difficult to control, which might unfavourably affect the dimensional accuracy of the extrudate. Thus, the backpressure was not recommended as a suitable process input parameter.

Costin *et al* suggested a method to develop a Multi-Input-Multi-Output (MIMO) extrusion model, where the individual SISO models were coupled based on relationships established though the process analysis. This method was adopted by Kaya and Rice (1985), in which a MIMO dynamic model was proposed to predict the extrudate flow rate and the melt temperature. Two SISO transfer functions relating the flow rate to the screw speed, and the melt temperature to the cooling water flow rate respectively were firstly identified. The MIMO dynamic model was then formed by coupling the two transfer functions. However, neither experimental verification, nor simulation of the MIMO model was demonstrated.

In the recent years, soft computing techniques have become a popular means to develop empirical models for many industrial processes. This is also true in the modelling of dynamic extrusion process. The techniques are founded on three major constituents, namely Artificial Neural Network, Genetic Algorithm and Fuzzy Rule Based System (Dubois and Parade, 1998).

Artificial Neural Network (ANN) is a technique with well-known ability to capture the non-linearity of process characteristics. The ability of an ANN model was evaluated by Wagner *et al* (1997) in predicting the extrudate viscosity during the steady state operation. The screw speed and additive dosage were used as the input parameters. The ANN model contained one hidden layer with four neurons. Each neuron in the hidden layer performed summation and sigmoidal processing. During the network training, the weights assigned to the linkages among the neurons were adjusted to improve the approximations of the I/O relationship of the parameters. The model showed reasonably good predictions during the model validation. However, it required a relatively large amount of data to identify a model.

Genetic Algorithm (GA) is basically a "systematic" random search technique. Its desirable properties as a "universal optimiser" include easy implementation, compact storage and simultaneous search in cases of multiple-objectives. The GA was employed by McKay *et al* (1996) to identify a dynamic viscosity model, through parallel search on both model structure and associated coefficients. The performance of thus obtained GA viscosity model was then compared to an ANN viscosity model. The results showed that the GA viscosity model was of better performance and having a simpler structure. However, the model identification process was time consuming and required intensive trials before a good model could be obtained.

Fuzzy Rule Based System (FRBS) is a means of linguistic approach normally used to exploit imprecise and incomplete information. The parameters of a FRBS model are defined by membership functions, which are related by a set of fuzzy "If... then" rules. This makes the FRBS model possible to be interpreted linguistically. However, the identification of the FRBS model could be problematic if it has a large number of input parameters, or more than one output parameters. Chiu and Pong (2001) proposed a FRBS dynamic model to approximate the melt viscosity during the extrusion process. The model contained a set of rules coupling the output viscosity with the input parameters of screw speed and viscosity. A reasonable agreement between the model predictions and the experimental data was achieved. The model was then used to design a fuzzy viscosity control system. The system was shown to be stable under the stability test proposed by Kiszka *et al* (1985).

The reviewed empirical modelling techniques provide varieties of model structures (Laplace transform, discrete time expression, ANN and FRBS) to develop an empirical model. Though, all of these techniques perform a similar function, which is curve-fitting the model predictions with the experimental data. Whilst these models are useful in their specific applications, they lack generality and physical meanings. Identifying a good empirical model is experimentally intensive, which can have a cost implication. On the other hand, the theoretical dynamic extrusion model is difficult to derive. It requires good knowledge of the process behaviour in both temporal and spatial domains. Besides, the accuracy of a prediction is affected by the process simplification assumptions. A research interest has been pointed to obtain a compromise between the empirical and theoretical modelling techniques, in which a semi-physical modelling technique is introduced (Lindskog and Ljung, 1994).

An example of a semi-physical model for the extrusion process is a macroscopic dynamic model proposed by Reber *et al* (1973). The model approximates the extrusion process as a series of repeating units. Each unit is governed by a set of ordinary differential equations derived from the conservation laws. Some complicated part of melting mechanisms, including the convections of solid and melt, are approximated by empirical equations. These equations are identified offline based on the flow rate data using a pattern search technique proposed by Wilde and Beightler (1967). The predictions on the melt temperature and the flow rate of the resultant semi-physical model were validated with the experimental data.

The semi-physical modelling technique has also found applications in other processes. Lindskog and Sjoberg (1995) demonstrated the technique in modelling a solar heated house. The aim of the model was to predict the behaviour of the storage temperature in response to the solar radiation and the pump speed. To achieve this, a sixth order linear model was first developed but the predictions were not satisfactory. Then, the energy conservation law was used to aid the model identification. A second order non-linear semi-physical model was obtained. The semi-physical model not only performed much better than the previous linear model, but also offered a means of physical interpretation.

Tan and Li (1997) proposed a semi-physical model for a twin tank liquid-level system. A nonlinear MIMO state space model was first derived from the Bernoulli's equation of

mass balance. The model contained some parameters that were difficult to measure accurately such as the discharge coefficient. These parameters were then identified using a hybrid of Simulated Annealing and Genetic Algorithm techniques. The semi-physical model produced encouraging results, which implied that the unknown empirical parameters had been adequately identified.

In a biochemical process, semi-physical models were developed to predict the *pH*-trajectory of a fed-batch penicillin conversion, given only the initial stage and the process input (Braake *et al*, 1999). The kinetic of penicillin conversion was approximated using a FRBS and an ANN separately. Both of them were then incorporated into the theoretical model governed by the chemical charge balance. The semi-physical models (with a FRBS sub-model and an ANN sub-model separately) predicted reasonably accurate *pH*-trajectories. The simulated results were then employed as training dataset to develop an ANN model for control applications.

2.5 Extrusion Control Systems

The aim of a control system is to stabilise an operation while achieving the desired outcome. The block diagram of a simplified control system is illustrated in Fig. 2-5. Within the boundaries of a specified operating region, the controller should be able to drive the plant output Y (controlled parameter) to match the desired value R (reference) as closely as possible, by imposing an adequate signal to the plant input U (manipulating parameter) automatically. To reach this aim, a dynamic process model is often used to aid the design of the controller.

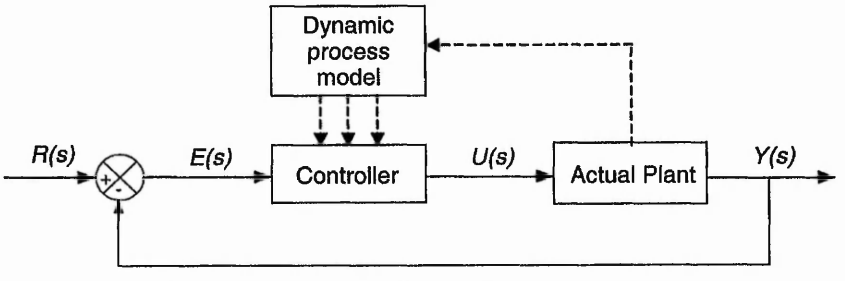

Fig. 2-5: A simplified closed loop control system.

During the past few decades, many controllers have been proposed to improve the quality of the polymer extrudate. The term "quality" was defined by Menges and Giegerich (1972) as the homogeneity of the polymer melt. They suggested several process parameters that might have most influent on the melt homogeneity. These include melt temperature, pressure, viscosity, tension, impurities, mixing homogeneity and throughput rate. Some of the parameters require special measuring devices that are expensive to install in practice.

The common process inputs (manipulating parameters) and outputs (controlled parameters) are depicted in Fig. 2-6. The manipulating parameters include the screw speed, the barrel temperature and the backpressure valve while the controlled parameters include the melt pressure, the flow rate and the melt temperature. The backpressure valve is used to adjust the die restriction to control the operating pressure while the pulling speed determines the rate of extrudate being drawn out from the die. These two parameters would control the size of the extrudate indirectly. The couplings of the manipulating parameters and the controlled parameters are shown in Fig. 2-7. The *x*-axis represents the controlled parameters while the manipulating parameters are listed in the legend. The information in the stacked bars is interpreted as follows.
Taking the first bar as an example, it is observed that about 30% of the surveyed literature considered the melt pressure at the die as an important controlled parameter. To regulate the melt pressure, the most popular method was by changing the screw speed. Alternatively, the backpressure valve was manipulated.

In a similar interpretation, it is realised that the melt temperature at the die (second bar) was regarded as the most commonly used parameter to indicate the melt quality. The popularity of this parameter is ascribed to the reliability and the cheaper cost of temperature measuring devices. For example, installing a thermocouple at the die is more economical than fabricating a unique device to measure the viscosity.

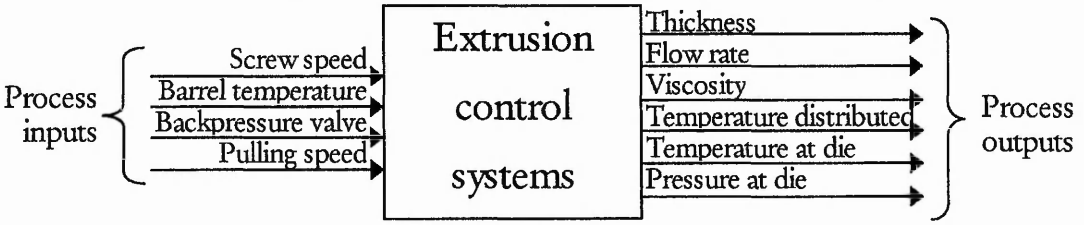

Fig. 2-6: Commonly employed process input and output parameters

The screw speed was treated as the single most important manipulating parameter to regulate nearly all the controlled parameters. The extrusion process responds relatively fast to changes in the screw speed. This is because the heat generated by viscous dissipation due to the rotating screw is the main energy source in the melting mechanism. In this research, the barrel temperature alone is considered insufficient to be used as the manipulating parameter. Details will be given in Chapter 6. It should be noted that the coupling of the process parameters could overlap for MIMO control systems. The overlapped couplings of parameters are difficult to illustrate in the graph, but will be elucidated in the following sections.

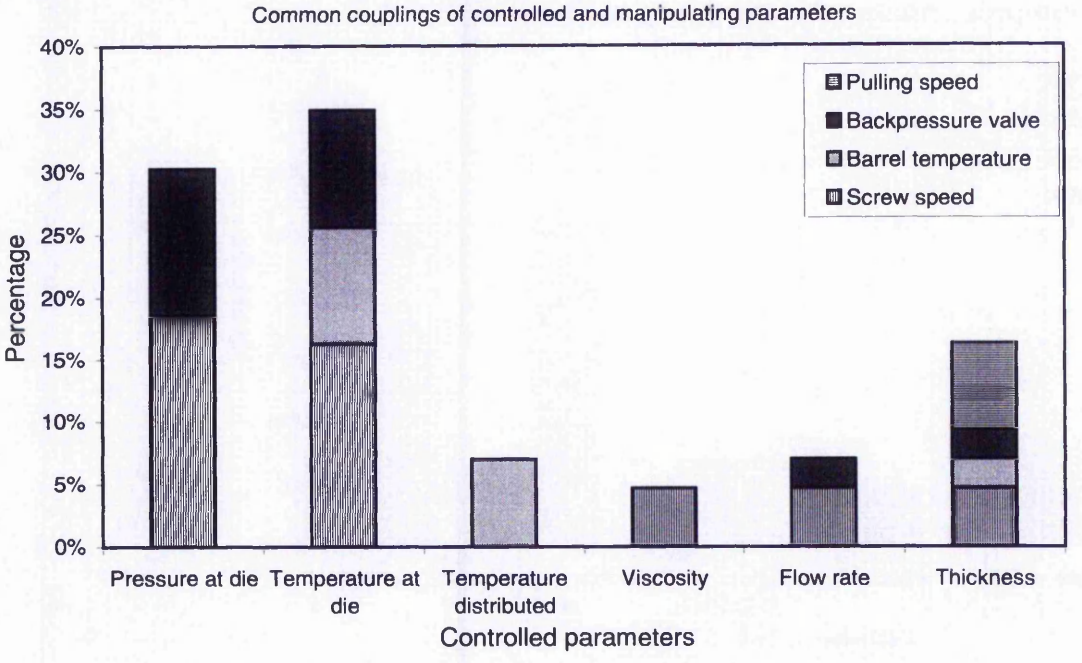

Fig. 2-7: Common couplings of controlled and manipulating parameters.

2.5.1 Conventional controllers

The simplest form of extrusion controller provides "on-off" control of heater/cooler system (Moore, 1989). The heater is fully switched on when the melt temperature is below the preset lower limit or vice versa. The preset lower and upper limits for turning-on and turning-off of the heater/cooler system are deliberately made to differ by a small amount. This is known as hysteresis, which is created to prevent noise from switching the heater rapidly and unnecessarily when the melt temperature is near the reference. In the least demanding circumstances, the on-off controller can give acceptable results. However, the melt temperature tends to cycle around the reference temperature. The

fluctuations are undesirable and normally with the peak-to-peak amplitude exceeding the hysteresis.

The performance of the on-off controller has been slightly improved by a 'time proportioning" approach (Weisbrod, 1969). In this approach, the controller varies the time-on/time-off ratio of the heater/cooler system to control the temperature. The time ratio is proportional to the ratio of the temperature deviation. The power supply is switched off for a shorter time when the measured temperature is closer to the reference temperature. The proportional gain is calculated only when the temperature is within a "proportional band", which is determined by the preset lower and upper temperature limits. The time proportioning controller helps to reduce the temperature overshoot and oscillation, yet the result is rather crude.

Proportional-Integral-Derivative (PID) controllers are designed subsequent to the development of potentiometric or bridge type circuitry. Its first application is dated back to 1922 on ship steering (Minorsky, 1922). This is then followed by intensive theoretical investigations and eventually promoted to industrial applications. It was reported that the PID controllers have been implemented in about 95% of close-loop industrial processes (Yamamoto and Hashimoto, 1991).

The basic elements of a PID controller are illustrated in Fig. 2-8. The controller comprises three strategies, namely Proportional control, Integral control and Derivative control, which play different roles during the operation. Taking the melt temperature control as an example, the results of the on-off controller may exhibit a large overshoot followed by oscillations around the reference temperature. This is because the on-off controller would either turn-on or turn-off the heater power when being triggered. The proportional control allows variable amount of power supply to the barrel heater when the melt temperature is in the proportional band. The proportional bandwidth is set to be 5% in a typical industrial PID extrusion controller (Whelan and Dunning, 1982). The setting is in relative to the heater power capacity and the properties of the barrel wall. When the melt temperature approaches the reference temperature, the power supply to the heater is reducing. The power supply is switched off totally when the melt temperature meets the reference. By this means, the overshoot and oscillating responses are minimised if the proportional band is set sufficiently wide. However, the wide

proportional band may adversely result in a large offset error (steady state error) due to the lower sensitivity of the controller. The final temperature would stay below the reference temperature because a temperature difference is required to keep the heater power on. Narrowing the proportional band may help to decrease the steady state error, but may also cause less control on the overshoot response. To reduce the overshoot while maintaining a narrow proportional band, a derivative control is incorporated with the proportional controller.

The derivative control operates on the basis of the rate of temperature change. When the temperature reaches the proportional band, the proportional control starts reducing the power supply to the heater. This gives a slowing rate of temperature change, and the derivative control introduces the information to the control action. The resultant control action will be a value less than the control action of a purely proportional control corresponding to that particular temperature difference. Therefore, the overshoot response is reduced more efficiently, if not eliminated. Although proportional-derivative control deals neatly with the overshoot problem, it does not overcome the problem of the steady state error. An error is still necessary to maintain the power supply to the heater. To minimise the steady state error, an integral control is needed.

The integral control accumulates the small steady state error over time so that eventually the accumulated value is large enough to trigger a corrective control action. This is similar to adding a bias signal to the control action automatically to compensate the steady state error. A common problem associated with the integral control is called integral wind-up. Since the integral control operates by accumulating the steady state error, the accumulated value will increase continuously if the error remains in the same direction (say the melt temperature consistently stays below the reference). This may happen when the capacity of the manipulating parameter cannot meet the demanding conditions.

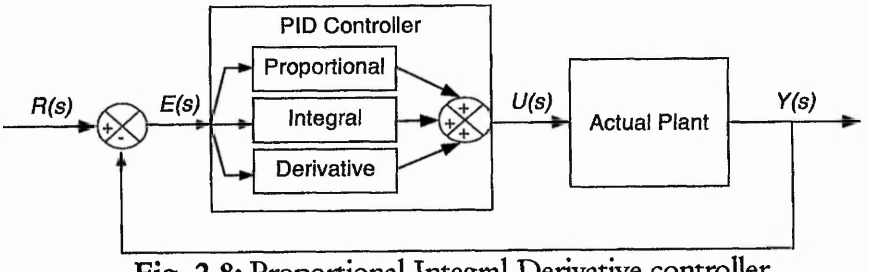

Fig. 2-8: Proportional-Integral-Derivative controller.

To illustrate the problem of integral wind-up, a case where a constant melt temperature to be maintained is considered. In a normal operation, the screw rotates at a constant speed to provide the heat energy by viscous dissipation while the electrical heater generates the heat energy to compensate for changes in ambient temperature. In one occasion, if the screw rotates at a speed slower than required due to the power disturbance, the heat energy by viscous dissipation is reduced. The controller will increase the heater power so that the total amount of heat energy required for the melting mechanism can be maintained. If the screw speed continues dropping, the heater will eventually fail to maintain the melt temperature even if it is fully switched on. Then, the integral control will accumulate this steady state error and the accumulated value will grow larger and larger. When the screw speed is restored, the heater will still fully on in response to the large accumulated error. Therefore, it is quite likely that the melt temperature may increase to overshoot the reference largely before the accumulated error drops to a point that the power to the heater starts reducing. The response can be sluggish. One of the solutions is by constraining the operation of the integral control within the proportional band. This is obtained by setting the integral control to zero when the melt temperature falling outside of the proportional band. Alternatively, a simpler solution is by resetting the accumulated error from time to time during the operation.

In general, the PID controller should provide good performance during the start-up and steady state operations. However, it was reported by Costin *et al* (1982b) that the derivative control might cause the system instability when regulating the process disturbances. The disturbances resemble a fast-changing error and every change in the error is magnified by the derivative control strategy. In this circumstance, Costin *et al* suggested to apply only a PI controller.

To benefit from computer technology, a number of existing analogue control algorithms are converted for digital implementation. These include the PID controllers for the polymer extrusion process. The performance of a digital PID controller to regulate the melt temperature was evaluated in Dormeier (1979). The heater power located at the final heating zone was regarded as the manipulating parameter. Disturbances were introduced by imposing step-changes in the heater power at the second zone. The digital PID controller was tuned off-line using a simulation study. Its

performance was shown to be better than an analogue PID control system, in minimising the long-term temperature deviation. The computer simulation was regarded as an effective and convenient tool for the tuning of the controller parameters.

The general applicability of the PID controller has been accompanied by the well-established theory of the PID control algorithms. If a process model is available, the controller parameters can be determined analytically. Even without a model, there are many rules that can be used to guide the parameter setting (Astrom and Hagglund, 1995; Ziegler and Nichols, 1942; Karaboga and Kahnh, 1996). Three classes of automated tuning methods for PID extrusion control were compared in Gawthrop *et al* (1990). These methods were Ziegler-Nichols-based tuning method, waveform-analysis tuning method, and least-square identification-based tuning method. A set of PID controllers was employed to control the melt temperature by manipulating the barrel temperature at different locations along the extruder separately. The results indicated that none of these methods could ideally met all the requirements, in tracking changes of reference signal and reducing the impact of process disturbances. A combination of the methods was recommended to widen the range of applicability.

A SISO PID controller in some situations may only achieve satisfactory but not optimal performance. This is especially true for the extrusion process with strong interrelationships between its process parameters. Taking the temperature control systems described in the previous paragraph as an example, different units of SISO PID controllers were developed to control the melt temperature at different locations along the extruder. The performance of these individual SISO PID controllers was found insufficient even though three tuning methods were attempted. The performance could be possibly improved if a MIMO control system was designed. One of the approaches to achieve the MIMO control is by implementing a cascade control scheme (Turnbull, 1972; Carr, 1985). The individual PID controllers are regarded as slave controllers to be managed by a master controller. Although the cascade control scheme offers an approach of MIMO control, the parameters of each PID controller are difficult to be tuned for optimal performance. The performance deteriorates especially if the process parameters are highly interrelated.

2.5.2 Adaptive controllers

Adaptive controllers are defined as those controllers with the automatic parameter tuning ability to improve the control actions. The concept of adaptive control has been developed since 1960s (Astrom, 1996). However, its applications at the time have been limited by the cost of implementations. Only with the development of a microprocessor, its impact on the industrial processes becomes obvious (Astrom and Wittenmark, 1995). Self-Tuning Regulator (STR), Model Base Predictive Controller (MBPC) and fuzzy controller are the examples of adaptive controllers found in the polymer extrusion control system.

Leffew *et al* (1987) applied a digital STR to regulate the melt temperature by manipulating the barrel temperature in the extrusion process. The STR was designed based on Dahlin control algorithm, in which the closed-loop step response of the system was modelled by a first order transfer function plus transport delay (Dahlin, 1968). The parameters of the model were updated online regularly through a linear least squares estimator. The results of the simulation study were quite promising but the STR required a correct estimation of the transport delay.

Costin *et al* (1982b) compared the performance of a STR and a PI controller. Both controllers were able to regulate the melt pressure in response to the low frequency disturbances using the screw speed. However, the performance of the PI controller deteriorated when a new type of polymer was fed to the extruder. This phenomenon was expected because the PI controller in the study was not adaptive to new operating conditions when the polymer properties were changed. To maintain its optimal performance, the parameters of the PI controller would require re-tuning. The automatic tuning ability of the STR was an expected solution, but in practise the tuning was found too sensitive to the measurement noises. Therefore, its installation was suggested to the location near the die, as the measurements were less distorted by the noises.

Bezanson and Harris (1986) developed two types of MIMO STR for the extrusion control, namely quadratic STR and state space STR. An optimal strategy of Gaussian quadratic cost function minimisation was used in the quadratic STR, while a state feedback strategy of pole placement was employed in the state space STR. Both STRs

operated on the basis of a second order MIMO empirical model. The melt pressure and the melt temperature at the die were coupled to the screw speed and the backpressure valve. The quadratic STR reduced the standard deviation of the melt temperature satisfactorily. However, the parameters in the quadratic cost function needed to tune by trial and error using offline simulations. Comparatively, the state space STR was recommended for the industrial application. It offers a stable approach for the initial process control when the process knowledge is limited. Though, the calculation was found to be more cumbersome.

Model Based Predictive Control (MBPC) is a suitable control methodology for MIMO processes especially when the process parameters exhibit large transport delays (Sanchez and Rodellar, 1996). A MBPC system operates based on a concept of a *receding horizon*, which can be illustrated as follows:

> For a Single-Input-Single-Output process, the reference, $r(k+n)$, is first planned to obtain in a specific length of future horizon by drawing an ideal trajectory. Based on the trajectory, a sequence of future manipulating signals is calculated such that the cost function is minimised. At each instant, only the first manipulating signal is applied to the plant although a sequence of manipulating signals has been calculated. The operation is repeated when the system advances to the next instant. The state of the predictive model is updated consistently. Under the ideal conditions, the controlled signal, $y(k+n)$, will eventually converge to the reference, $r(k+n)$, at the future horizon.

This concept of MBPC was combined with feedback control theory to control the single screw extrusion process (Yang and Lee, 1986a and 1986b). The resulted controller was namely an Adaptive Feedforward Feedback Controller (AFFC). The control system employed the extrudate thickness as the controlled parameter and the pulling speed as the manipulating parameter. Changes in the screw speed and the feed polymer properties were imposed to create disturbances to the thickness of extrudate. The AFFC was shown to respond faster to the disturbances than the digital PI controller. The combination of feedback and feedforward controllers was constructive. The adaptive ability of the control algorithm helped to improve the prediction of the predictive model.

Tsai and Lu (1998a) proposed a MIMO adaptive predictive controller for a plastic injection moulding process. It is remarked that the operation of the injection moulding process is periodic in nature while the extrusion process is continuous. However, the melting mechanisms in both processes are similar, if the same type of extruder is employed. The heater powers at four different locations along the extruder were manipulated to control the melt temperature. The control signal was generated using a predictive control law derived by minimising a quadratic cost function. Under the assumptions of constant reference temperature and unity control horizon, the predictive control law would resemble the function of a PI controller. This implied that the assumptions would help the controller to compensate for the modelling error. The performance of the predictive controller was validated against experimental evaluations in aspects of process disturbances, step-changes in reference, and variations in model parameters.

Research on the soft computing techniques has sparked a new era in the design of adaptive controllers. The constituents of the techniques have been described earlier in Section 2.4. The techniques, in general, emulate various aspects of natural intelligence to create the unique approaches of resources utilisation. A soft computing controller can be realised purely based on the techniques, or by integrating the techniques with other control methodologies (Mahfouf *et al*, 2002a; Tsai and Lu, 1998b). This flexibility promotes the applicability of the soft computing controller to a wider range of industrial processes. Many successful examples have been reported (Maeda *et al*, 1995; Espinosa and Vandewalle, 1998; Jha and He, 2002).

An Active Recognition and Adaptive Control system was proposed for the extrusion process in Guo *et al* (1993). The system comprised two interactive strategies, namely pattern analysis and adaptive control, which were developed based on the FRBS. These strategies helped the system to mimic an experienced expert in controlling the extrusion operation. However, the proposed control system lacked of proper evaluation.

Chiu and Pong (1999) developed a fuzzy gain-scheduled PID controller to control the melt viscosity by manipulating the screw speed. A second-order empirical model was identified to assist the controller design. The effectiveness of the fuzzy gain-scheduling method was compared to the Ziegler-Nichols tuning method. The performance of both

control systems was evaluated by means of experimental study and computer simulation. The results were conclusive, indicating the fuzzy gain-scheduled PID controller provided a tighter control of the melt viscosity. Chiu and Pong (2001) conducted further work to develop a complete fuzzy control system using the same coupling of process parameters. A fuzzy controller was identified to substitute the described fuzzy gain-scheduled PID controller. The authors concluded that the fuzzy controller has the capability to exploit imprecise measurements of the viscosity and generated an appropriate control action during the extrusion process.

It should be noted that the effectiveness of various types of controllers previously discussed is confined to specific locations along the extruder. To achieve a full control for a distributed parameter system such as the extrusion process, a PDEs-based control methodology is suggested (Banks, 1990; Zhang, 2002). The control methodology was demonstrated through a case study of noise control in a three-dimensional structural acoustic system (Banks *et al*, 1994). Piezoceramic patches were used as control elements, which would generate bending moments in response to the applied voltage. The system was modelled in the form of coupled PDEs, with some parameters to be identified using the experimental data. This is similar to the semi-physical model presented in previous section. The PDEs-based model was transformed to a matrix structure to obtain a feedback controller through an optimal control theory. Although this idea is very appealing, the technique of inversing the PDEs-based model is very complicated and also dedicated to the investigated acoustic system. Its application in other distributed parameter processes including the polymer extrusion is difficult to be evaluated without having detailed information.

2.6 Learning Methods

The controllers developed based on soft computing techniques require learning methods to improve the control performance. The learning methods can be classified into the direct or indirect learning category. The direct learning method tunes the controller parameters using the plant output information. As illustrated in Fig. 2-9a, the method normally requires a process model to facilitate the learning operation. Assuming that an ideal process model is available, the direct learning method is possibly described as follows (Jang and Sun, 1995):

1. calculate the gradient of cost function with respect to the controlled signal, $\partial J/\partial y$. The cost function is formulated using the controlled error, e_y;
2. calculate the gradient of the controlled signal with respect to the manipulating signal, $\partial y/\partial u$ using the process model;
3. calculate the gradient of the manipulating signal with respect to the controller parameter, $\partial u/\partial \omega$; and
4. update the controller parameter using the gradient descent algorithm given below;

$$\omega(k+1) = \omega(k) - \eta \frac{\partial J(k)}{\partial \omega(k)} \qquad (2\text{-}2)$$

where η is the learning rate, J is the cost function, y is the controlled signal, ω is the controller parameter and $\partial J/\partial \omega$ is the gradient vector obtained from the chain rule;

$$\partial J/\partial \omega = \partial J/\partial y \times \partial y/\partial u \times \partial u/\partial \omega \qquad (2\text{-}3)$$

where u is the manipulating signal.

The process model in some cases might not be available, which prohibits the calculation of the gradient information $\partial y/\partial u$. This problem has been investigated in the past and several indirect learning algorithms were developed. The algorithm proposed by Albus (1975) was referred to as a time inversion technique, which was applied to tune a Cerebellar Model Articulation Controller (CMAC) network. The algorithm proposed by Andersen *et al* (1997) was named as a Controller Output Error Method (COEM), which was used to tune a fuzzy controller. The fundamental concepts of these two algorithms were discussed in Reay (1999) and found to be similar. The tuning of the controller

parameters relies on the deviation of the manipulating signals rather than the controlled error. The concept of indirect leaning is explained as follows by use of Fig. 2-9:

In one occasion, a controller is required to drive a plant output to match a reference as closely as possible. To meet this requirement, the controller generates a manipulating signal, u, and applies to the plant. Subsequently, an output of the plant is measured as a controlled signal, y. A controlled error, e_y, exists if there is a difference between the controlled signal, y and the reference, r. A direct learning algorithm depicted in Fig. 2-9a tunes the controller parameters based on this error.

The indirect learning algorithm advances a step further. It is known that the controlled signal, y, is measured when the manipulating signal, u, is applied to the plant, in which the manipulating signal, u, is calculated based on the reference, r. The controller depicted in Fig. 2-9b is now required to reproduce a manipulating signal based on the measured controlled signal, y. It is apparent that the reproduced manipulating signal, u', will differ from the applied manipulating signal, u, if the measured controlled signal, y is varied from the reference, r. This implies that at a time when $u' \approx u$, the measured controlled signal, y would have also reached the reference, r. Therefore the proposed algorithm attempts to minimise the manipulating error, e_u ($e_u = u' - u$), which indirectly reduces the controlled error, e_y.

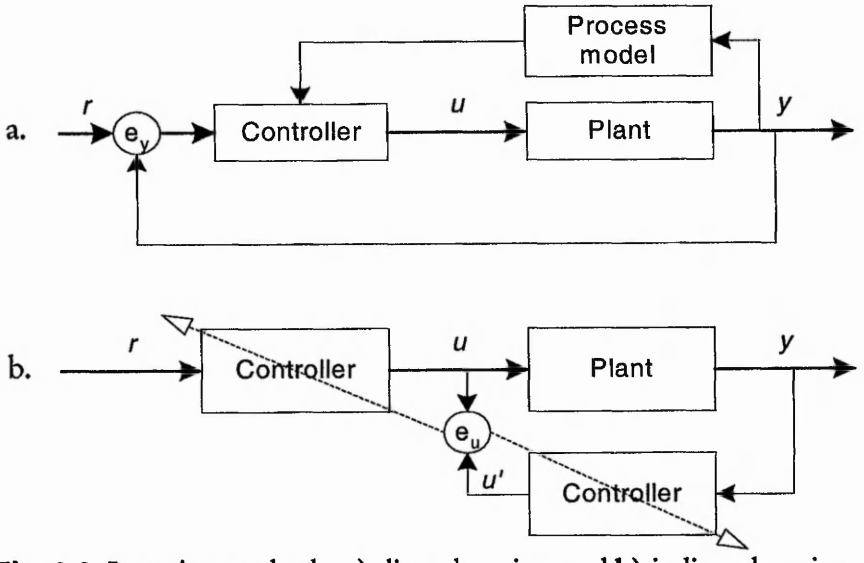

Fig. 2-9: Learning methods: **a)** direct learning, and **b)** indirect learning.

The indirect use of controlled signal in the algorithm to tune the controller parameters is referred to as "indirect learning method" in the present study (Psaltis *et al.*, 1988). Elsewhere in the literature, the applications of the indirect learning method are described. Miller *et al* (1987) designed a CMAC network to generate the required actuator torques to follow desired trajectories in robot arm applications. The indirect learning method was employed to adjust the weights in the CMAC network. The application of the similar CMAC network was also investigated by means of simulation for a hydro-mechanical system (Chan and Asokanthan, 2001). Abonyi *et al* (1997) developed a fuzzy controller to control the temperature of batch polymerisation reactors. The method was used to partially updating the fuzzy controller, where only the parameters of the rule consequents were tuned.

Some common characteristics of the indirect learning method could be realised from the above applications. These characteristics are described as follows:

1. inverse process model was not required;
2. two manipulating signals were calculated in each control cycle; one was applied to the plant, while another was only used for learning purpose; and
3. a stable controller was required before commencing the indirect learning method.

The first characteristic is particularly attractive for complicated processes, when the process model for direct learning is difficult to acquire. Characteristics two and three are the weaknesses of the indirect learning method. Calculating two manipulating signals in each control cycle are compulsory and this induces extra computational work. It is therefore desired to simplify the calculations as compensation. The indirect learning method represents only a fine-tuning algorithm. It needs a stable controller to function properly. This weakness, conversely, offers flexibility for the method to be implemented in any intelligent controller provided that it is stable (Pomares *et al*, 2001; Angelov, 2002).

2.7 Summary Remarks

Single screw extruder is the primary device that continuously melts and supplies molten polymer for different types of downstream orienting processes. It is therefore very important that the output molten polymer is of consistent conditions. During the past decades, knowledge of the melting behaviour inside the extruder has been developed through experimental observations and analytical analyses. However, most of the analyses are established based on the steady state conditions for screw design purposes.

Both theoretical and empirical modelling techniques have been attempted to develop suitable dynamic extrusion models. The development of a theoretical dynamic extrusion model has been laborious since it requires detailed knowledge of the process. Consequently, it is of no surprise to learn that most dynamic extrusion models for control applications are empirical. Although an empirical dynamic extrusion model is easier to be obtained, an extensive experimental data is often essential. This may have a cost implication, as the polymer material is not necessarily cheap. Moreover, the empirical model lacks generality. The validity is likely to be restricted to the operating regions within which the model has been identified. When both theoretical and empirical modelling techniques are combined, a semi-physical model is obtained. Many semi-physical models have been successfully employed in industrial control systems. Some common advantages include effectiveness of resource utilisation during the model identification, wide range of validity and good accuracy of predictions during the operation. The identification of a semi-physical model is case dependent. Its suitability for the single screw extrusion process will be investigated in Chapter 4.

Both analogue and digital PID controllers are commonly applied in the industrial extrusion process. Their popularity is mainly attributed to the simple implementation and the convenient of parameter tuning. Adaptive controllers are designed when conventional controllers with fixed parameters including the PID controller are found insufficient to meet demanding criteria. Self-tuning regulator, predictive controller and soft computing controller are some examples of the adaptive controllers. The predictive controller, in particular, has demonstrated its effectiveness for the MIMO complex systems. However, the approach of predictive controller in formulating an optimal control law has limited its predictive model to certain model structures. This limitation will be discussed in Chapter 5.

Chapter 3
Data Review and Signal Processing

3.1 Introduction

This chapter presents a preliminary work for the current research on dynamic modelling and intelligent control of the extruder. Data collected in the Phase 1 of research programme is reviewed here for the following purposes (Qiu, 1998):

- to examine the extrusion process behaviour and to verify the occurrences of process disturbances on the melt pressure and the melt temperature;
- to propose appropriate signal-conditioning methods.

In the Phase 1 of research programme, the data was interpreted from the perspective of screw design. Mean values of measurements with respect to screw geometries were calculated to obtain melt pressure profiles, barrel temperature profiles and screw temperature profiles. These profiles were useful to evaluate the performance of the extruder with respect to different screw designs. From the perspective of control system design, the profile information is not sufficient. It is more important that the inconsistency of the melt condition could be investigated. The variations in the measured signals, which indicate the inconsistencies of melt condition, are therefore analysed in this chapter.

The melt pressure and the melt temperature data of High Density Polyethylene (HDPE), Medium Density Polyethylene (MDPE) and Linear Low Density Polyethylene (LLDPE) polymers are reviewed. The properties of these polymers are specified in Appendix 1. For the convenient of presentation, the graphs obtained by data interpolation are shown but experimental data points are indicated where appropriate. To make the thesis self-contained, it is considered prudent to provide a brief description on the specifications of the in-house extruder (Francis Shaw, 1971). The operating ranges and locations of each physical part including the motor, the heating/ cooling units, the pressure transducers and the thermocouples are described in the following section.

3.2 In-house Extruder

The in-house extruder, MK 3 thermatic extruder with a 63.5 mm diameter barrel, is illustrated in Fig. 3-1. The barrel is cylindrical and it is of bimetal construction with the interior being made of wear resistant alloy. This construction provides the barrel with strength to withstand the working pressure up to 70 MPa. Inside the barrel is a standard screw of 63.3 mm diameter with 25.5:1 screw length-to-diameter ratio. It is made of alloy steel with the flight tips harden to reduce wear.

During the operation, the screw is driven by a 30 kW DC motor located at the beginning of the extruder. A poly-phase tachogenerator is installed to measure the rotational speed of the screw. By adjusting the voltage supply to the motor, the screw may rotate at any speed from virtually zero to over 140 rpm. Five heating/cooling units are installed at five zones along the barrel to control the barrel temperature. Each heating/cooling unit consists of a tubular resistance heater, a liquid-cooling system and an electric fan. The heater is made of cast aluminium with a heating capacity of 5 kW. This allows settings of the barrel temperature to a maximum of 400°C. The cooling units include a liquid-cooling system and electric fans. The liquid-cooling system is activated only in the crash-cooling operation to acquire information of solid bed deformation. In any event the barrel requires cooling during the normal operation, electric fans are activated. The air-cooling capacity at each zone may achieve a maximum of 17 m^3/min. However, it is remarked that an efficient melt temperature control should achieve without the cooling operation, as it implies energy lost. The screw speed and the barrel temperature are two parameters that affect the extrusion melting conditions. They are regarded as the manipulating parameters in the extrusion.

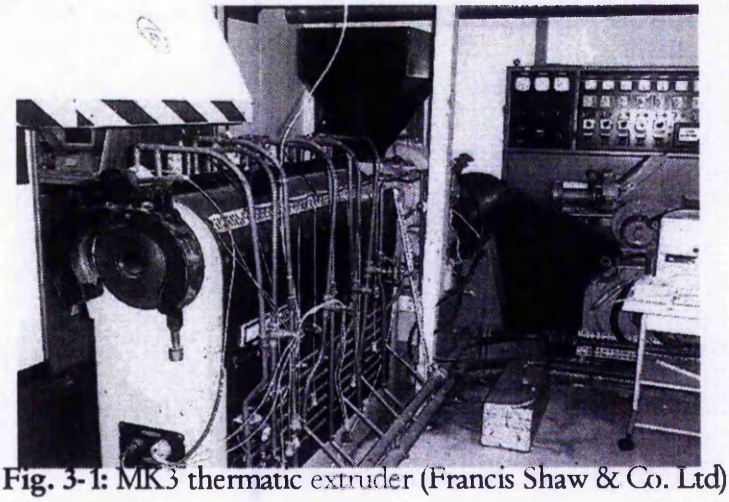

Fig. 3-1: MK3 thermatic extruder (Francis Shaw & Co. Ltd).

Pressure transducers (models 0120[2] and PT420A[3]) and thermocouples (J type) are installed to measure the melt pressure and the melt temperature respectively. The barrel is fitted with eleven pressure transducers and five thermocouples at different locations. In Fig. 3-2, the pressure transducers and the thermocouples are designated as PB and TB respectively. The screw is also equipped with nine thermocouples designated as TS at the positions depicted in Fig. 3-3. The pressure transducers are capable of measuring the melt pressure to a maximum of 34.5 MPa under normal working conditions. The pressure is converted to a proportional voltage output signal using bonded strain gauge principles. The transducers require an excitation voltage ranging from 6 to 12 V to produce a sensitivity of 3.3 mV/V. The thermocouples operate based on thermoelectric effect, in which an electromotive force is developed when two different metals are subjected to different temperature at the jointed ends. The working temperature range of the measuring junction is approximately 20 °C to 700 °C. The melt pressure and the melt temperature are measured to estimate the quality of the product. They are referred to as the controlled parameters.

The signals from the pressure transducers and the thermocouples require proper signal conditioning to enable accurate and convenient means of data logging. The voltage output signals of the pressure transducers in mV range are amplified using a DC amplifier, model FE.359.TA[4], to a range of 1 to 10 V. The amplified analogue signals are then converted to digital signals by a 12 bits analogue-to-digital converter, model PC26AT[5]. A software program named *Unimas*[6] is installed to a computer to record the pressure data automatically from all the pressure transducers. The program allows a range of 1 to 20 samples to be taken in every second for each transducer. The melt temperature measured by fourteen thermocouples (five at barrel and nine at screw) are connected to a C9001 thermometer[7] through a twenty channels selector unit[8]. The output signals of different individual thermocouple are then selected, read and recorded

---

[2] Manufactured by Industrial Sensors Incorporated (ISI), England.

[3] Manufactured by Dynisco (UK) Limited, England.

[4] Manufactured by FYLDE Electronic Laboratories Ltd., England

[5] Manufactured by Amplicon Liveline Limited, England

[6] Produced by Marandy Computers Ltd., England

[7] Manufactured by KM. Comark test & measurement, England

[8] Manufactured by Comark Electronic Ltd., England.

manually. The built-in signal conditioning function of the thermometer provides digital output signals with 0.1 °C resolution and response time of 1 second to full accuracy.

3.3 Review of Melt Pressure Data

This section reviews the melt pressure data of HDPE, MDPE and LLDPE polymers. The pressure signals were recorded at the interval of 0.1 second. In Fig. 3-4, the distributions of the mean pressure along the extruder are found to be similar for these three polymers. The melting mechanism starts in the feed section at the axial location of 0.3 m from the hopper. When the melt enters the compression section, the pressure increases rapidly until a maximum pressure is reached at the end of the compression section, which is approximately at 1.0 m axial location. After passing the peak, the melt pressure decreases gradually in the metering section. This behaviour of the melt pressure with respect to the screw geometry is termed as the pressure profile.

To investigate the pressure disturbances, the pressure signal collected from the pressure transducer designated as PB0 shown in Fig. 3-2 is analysed. The location of the transducer is nearest to the die exit, hence is the most appropriate indication to the dimensional accuracy of the end product. The variations in the melt pressure for two polymers are shown in Fig. 3-5 at the time scale of 10 seconds. The solid lines represent the pressure measurements of the HDPE polymer while the dotted lines represent the pressure measurements of the MDPE polymer. The polymers were processed at the screw speeds of 30 rpm, 60 rpm and 90 rpm depicted in Fig. 3-5a, Fig. 3-5b and Fig. 3-5c respectively. It is observed that the pressure fluctuates at the same frequencies as the screw rotational speeds. The cyclic interval is 2 seconds (0.5 Hz) for 30 rpm, 1 second (1 Hz) for 60 rpm, and 0.7 second (1.4 Hz) for 90 rpm screw speeds. These variations are regarded in the literature as high frequency disturbances (Tadmor and Klein, 1970; Costin *et al*, 1982). The disturbances are mainly due to the periodical interference of the screw flight on the operation of the pressure transducer. Quite often, the disturbances are also referred to as "flight noises".

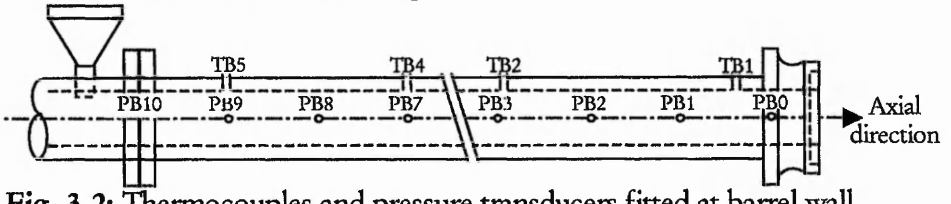

Fig. 3-2: Thermocouples and pressure transducers fitted at barrel wall.

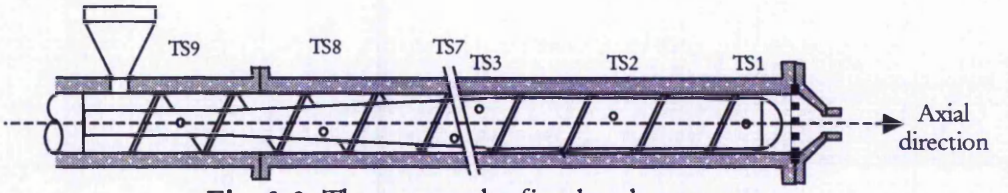

Fig. 3-3: Thermocouples fitted at the screw.

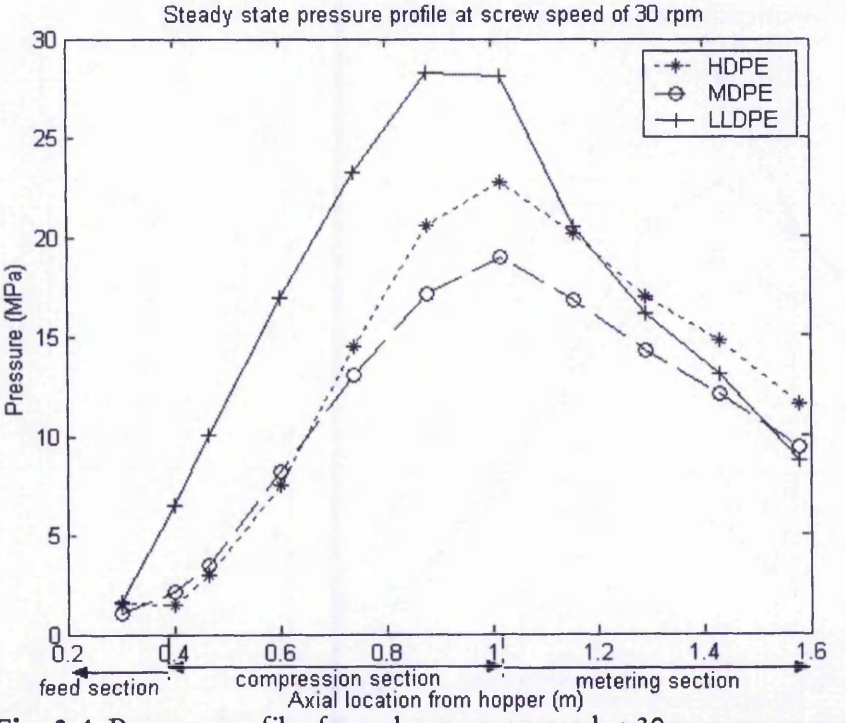

Fig. 3-4: Pressure profiles for polymers processed at 30 rpm screw speed.

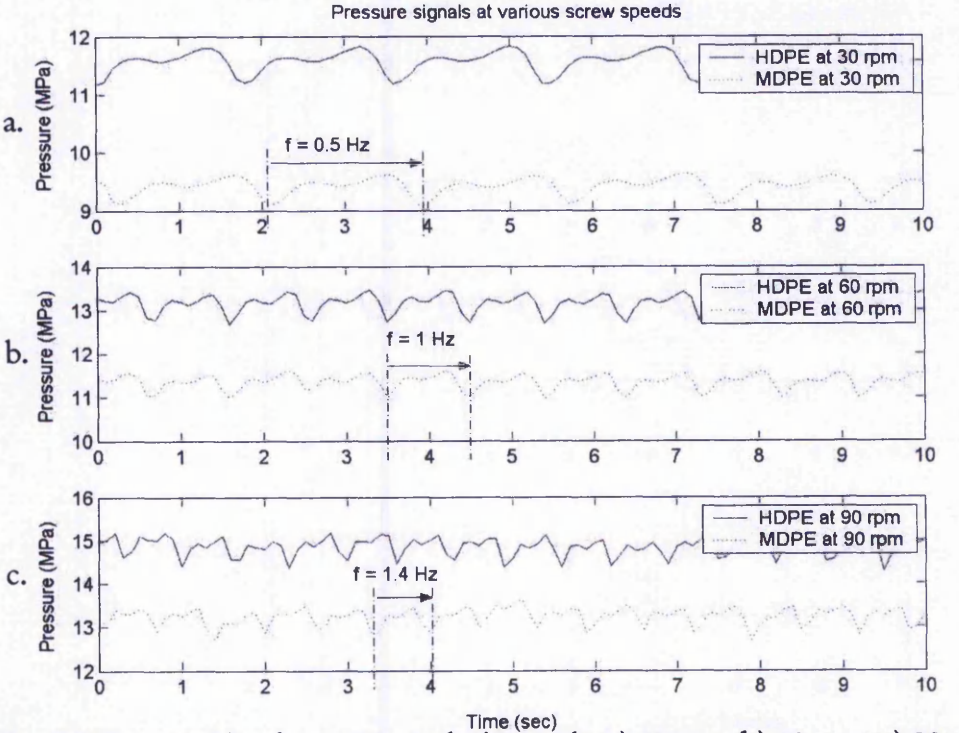

Fig. 3-5: Pressure signals at 10 seconds time scale: **a)** 30 rpm, **b)** 60 rpm, **c)** 90 rpm.

The hypothesis for the occurrence of the flight noises could be described by use of Fig. 3-6. For the sake of explanation, the surface of the screw flight in the same direction as the screw motion is named as an advancing flight while the opposite direction is a trailing flight. The pressure transducer is stationary and the screw flight passes the tip of the transducer periodically. At the time when the trailing flight has just passed the tip of the transducer, a low melt pressure is measured (Fig. 3-6a). Thereafter, the pressure is gradually built as the melt in the screw channel is being pushed by the advancing flight (Fig. 3-6b). A high melt pressure is measured when the advancing flight reaches the position just before the tip of the transducer (Fig. 3-6c). Once the screw flight passes the transducer, the pressure drops instantly and the cycle is repeated.

The data representation in the frequency domain depicted in Fig. 3-7 could further prove the occurrence of the flight noises. The time-to-frequency transformation is achieved using Fast Fourier Transformation (FFT) algorithm by assuming that the 'windowed' signal has reached its steady state conditions (Denbigh, 1998). The signal frequencies in Power Spectrum Density (PSD) signify that the melt pressure of HDPE polymer contains major components at around 0.5 Hz for the screw speed of 30 rpm (Fig. 3-7a), 1 Hz at 60 rpm (Fig. 3-7b), and 1.5Hz at 90 rpm (Fig. 3-7c). The frequencies of the disturbances and the screw speeds are coincident.

The existence of flight noises in the measurements might affect the performance of the control system. Therefore, a low pass filter is suggested as a signal-conditioning approach to filter out the effect of flight noises in the pressure measurements.

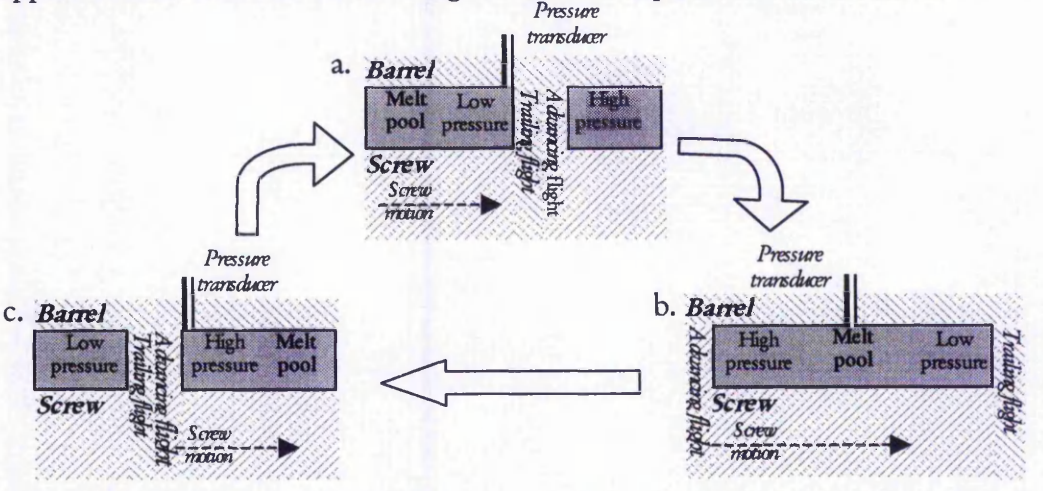

Fig. 3-6: A complete cycle of flight noises: **a)** after trailing flight, **b)** middle of channel, and **c)** upon advancing flight.

Examples of the low pass filtered pressure signals for HDPE polymer are represented as solid lines in Fig. 3-8 for different screw speeds. The filtered pressure signals are observed fluctuating at lower frequencies in comparison with the unfiltered pressure signals represented as dotted lines. This indicates that the impact of flight noises has been reduced.

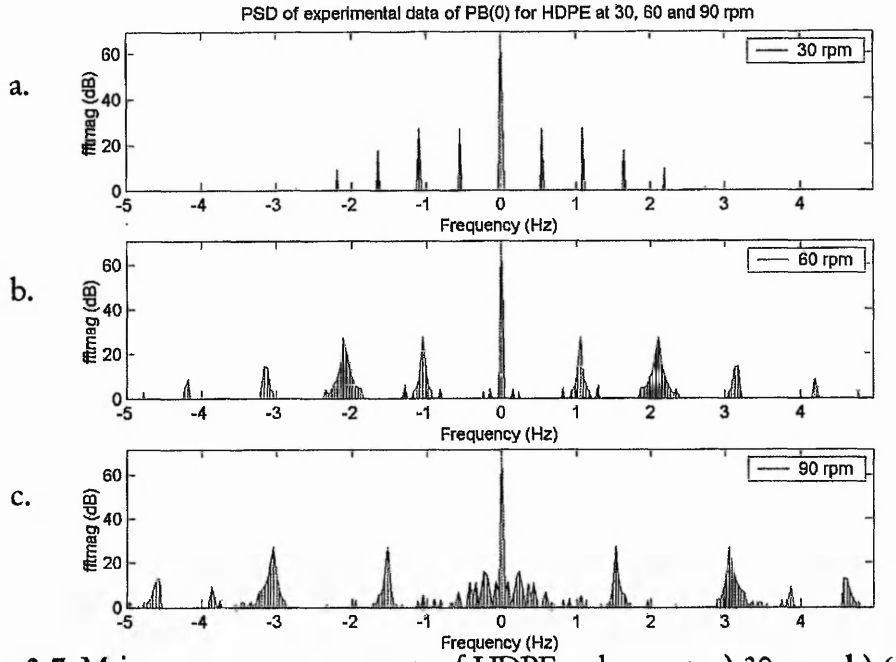

Fig. 3-7: Major spectrum components of HDPE polymer at: **a)** 30 rpm, **b)** 60 rpm, and **c)** 90 rpm screw speeds.

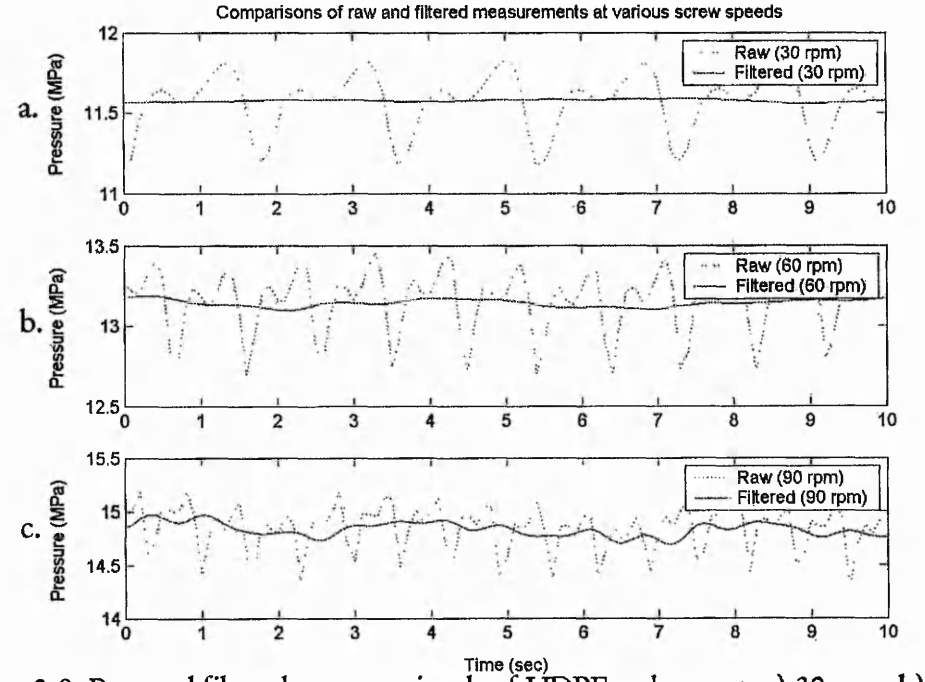

Fig. 3-8: Raw and filtered pressure signals of HDPE polymer at: **a)** 30 rpm, **b)** 60 rpm, **c)** 90 rpm screw speeds.

The variations in the pressure signals at the lower frequencies shown in Fig. 3-8 are the impact of intermediate and low frequency disturbances. It is difficult to determine the exact frequency ranges of these two disturbances. Roughly, the intermediate frequency disturbances for the HDPE melt pressure in the study are ranged from 0.17 to 0.25 Hz. Table 3-1 indicates that the amplitude and the standard deviation of the disturbances are reliant upon the screw speed. The disturbances are more significant if the screw rotates at a higher speed. A similar result was also reported in Costin *et al*, (1982a). It is widely accepted that the disturbances are mainly ascribed to the breaking-up of the solid bed during the melting process (Tadmor and Klein, 1970; Rauwendaal, 1986; Wong *et al*, 1998). The solid bed begins to break randomly at a point when its bonding strength is weaker than the shear strength induced by the relative motion of the rotating screw and the stationary barrel. The broken solid particles float at different speeds within the melt, causing irregular melt pressure measured by the transducer. In a higher screw speed, the magnitude of pressure irregularity is larger. Another possible reason is that when the solid bed breaks-up, the air entrapped within the solid bed is released as bubbles. The mixture of broken solid bed, melt and bubbles in the screw channel could be a reason for the pressure irregularity.

To observe the impact of low frequency disturbances in the melt pressure data, the time scale of same filtered data shown in Fig. 3-8 is contracted from 10 seconds to 300 seconds. The solid lines in Fig. 3-9 indicate that the fluctuations of the melt pressure are non-periodical. The occurrences of the low frequency disturbances are independent of the screw speed but usually affected by the inconsistency of external conditions. The instability of power supply, the variations in the ambient humidity and the properties of processing polymers are examples of inconsistency of external conditions (Medora and Kusko, 1995).

The HDPE melt pressure in response to the changes in screw speed is shown in Fig. 3-10. The data is filtered after 100 seconds to reduce the flight noises. The screw speed is changed from 30 rpm to 60 rpm at a time of 1000 seconds, and from 60 rpm to 90 rpm at 2700 seconds. When the screw speed increases, the melt pressure rises rapidly with a noticeable overshoot. This response suggests that additional quantity of melt has been delivered quickly and compressed in the die cavity. Then, the pressure decays to a new steady state value when the melt exits through the die. The figure also indicates that

as the screw rotates at higher speeds, the pressure fluctuations are more obvious due to the greater disturbances occur at intermediate frequencies. Similar observations on both the transient and the steady state responses are depicted in Fig. 3-11, when the MDPE polymer is processed. The steady state response of the MDPE melt pressure, in addition, contains several intervals of abrupt fluctuations. The fluctuations might be caused by the faulty readings of the pressure transducer.

Table 3-1: Intermediate and low frequency disturbances for different polymers.

Characteristics	HDPE	MDPE	LLDPE
Amplitude (MPa):			
30 rpm:	0.0246	0.0435	0.0442
60 rpm:	0.0776	0.1699	N/A
90 rpm:	0.3257	0.4457	N/A
Standard deviation (MPa)			
30 rpm:	0.0080	0.0109	0.0091
60 rpm:	0.0229	0.0332	N/A
90 rpm:	0.0661	0.0975	N/A

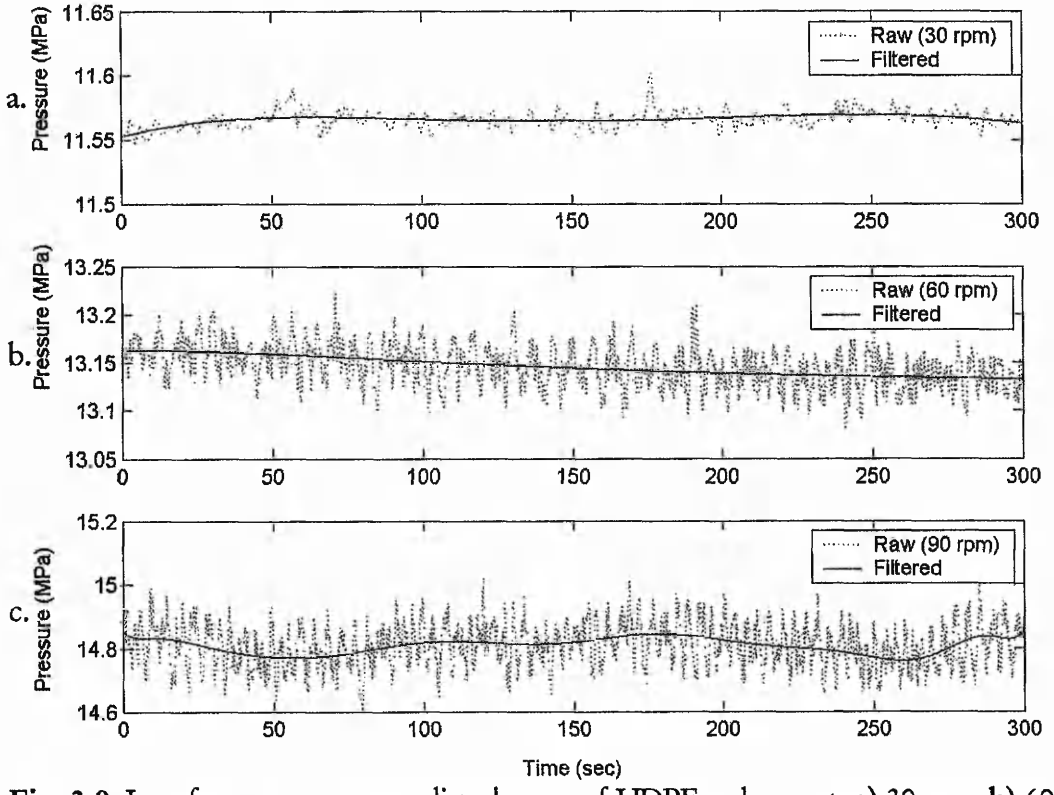

Fig. 3-9: Low frequency pressure disturbances of HDPE polymer at: **a)** 30 rpm, **b)** 60 rpm, **c)** 90 rpm screw speeds.

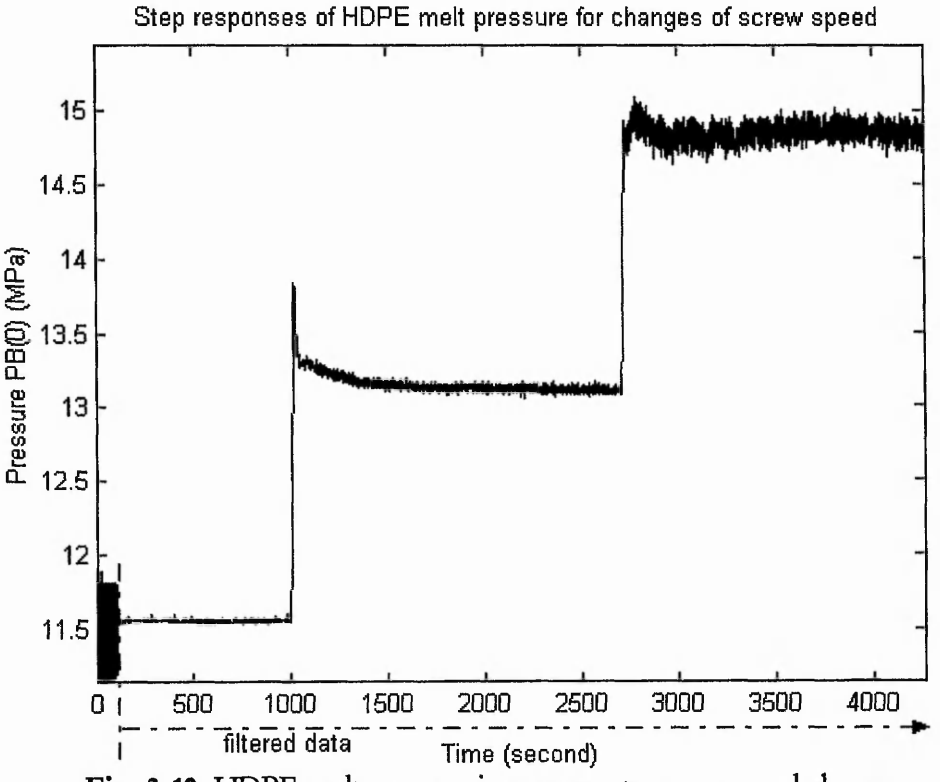

Fig. 3-10: HDPE melt pressure in response to screw speed changes.

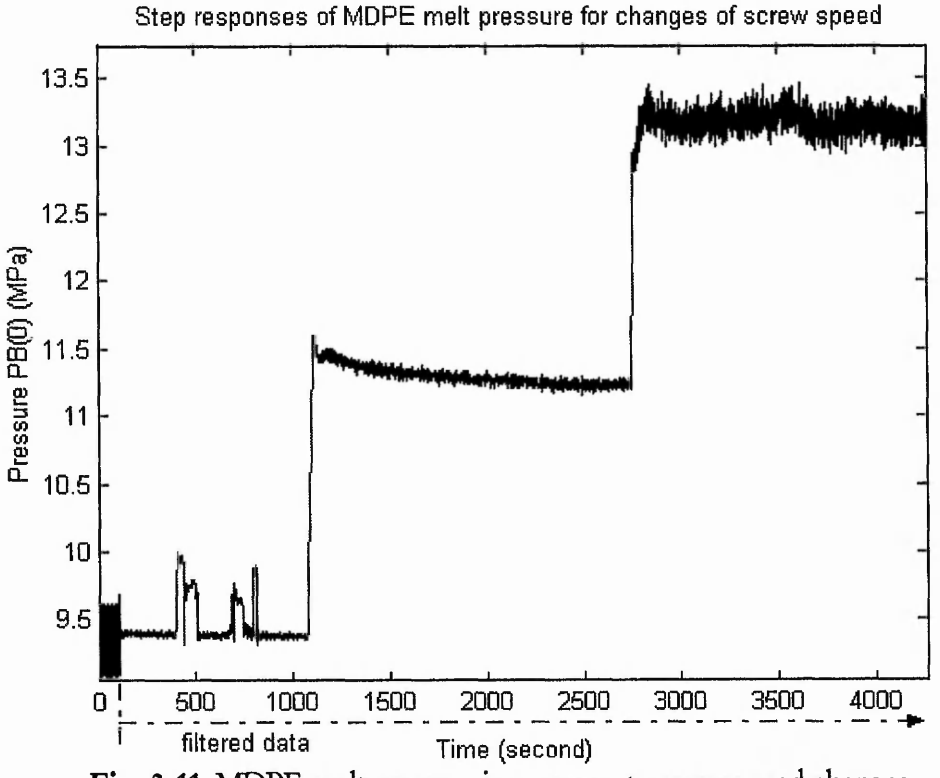

Fig. 3-11: MDPE melt pressure in response to screw speed changes.

3.4 Review of Melt Temperature Data

This section reviews and analyses the melt temperature data of HDPE and MDPE polymers. The temperature measurements along the extruder were recorded at 5 minutes interval, with fourteen measurements at each interval. The screw and the barrel temperature profiles of the HDPE polymer melt are depicted in Fig. 3-12. The solid lines denote the screw temperature profiles (T_{scr}) while the dotted lines represent the barrel temperature profiles (T_{bar}). Large differences are observed between the screw temperature measurements and the barrel temperature measurements at the beginning of compression section. Thereafter, the screw temperature increases rapidly until meeting the barrel temperature. The screw temperature exceeds the barrel temperature at the beginning of metering section and continues to rise slowly. The melting mechanism that leads to these temperature profiles has been explained in Section 2.3 of Chapter 2. The barrel temperature profiles exhibit a steadier behaviour. The barrel temperature remains at the preset value in the compression section, and slightly increases when approaching the end of the metering section. Similar screw and barrel temperature profiles are observed in Fig. 3-13 for the MDPE polymer.

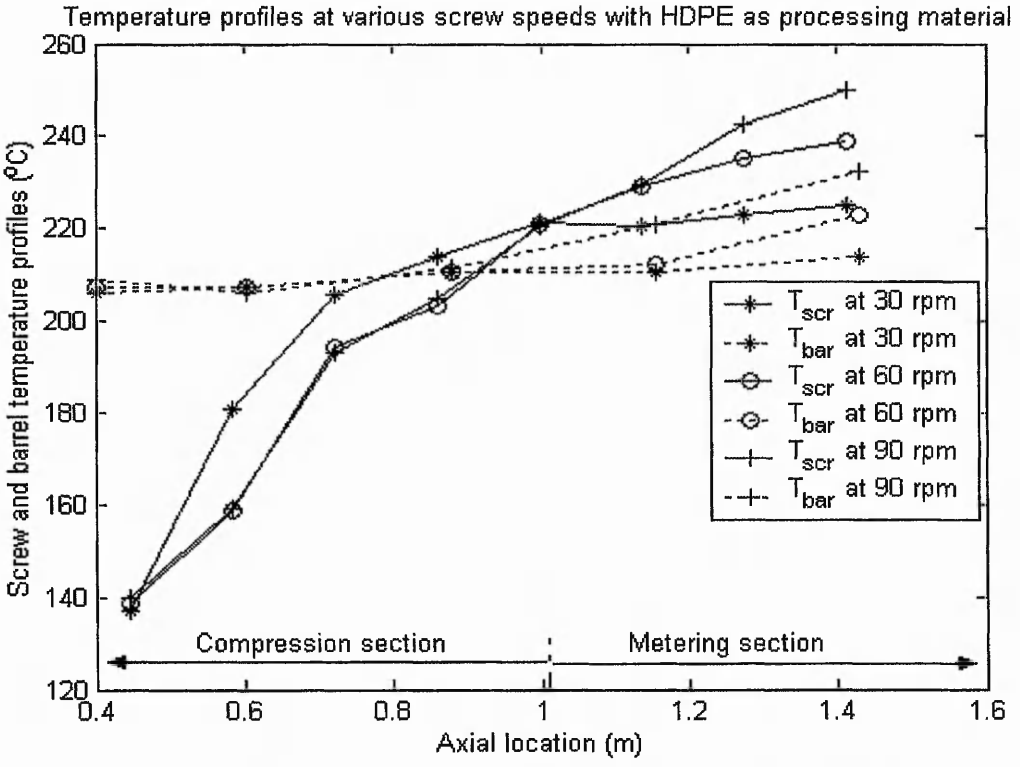

Fig. 3-12: Screw and barrel temperature profiles for HDPE polymer.

The impact of the screw speeds on the melt temperature is also depicted in Fig. 3-12 and Fig. 3-13. The lines marked with asterisk (*), circle (o) and cross (+) represent the screw speeds at 30, 60 and 90 rpm respectively. At the beginning of the compression section, a higher screw speed induces a lower rising rate in the screw temperature. The high screw speed in general would shorten the residence time of the polymer inside the extruder. Therefore, the surface of the polymer particles in conta- might have insufficient time to acquire necessary amount of con the melting point. The forming of a thin melt film, which is nece- by viscous dissipation, might have been delayed and this might h screw temperature rising rate. Beyond the point when melti temperature increases at a higher rate for a higher screw speed, sl Fig. 3-13 at locations between 0.6 and 1.0 m. When the polymer s screw speed results a more intensive melt film-shearing activi generated by the viscous dissipation. At the end of metering secti- the screw temperature stays higher for a faster screw speed. When the polymer is fully melted, more excessive heat energy is generated if the screw is rotating faster. Therefore, both of the barrel temperature and the screw temperature remain high.

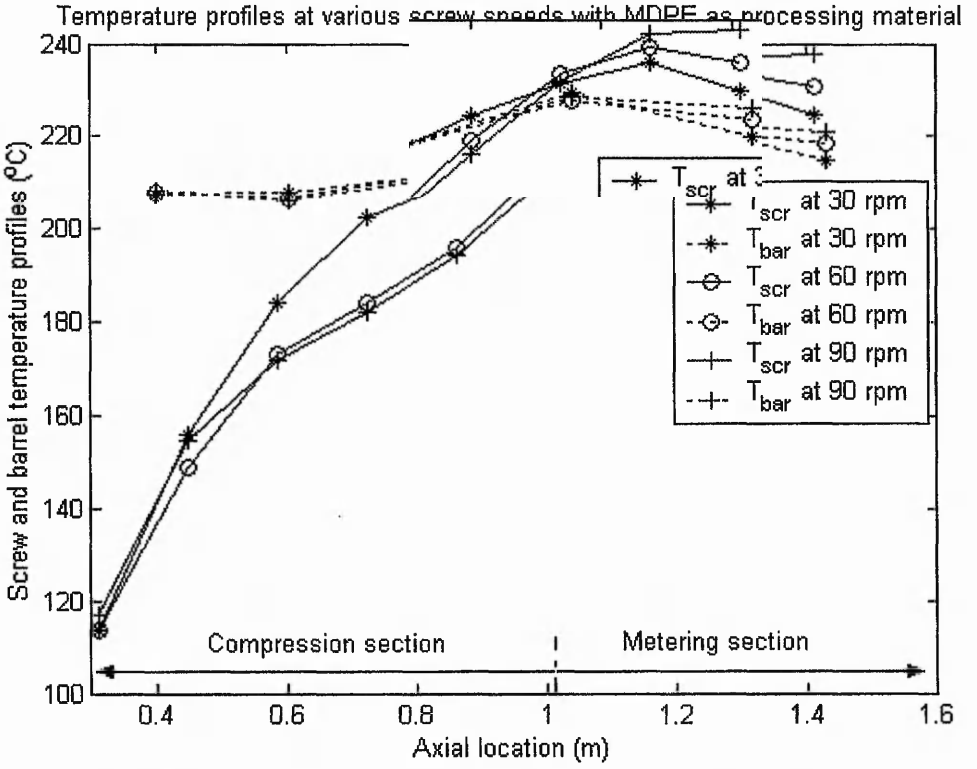

Fig. 3-13: Screw and barrel temperature profiles for MDPE polymer.

The analysis of the melt temperature disturbances is limited by the data available. The screw and barrel temperature signals for the HDPE polymer measured by the thermocouples near the die are shown in Fig. 3-14. The signals might enclose only the low frequency disturbances because the 300 seconds sampling interval is far beyond the range of high and intermediate frequencies. Both screw temperature and barrel temperature increase with the screw speed. It is found that the temperature signals vary even when the screw speed remains constant. This signifies the occurrence of the low frequency disturbances. Similar results are observed in Fig. 3-15 for the MDPE polymer.

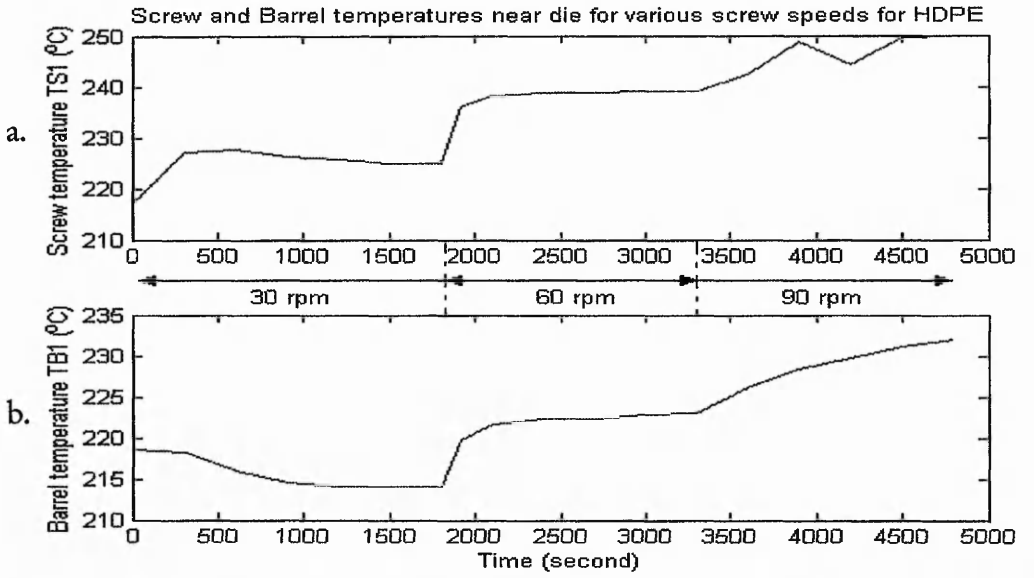

Fig. 3-14: Temperature signals at the die for HDPE polymer: **a)** screw temperature, and **b)** barrel temperature.

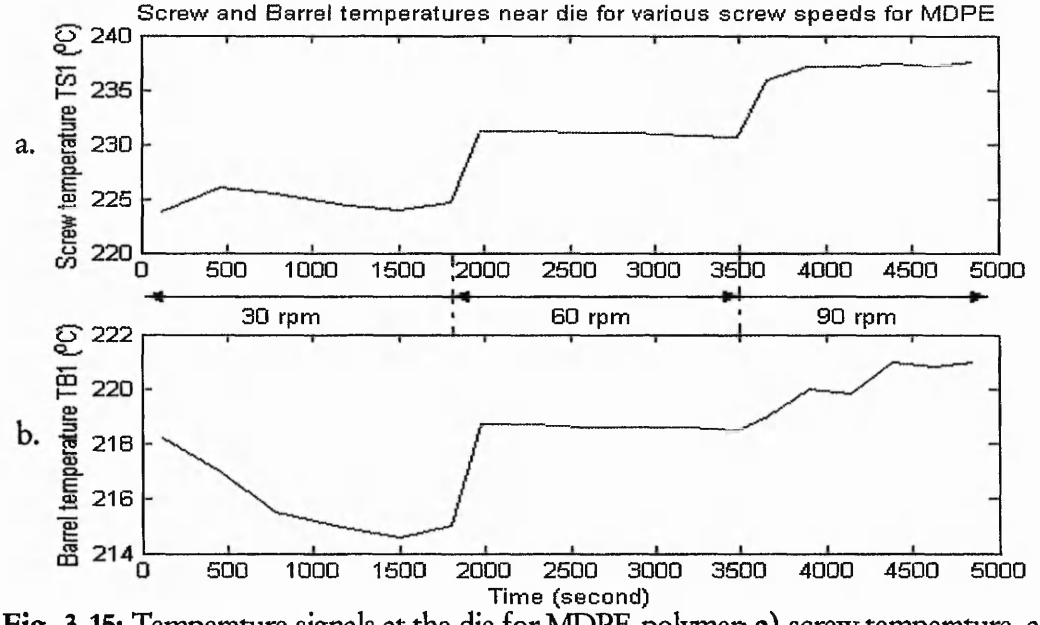

Fig. 3-15: Temperature signals at the die for MDPE polymer: **a)** screw temperature, and **b)** barrel temperature.

3.5 Filtering High Frequency Disturbances

The high frequency disturbances (flight noises) in the data have been recognised as the technical faulty readings due to the interference of the screw flight. A low pass filter is suggested to reduce the noises and this has been shown in Fig. 3-8 to be effective. In this section, the performance of two filters is studied using the pressure data of HDPE polymer at the screw speed of 30 rpm. The filter with better performance is then further discussed in aspects of filter realisation and functional stability.

The common requirements for the filters are high attenuation in the stopband, high roll-off rate and low ripple in the passband. A number of digital filter designs have been investigated under MATLAB environment to meet the above requirements. Two examples of the filters, namely an Elliptic filter and a Butterworth filter are selected to evaluate their performance here. The eighth-order Elliptic low pass filter, with the specifications of 0.01 dB allowable ripple at the passband and a minimum stopband attenuation of 50 dB, is designed with 0.4 Hz cut-off frequency for the screw speed of 30 rpm. The cut-off frequency is obtained based on the results of the data analysis shown in Fig. 3-7. The Butterworth low pass filter is also designed with the same specifications for the performance comparison.

The results indicate that the output signal of the Elliptic filter in Fig. 3-16a fluctuates at a lower frequency in comparison to the output signal of the Butterworth filter in Fig. 3-16b. The Power Spectrum Densities (PSDs) of both filtered signals are depicted in Fig. 3-16c and Fig. 3-16d separately. It is evident that the Elliptic filtered signal (Fig. 3-16c) is clear of the high frequency component caused by the flight noises, in comparison with the result achieved by the Butterworth filter (Fig. 3-16d). The frequency responses of both filters are shown in Fig. 3-17. Having the same order for both filters, the Elliptic filter provides a higher roll-off rate as shown in Fig. 3-17a. Consequently, it is more efficient in reducing the signals with unwanted frequencies without affecting the amplitude of the desired signal. The phase responses of both filters in Fig. 3-17b are similar within the cut-off frequency of 0.4 Hz. The design of the Elliptic filter which shows a better performance will be elaborated in the following paragraphs.

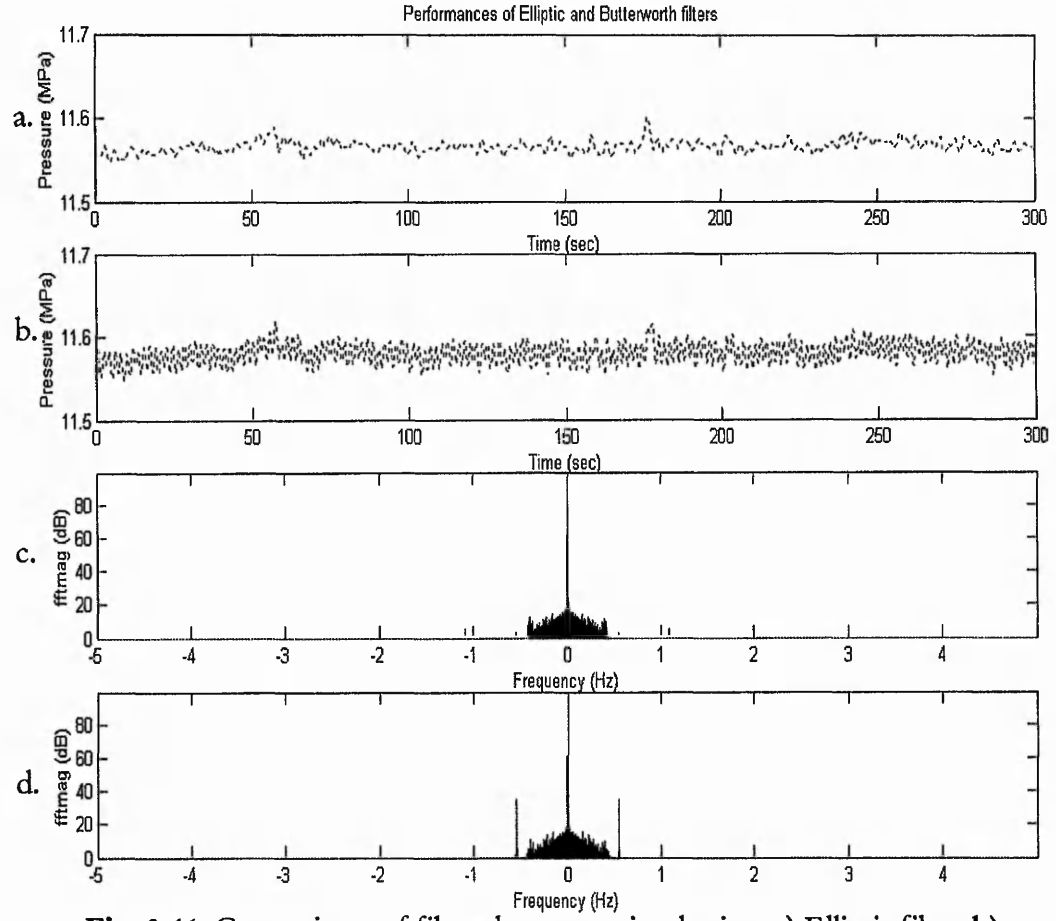

Fig. 3-16: Comparisons of filtered pressure signal using: **a)** Elliptic filter, **b)** Butterworth filter, and PSD of **c)** Elliptic filter, **d)** Butterworth filter.

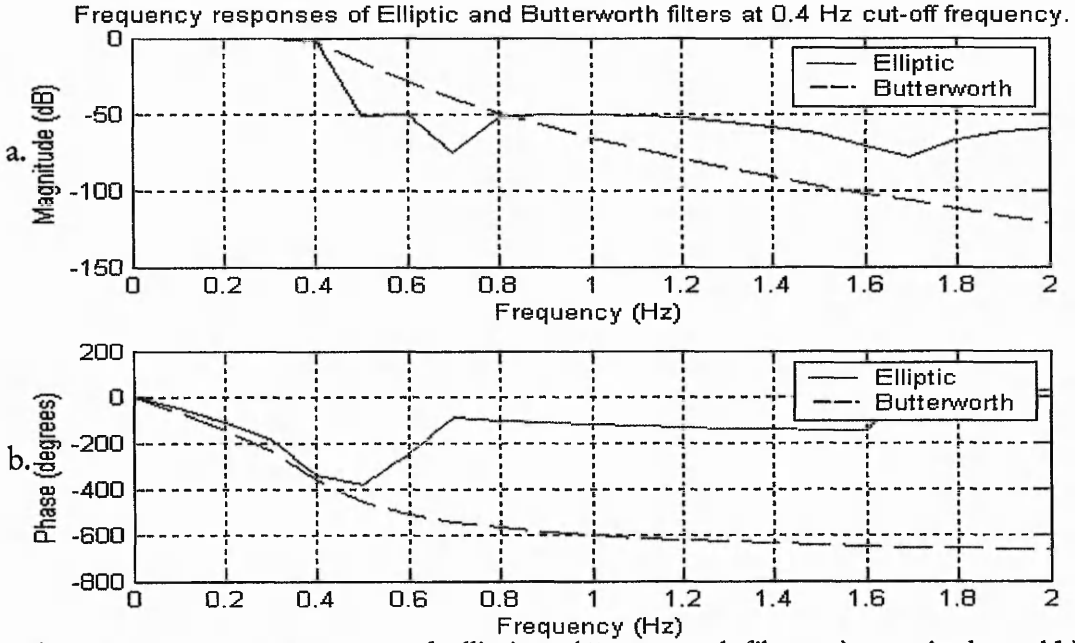

Fig. 3-17: Frequency responses of Elliptic and Butterworth filters: **a)** magnitude, and **b)** phase.

The function of the eighth-order Elliptic filter, $H(z)$, is expressed below:

$$H(z)=\frac{0.0033-0.0219z^{-1}+0.0665z^{-2}-0.1220z^{-3}+0.1480z^{-4}-0.1220z^{-5}+0.0665z^{-6}-0.0219z^{-7}+0.0033z^{-8}}{1-7.2524z^{-1}+23.1686z^{-2}-42.5694z^{-3}+49.1904z^{-4}-36.5978z^{-5}+17.1177z^{-6}-4.6012z^{-7}+0.5441z^{-8}} \quad \textbf{(3-1)}$$

To realise a digital filter, the coefficients of the filter function need to be converted into n-bit binary words. The conversion may introduce inaccuracy of coefficient representation, depending on the rounding-off condition of the coefficient and the resolution of the coding operation. The accuracy deteriorates especially for a higher-order filter, which may subsequently cause instability of the filter operation.

As a remedy, the high-order filter is reconstructed by cascading a sequence of second-order filters. The reconstruction is accomplished using a command **zp2sos** under the MATLAB environment. The filter function, $H(z)$, in Equation (3-1) is optimally broken down into a cascade of second-order functions, $H_{1,2,3,4}(z)$, written as:

$$H(z)=H_1(z)\times H_2(z)\times H_3(z)\times H_4(z) \quad \textbf{(3-2)}$$

where:

$$H_1(z)=\frac{0.003-0.003z^{-1}+0.003z^{-2}}{1.000-1.691z^{-1}+0.720z^{-2}} \qquad H_2(z)=\frac{1.000-1.813z^{-1}+1.000z^{-2}}{1.000-1.784z^{-1}+0.831z^{-2}}$$

$$H_3(z)=\frac{1.000-1.893z^{-1}+1.000z^{-2}}{1.000-1.865z^{-1}+0.927z^{-2}} \qquad H_4(z)=\frac{1.000-1.911z^{-1}+1.000z^{-2}}{1.000-1.912z^{-1}+0.980z^{-2}}$$

A total of four second-order functions are cascaded to approximate the eighth-order filter function. The diagram of the cascaded Elliptic filter is illustrated in Fig. 3-18.

Two methods, namely z-plane and impulse response estimation, are adopted to analyse the stability of the cascaded Elliptic filters with 0.4, 0.9 and 1.4 Hz cut-off frequencies. The cascaded filters are found to be stable, since all poles and zeros of each filter are located within each unit circle shown in Fig. 3-19, Fig. 3-20 and Fig. 3-21. The results of the impulse response estimation further confirm the stability of the filters, as decaying responses are observed in Fig. 3-22, Fig. 3-23 and Fig. 3-24.

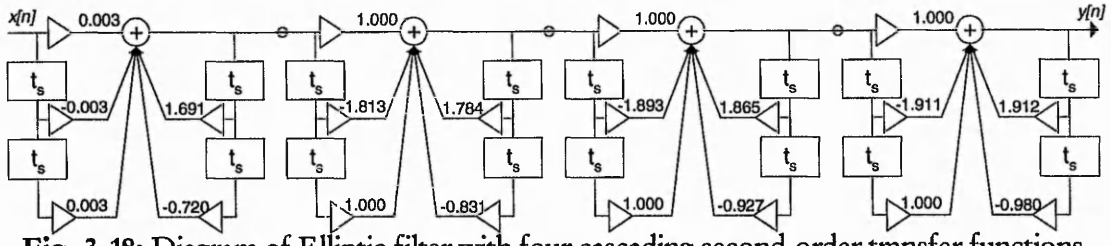

Fig. 3-18: Diagram of Elliptic filter with four cascading second-order transfer functions.

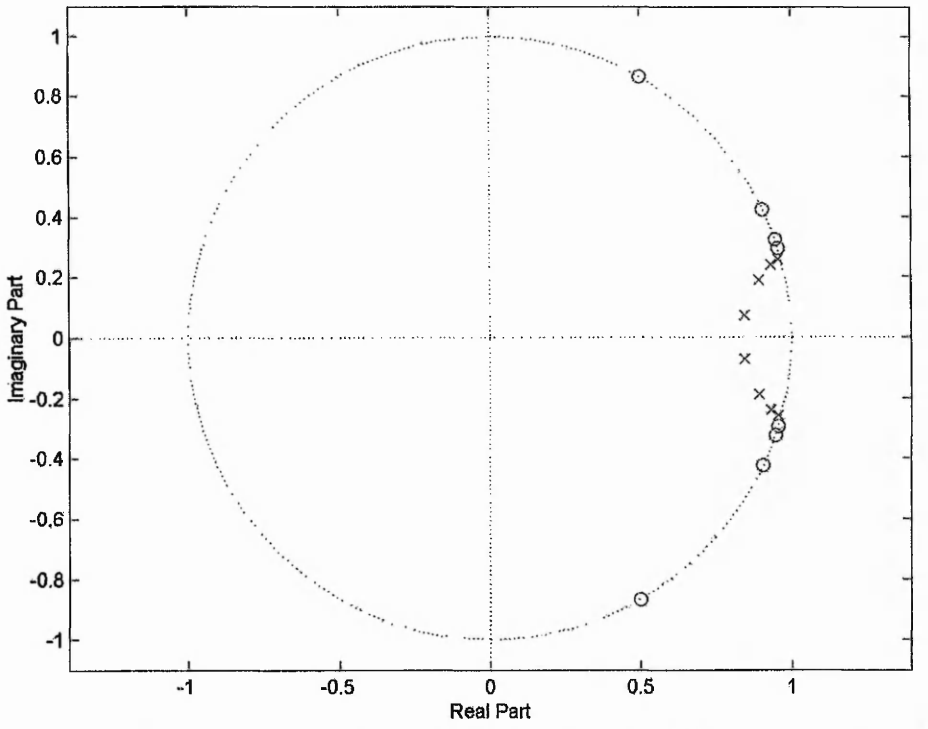

Fig. 3-19: Locations of poles-zeros of Elliptic filter (0.4 Hz cut-off frequency).

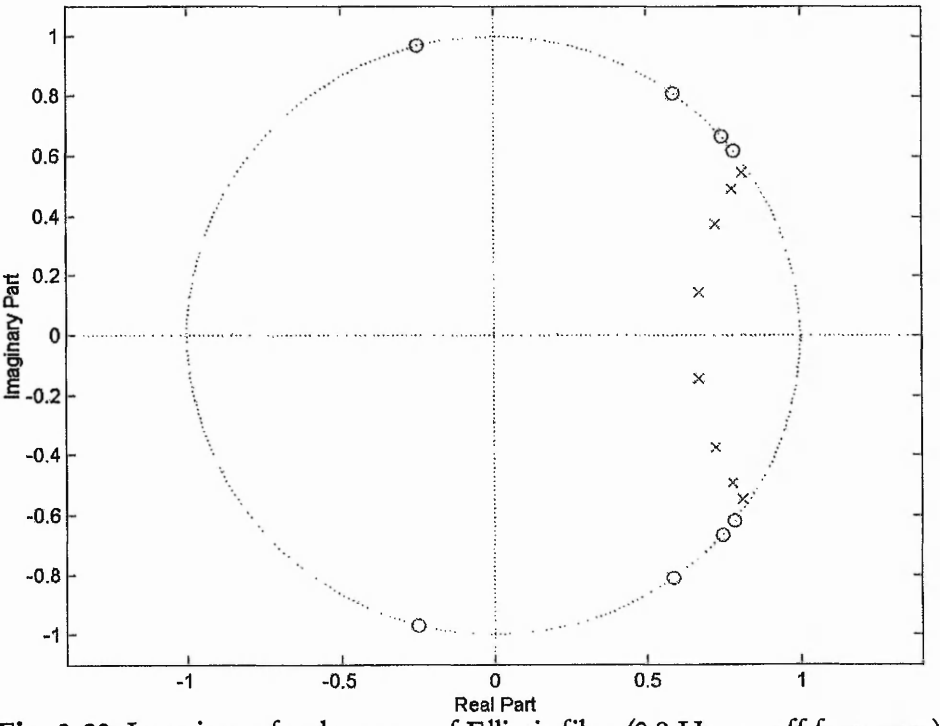

Fig. 3-20: Locations of poles-zeros of Elliptic filter (0.9 Hz cut-off frequency).

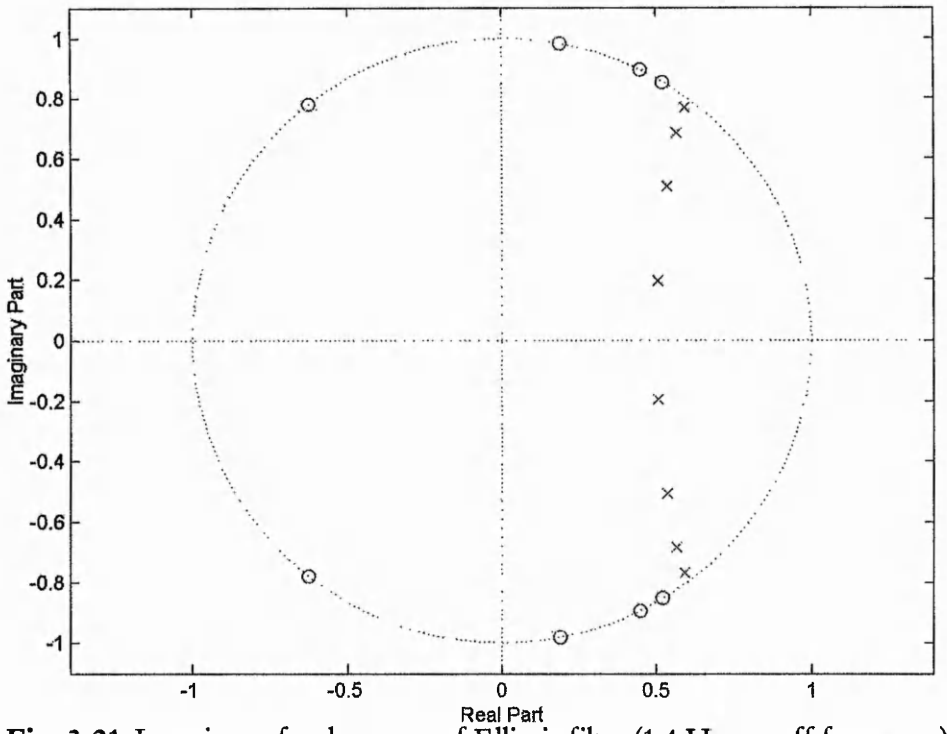

Fig. 3-21: Locations of poles-zeros of Elliptic filter (1.4 Hz cut-off frequency).

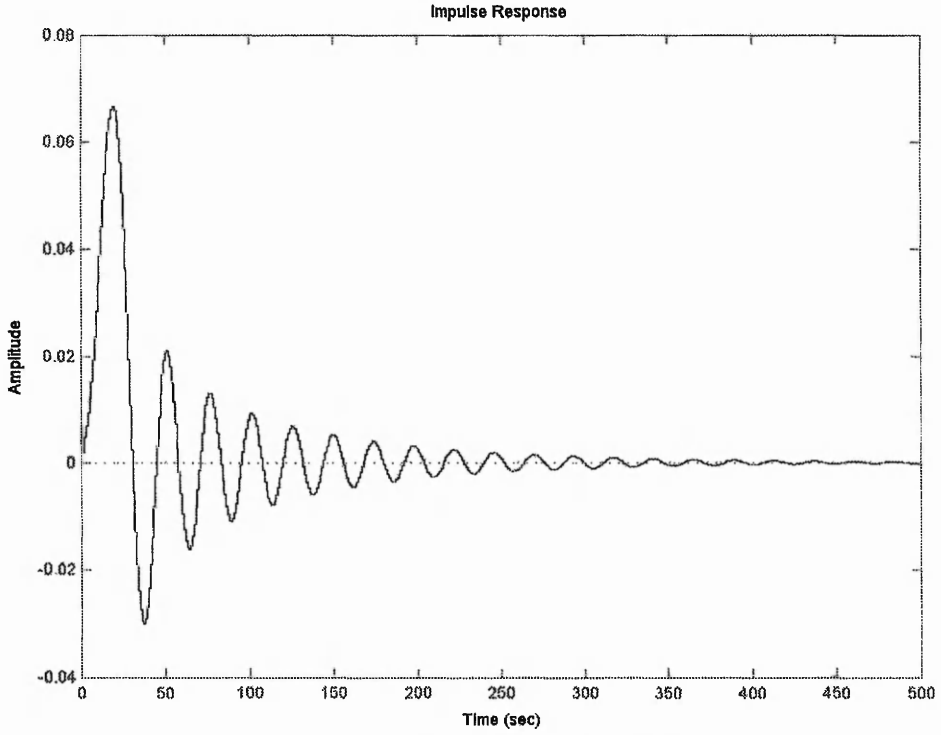

Fig. 3-22: Impulse response of Elliptic filter (0.4 Hz cut-off frequency).

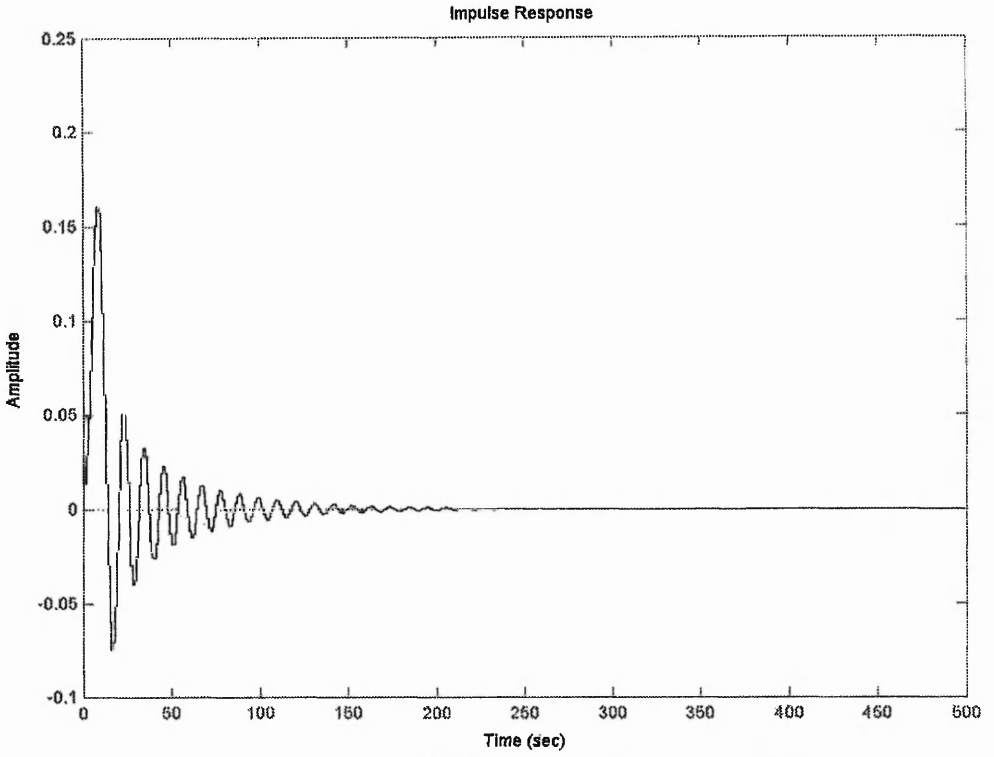

Fig. 3-23: Impulse response of Elliptic filter (0.9 Hz cut-off frequency).

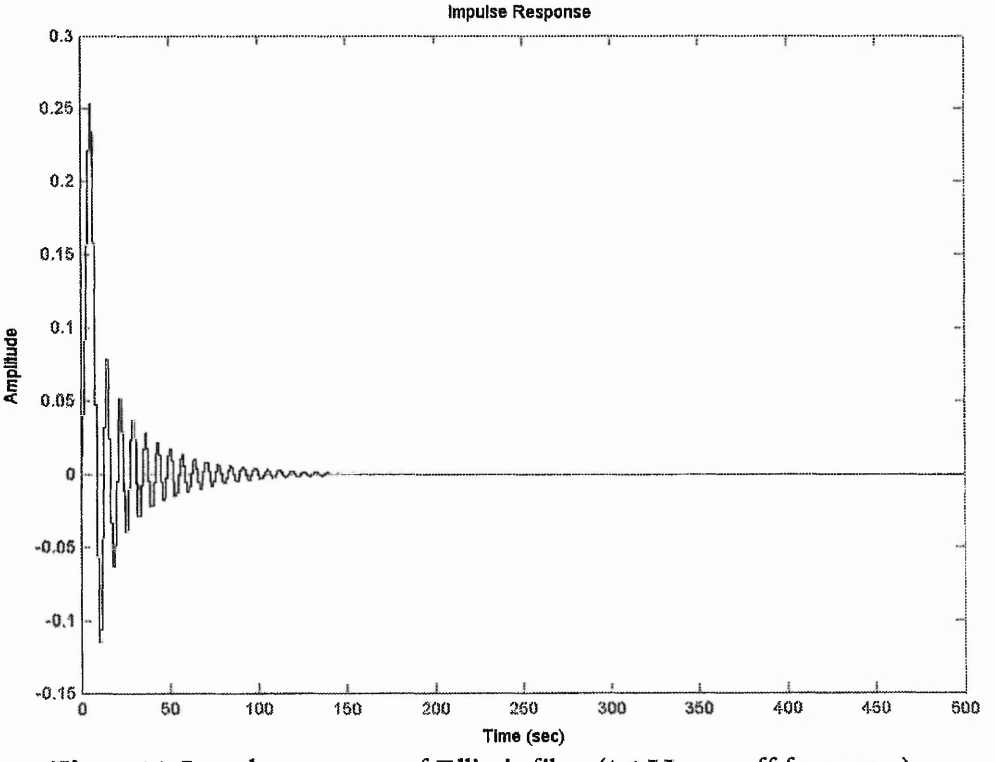

Fig. 3-24: Impulse response of Elliptic filter (1.4 Hz cut-off frequency).

3.6 Deducing True Melt Temperature

The melt temperature analyses in Section 3.4 are established on the basis of melt temperature measured at surfaces of the screw and the barrel. The measurements at the screw and the barrel differ largely and might not truly represent the melt temperature within the screw channels due to the poor thermal conductivity of the polymer. Meanwhile, the melt temperature within the screw channel is impossible to measure directly due to the operational constraints. The screw flight continuously 'scrapes off' the melt adhered to the inner barrel surface. The scraping motion of flight prohibits a thermocouple to be protruded from the barrel to measure the melt temperature at the mid-channel. Some experimental studies protruded a thermocouple from the screw to the mid-channel (Tadmor and Klein, 1970). This installation is not economical for industrial application, and may also alter the melt flow pattern. Infrared sensor has been proposed as an advance technique to measure the melt temperature (Sabota *et al*, 1995). However, the effective measurement is limited to the melt surface temperature due to the opacity of the polyethylene polymer. Therefore, an approach to deduce the true melt temperature within the screw channel is proposed as follows.

The true melt temperature is deduced based on the Maddock melting model described in Chapter 2. The assumptions include 1) the temperature profile of the steady state operation is fully developed, where the local melt temperature at any spatial domain is constant with time, and 2) the readings of the thermocouples truly indicate the melt temperature at the contacted surfaces. The cross sectional contents of the helical screw channels at different locations are depicted in Fig. 3-25. The melting mechanisms commence approximately at the beginning of the compression section, become very rapid at the middle of the compression section and complete at the end of the compression section.

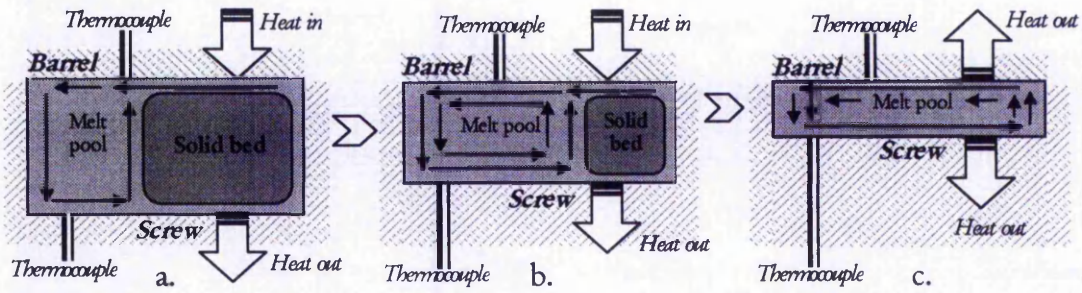

Fig. 3-25: Melting mechanisms: **a)** at the beginning, **b)** at the middle, and **c)** at the end of compression section.

At the beginning of the compression section, the heat source of the polymer melting is mainly by conduction from the hot barrel wall. Regardless of the poor thermal conductivity of the polymer properties, the polymer contacting with the barrel wall would melt due to the large temperature difference between the barrel inner wall and the solid polymer. When a first trace of melt is formed at the barrel surface, the relative motion between the barrel and the screw continuously drives the melt film towards the advancing flight of the channel. Upon meeting the flight, the melt film is 'scratched' from the barrel surface and accumulated in a melt pool. The heat within the melt pool is inhomogeneous. It is shown in Fig. 3-25a that the heat is partially conducted away when the melt touches the cooler screw surface. The melt temperature at this location (beginning of the compression section) is given in Fig. 3-26. The maximum melt temperature ($*_a$) is measured at the barrel surface and the minimum melt temperature is measured at the screw surface (o_a). The difference between the maximum and the minimum temperature signals of the melt is large because of the deep screw channel and the poor thermal conductivity of the polymer. The true melt temperature within the melt pool at this location ($+_a$) is taken as an average of the melt temperature measured at the surfaces of the barrel wall and the screw.

At the middle of the compression section, the conversion of solid polymer to the molten polymer is very rapid. The size of melt pool grows while the solid bed diminishes. It is noticed in Fig. 3-25b that the depth of channel in compression section is shallower. Reducing in channel depth creates a high pressure to push the melt towards the metering section. The pressure also rearranges the solid bed to maintain the melt film thickness throughout the melting process. The melting mechanisms at this location (middle of the compression section) is similar to those in Fig. 3-25a. Therefore the true melt temperature ($+_b$) in Fig. 3-26 is deduced on the same consideration as previous melt temperature ($+_a$), which is the average of the measured temperature at the surfaces of the barrel and the screw.

At the end of the compression section, the melting of solid polymer is normally completed. The depth of the screw started from this location (Fig. 3-25c) is very shallow. The shallow depth improves the temperature and the pressure homogeneities through better melt circulation within the screw channel. Consequently, the melt temperature signals exhibit less temperature difference. From the temperature profile shown in Fig.

3-26, the screw temperature (o) is observed to be slightly higher than the barrel temperature (*). The barrel temperature in the experiment is set constant at 210 °C. When the temperature exceeds the preset value, the heater power is turned off. Without the power supply, the barrel temperature starts decreasing when the heat is dissipated to the surroundings. Meanwhile, the screw temperature can be maintained because the screw is inside the extruder. Therefore, the melt temperature (+) measured at the surface of the screw can be best taken as the true melt temperature.

The dashed line in Fig. 3-26 shows the complete true melt temperature. Similar trends were observed in published experimental results (Tadmor and Klein, 1970). The experiments were conducted at the screw speed of 80 rpm in a 2.5 inches diameter extruder to process the LDPE polymer. A few thermocouples were installed in the middle of screw channels throughout the screw, near the advancing flight in the feed section and near the trailing flight in the metering section. Comparable observations were also obtained in the experiments conducted on an 8 inches diameter extruder. These results help to justify the applicability of the deduced melt temperature as the true melt temperature.

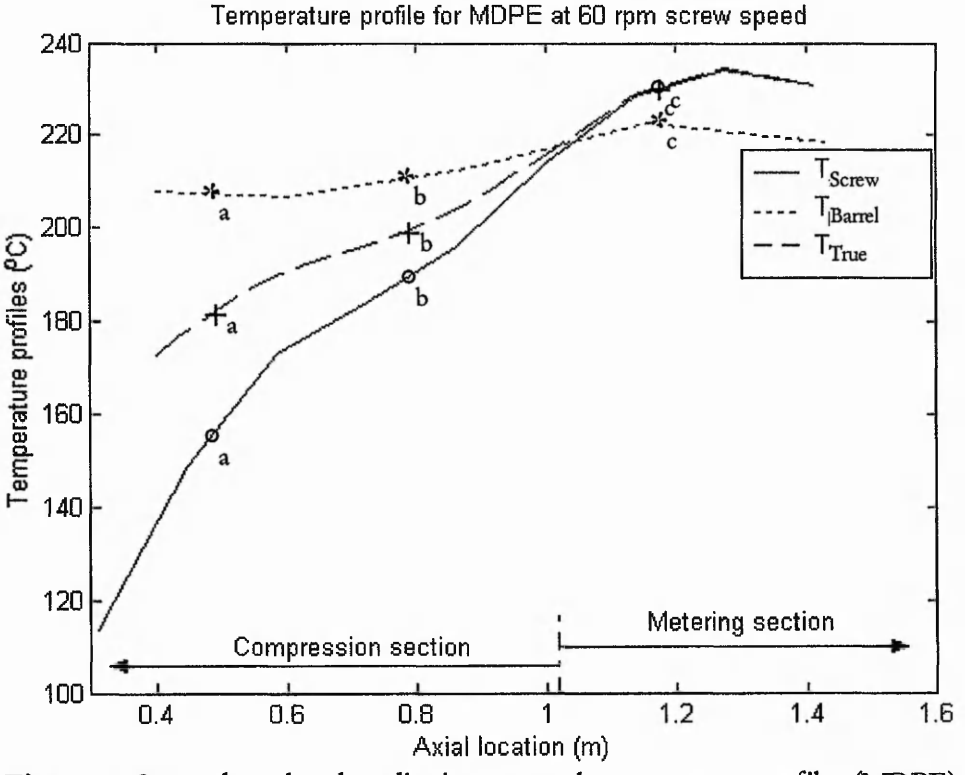

Fig. 3-26: Screw, barrel and qualitative true melt temperature profiles (MDPE).

3.7 Summary Remarks

In this chapter, the physical elements and the experimental data of a single screw extrusion system have been reviewed. The extruder consists of a cylindrical barrel with a screw inside. During the operation, the screw rotational speed is controlled by a DC motor while the barrel temperature is controlled by a heating/ cooling unit. The screw speed and the barrel temperature are regarded as the manipulating parameters. Changing these parameters can alter the polymer melt conditions. The melt conditions in the study are indicated by the melt pressure and the melt temperature, which are referred to as the controlled parameters.

The review of data has improved the understanding of the extrusion behaviour. The polymer extrusion is found to be a distributed parameter process. Different values of melt pressure and melt temperature are observed at different locations of extruder under a constant operating condition. The process parameters are interrelated. For example, a change in the screw speed would affect both of the melt pressure and the melt temperature simultaneously. The data review also verifies the occurrences of high, intermediate and low frequency disturbances during the operation. The high frequency disturbances or flight noises occur due to the periodical interference of the screw flight passing the pressure transducer. The disturbances could be regarded as signal distortions. The intermediate and low frequency disturbances occur due to the inconsistency of melt conditions such as the irregularity of melt velocity. Minimising the impact of these two disturbances requires a suitable control system. A design of the control system will be described in Chapter 5.

The eighth-order Elliptic low pass filter has demonstrated its efficiency in reducing the flight noises in the pressure data. The transfer function of the filter is reconstructed by cascading four second-order transfer functions. This decreases the sensitivity of the filter function to the inaccuracy of coefficient representation and helps to realise a stable filter.

Neither the screw temperature nor the barrel temperature is regarded as the true melt temperature. A qualitative approach to deduce the true melt temperature based on the screw temperature and the barrel temperature has been presented. The deduced melt temperature will be referred to as the melt temperature in the remaining chapters.

Chapter 4
Extrusion Modelling

4.1 Introduction

Dynamic modelling of the melting mechanism inside the extruder allows predictions to be made on the extruder performance in response to changes in operating conditions. The predictions help to reduce the amount of experimental works required for designing a feasible control system. Basically, there are two methods available to model the extrusion process, namely a theoretical modelling method and an empirical modelling method. The theoretical modelling method develops a process model based on physical knowledge of the melting mechanism, while the empirical modelling method identifies a process model based on experimental observations.

The complexity of process behaviour represents one of the difficulties to develop a process model. The extrusion behaviour identified from the data review may be summarised as follows:

- the process parameters are distributed in that different values of temperature and pressure are measured at different locations along the extruder;
- the process parameters are interrelated in that a change in the screw speed would lead to changes in the melt temperature and the melt pressure;
- the operating conditions may be varying and the impact of the variations could be seen from the inconsistency of the melt temperature and the melt pressure.

In the past, both theoretical and empirical models have been developed when attempting to address the above extrusion behaviour. It is found from the literature survey that the majority of dynamic extrusion models are empirical (Costin *et al*, 1982a; Nelson *et al*, 1986; McKay *et al*, 1996; Chiu and Pong, 2001). This is probably due to the fact that an empirical model is easier to obtain. While the empirical models might be suitable for specific applications, they lack generality and proper structures to describe the distributed process parameters. The validity of an empirical model is limited to a specific location and operating condition. Relatively few theoretical dynamic extrusion

models are available (Tadmor *et al*, 1974; Brauner *et al*, 1977). A theoretical extrusion model is not easy to derive, as detailed extrusion knowledge in both temporal and spatial domains is required. The available theoretical models have shown the ability to address the distributed and interrelated characteristics of the process parameters, but their practical applications in controller design are limited. The models are developed using simplifying assumptions that may not be valid in practice. Some process parameters, that ought to be sensitive to the operating conditions, are assumed to be constant during the operation. Consequently, a modelling error will be resulted when the operating conditions are varying.

There is a need for an alternative method that will develop an extrusion model with better performance. In this chapter, an overlapping of theoretical and empirical modelling techniques is investigated. Subsequently, a semi-physical dynamic extrusion model is developed by combining a theoretical model and empirical FRBS sub-models with the following purposes:

- a theoretical model offers a suitable model structure for predicting the distributed and interrelated process parameters;
- empirical FRBS sub-models introduce adaptive ability to the semi-physical model by allowing the approximations of the operational-sensitive parameters to change accordingly to the variations in the operating conditions.

An overview of the semi-physical model development is shown in Fig. 4-1. More details of the theoretical model, the FRBS sub-models and the simulation method of the semi-physical model will be presented. Based on the simulation, the predictive ability and the adaptive ability of the semi-physical model will be evaluated.

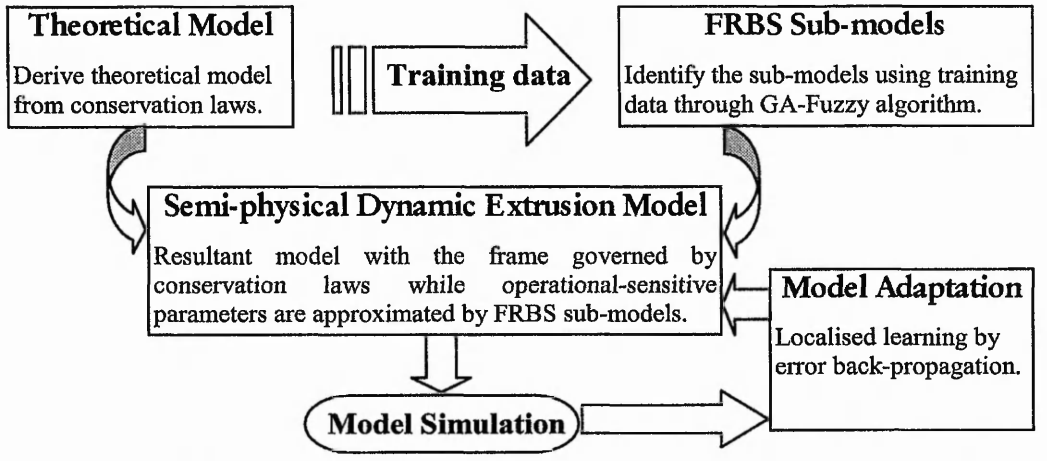

Fig. 4-1: Overview of semi-physical dynamic extrusion model development.

4.2 Theoretical Dynamic Extrusion Model

The theoretical dynamic extrusion model describes the states of the extrusion process based on the transient responses of the Solid Bed Profile (SBP) and the Melt Temperature Profile (MTP). The dynamic conditions are assumed to prevail only when the polymer starts melting, i.e. in the melting and the melt conveying mechanisms. The governing equation for the dynamic SBP is derived from differential mass balance of the solid bed, given in Equation (4-1), whereas the dynamic MTP is governed by differential energy balance on the melt pool, written in Equation (4-2). The original MTP governing equation in Tadmor *et al* (1974) is found to be erroneous. The details of the correction are noted in Appendix 3.

$$\frac{\partial X}{\partial t} + v_{sz}\frac{\partial X}{\partial z} = -\frac{\phi X^{1/2}}{\rho_s H} + \frac{A v_{sz}}{H} X \tag{4-1}$$

$$\frac{\partial T}{\partial t} + v_{mz}\frac{\partial T}{\partial z} = \frac{\phi X^{1/2}(T_f - T)}{\rho_m H(W - X)} + \frac{q_{tr} + q_{vc}}{C_m \rho_m H(W - X)} \tag{4-2}$$

In the above equations, X is the solid bed width, T is the melt temperature, z and t are the helical down channel distance and time instant respectively, v_{sz} and v_{mz} are the down channel velocity of solid and melt respectively, ρ_s and ρ_m are the density of solid and melt, A is the channel taper, H is the channel depth, T_f is the film temperature, ϕ is the melting coefficient, C_m is the heat capacity of melt, W is the channel width, q_{tr} is the heat transfer rate through barrel wall and q_{vc} is the viscous dissipation rate.

The volumetric flow rate and the melt pressure are interdependent. It is assumed that the responses of these two parameters are relatively rapid and steady state conditions are obtained before any changes in SBP and MTP taken place. Therefore, the parameters could be calculated using steady state equations based on instantaneous local conditions. The volumetric flow rate, Q, is determined by summation of the drag flow and the pressure flow given below:

$$Q = p\frac{v_{bz} WH}{2} F_{dr} + p\frac{WH^3}{12\eta}\left(-\frac{\partial P}{\partial z}\right) F_{pr} \tag{4-3}$$

where p is the number of channel in parallel, which is one for the standard single channel screw, η is the viscosity, F_{dr} and F_{pr} are 'shape factors' for the drag and the pressure flows respectively. Other symbols are denoted in the Nomenclature section.

In an 'imaginary' case where the flow control valve at the die is fully closed, the extruder is operating at a no-discharge condition ($Q = 0$). Taking $p = 1$ and neglecting the shape factors, Equation (4-3) is simplified to:

$$\frac{\partial P}{\partial z} = \frac{6\eta v_{bz}}{H^2} \tag{4-4}$$

where v_{bz} is the barrel velocity in the down channel direction. In an operation with throughput, Q, the pressure loss due to the throughput could be calculated by neglecting effect of drag flow and shape factor in Equation (4-3) as follows:

$$\frac{\partial P}{\partial z} = \frac{12Q\eta}{WH^3} \tag{4-5}$$

Therefore, the net pressure gradient for an operation with throughput, Q, is determined by a balance of pressure developed and the pressure loss.

$$\frac{\partial P}{\partial z} = \frac{6\eta v_{bz}}{H^2} - \frac{12Q\eta}{WH^3} \tag{4-6}$$

The first term on the right hand side of the equation is the pressure developed at the no-discharge condition and the second term defines the pressure loss due to the throughput. The variation of the melt pressure along the screw channel in helical direction is termed as "Pressure Profile" (PP).

The above equations represent the basic governing equations for the theoretical dynamic model. Within the model, several process parameters are sensitive to the variations in the operating conditions. These operational-sensitive parameters are the viscosity of the molten polymer, the melting rate, the viscous dissipation rate and the heat transfer rate. In the theoretical model, the operational-sensitive parameters are expressed as follows.

The viscosity of molten polymer exhibits linear relationships between shear stress and shear rate (Newtonian flow behaviour) at low and high shear rate ranges. In the intermediate range, where most polymers processing occur, the relationships are nonlinear (non-Newtonian flow behaviour). A popular method to approximate the viscosity of non-Newtonian flow is by means of a "power law" model. For convenient of computer calculation, the equation of the power law model is quite often expressed in a logarithmic form given in Equation (4-7):

$$\log\eta = a_0 + a_1 \log\dot{\gamma} + a_{11}(\log\dot{\gamma})^2 + a_2 T + a_{22} T^2 + a_{12} T \log\dot{\gamma} \qquad (4\text{-}7)$$

where $\dot{\gamma}$ is the shear rate, and a is a set of coefficients obtained by a linear regression analysis on a logarithmic scale graph. The values of the coefficients are determined from experimental data obtained on a rheometer.

The melting rate, ϕ, determines the efficiency of state conversion from solid to melt. The expression of the melting rate is given in Equation (4-8) where the numerator signifies the rate at which heat is being supplied. The denominator represents the heat used for the melting.

$$\phi = \sqrt{\frac{v_{bx}\rho_m\left[K_m(T_b - T_m) + \frac{\eta}{2}v_j^{\,2}\right]}{2\left[C_s(T_m - T_s) + \lambda\right]}} \qquad (4\text{-}8)$$

In the above equation, T_b is the barrel temperature, T_s is the temperature of solid polymer, v_j is the velocity difference between barrel and solid bed, λ is heat of fusion and K_m is thermal conductivity of polymer melt.

The viscous dissipation rate, q_{vc}, defines the energy generated subsequent to the shear action in polymer melt created by the relative motion of the rotating screw in the stationary channel. It is calculated as follows:

$$q_{vc} = \frac{p\eta\pi^2 N^2 \overline{D}^2}{\sin\overline{\theta}}\left(\frac{W}{H}\right)\left[\cos^2\overline{\theta} + 4\sin^2\overline{\theta} + 3\cos^2\overline{\theta}\left(\frac{Q_{pr}}{Q_{dr}}\right)^2 + \frac{\eta_f}{\eta}\frac{H}{W}\frac{e}{c}\right] \qquad (4\text{-}9)$$

where Q_{pr} and Q_{dr} are the volumetric flow rates attributed to the pressure and drag flow.

The heat transfer rate, q_{tr}, given in Equation (4-10) specifies the heat gained or lost by the melt through the barrel wall in radial direction:

$$q_{tr} = \rho_m C_m H(\overline{T}_c - T)W - X\left(\frac{\Delta z}{t_n}\right) \qquad (4\text{-}10)$$

where t_n is the heat transfer time and $\overline{T}_c$ is the average melt temperature in the channel.

It is argued that Equations (4-7) to (4-10) which are expressed in a deterministic manner might not be suitable for approximating the behaviour of the operational-sensitive parameters. The justifications for this argument are given as follows:

- The power law model in Equation (4-7) might not be able to predict the instantaneous viscosity of the molten polymer during the operation. The validity of the power law model is limited to the intermediate shear rate range. In practice, this range is difficult to determine. Besides, the preset values assigned as the empirical coefficients in the power law model might also make the prediction impractical because the polymer properties are inconsistent. The properties for the same type of polymers supplied from the same manufacturer may vary from batch to batch, not to mention if from different suppliers. Furthermore, regrind polymers are often mixed with fresh polymers feeding to the extruder. The practice of polymer recycling is common in the polymer processing industry under the legislation.

- The deterministic equations of the melting rate, ϕ, the viscous dissipation rate, q_{vc}, and the heat transfer rate, q_{tr}, given in Equations (4-8) to (4-10) respectively are in the simplest form of analytical expressions. Their validity is confined to the assumptions of polymer melt with Newtonian flow behaviour and negligible effect of the barrel curvature. The analytical expressions of these process parameters for more complicated situations are possible to derive, when more simplifying assumptions are waived. The complicated expressions, however, are meaningless as these process parameters are impossible to measure during the extrusion process and cannot be validated. Apart from this, the equations may also become invalid when the operating conditions vary, including mechanical depreciation of the extruder.

The above justifications argue the inadequacy of employing the deterministic equations to approximate the operational-sensitive parameters. A modification is introduced to the theoretical model so that these operational-sensitive parameters could be approximated using a more suitable approach. Considering the characteristics of the parameters described above, Fuzzy Rule Based System (FRBS) would be the approach of choice. The modification to the theoretical model using the FRBS will be described in the next section.

4.3 FRBS Sub-models

Fuzzy Rule Based System (FRBS) is introduced as a tool to develop sub-models to substitute the deterministic equations of the operational-sensitive parameters. This strategy provides flexibility for the process model to cope with the incomplete process information and the changes in the operating conditions during the extrusion process. The nonlinear functions, $f_{fz(.)}$, of the sub-models for the parameters η, ϕ, q_{vc}, and q_{tr} are expressed in Equations (4-11) to (4-14) respectively.

$$\eta = f_{fz(\eta)}(\omega, X, T) \tag{4-11}$$

$$\phi = f_{fz(\phi)}(\omega, T_b) \tag{4-12}$$

$$q_{tr} = f_{fz(tr)}(\omega, T_b, X) \tag{4-13}$$

$$q_{vc} = f_{fz(vc)}(\omega, T_b, T, H) \tag{4-14}$$

The input parameters in the above nonlinear functions are determined by a measure of correlation. A hybrid GA-Fuzzy algorithm is then employed to identify the optimal structure for each sub-model (Cordon *et al*, 2001). The data for the sub-model identification is acquired from a simulator that has been constructed based on the theoretical dynamic model. The details of the simulator are given in Appendix 4.

The GA-Fuzzy algorithm utilises a special form of representation, namely chromosome, during the identification of a sub-model. A chromosome represents a complete Knowledge Base (KB) of an operational-sensitive parameter that consists of a Data Base (DB) and a Rule Base (RB). The potential solutions for a sub-model of m inputs, n outputs and r rules are coded into a population of chromosomes with a fixed binary number of s bits. The input and output (I/O) parameters have their own sets of Membership Functions (MFs), q. Each I/O parameter is initialised with a maximum number of MFs, i.e. $q = r$. As all the sub-models are of zero-order Sugeno type with symmetric Gaussian MF (with two MF parameters), the total length of a chromosome is $L = s \times r\ (2 \times m + n)$. The GA-Fuzzy algorithm is programmed with a flexible coding length to deal with the descending number of rules and MFs during the identification.

The procedure of structure optimisation of a sub-model is depicted in Fig. 4-2. The sub-model structure is defined by the number of rules and MFs. The initial setting specifies the criteria of the optimisation. For example, the maximum number of desired rule, the

type of genetic operator and the criteria of convergence are determined. It is also possible to translate the expert knowledge in the initial setting.

During the DB optimisation, fitness indices are assigned to all chromosomes within the population. The definition of the best fitness depends on several conditions proposed by Surmann and Selenschtschikow (2002). In the present study, the fitness index is determined by the inverse of mean square error given below:

$$F^{1/o} = \frac{V}{\sum_{j=1}^{V} (o_j - \hat{o}_j)^2} \tag{4-15}$$

where V is number of data pairs, $\hat{o}$ and o are predicted and desired outputs respectively.

A few chromosomes with high fitness are kept for the next generation and the genetic operators are applied to the current population. The genetic operators are the functions that act on the chromosomes to diversify the possible solutions. The commonly used operators include **selection, crossover** and **mutation** (Whitley, 1993). The DB optimisation process is repeated until the convergent criterion is met. When this happens, the population with the selected chromosomes proceeds to Knowledge Base (KB) optimisation.

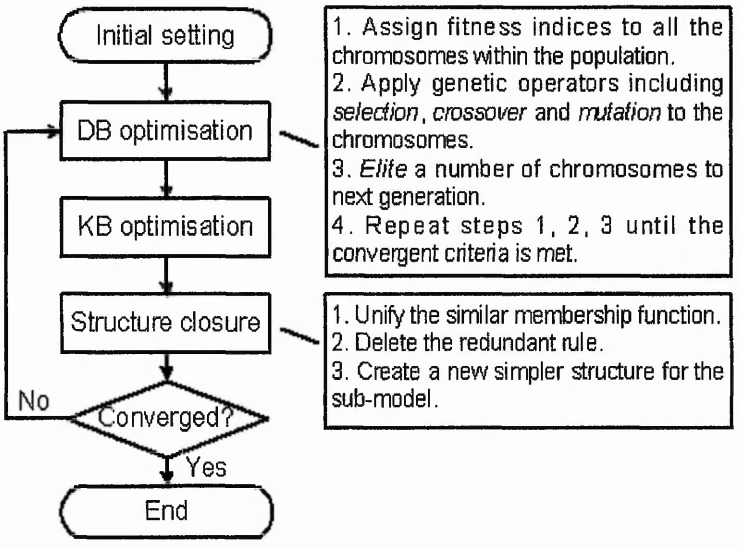

Fig. 4-2: GA-Fuzzy algorithm for structure optimisation of sub-model

The Knowledge Base (KB) optimisation step is similar to that of the Data Base (DB) optimisation except that three extra fitness indices, namely the entropy of the FRBS (F^E), the MF similarity (F^S), and the rule activation (F^Z), are included with assigned weights. Introducing F^E into the criterion encourages an adequate overlapping of MFs, F^S to reduce the tendency of having similar MFs and F^Z to penalise the redundant rules of the sub-models.

$$F^E = \frac{1}{\chi\left(\frac{\bar{r}}{r_{\max}} - 1\right) + \varsigma\left(\frac{\bar{r}}{r_{act}} - 1\right) + 1} \tag{4-16}$$

$$F^S = 1 + \nu \frac{S}{(m+n)r_{tot}} \tag{4-17}$$

$$F^Z = \psi \frac{Z}{(m+n)r_{tot}} + 1 \tag{4-18}$$

The fitness indices given in Equations (4-15) to (4-18) are then combined in a single convergent criterion written in Equation (4-19).

$$F^A = F^{I/O} \text{ x } F^E \text{ x } F^S \text{ x } F^Z \tag{4-19}$$

Upon convergence of the KB optimisation, only the best chromosome is selected for the structure closure step. A new simpler structure is produced by unifying the similar MFs and deleting the redundant rules. Then, a new generation of the chromosomes having this new structure is created and the entire GA-fuzzy optimisation process is then repeated. While the convergences of the DB and the KB optimisations are decided by the predefined number of generations or error limits, the optimisation of the structure of the sub-model is deemed to have converged only if the closure step cannot be further executed.

Table 4-1 tabulates the initial settings for the sub-model identifications and the corresponding final structures of the sub-models. The size of the population is set in proportion to the number of inputs in each sub-model. A larger population enhances the diversity that is especially important for a lengthy chromosome. The parameters of MF are converted into 6 bits binary code, in which a range of 64 discrete values is produced. The resolution should be high enough as the parameters represent only the width and the location of the MF within a bounded operating range.

The strategies for applying the genetic operators are tournament selection, multiple-points crossover with crossover rate of 1 and randomised mutation with a trigger weight function of 0.1. **Elitism** is applied as a special policy for each generation to keep a group of fittest chromosomes. The properties of elite chromosomes are exceptional and are excluded from the genetic operations. A total of 5 chromosomes with the highest fitness within the current generation are elite to the next generation. This policy helps to ensure that the fitness of the chromosomes in the next generation will be at least maintained as, if not higher than, the current generation. To a certain extent, if all the chromosomes in the current generation are elite to the next generation, the fitness of the chromosomes in the next generation will never be improved.

The results given in Table 4-1 indicate that the final sub-models contain fewer MFs and smaller number of rules. The advantages of the simpler structure include easier model interpretation, less computational demanding and higher efficiency of model adaptation. The sub-models with the optimised structures (Equations (4-11) to (4-14)) are then substituting the deterministic equations (Equations (4-7) to (4-10)) to approximate the operational-sensitive parameters, forming the semi-physical dynamic extrusion model.

Table 4-1: Sub-model identification and corresponding final structures.

Properties	**ϕ sub-model**	**q_{vc} sub-model**	**q_{tr} sub-model**	**η sub-model**
Number of inputs	2	4	3	3
Size of population	40	60	50	50
Initial number of rules	27	36	30	30
Initial number of MFs	27 x 3	36 x 5	30 x 4	30 x 4
Final number of rules	5	3	5	2
Final number of MFs	5 x 5 x 5	2 x 3 x 2 x 3 x 3	5 x 5 x 5 x 5	2 x 2 x 1 x 2

4.4 Adaptation Mechanism

The semi-physical dynamic extrusion model allows predictions on several process parameters. In this study, the predictions on the melt temperature and the melt pressure are taken as indications to the accuracy of the model predictions because these two parameters are measurable during the operation. The deviation between the model prediction and the experimental measurement is referred to as a prediction error. When

the prediction error is beyond a preset tolerance, the adaptation mechanism is activated to tune the sub-models to reduce the prediction error.

It is remarked that the sub-models approximate only the operational-sensitive parameters but not the melt temperature and the melt pressure. These sub-models will then be part of the semi-physical model to predict the melt temperature and the melt pressure. To facilitate the adaptation mechanism, a technique is required to transfer the information of the prediction error to the sub-models. In the study, an error back-propagation technique is employed.

The concept of the error back-propagation technique is shown in Fig. 4-3. In the forward sequence (left to right), a small change in the MF parameter, g, will affect the inferential membership grade of an input, w. The influence is further reflected on the approximation of the sub-model, $f_{fz(.)}$. This in turn will affect the prediction of the semi-physical model, $\hat{o}$. It is realised that the prediction error can be minimised if the effects of the changes at individual level are known, which are the gradient vectors of the causal relationship. Therefore, information of prediction error can be passed from the output level, and going backward level by level, to the first level as depicted in the backward sequence (right to left). The total gradient vectors in the backward sequence are effectively represented by a chain rule generalised as:

$$\frac{\partial J}{\partial g_q^i} = \frac{\partial J}{\partial f_{fz(.)}^i} \sum \frac{\partial f_{fz(.)}^i}{\partial w_q^i} \times \frac{\partial w_q^i}{\partial g_m^i} \qquad (4\text{-}20)$$

where J and i are the cost function and the sub-model index respectively. The corresponding MF parameter is then updated using a gradient descent algorithm. The MF parameters are tuned based on the cost function, J, calculated from the sum of the squared error between the experimental measurements and the model predictions.

$$J = \sum (o - \hat{o})^2 \qquad (4\text{-}21)$$

where o is the experimental measurements and $\hat{o}$ is the model predictions.

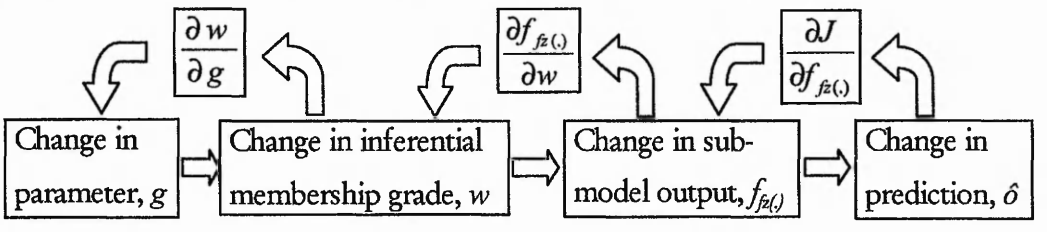

Fig. 4-3: Causal relationship of MF parameters to the model prediction.

4.5 Simulation Method

The governing equations of the semi-physical model are rather complex. It comprises the Partial Differential Equations (PDEs), the algebraic equations and the FRBS sub-models. A computation path is employed to guide the model programming, so that the calculations follow a correct sequence to realise the model simulation. The PDEs in the semi-physical model are solved using the Finite Volume Method (FVM).

4.5.1 Computation path

The computation path of the semi-physical model is illustrated in Fig. 4-4. The program is initially provided with the following data:

- geometry parameters such as channel depth;
- material properties such as density of solid polymer;
- barrel temperature setting as a function of time, $T_b(t)$;
- screw speed as a function of time, $\omega(t)$;
- initial profile at time t_0 for the solid bed $X(z,t_0)$, and the melt temperature $T(z,t_0)$;
- location of the melting process commences;
- initial estimation of the flow rate at the die, $G(t_0)$.

The flow rate at the die, G, is initialised by the flow rate taken from the previous steady state condition. When the operating condition changes with time, the program is iterated until new steady state condition is reached. The prediction of the flow rate improved during the iteration. The relationship between the flow rate and the pressure-drop at die, ΔP_{die}, is given below:

$$G = K_{die}\rho_m \frac{\Delta P_{die}}{\eta_{die}} \tag{4-22}$$

where K_{die} is the die constant and η_{die} is the viscosity of the melt at the die.

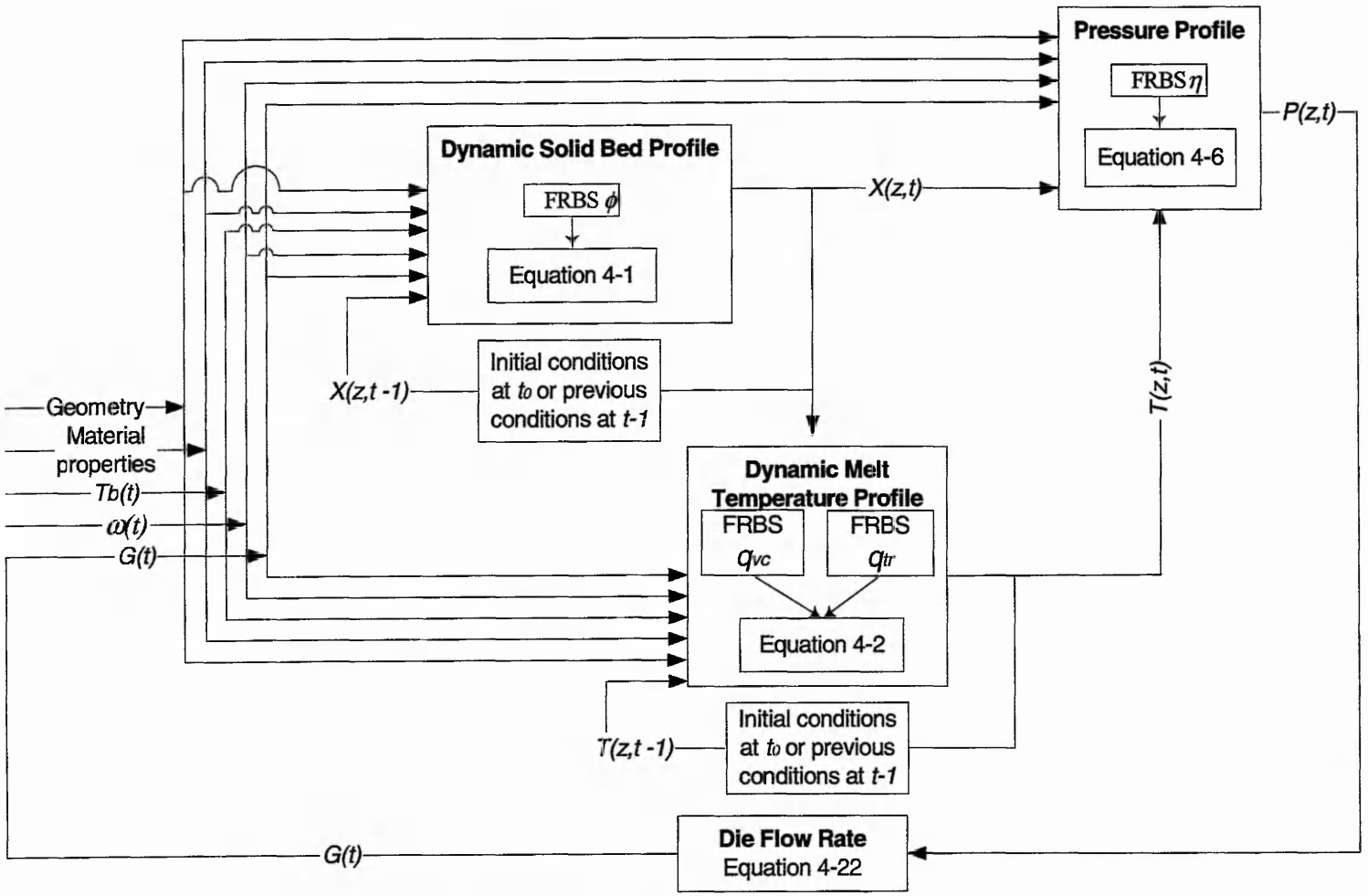

Fig. 4-4: Computation path of semi-physical dynamic extrusion model.

4.5.2 PDEs solution

The partial differential governing equations of the Solid Bed Profile (SBP) and the Melt Temperature Profile (MTP) are solved numerically using the FVM (Versteeg and Malalasekera, 1995). The procedure of the FVM consists of the following steps:

- integrate the governing equations over finite units of control volume of the solution domain;
- covert the finite integral equations into a finite set of linear algebraic equations by means of discretisation;
- obtain the solution of the algebraic equations.

The first step, the control volume integration, distinguishes the FVM from all other numerical methods including the Finite Element Method. The integration helps to conserve the relevant properties of an original PDE for each finite size cell and hence presents a clear relationship between the numerical algorithm and the underlying physical conservation law. The discretisation procedure of the FVM is illustrated in Fig. 4-5. The continuum domain of each PDE is firstly divided into a series of non-overlapping control volumes (sub-domains), with each control volume surrounding a representative discrete point. The relationships between the representative points are then established by integrating the PDE both spatially and temporally over each confined control volume. The nonlinear continuous function of the PDE is thus converted into a finite set of discrete functions, with each discrete function expressed in a linear algebraic equation. The algebraic equations for the SBP and the MTP are given in Equation (4-23) and Equation (4-24) respectively. The derivations of the equations are detailed in Appendix 5. The discrete function shows a clear physical interpretation. For example, the Equation (4-23) signifies that the rate of change of solid bed, X_p, in a control volume, P, is dependent on the net flux of X_w due to convection into the control volume and the rate of increase due to the sources, X_p^0.

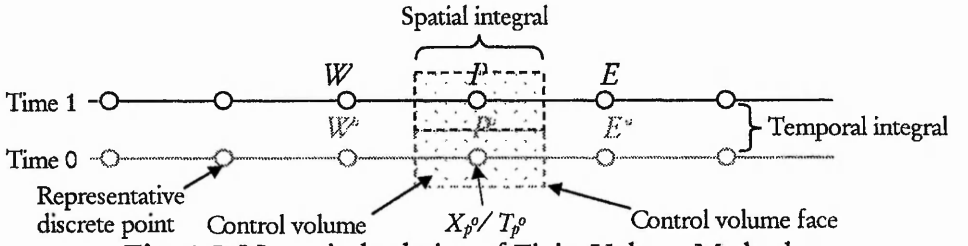

Fig. 4-5: Numerical solution of Finite Volume Method.

$$(\rho_s h + \frac{\phi}{H\sqrt{X_p^o}} hk + \rho_s v_{sz} k) X_p = \rho_s v_{sz} k X_w + (\rho_s h + \frac{A\rho_s v_{sz}}{H} hk) X_p^0 \quad (4\text{-}23)$$

$$(\rho_m h + \rho_m v_{mz} k + \frac{\phi\sqrt{X}}{H(W-X)} hk) T_p \quad (4\text{-}24)$$

$$= k\rho_m v_{mz} T_w + (\frac{\phi\sqrt{X} T_f}{H(W-X)} + \frac{q_{vc} + q_{tr}}{C_m H(W-X)}) hk + \rho_m h T_p^o$$

Subscripts p and w denote the current and previous control volume respectively. Superscript o denotes previous time level.

The algebraic equation sets for the SBP and the MTP at a time level can be arranged to form tri-diagonal matrices separately. An example of the matrix is given below:

$$[E][x] = [b] \quad (4\text{-}25)$$

where $[x]$ is the column vector of dependent variables, $[b]$ is the source vector of the algebraic equations and $[E]$ is a tri-diagonal matrix in the following form:

$$[E] = \begin{bmatrix} -d_{w,t} & d_{p,t} & 0 & \cdots & \cdots & \cdots & 0 \\ 0 & -d_{w,t} & d_{p,t} & 0 & \cdots & \cdots & 0 \\ 0 & \ddots & \ddots & \ddots & 0 & \cdots & 0 \\ 0 & \cdots & \cdots & \cdots & \cdots & -d_{w,t} & d_{p,t} \end{bmatrix}$$

where d is the coefficients derived from the algebraic equations and t represents the time level.

The tri-diagonal matrices for the SBP and the MTP are solved using tri-diagonal matrix algorithm (Patankar, 1980). This algorithm provides a fast and economical means of solutions. Starting with the initial profile at time t, the coefficients and the source vector expressed in Equation (4-25) are solved through forward elimination and back-substitution strategies. A new profile is thus obtained for the dependent variables at time $t+1$. Next, the new profile is assigned to the source vector and the calculation proceeds to the next time level until the steady state condition is reached.

4.6 Model Evaluation

The semi-physical dynamic extrusion model is evaluated on the basis of consistency of the model predictions with the experimental observations presented in Chapter 3. The model is simulated with step-changes in the screw speed and the barrel temperature separately. The melt pressure and the temperature at the die are shown in Fig. 4-6 and Fig. 4-7 in response to the changes in the screw speed. The screw initially rotates at a speed of 60 rpm and the extrusion process is assumed to operate under steady state conditions. The dashed lines represent the steady state responses of the process; the dotted lines are the responses to a positive step-change from 60 rpm to 70 rpm whereas the solid lines are the responses to a negative step-change from 60 rpm to 50 rpm. The model predicts immediate changes in the melt pressure at die as depicted in Fig. 4-6. An overshoot is noticeable before the pressure decays to a new steady state value. Similar pressure responses are also found in the experimental data illustrated in Fig. 3-10 and Fig. 3-11 of Chapter 3, when processing HDPE polymer and MDPE polymer respectively. In Fig. 4-7, a slow temperature increment is predicted when a positive screw speed change is applied. This slow temperature response is also observed in the experimental data shown in Fig. 3-14 and Fig. 3-15.

The model is also evaluated under a case study that the barrel temperature is employed to control the melt temperature at the die. The settings of the barrel temperature are indicated in the legend of Fig. 4-8. The model shows the melt temperature increases when the barrel temperature is set high, but an inverse response occurs initially. The inverse response appears especially when small step-change is applied, such as in the step-change from 180 °C to 190 °C. Logically, the inverse response should not exist when the barrel temperature is increased. This effect could be caused by modelling errors of the semi-physical extrusion model.

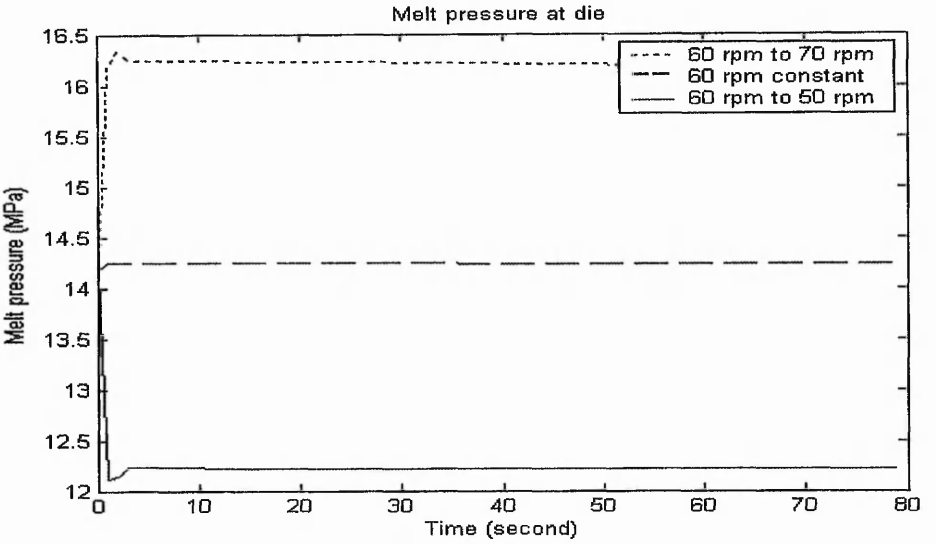

Fig. 4-6: Transient responses of melt pressure to step-changes in screw speed.

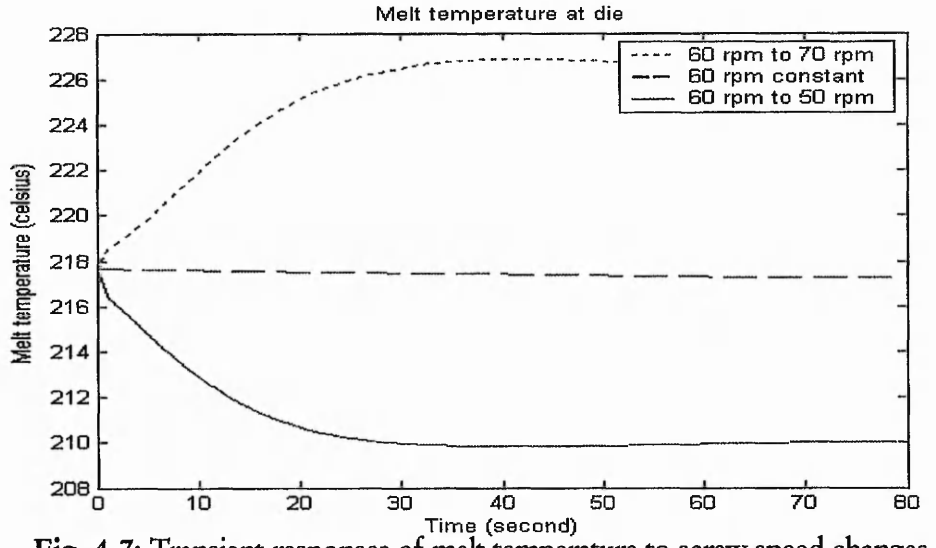

Fig. 4-7: Transient responses of melt temperature to screw speed changes.

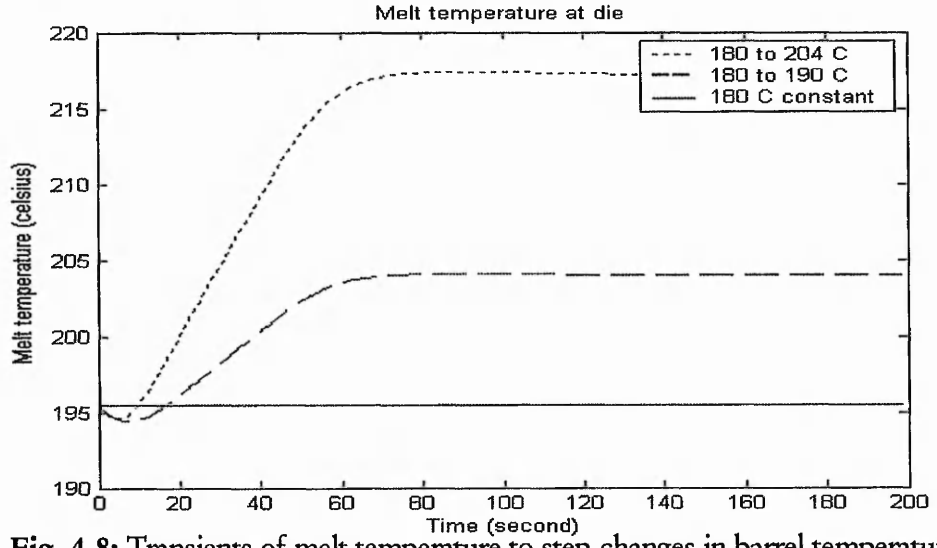

Fig. 4-8: Transients of melt temperature to step-changes in barrel temperature.

The evaluations presented earlier are with the assumption that the model has reasonably described the behaviour of the extrusion process. The assumption could be invalid in many practical situations due to the process disturbances. Therefore, an adaptive model would be useful.

The effectiveness of model adaptation with respect to changes in the polymer properties as a possible disturbance is shown in Fig. 4-9. The evaluation is performed to an extent that the feed polymer is changed from LDPE polymer to HDPE polymer. The star-dotted points represent the published melt temperature measurements at five locations distributed along the barrel, when processing a new type of polymer (HDPE) (Qiu, 1998). The dotted line indicates that the initial prediction of the semi-physical extrusion model produces an obvious prediction error. This prediction is made before the model adaptation. The sub-models are still using the information of the old polymer material (LDPE). The smooth line is the prediction after the model adaptation. The semi-physical model with trained sub-models is able to give a reasonably good result.

The trained semi-physical model is further evaluated by predicting the MTP when the screw is rotating at the speed of 90 rpm. In Fig. 4-10, it is observed that the prediction shows only a small deviation from the experimental data. This implies that the sub-models have been tuned correctly to approximate the operational-sensitive parameters in the new operating environment. The prediction errors of the semi-physical model at different stages are indicated in Table 4-2. The prediction errors in the initial stage and the training stage are calculated from the data in Fig. 4-9, while the prediction error in the validation stage is calculated from the data in Fig. 4-10. The percentage error is calculated as follows:

$$\%Error = \frac{\sum Prediction\ Error}{\sum Prediction} \times 100 \qquad (4\text{-}26)$$

Prediction errors in:	Initial	Training	Validation
Root mean square error	15.0408	4.4641	5.0616
Percentage error (%)	6.2735	1.8746	1.7298

Table 4-2: Prediction errors of the semi-physical model at different stages.

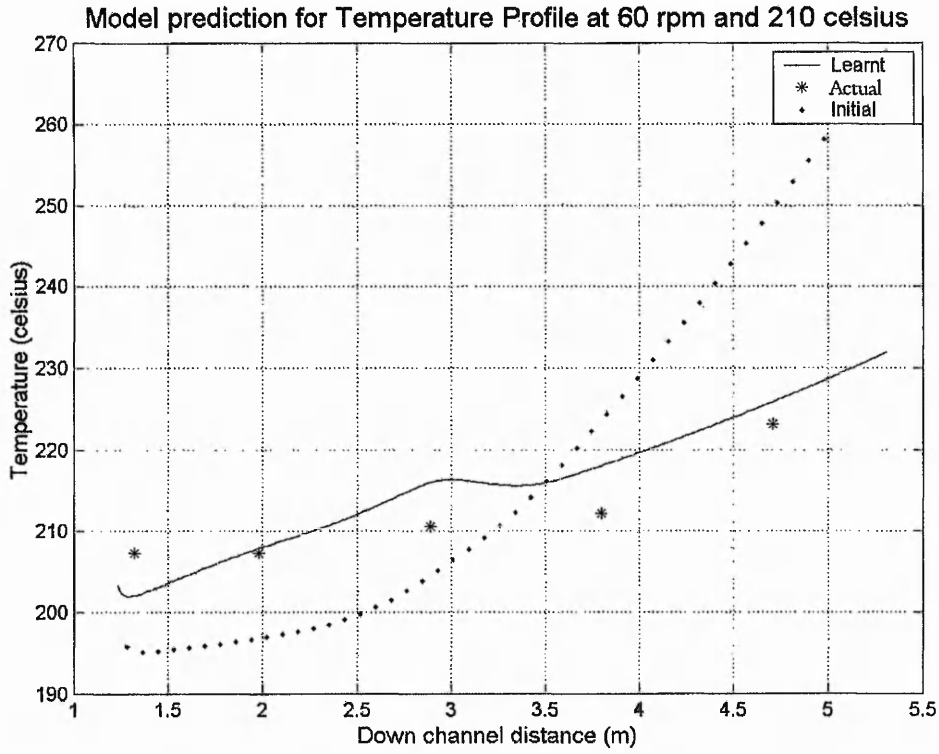

Fig. 4-9: Effectiveness of model adaptation for different processing material.

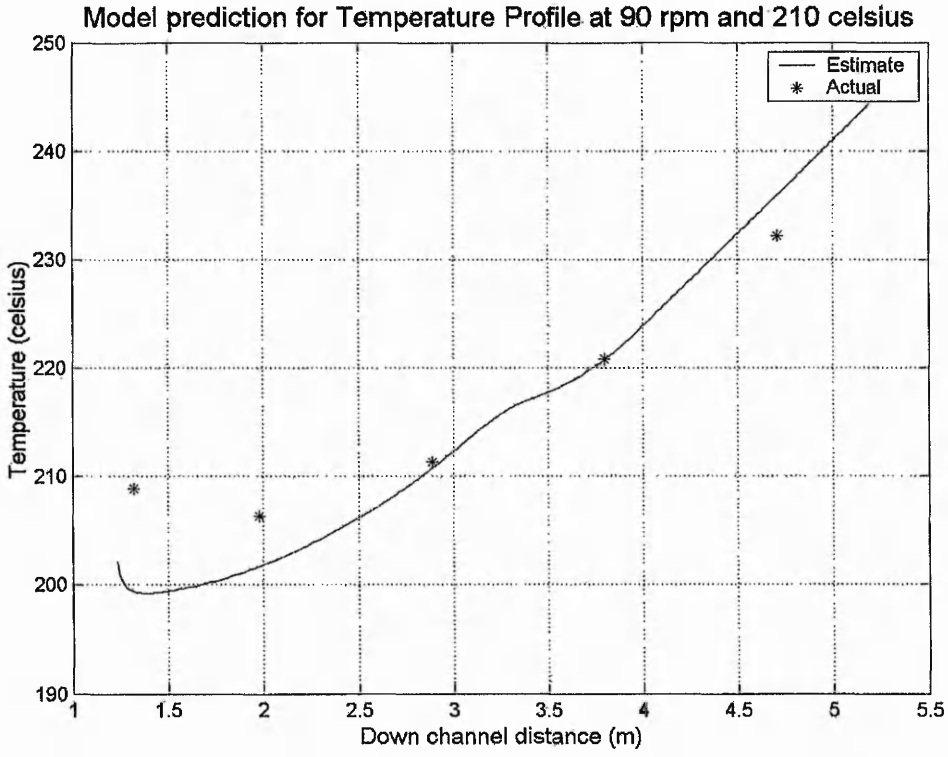

Fig. 4-10: Validation of the trained semi-physical dynamic extrusion model.

4.7 Summary Remarks

To design an effective control system for the extrusion process, a suitable model is required to predict the behaviour of the process. In the past decades, both empirical and theoretical dynamic extrusion models have been developed. However, these models are insufficient to address the behaviour of the extrusion parameters that are distributed, interrelated and sensitive to the variations in the operating conditions. Therefore, there is still a need for a more suitable extrusion model.

It has been demonstrated in this chapter that by overlapping the theoretical and the empirical modelling techniques, an extrusion model with encouraging performance could be obtained. The extrusion model, namely a semi-physical dynamic extrusion model, is developed based on a theoretical model, which provides a proper structure to predict the distributed and interrelated characteristics of the process parameters. It is argued that the operational-sensitive parameters within the theoretical model are inadequately expressed in a deterministic manner. Based on the characteristics of the operational-sensitive parameters, a FRBS is utilised as a tool to develop sub-models to substitute those deterministic equations. The sub-models are adaptive during the operation so that the semi-physical model is responsive to the variations in the operating conditions.

The computation of the semi-physical model is rather complex, as it is governed by a mixture of partial differential equations, algebraic equations and FRBS sub-models. The sequence of calculating each element of the model is illustrated through a computation path. Finite Volume Method is used to solve the partial differential equations.

The semi-physical model has exhibited its desired characteristics for the extrusion control design during the model evaluations. It predicted the melt temperature and the melt pressure in response to changes in the screw speed and the barrel temperature reasonably well. The adaptive ability of the model was also shown useful when the polymer properties were varied.

Chapter 5
Control System Design

5.1 Introduction

In practice, the polymer extrusion operation can be taken as steady but the operating conditions may vary. This is evidenced by the variations in the melt temperature and the melt pressure as detailed in Chapter 3. Therefore, the objective of an extrusion control system is to minimise the impact of inconsistency of operating conditions, hence reducing the variations in the melt temperature and the melt pressure. However, this objective is not easily achievable. The extrusion behaviour is complicated. The process parameters are distributed along the extruder and interrelated. For example, a change in the screw speed can cause simultaneous changes in both melt temperature and melt pressure along the extruder. This implies that without a proper control system, regulating one process parameter may lead to deviation of other parameters.

To control the extrusion process effectively, a Multi-Input-Multi-Output (MIMO) control system could be helpful. Literature survey suggests that a Model Based Predictive Control (MBPC) is a promising method to develop a MIMO control system (Morari and Lee, 1999). There are three desirable features that lead to its popularity. Firstly, the incorporation of an explicit model into the formulation of control law allows a MBPC system to deal with the complicated process behaviour. Secondly, the concept of receding horizon makes the optimisation of control performance efficient. A closed loop optimal control solution is obtained by repeatedly optimising an open loop control solution with every initial condition updated at each time instant. Finally, the system has the ability to deal with constraints of its input and output parameters. Nevertheless, the type of process model that could be incorporated into a MBPC system is very limited. The model is normally expressed in a form of standard linear difference equation (Sanchez and Rodellar, 1996). This is the main drawback of the MBPC.

It is expected that the combination of the semi-physical dynamic extrusion model and the concept of the MBPC will be a solution for an effective extrusion control. The semi-

physical model predicts the complex behaviour of the extrusion process, while using the concept of MBPC to calculate the appropriate control solution based on the model prediction to control the extrusion process. However, this combination requires some modifications because the structure of process model suitable to be used in the MBPC as the predictive model is limited.

In this chapter, a Fuzzy supervisory indirect Learning Predictive Control (FsiLPC) is proposed. The operating mechanism of a FsiLPC system is basically similar to a MBPC system. One distinguishing strategy is introduced where the Fuzzy Rule Based System (FRBS) is used in a form of a fuzzy supervisory unit in the FsiLPC system to generate a control action. To obtain suitable control actions, the fuzzy supervisory units are tuned using the Controller Output Error Method (COEM) during the operation. This strategy allows the FsiLPC system to implement the concept of the MBPC using a predictive model of any structure, including the semi-physical model. The fundamental concept of the FsiLPC system will be described using standard terminology of the control system. Several terms used extensively in the chapter are noted here. A process input parameter is denoted as **manipulating parameter** and its signal is **manipulating signal**, $U(k)$. Likewise, a process output parameter is named **controlled parameter** and its signal is **controlled signal**, $Y(k)$. The discrepancy between a controlled signal, $Y(k)$, and a **reference signal**, $Y_r(k)$ is **error signal**, $E(k)$. The notation with lowercase is a scalar variable while uppercase is a vector variable.

5.2 Background Knowledge: Operation of Model Based Predictive Control (MBPC) System

The concept of the FsiLPC is established based on the MBPC, which has been introduced by Sanchez (1976). The principle of MBPC is expressed as: *Based on a model of the process, predictive control is the one that makes the predicted process dynamic output equal to a desired dynamic output conveniently predefined.* To make the chapter self-contained, the operation of a MBPC system is given as follows (Sanchez and Rodellar, 1996).

A MBPC system consists of a trajectory planner and a predictive model (Fig. 5-1). The trajectory planner generates a trajectory of desired controlled signal, $Y_d(k+j)$, that guides the actual controlled signal, $Y(k)$, to the reference signal, $Y_r(k+j)$, in a predefined pattern.

Then, the controller calculates a predicted manipulating signal trajectory, $\hat{U}(k+l)$, to minimise the deviation between the predicted controlled signal trajectory, $\hat{Y}(k+j)$, and the desired controlled signal trajectory, $Y_d(k+j)$.

Assuming that a plant with the process dynamics could be described in general as:

$$Y(k) = \sum_{i=1}^{n} A_i Y(k-i) + \sum_{i=1}^{m} B_i U(k-i) \qquad (5\text{-}1)$$

where m and n denote the order of the process behaviour, A_i and B_i are the coefficients of the ideal model. To drive the controlled signal, $Y(k)$, to reach the desired value in a satisfactory manner, the MBPC system performs several calculations based on a procedure presented below:

1. Calculate the desired controlled signal trajectory, $Y_d(k+j)$, using the equation:

$$Y_d(k+j) = \sum_{i=1}^{p} \alpha_i Y_d(k+j-i) + \sum_{i=1}^{q} \beta_i Y_r(k+j-i) \qquad (5\text{-}2)$$

$j = 1, 2, 3, \ldots \lambda$

where j is the predictive step, λ is the prediction horizon, α and β are the coefficients of trajectory planner, p and q represent the order of the trajectory. To improve the practicability of the calculated output, the measured controlled signal, $Y(k+1-i)$, is used to update the planner in Equation (5-2) where:

$$Y_d(k+1-i) = Y(k+1-i) \qquad (5\text{-}3)$$

2. Define a cost function to measure the system ability to achieve the desired trajectory, $Y_d(k+j)$. A simple but popular cost function, $\hat{J}(k)$, is:

$$\hat{J}(k) = \left[\hat{Y}(k+j) - Y_d(k+j)\right]^T \left[\hat{Y}(k+j) - Y_d(k+j)\right] \qquad (5\text{-}4)$$

$j = 1, 2, 3, \ldots \lambda$

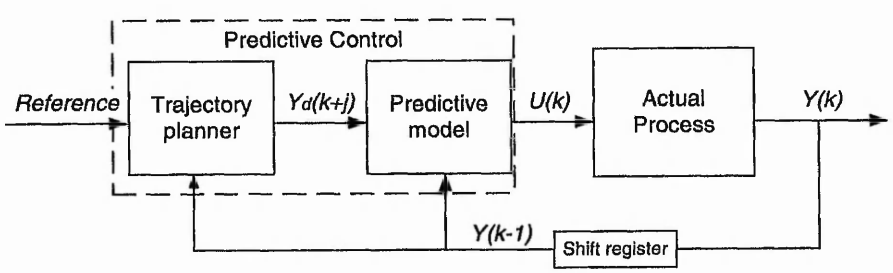

Fig. 5-1: Block diagram of a MBPC system.

The predicted trajectory, $\hat{Y}(k+j)$, in Equation (5-4) is calculated using a predictive model given below:

$$\hat{Y}(k+j) = \sum_{i=1}^{\hat{n}} \hat{A}_i \hat{Y}(k+j-i) + \sum_{i=1}^{\hat{m}} \hat{B}_i \hat{U}(k+j-i) \qquad (5\text{-}5)$$

$j = 1, 2, 3, \ldots \lambda$

where $\hat{A}$ and $\hat{B}$ are the coefficients of the predictive model, $\hat{n}$ and $\hat{m}$ are the order of the predicted process behaviour. It is to be noted that $\hat{A}$, $\hat{B}$, $\hat{m}$ and $\hat{n}$ may not be identical to those of ideal model in Equation (5-1) as a result of the modelling error. The predictive model expressed in Equation (5-5) is also updated with the measured signals to enhance the practicability of the prediction, where:

$$\begin{aligned} \hat{Y}(k+1-i) &= Y(k+1-i) \qquad i = 1, 2, \ldots, \hat{n} \\ \hat{U}(k+1-i) &= U(k+1-i) \qquad i = 1, 2, \ldots, \hat{m} \end{aligned} \qquad (5\text{-}6)$$

To express the predictive model in terms of the measured signals and the predicted manipulating trajectory, $\hat{U}(k+l)$, the Equation (5-5) is rewritten as:

$$\hat{Y}(k+j) = \sum_{i=1}^{\hat{n}} \hat{E}_i^{(j)} Y(k+1-i) + \sum_{i=2}^{\hat{m}} \hat{F}_i^{(j)} U(k+1-i) + \sum_{l=0}^{j-1} \hat{F}_l^{(j-l)} \hat{U}(k+l) \qquad (5\text{-}7)$$

$j = 1, 2, 3, \ldots \lambda$

where $\hat{E}$ and $\hat{F}$ are the new sets of coefficients formulated based on the recurrent calculation of coefficients $\hat{A}$ and $\hat{B}$.

3. Calculate the predicted manipulating trajectory, $\hat{U}(k+l)$, according to the cost function, $\hat{J}(k)$, written in Equation (5-4). The trajectory, $\hat{U}(k+l)$, is obtained using the equation given below:

$$\hat{U}(k+l) = \frac{Y_d(k+j) - \sum_{i=1}^{\hat{n}} \hat{E}_i^{(j)} Y(k+1-i) + \sum_{i=2}^{\hat{m}} \hat{F}_i^{(j)} U(k+1-i)}{\sum_{l=0}^{j-1} \hat{F}_l^{(j-l)}} \qquad (5\text{-}8)$$

$j = 1, 2, 3, \ldots \lambda$ and $l = j-1$

4. Apply the first predicted manipulating signal, $\hat{U}(k)$, to the process.

5. Measure the actual controlled signal, *Y(k)*, and manipulating signal, *U(k)*.

6. Update the trajectory planner and the predictive model.

7. Repeat Steps 1 to 6 for the next control cycle.

Steps 2 and 3 are complicated and computationally demanding. The calculations involve λ number of unknowns predicted manipulating signals in the trajectory, $\hat{U}(k+l)$, that must be solved simultaneously. The calculations could be simplified if the number of unknown is decreased. This is possibly obtained by imposing a predetermined pattern of predicted manipulating trajectory, $\hat{U}(k+l)$.

Step predicted manipulating trajectory has been shown as an effective pattern to reduce the number of unknown (Sanchez and Rodellar, 1996). The number of unknown is reduced to only one, when the predicted manipulating signal, $\hat{U}(k)$, remains constant within the prediction horizon, λ, such that:

$$\hat{U}(k)=\hat{U}(k+1)=\hat{U}(k+2)=...=\hat{U}(k+\lambda-1)=U(k) \qquad (5\text{-}9)$$

Imposing the step predicted manipulating trajectory also helps to evaluate the process dynamics within the prediction horizon. It is an analogy to a case when investigating the step response of a process. The magnitude of the manipulating signal, *U(k)*, depends not only on the discrepancy between the desired and the current controlled signal, but also the prediction horizon allowable for the process dynamics to evolve. The manipulating signal, *U(k)*, is less demanding for a longer prediction horizon.

The block diagram of the MBPC system with the step predicted manipulating trajectory is shown in Fig. 5-2. When this trajectory is imposed, the calculation of the desired trajectory, $Y_d(k+j)$, is not required. Instead, only the output of the trajectory planner at the end of prediction horizon, $Y_d(k+\lambda)$, is needed. Therefore, the trajectory planner in Fig. 5-2 provides only a desired signal, $Y_d(k+\lambda)$, rather than a desired trajectory, $Y_d(k+j)$,

as depicted earlier in Fig. 5-1. The desired signal, $Y_d(k+\lambda)$, and the predicted signal, $\hat{Y}(k+\lambda)$, will coincide if the applied manipulating signal is appropriate.

The operating procedure for the MBPC system with the step predicted manipulating trajectory is altered from the presented MBPC system as follows:

1. Calculate the desired controlled signal, $Y_d(k+\lambda)$, according to the measured controlled signals, $Y(k+1-i)$, the past reference signals, $Y_r(k+1-i)$, and the future reference signals, $Y_r(k+i)$, using the following expression:

$$Y_d(k+\lambda) = \sum_{i=1}^{p} \chi_i^{(\lambda)} Y(k+1-i) + \sum_{i=2}^{q} \gamma_i^{(\lambda)} Y_r(k+1-i) + \sum_{i=0}^{\lambda-1} \gamma_1^{(\lambda-i)} Y_r(k+i) \quad (5\text{-}10)$$

   where χ and γ are the new sets of coefficients formulated based on the recurrent calculation of coefficients α and β in Equation (5-2).

2. When the step predicted manipulating trajectory is imposed, the cost function, $\hat{J}(k)$, is simplified to:

$$\hat{J}(k) = \left[\hat{Y}(k+\lambda) - Y_d(k+\lambda)\right]^T \left[\hat{Y}(k+\lambda) - Y_d(k+\lambda)\right] \quad (5\text{-}11)$$

   The predicted controlled signal, $\hat{Y}(k+\lambda)$, is calculated in terms of the measured signals and a predicted manipulating signal, $\hat{U}(k)$, as follows:

$$\hat{Y}(k+\lambda) = \sum_{i=1}^{\hat{n}} \hat{E}_i^{(\lambda)} Y(k+1-i) + \sum_{i=2}^{\hat{m}} \hat{F}_i^{(\lambda)} U(k+1-i) + \hat{H}^{(\lambda)} \hat{U}(k) \quad (5\text{-}12)$$

   where, $\hat{H}^{(\lambda)} = \hat{F}_1^{(\lambda)} + \hat{F}_1^{(\lambda-1)} + \hat{F}_1^{(\lambda-2)} + \ldots + \hat{F}_1^{(1)}$

3. Calculate the predicted manipulating signal, $\hat{U}(k)$, using the equation below:

$$\hat{U}(k) = \frac{Y_d(k+\lambda) - \sum_{i=1}^{\hat{n}} \hat{E}_i^{(\lambda)} Y(k+1-i) + \sum_{i=2}^{\hat{m}} \hat{F}_i^{(\lambda)} U(k+1-i)}{\hat{H}^{(\lambda)}} \quad (5\text{-}13)$$

4. Execute Steps 4, 5, 6 and 7 of the previously described MBPC system.

From the descriptions of the operating procedure, it should be realised that the MBPC system calculates the manipulating signal, $U(k)$, in every control cycle with respect to the

instantaneous states of the process and the cost function. To calculate the manipulating signal, $U(k)$, a predictive model is needed to predict the controlled signal, $\hat{Y}(k+\lambda)$. The predictive model expressed in Equation (5-12) represents the standard form of predictive model used in the MBPC system, namely a linear difference equation model. The simple structure of the linear difference equation model allows the calculations in Steps 2 and 3 to be accomplished conveniently.

It is remarked that a process model could be developed in many other forms including the fuzzy model, the PDE-based model and the semi-physical model as described in the previous chapters. To convert these other forms of model into a linear difference equation model, there is a need to decouple the parameters of the model but sometimes this is impractical. Therefore, their applications in the MBPC system are very limited.

Consequently, there is a need to find a method to combine the concept of the MBPC system with these other forms of model. In the present study, a Fuzzy supervisory indirect Learning Predictive Control (FsiLPC) is proposed. The operating mechanism of the FsiLPC system is similar to the MBPC system, but a different strategy is applied to calculate the manipulating signal, $U(k)$. The details of the FsiLPC system will be given in the rest of this chapter.

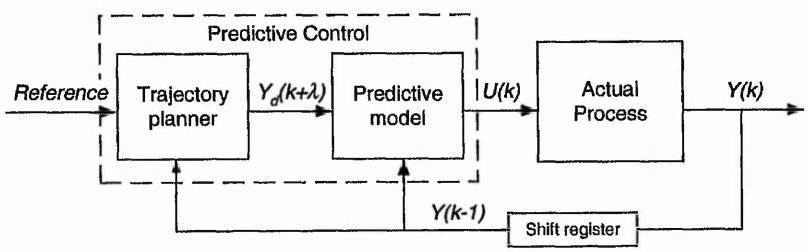

Fig. 5-2: MBPC system with step predicted manipulating trajectory.

5.3 Overview of Fuzzy supervisory indirect Learning Predictive Control (FsiLPC) System

In this section, an overview of the FsiLPC system by means of operating procedure is presented. The block diagram of the FsiLPC system is illustrated in Fig. 5-3. By visual comparison with the MBPC system depicted in Fig. 5-2, the FsiLPC system contains a functional block namely a fuzzy supervisory unit. The fuzzy supervisory unit is included to serve two functions. Firstly, it generates the manipulating signal, *U(k)*, to be applied to the process. Secondly, it also generates an 'imaginary' manipulating signal, $U'(k)$, to be used for the optimisation purpose. For the convenient of explanation, the fuzzy supervisory unit in executing the second function is designated as 'imaginary' fuzzy supervisory unit. The operating procedure of the FsiLPC system is presented as follows:

1. Calculate the desired controlled signal, $Y_d(k+\lambda)$, using Equation (5-10) in the trajectory planner.

2. Generate a manipulating signal, *U(k)*, using a fuzzy supervisory unit according to the desired controlled signal, $Y_d(k+\lambda)$.

3. Apply the manipulating signal, *U(k)*, to the process and the predictive model.

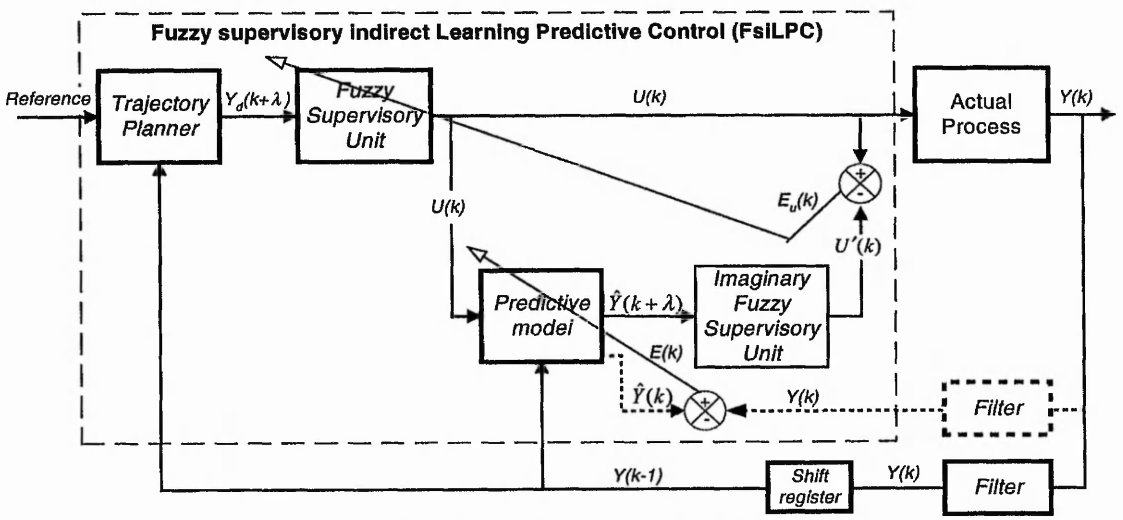

Fig. 5-3: Block diagram of the FsiLPC system.

4. Input the predicted process output, $\hat{Y}(k+\lambda)$, to the imaginary fuzzy supervisory unit. Compare the imaginary manipulating signal, $U'(k)$, and the applied manipulating signal, $U(k)$, to acquire a discrepancy. The discrepancy is termed as supervisory output error, $E_u(k)$, where:

$$E_u(k) = U'(k) - U(k) \tag{5-14}$$

5. Tune the fuzzy supervisory unit based on a cost function, $J_u(k)$, given below.

$$J_u(k) = E_u(k)^T E_u(k) \tag{5-15}$$

6. Measure the actual controlled signal, $Y(k)$, and the manipulating signal, $U(k)$.

7. Update the trajectory planner and the predictive model with the measurements.

8. Repeat Steps 1 to 7 for the next control cycle.

The FsiLPC system can be extended to be adaptive. This helps to improve the prediction of the model. The functional blocks for the adaptive mechanism are shown as dotted lines in Fig. 5-3. The procedure for the adaptive system is extended from previously described Step 7 as follows:

1. – 7. Identical to presented Step 1 – 7 in the non-adaptive FsiLPC system.

8. Compare the predicted controlled signal, $\hat{Y}(k)$, with the actual signal, $Y(k)$, to obtain the discrepancy of the prediction. The error signal, $E(k)$, is given as:

$$E(k) = \hat{Y}(k) - Y(k) \tag{5-16}$$

9. Tune the parameters of the predictive model according to the error signal, $E(k)$, using a cost function, $J(k)$, given in equation below.

$$J(k) = E(k)^T E(k) \tag{5-17}$$

10. Update the trajectory planner and the predictive model with the measurements.

11. Repeat Steps 1 to 10 for the next control cycle.

5.4 Operating Mechanism of FsiLPC System

This section describes the operating mechanism of the FsiLPC system. The block diagram in Fig. 5-4 shows different operating phases of the FsiLPC system. They are,

i) Control Phase (CP),

ii) Manipulating Signal Optimisation Phase (MSOP) and,

iii) Model Adaptation Phase (MAP).

These phases are executed sequentially in a complete control cycle as illustrated in Fig. 5-5. The manipulating signals are calculated and applied to the actual process and the predictive model during the CP, the fuzzy supervisory unit is tuned during the MSOP and the predictions of the predictive model are improved during the MAP. In the following sub-sections, these three operating phases will be detailed.

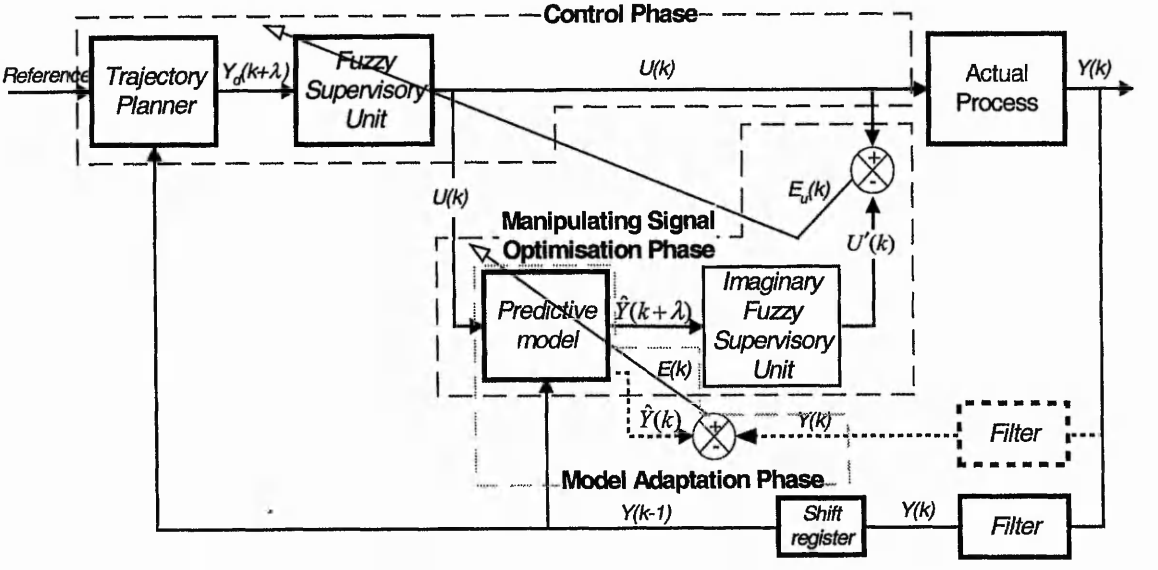

Fig. 5-4: Block diagram of FsiLPC system with operating phases.

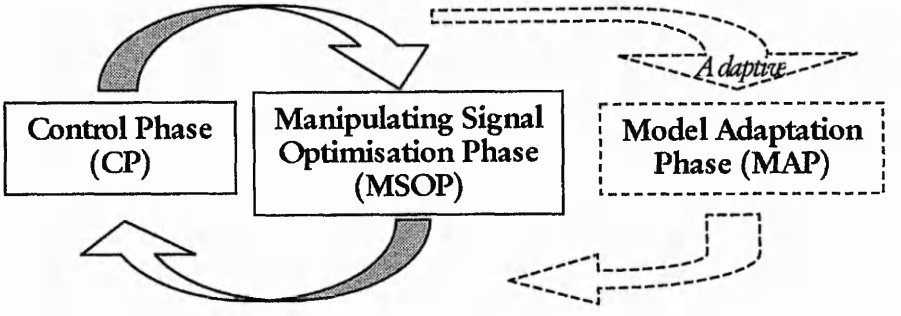

Fig. 5-5: A complete control cycle

5.4.1 Control phase

In the control phase, a manipulating signal, $U(k)$, is calculated and applied to the process. The functional blocks in this phase comprise a trajectory planner and a fuzzy supervisory unit as illustrated in Fig. 5-4.

The objective of the **trajectory planner** is to guide the controlled signal, $Y(k)$, to the reference signal, $Y_r(k)$, in a satisfactory manner. The function of a planner is expressed mathematically in Equation (5-10) to calculate only a desired signal at the end of the prediction horizon, $Y_d(k+\lambda)$. It is remarked that the parameters of the Equation (5-10) are different from the predictive model written in Equation (5-13). This means that the calculation for the desired signal, $Y_d(k+\lambda)$, is independent of the process dynamics. The function of the trajectory planner is normally developed upon the measured signal, $Y(k)$, and the reference signal, $Y_r(k)$. Therefore, the planner must be updated with the measurements in every control cycle to enhance the practicability of the calculation.

The **fuzzy supervisory unit** is developed to linguistically approximate the function of a manipulating parameter such as the screw speed and the barrel temperature in the extrusion process. It generates a manipulating signal, $U(k)$, based on the desired signal, $Y_d(k+\lambda)$, and is applied to the actual process and the predictive model. The function of the fuzzy supervisory unit, $\hat{G}_c(.)$, is given as:

$$u_\varphi(k) = \hat{G}_c(Y_d(k+\lambda), \hat{w}_\varphi(k)), \quad \varphi = 1, 2, 3, \ldots H \tag{5-18}$$

where $\hat{w}(k)$ is the parameter set of fuzzy supervisory unit, subscript φ is the label of the fuzzy supervisory unit and h is the number of the unit.

The fuzzy supervisory unit offers a flexibility to facilitate the parameter tuning so that an optimal manipulating signal could be produced. Although the input of the unit is only the desired signal, $Y_d(k+\lambda)$, the parameters of the unit, $\hat{w}(k)$, could be actively tuned to minimise the cost function given in Equation (5-15). The details of the fuzzy supervisory unit optimisation will be described in the next sub-section.

5.4.2 Manipulating signal optimisation phase

In this phase, the parameters of the fuzzy supervisory unit, $\hat{w}(k)$, are tuned so that the manipulating signal at next instant, $U(k+1)$, is optimised to drive the process output to the desired value. The functional blocks of this phase consist of a predictive model, an imaginary fuzzy supervisory unit and a comparator.

The **predictive model** predicts the future controlled signal, $\hat{Y}(k+\lambda)$, in response to the applied manipulating signal, $U(k)$, and the current states of the process. It should be realised that the FsiLPC system requires only the value of predicted signal, $\hat{Y}(k+\lambda)$, to perform the manipulating signal optimisation. The value of the predicted signal, $\hat{Y}(k+\lambda)$, is obtained through model simulation and this avoids the need of complicated formulation such as Equation (5-12). Therefore, the predictive model in the FsiLPC system could be considered as a 'black-box'. This provides the system with flexibility to incorporate any type of predictive model.

Regarding the predictive model as a black box requires the FsiLPC system to employ an indirect learning method, namely Controller Output Error Method (COEM), to optimise the manipulating signal. The underlying principle of the method is stated as follows. *Each time the response of a plant to a set-point signal is observed, we learn how to repeat that response, should it be required in future* (Andersen *et al*, 1997). In other words, the method requires the controller to learn from its experience. A simplified block diagram to illustrate the method is shown in Fig. 5-6. In Stage 1, the relationship of the action-consequence is observed. This information is then translated in Stage 2 by inputting the newly measured process output to the controller. Subsequently, an imaginary manipulating signal, $U'(k)$, is calculated. The controller function is then tuned based on the difference between the applied manipulating signal, $U(k)$, and the imaginary manipulating signal, $U'(k)$.

This concept of indirect learning is implemented in the FsiLPC system to tune the fuzzy supervisory unit. The predictive model provides the predicted controlled signal, $\hat{Y}(k+\lambda)$, in response to the manipulating signal, $U(k)$, being applied. To evaluate whether the signal $U(k)$ is optimal, a functional block namely **imaginary fuzzy supervisory unit** is assigned. The predicted controlled signal, $\hat{Y}(k+\lambda)$, is inputted to the imaginary fuzzy

supervisory unit to produce an imaginary manipulating signal, $U'(k)$. It should be clarified that the imaginary fuzzy supervisory unit in this phase (MSOP) and the fuzzy supervisory unit in the control phase (CP) belong to the same unit. The term 'imaginary' is used purely to distinguish the unit executed in two different phases. Therefore, the function of an imaginary fuzzy supervisory unit, $\hat{G}_c(.)$, is identical to the fuzzy supervisory unit,

$$u'_{\varphi}(k) = \hat{G}_c(\hat{Y}(k+\lambda), \hat{w}_{\varphi}(k)), \quad \varphi = 1, 2, 3, \ldots . H \tag{5-19}$$

where $u'_{\varphi}(k)$ is the imaginary manipulating signal.

Comparing Equation (5-18) and Equation (5-19), a difference in the input parameters of the imaginary fuzzy supervisory unit and the fuzzy supervisory unit can be noticed. The input parameter for the imaginary fuzzy supervisory unit is the predicted signal, $\hat{Y}(k+\lambda)$, while the desired signal, $Y_d(k+\lambda)$, is applied to the fuzzy supervisory unit. This implies that a discrepancy between the imaginary manipulating signal, $U'(k)$, and the actual manipulating signal, $U(k)$, exists due to the discrepancy between the predicted signal, $\hat{Y}(k+\lambda)$, and the desired signal, $Y_d(k+\lambda)$. The discrepancy in the manipulating signal is termed as the supervisory output error, $E_u(k)$, expressed in Equation (5-14).

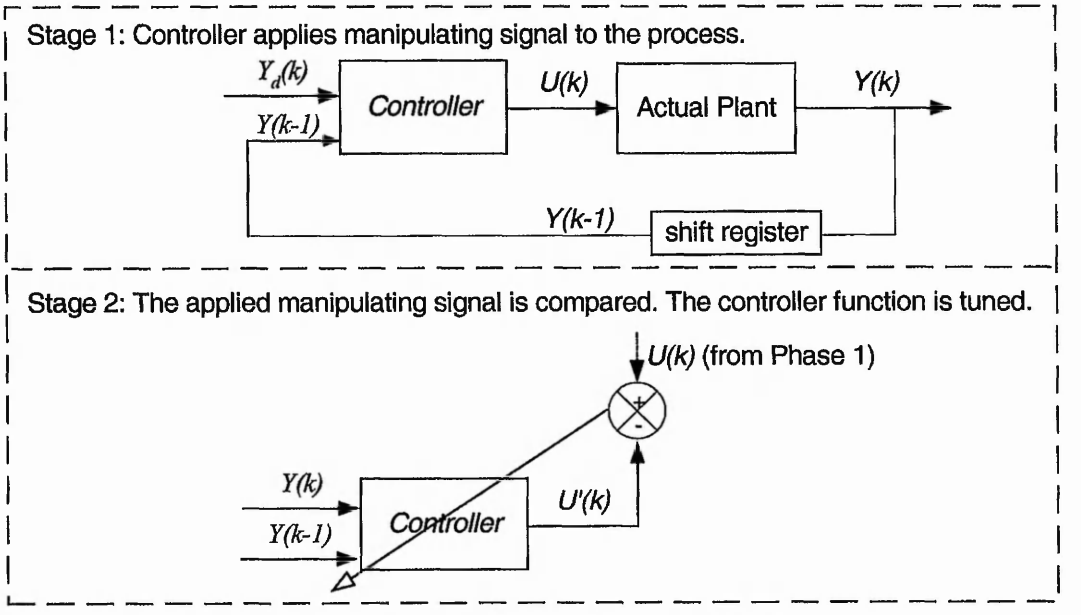

Fig. 5-6: Simplified diagram of control system employing COEM.

A cost function, $J_u(k)$, is introduced as a reference to minimise the supervisory output error, $E_u(k)$. The cost function given in Equation (5-15) is simple to apply but might lead to a localised optimum. A technique namely deadzone assumption is introduced as a remedy (Chen and Khalil, 1992). This technique keeps the system from over-fitting to the current operating region. The deadzone radius, δ, specifies the absolute lower limit to the activation of the manipulating signal optimisation. The squared error, x, is compared to the deadzone radius, δ, before any parameter tuning taken place. Therefore, the cost function in Equation (5-15) is rewritten under deadzone assumption as:

$$J_u(k) = \tfrac{1}{2} D[E_u(k)^T E_u(k)] = \tfrac{1}{2} D[x] \tag{5-20}$$

$$\text{Where, } D[x] = \begin{cases} x + \delta & \text{if } x < -\delta \\ 0 & \text{if } |x| < \delta \\ x - \delta & \text{if } x > \delta \end{cases}$$

The optimisation of the manipulating signal commences only if the squared error is greater than the radius. The gradient vector, $\partial J_u(k) / \partial \hat{W}(k)$, is calculated and the parameters of the fuzzy supervisory unit, $\hat{w}_\varphi(k)$, in Equation (5-18) are updated using the gradient descent method given below:

$$\hat{W}(k+1) = \hat{W}(k) - \eta \frac{\partial J_u(k)}{\partial \hat{W}(k)} \tag{5-21}$$

where η is the learning rate and $\hat{W}(k)$ is the vector of $\hat{w}_\varphi(k)$.

In an ideal case when the cost function is minimised, the imaginary manipulating signal, $U'(k)$, and the actual manipulating signal, $U(k)$, will converge. This indirectly means that the actual signal, $Y(k)$, should coincide with the reference signal, $Y_r(k)$, if the prediction of the model is accurate.

5.4.3 Model adaptation phase

Model adaptation phase is executed when the prediction error is beyond a preset tolerance. The adaptive ability of model is especially useful for a complicated process like the polymer extrusion process. In practice, the information of the process might be incomplete during the model identification and this subsequently introduces modelling

error. Furthermore, the parameters of the process might also vary. Therefore, it is required to tune the model parameters accordingly.

The functional blocks of the model adaptation phase include a predictive model and a comparator. When the control phase operation is completed, the actual signal, $Y(k)$, is measured and compared to the predicted signal, $\hat{Y}(k)$, to evaluate the accuracy of the prediction. The signal, $Y(k)$, should be filtered to represent only the instantaneous dynamics of the operating conditions. The cost function, $J(k)$, given in Equation (5-17) is formulated using the prediction error. The parameters of the model are then tuned based on the cost function through various techniques including error back-propagation and least square error method (Hsia, 1977). The details of the adaptation mechanism are described in Section 4.4 and they will not be repeated here.

The subsections above have elucidated the operating mechanisms at different phases of the proposed control system, which are summarised below:

- **Control phase:** Apply the manipulating signal, $U(k)$, generated by the fuzzy supervisory unit to the actual plant and the predictive model simultaneously.

- **Manipulating signal optimisation phase:** Compare the imaginary manipulating signal, $U'(k)$, and the actual manipulating signal, $U(k)$. Tune the parameters of the fuzzy supervisory unit so that at next instant, $k+1$, the discrepancy between these two manipulating signals is reduced. The convergence of the manipulating signals implies that the controlled signal, $Y(k)$, will also converge to the reference signal, $Y_r(k)$, if the prediction of the model is accurate. The control cycle is completed and to be repeated at the next instant, $k+1$, if the model adaptation phase is not activated.

- **Model adaptation phase:** Minimise the prediction error by tuning the model parameters according to the cost function, $J(k)$. The cost function is formulated by comparing the consistency between the predicted output and the process output. This phase is executed only when the prediction error is beyond the preset tolerance.

5.5 An Illustrative Example

Non-minimum phase dynamics are reported in several processes including ship navigation, missile autopilot, and aircraft aviation (Lopez and Rubio, 1992; Menon and Yousefpor, 1996; Chodavarapu and Spong, 1996; Tomlin *et al*, 1995). This case study demonstrates the development and the performance of the proposed FsiLPC system for a process with this behaviour. The system is developed under the assumptions of:

- the responses of the manipulating parameters are fast when compared with the transient responses of the process;
- an ideal dynamic process model is possible to obtain;
- the tuning of the fuzzy supervisory unit by the Controller Output Error Method (COEM) commences only when the closed-loop control system is stable;
- the reference signals are within the operating boundary of the fuzzy supervisory unit as in the identification process.

To illustrate the control of a system with non-minimum phase dynamic response, the following simple Single-Input-Single-Output transfer function, $G(z)$, is considered.

$$G(z) = \frac{-0.1274z + 0.1715}{z^2 - 1.332z + 0.4204} \qquad (5\text{-}22)$$

The step response of the process with the transfer function, $G(z)$, is shown in Fig. 5-7. The x-axis defines the duration while the y-axis denotes the amplitude of the response. The process output, $y(z)$, is driven initially to a negative direction when a positive step input, $u(z)$, is applied. The response of the process reaches a steady state condition after 30 seconds.

The stability of the process is estimated based on the locations of poles and zeros at a z-plane unit circle. The process has an unstable zero lying outside of the unit cycle as indicated in Fig. 5-8. This means that the manipulating signal trajectory, $u(.)$, needs to be unbounded in order to drive the output, $y(z)$, to the reference signal, $y_r(z)$. Unbounded manipulating signal is practically unrealisable, despite the system being theoretically stable. A possible solution might be applying a zero-pole cancellation technique, where the controller is designed with an unstable pole to cancel the unstable zero of the process. However, it requires accurate knowledge that might be impossible

to acquire for a complicated process. In the next sub-section, the ability of the FsiLPC system to deal with the problem without cancelling the unstable zero is presented.

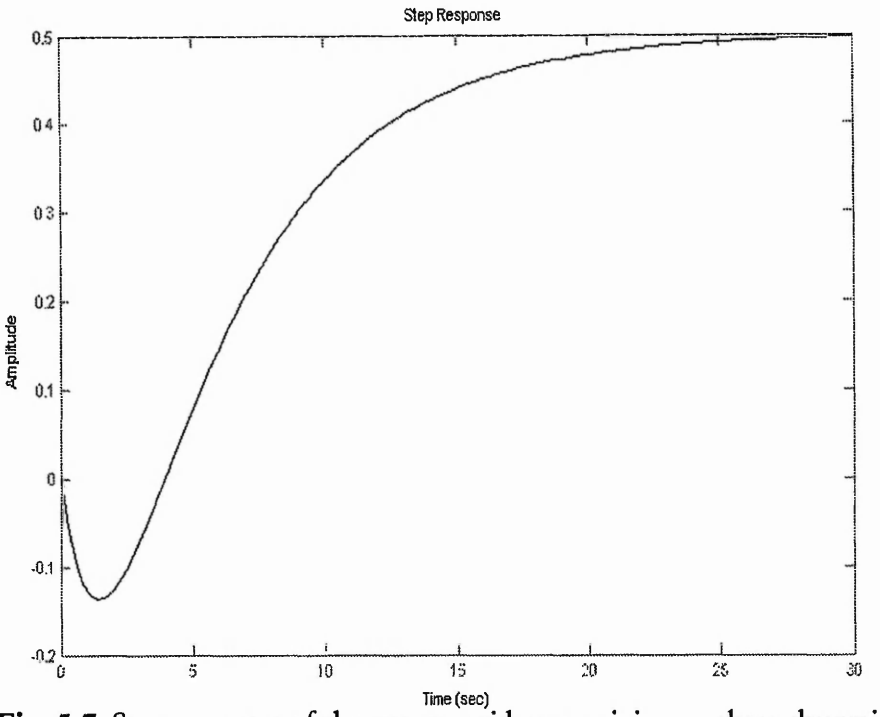

Fig. 5-7: Step-response of the process with non-minimum phase dynamics.

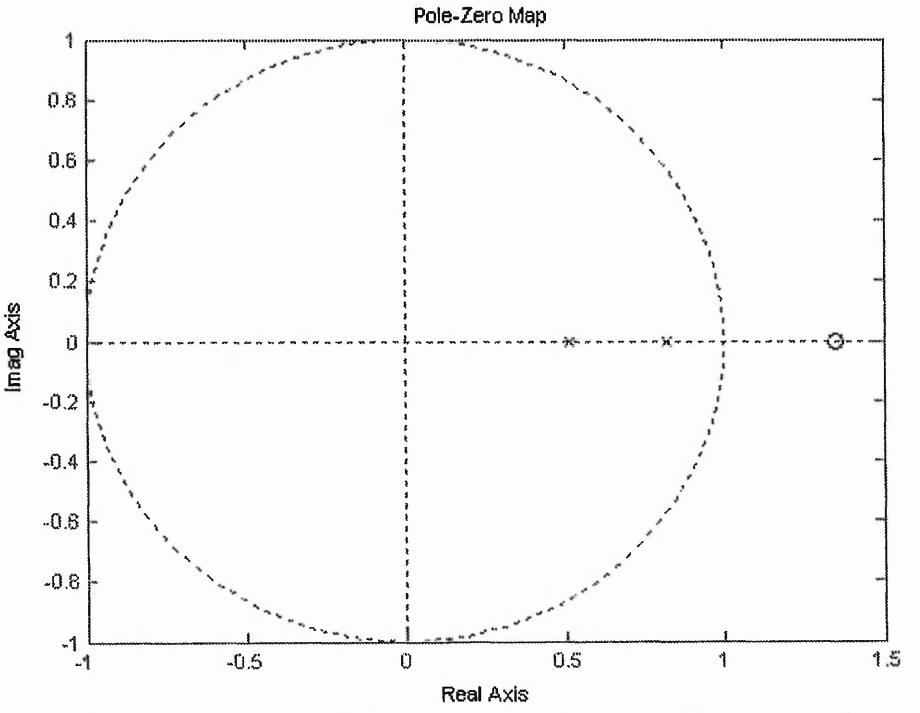

Fig. 5-8: Stability analysis of the process in the *z*-plane unit circle.

5.5.1 Development of a FsiLPC system

A one-input-one-output Fuzzy supervisory indirect Learning Predictive Control (FsiLPC) system is developed for the case study with the architecture shown in Fig. 5-9. The value of desired controlled signal is assumed to be constant during the prediction horizon, λ, and is taken to be the value of the reference signal, $y_r(k)$. Therefore, the function of the trajectory planner is simplified to:

$$y_d(k+\lambda) = y_r(k) \tag{5-23}$$

The fuzzy supervisory unit is a zero-order Sugeno-type of FRBS (Takagi and Sugeno, 1985). To produce data for identification of the unit, a range of manipulating signals is applied to the process, and the steady state process outputs are recorded. Then, the structure of the unit is obtained using the grid partition method based on the recorded data pairs. The input universe is divided into five regions with each region covered by a membership function, while the output universe is specified by five constants. Thus, only five rules are developed for the fuzzy reasoning. This initial structure of the fuzzy supervisory unit is then trained offline using a hybrid of least square and gradient descent error back-propagation methods to improve its approximating ability.

The predictive model is described by second order transfer functions with three sets of coefficients separately. This intends to evaluate the system performance in existence of the modelling error. The first model, $\hat{G}_1(z)$, is identified with the transfer function exactly given in Equation (5-22), to resemble an ideal model.

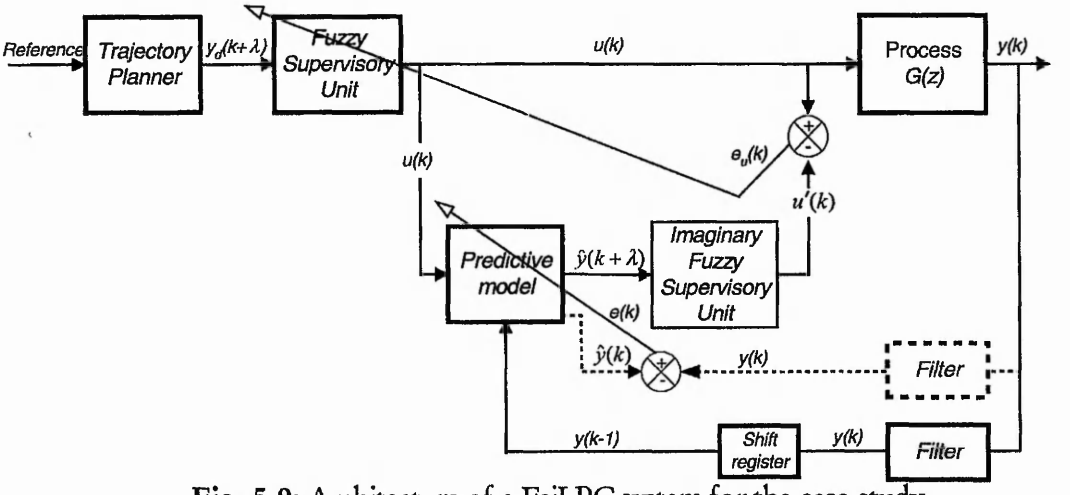

Fig. 5-9: Architecture of a FsiLPC system for the case study.

To evaluate the performance of the system in existence of modelling error, the second model is initiated with the coefficients of 10% deviation to the exact values. The transfer function, $\hat{G}_2(z)$, of the model is given in equation below.

$$\hat{G}_2(z) = \frac{-0.1401z + 0.1887}{z^2 - 1.4652z + 0.4522} \tag{5-24}$$

The case study also examines a situation when online identification of the process model is required due to the lack of information during the model development. The third model, $\hat{G}_3(z)$, is hence initiated with all coefficients set to a value of one.

$$\hat{G}_3(z) = \frac{z + 1}{z^2 + z + 1} \tag{5-25}$$

5.5.2 Results of simulations

The response of the FsiLPC system without tuning the fuzzy supervisory unit (open loop) is depicted as dotted line in Fig. 5-10. The transient response of process output, $y(k)$, (dotted line) is slow and a steady state error is noticeable. The figure also shows the performance of the system when the fuzzy supervisory unit is tuned. The system is assumed to have an ideal predictive model, $\hat{G}_1(z)$, and the settings of the prediction horizon are specified in the legend. When the prediction horizon is set to ten-steps-ahead, the controlled signal, $y(k)$, converges to the reference signal, $y_r(k)$, sooner with slightly overshooting (solid line). To evaluate the performance of the system on steady state error rejection, a sixty-steps-ahead prediction horizon is set. This resembles the prediction horizon of infinity. The result (heavy-dotted line) appears similar to the open loop system but the steady state error is significantly reduced. The dotted-dashed line shows the result of one-step-ahead prediction in which the actual signal, $y(k)$, diverges from the reference signal, $y_r(k)$. The manipulating signal, $u(k)$, in Fig. 5-11b is going unbounded until reaching the maximum limit of the fuzzy supervisory unit. The limit prevents the signal to continue diverging, which might lead to system instability.

The performance of the FsiLPC system is also compared to the MBPC system in three cases where the ideal predictive model, $\hat{G}_1(z)$, the model with 10% deviation in coefficients, $\hat{G}_2(z)$, and the model with unit coefficients, $\hat{G}_3(z)$, are employed. Both systems in all cases are subjected to a step-change in the reference signal. The prediction horizons of the systems are set to ten-step-ahead.

The responses in Fig. 5-11 indicate that a better performance is obtained for the MBPC system in the case when an ideal model is available. The manipulating signal, *u(k)*, is calculated accurately using Equation (5-13) to achieve a desired outcome, where the controlled signal, *y(k)*, (solid line in Fig. 5-11a) converges to the reference signal smoothly. The signal, *y(k)*, of the FsiLPC system (dotted line) is comparatively less ideal because of a greater overshoot and longer settling time.

The responses in Fig. 5-12a show that the outputs of both systems are not affected if the modelling error is subjected to only 10% deviation. The modelling error might have been corrected by the model adaptation phase during the operation. The FsiLPC system performs satisfactorily in the case when the coefficients of model are initialised with the value of one. The signal, *y(k)*, (dotted line) shown in Fig. 5-12b is more stable without radical changes when compared with the signal, *y(k)*, (solid line) for the MBPC system. These behaviours are attributed to different strategies employed to optimise the manipulating signal. The manipulating signal, *u(k)*, in the MBPC system is optimised mathematically, while the signal, *u(k)*, is optimised using the Controller Output Error Method in the FsiLPC system.

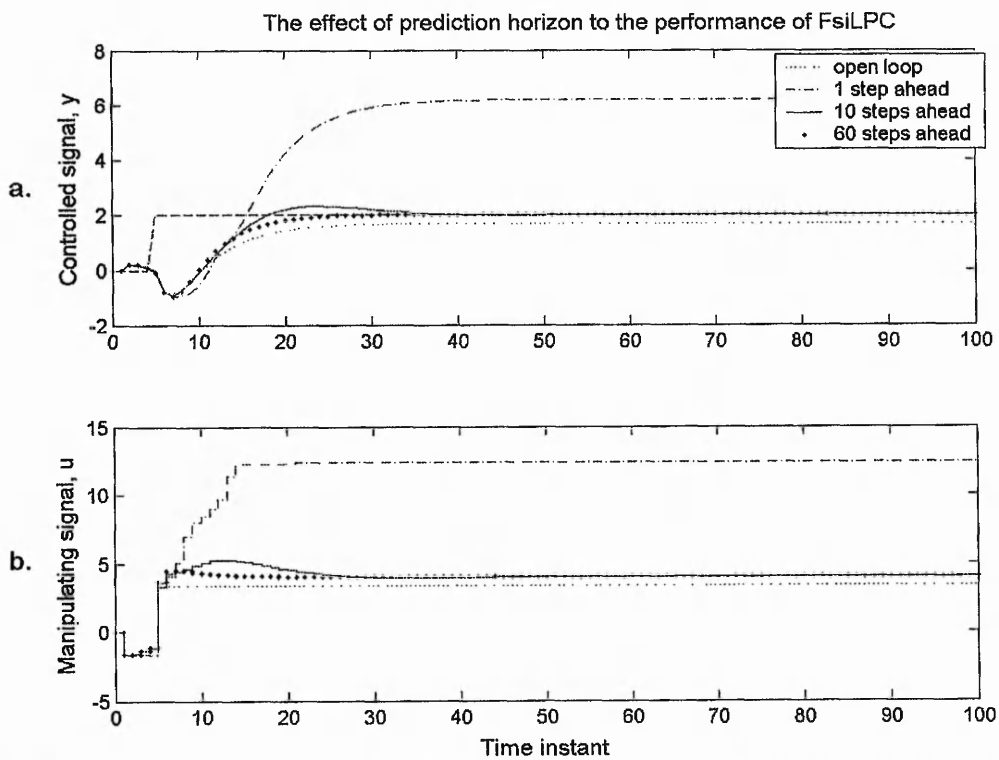

Fig. 5-10: FsiLPC system with different prediction horizon in tracking a step-change in reference signal: **a)** controlled signal, and **b)** manipulating signal.

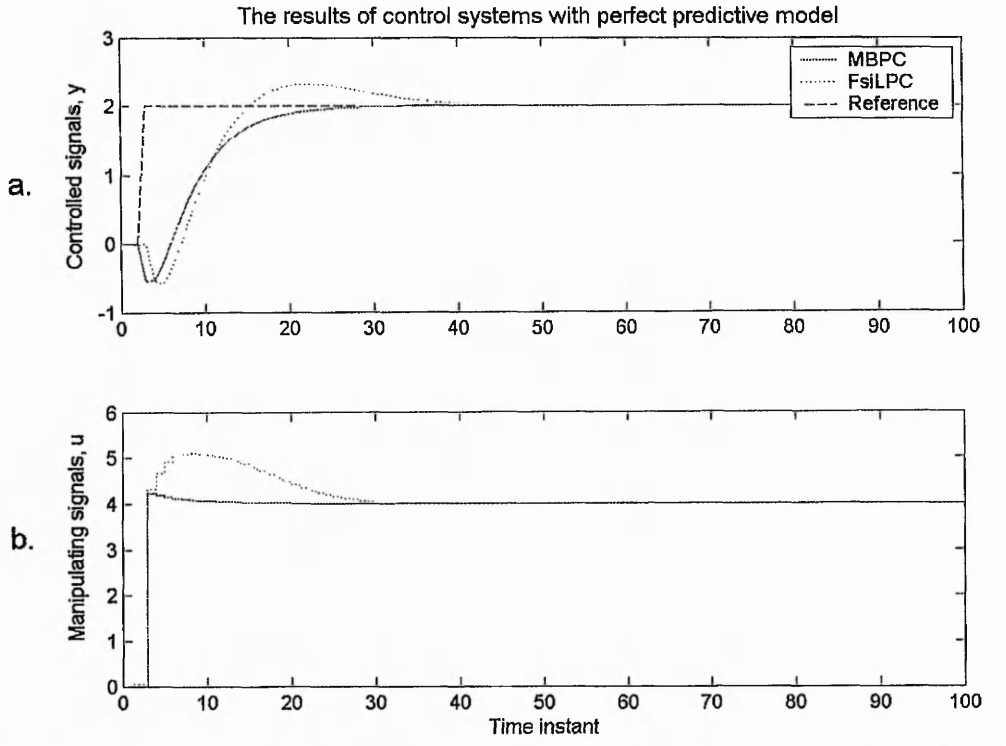

Fig. 5-11: Result comparison for the MBPC and the FsiLPC systems with ideal model: **a)** controlled signal, and **b)** manipulating signal.

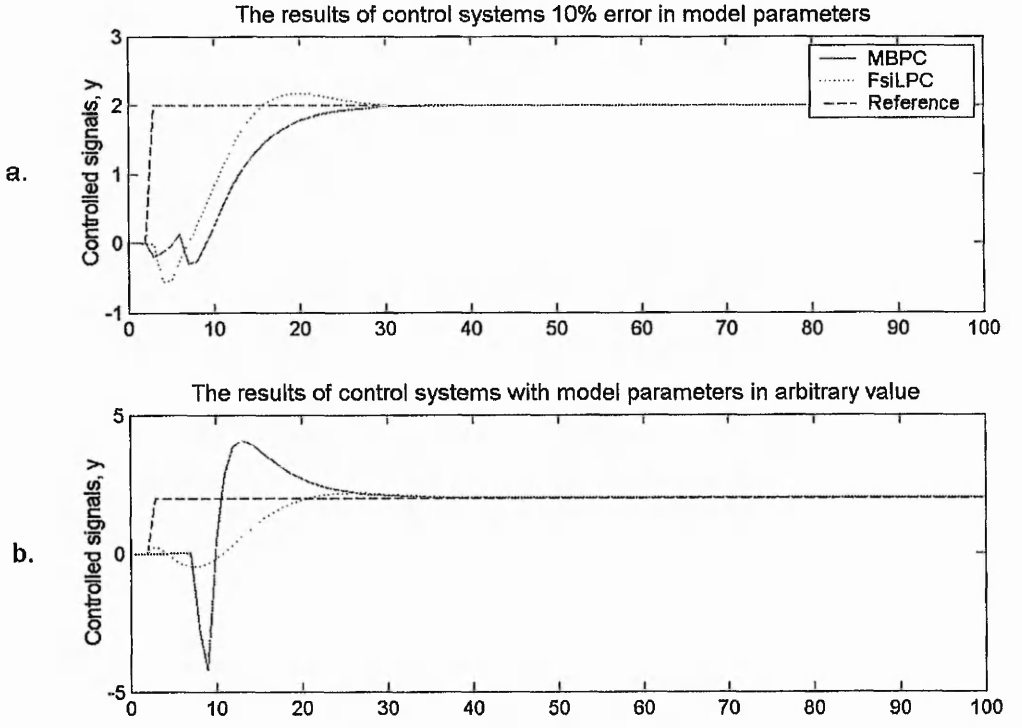

Fig. 5-12: Result comparison for the MBPC and the FsiLPC systems with model parameters of **a)** 10% error, and **b)** unit values.

5.6 Summary Remarks

Model Based Predictive Control (MBPC) is a useful control algorithm to develop a control system for the complicated process. A MBPC system utilises the process knowledge in a form of predictive model to optimise the control performance effectively. Nevertheless, the type of predictive model suitable for the MBPC system is found to be very limited. Most of the applications involve the use of linear difference equation models attributed to the simple structure. To combine the concept of MBPC with the semi-physical extrusion model, some modifications to the operating mechanism of the MBPC system are necessary.

It is demonstrated in this chapter that by using a different strategy to optimise the manipulating signals, the concept of the MBPC can be implemented using the semi-physical model as the predictive model. The operating mechanism of the resultant control system, namely Fuzzy supervisory indirect Learning Predictive Control (FsiLPC) system, has been described with reference to three phases. In the control phase, a fuzzy supervisory unit generates a manipulating signal in response to the reference signal. This manipulating signal is then applied to the actual process and the predictive model. In the manipulating signal optimisation phase, the parameters of the fuzzy supervisory unit are tuned using the COEM. The tuning process is dependent on the discrepancy between the applied manipulating signal and the imaginary manipulating signal. The convergence of these two manipulating signals will lead to the convergence of the reference signal and the actual controlled signal. In the model adaptation phase, the parameters of the predictive model are tuned to improve accuracy of the predictions. Similar to the MBPC system, the accuracy of the model predictions is also very important in the FsiLPC system.

A simple case study was presented as an example to illustrate the development of the FsiLPC system. The performance of the FsiLPC system was compared with the MBPC system in tracking a step-change in the reference signal. The results were promising. Therefore, it is expected that the FsiLPC system will also enhance the performance of the extrusion process. The development and the performance of the FsiLPC system for the extrusion process will be evaluated in the next chapter.

Chapter 6
Simulation Studies

6.1 Introduction

The concept of the Fuzzy supervisory indirect Learning Predictive Control (FsiLPC) has been elaborated in the previous chapter. This approach has the capability of using a predictive model of any structure. In this chapter, the development and the implementation of a FsiLPC system for the extrusion process are presented. The melt temperature and the melt pressure are the controlled parameters while the screw speed and the barrel temperature are the manipulating parameters.

The performance of the FsiLPC system for the extrusion process is evaluated by means of simulation studies namely a parametric study and a comparative study. The parametric study investigates the response of the system with respect to changes in process parameters, determines the suitable setting of system parameters and evaluates the system robustness. The comparative study is conducted to compare the performance of the FsiLPC system with the conventional extrusion control systems namely the PI and the Self-Tuning Regulator (STR) control systems. These three control systems are evaluated with respect to the performance of:

- tracking the changes of reference signals;
- minimising the impact of the process disturbances.

In practice, the reference signals are seldom changed during the operation. However, it is considered prudent in the simulation studies to observe the tracking performance of the control systems, which would provide a convenient measure of the system ability in driving the controlled signals. The second evaluation examines the ability of the control systems in minimising the variations in the melt temperature and the melt pressure due to the process disturbances. The disturbances in the case studies resemble the actual process disturbances as detailed in Chapter 3.

6.2 Development of a FsiLPC System for the Extrusion Process

A two-input-two-output FsiLPC system is developed, which comprises a trajectory planner, two fuzzy/imaginary fuzzy supervisory units, a predictive model, and filters as depicted in Fig. 6-1. The trajectory planner is designed with a simple function. The desired controlled signal vector is assumed to be constant during the prediction horizon, and taken to be the reference signal vector. This is expressed as follows:

$$P_d(k+\lambda) = P_r(k) \tag{6-1}$$

$$T_d(k+\lambda) = T_r(k) \tag{6-2}$$

where P_d is the desired melt pressure, T_d is the desired melt temperature, λ is prediction horizon, P_r and T_r are the reference pressure and temperature respectively.

Each fuzzy supervisory unit consists of only two inputs and one output. The inputs to the fuzzy supervisory unit of screw speed are the reference melt temperature, $T_r(k)$, and the reference pressure, $P_r(k)$, while the output is the screw speed, $\alpha(k)$. For the fuzzy supervisory unit of barrel temperature, the inputs are also the reference melt temperature, $T_r(k)$, and the reference pressure, $P_r(k)$, while the output is the barrel temperature, $T_b(k)$. The fuzzy supervisory units are initialised with nine rules and three membership functions for each input universe. To improve the accuracy of approximation, a hybrid least square and gradient descent error back-propagation method is employed to train the initialised fuzzy supervisory units.

The predictive model employed in the FsiLPC system is the semi-physical dynamic extrusion model described in Chapter 4. The model is governed by a set of complex equations with the operational-sensitive parameters approximated by the FRBS sub-models. Numerical calculation method is required for the model simulation. The initial conditions of the predictive model are always taken from the updated measurements of the process parameters. Filters are used to eliminate signals with undesired frequencies during the operation. The effective cut-off frequencies of the filters for given operating conditions are obtained from Chapter 3.

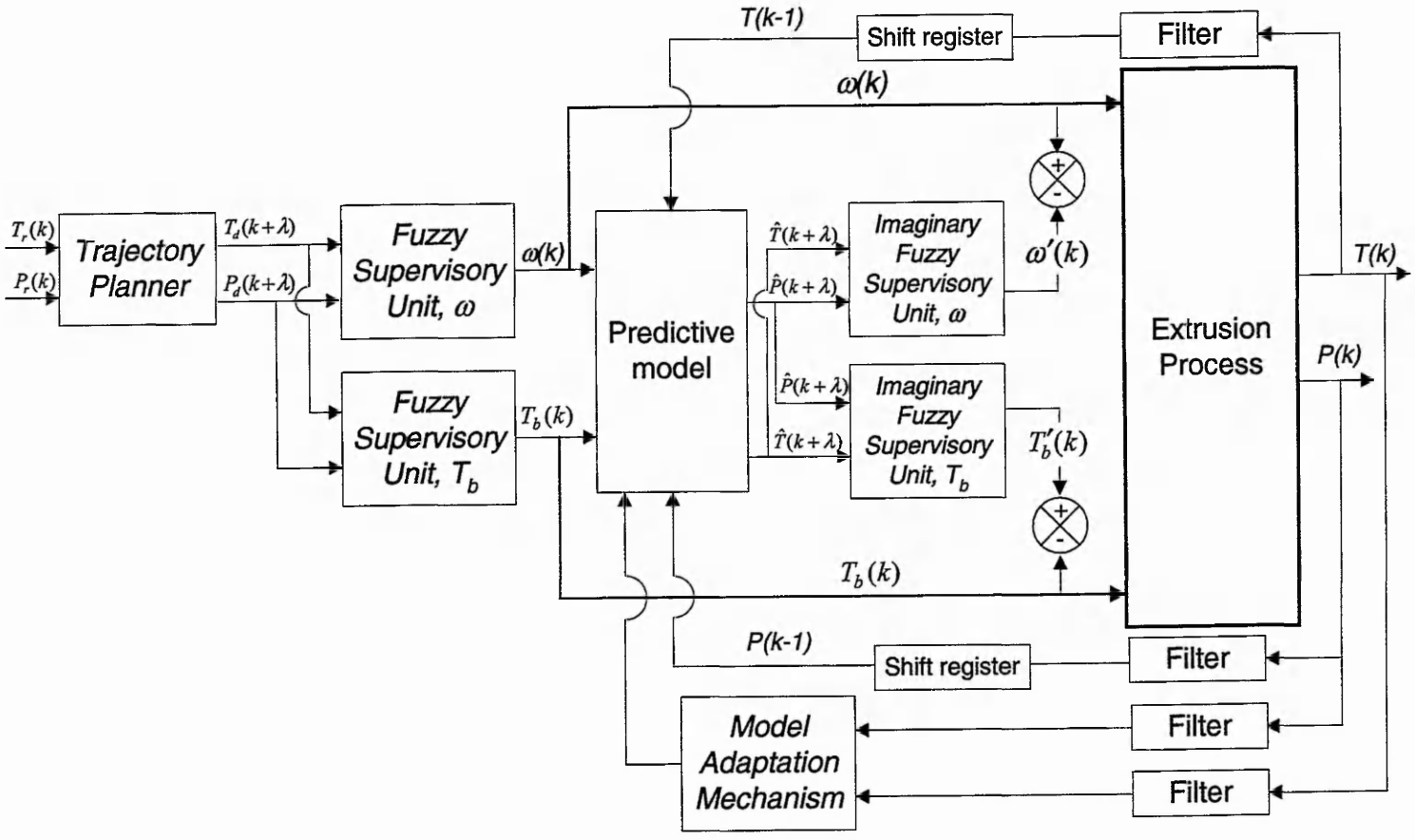

Fig. 6-1: Architecture of the FsiLPC system for the extrusion process.

6.3 A Parametric Study

To estimate the characteristics of a control system, a parametric study may prove useful. In this parametric study, the effects of possible variations in the system parameters are investigated. The study firstly examines the response of the system with respect to the variations in the screw speed and the barrel temperature, to be followed by the dynamic response of barrel temperature. Then, the system performance with respect to the changes in the reference signals, the parameter settings and the variations in the process disturbances is also evaluated.

6.3.1 Screw speed and barrel temperature

This section investigates the open loop response of the system to changes of the screw speed and the barrel temperature. It is shown in Fig. 6-2 that the melt temperature increases with the barrel temperature and the screw speed. When the barrel temperature is set to a high value, an increment in the screw speed has less impact on the system response. The response in Fig. 6-3 indicates that the melt pressure is strongly controlled by the screw speed, while the barrel temperature produces only a negligible impact. The latter could be the reason to find that none of the melt pressure control in the literature (first bar in Fig. 2-7) uses the barrel temperature as the manipulating parameter.

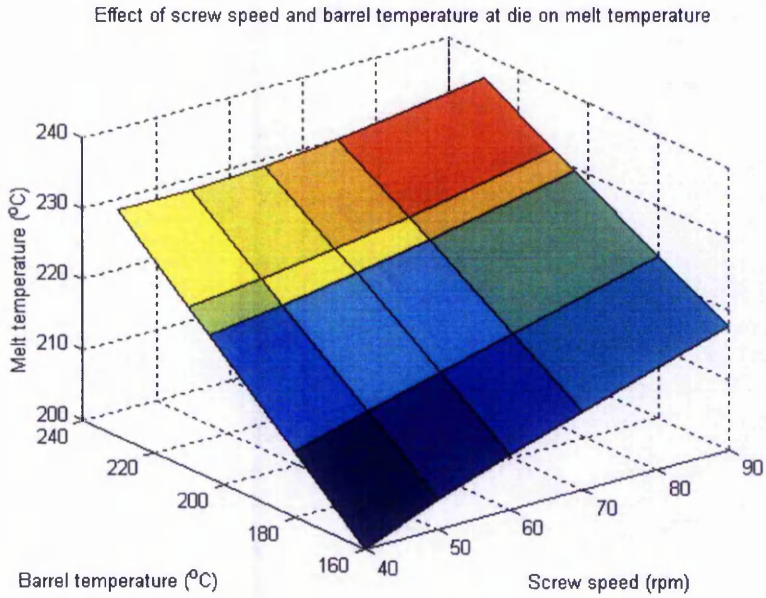

Fig. 6-2: Variations in manipulating parameters to the melt temperature.

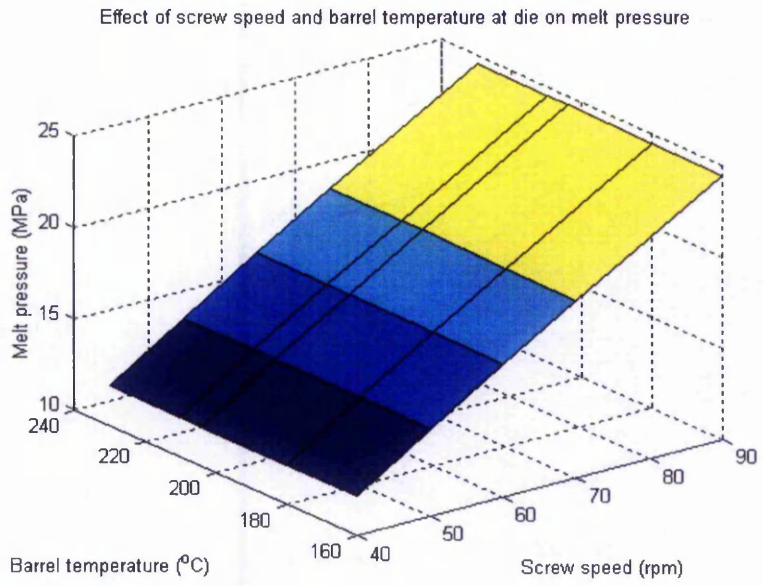

Fig. 6-3: Variations in manipulating parameters to the melt pressure.

6.3.2 Dynamic response of the barrel temperature

The dynamic response of the screw speed is mainly determined by the electric motor. It is relatively fast if compared with the process dynamics. Meanwhile, the dynamic response of the barrel temperature is determined by the barrel heater. The response is relatively slow and exhibits a large transportation lag (pure time delay). The delay occurs when the heat is transferred from the outer barrel wall to the inner barrel wall surface that contacting with the polymer melt. In general, the barrel temperature response could be approximated by a first order transfer function with a pure time delay. The case study investigates the closed loop response of the FsiLPC system in rejecting the process disturbances, when the time constant and the pure time delay of the barrel temperature response are varied.

From the results in Section 6.3.1, it is realised that changes in the barrel temperature would only affect the consistency of the melt temperature but not the melt pressure. Therefore, the current case study evaluates the performance of the FsiLPC system with reference to the standard deviation of the melt temperature as shown in Fig. 6-4. The flat mesh plane represents the standard deviation of the open loop system. The surface below the flat mesh plane represents the FsiLPC system with better performance than

that of the open loop system and vice versa. Increasing the pure time delay causes a larger deviation and the effect is seen clearly when the time constant is small. The standard deviation enters a high plateau when the time constant is above 100 seconds. This suggests that the barrel heater becomes ineffective when the time constant is larger than 100 seconds, even without any pure time delay. The changes of the actual heat supply are too slow when compared with the disturbances on the melt temperature.

The standard deviation surface in Fig. 6-4 can also be served as a guideline to design an effective barrel heater for the control system. For instance, it suggests that the barrel heater with a pure time delay below 40 seconds and a time constant below 100 seconds is useful. The requirements may be fulfilled if the barrel heater is located nearer to the melt by having a thinner wall, or the wall is fabricated with the materials of good heat conductivity such as the aluminium alloy. The design of the barrel wall, however, must always account for the enormity of the melt pressure during the operation. The pressure is especially high in the compression section of the extruder.

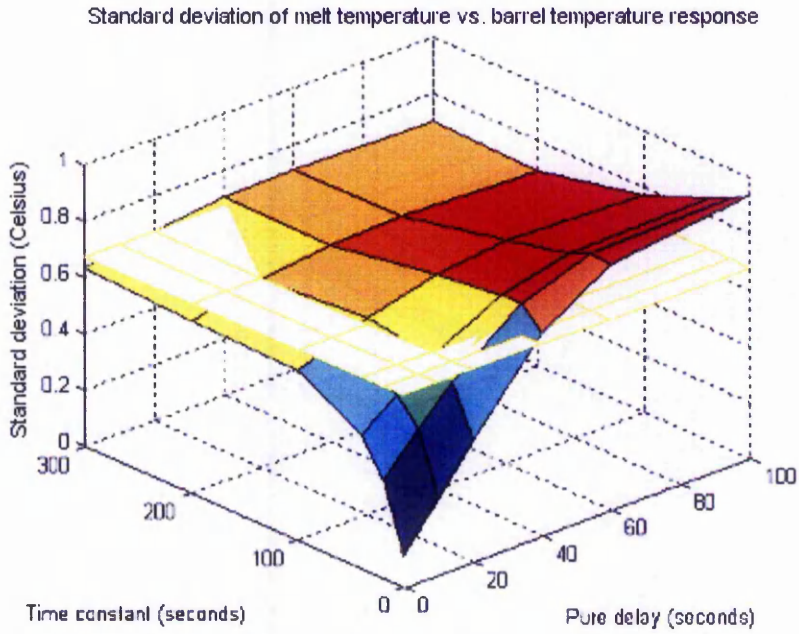

Fig. 6-4: Variations in barrel temperature response to system performance.

6.3.3 Changes in the reference signals

In this section, the response of the FsiLPC system with respect to the changes in the reference signals is examined. The reference signals are changed at a range of frequency from every 50 seconds (Fig. 6-5) to every 1 second (Fig. 6-6). The FsiLPC system performs reasonably well when the reference signals are slowly changed. The controlled signals converge to the reference signals as indicated in Fig. 6-5. However, the system performance deteriorates when the changes in the references are rapid. The melt temperature in Fig. 6-6 almost remains constant while the melt pressure responds in opposite direction at some instances. The system performance in response to various frequencies of changes in the references is depicted in Fig. 6-7. It is noticed that the root-mean-square errors of the melt temperature and the pressure increase with the frequencies of changes. The dynamic response of the system could find it difficult to cope with the rapid changing references. This observation also implies the system inability to respond to the rapid-changing disturbances.

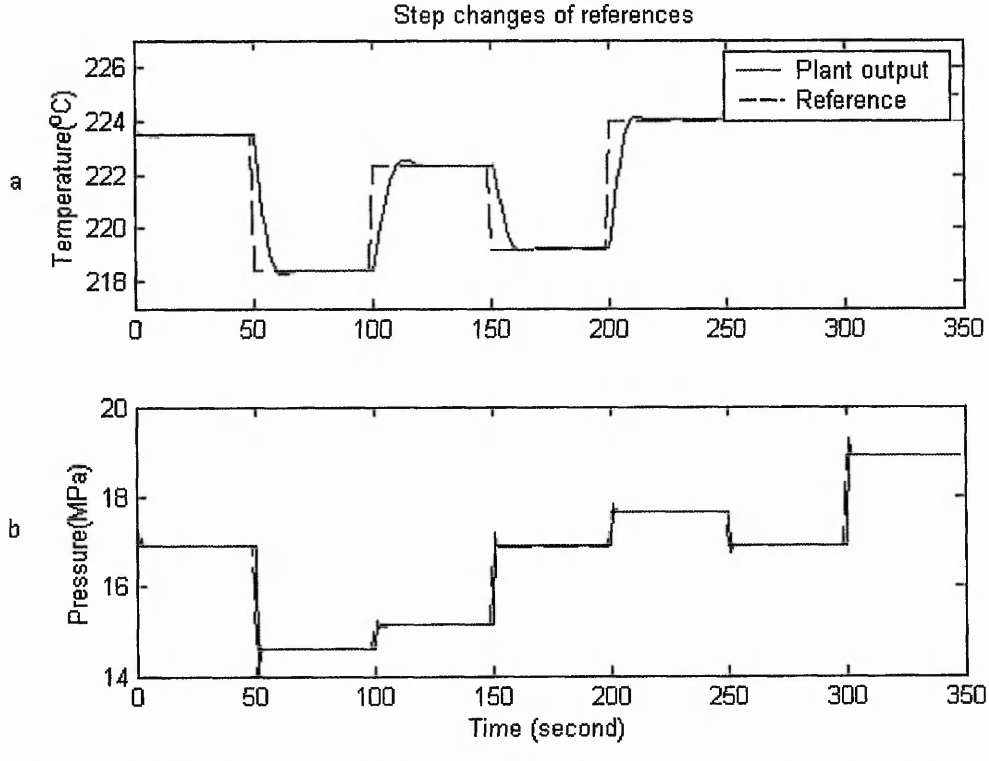

Fig. 6-5: Reference signals change at every 50 seconds: **a)** melt temperature, and **b)** melt pressure.

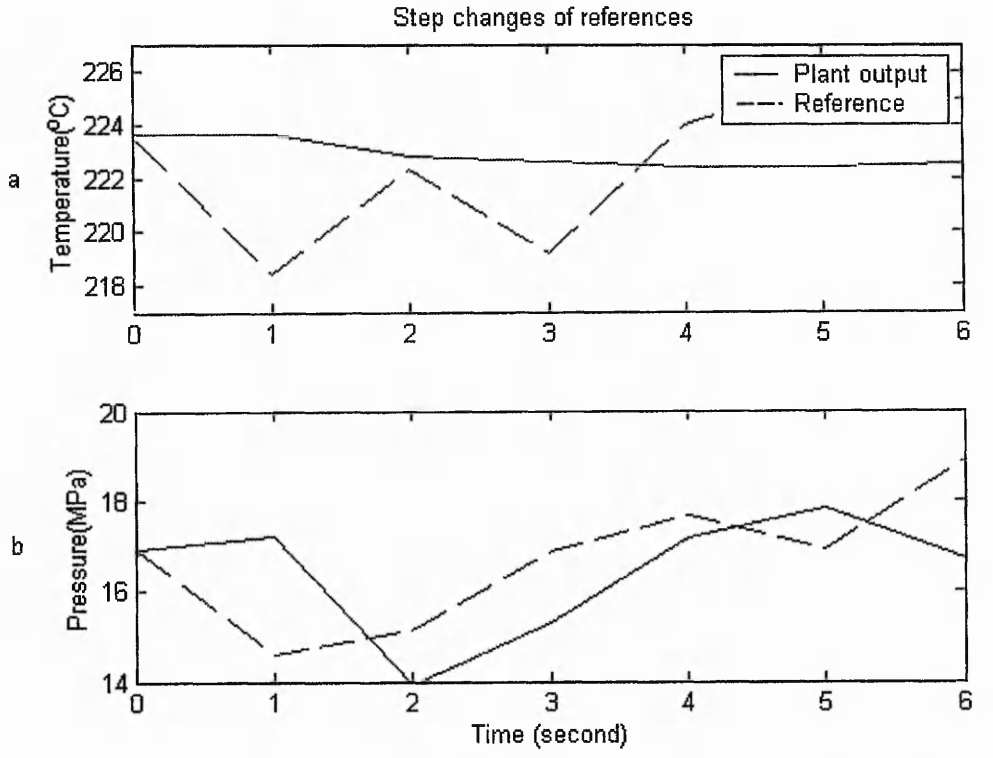

Fig. 6-6: Reference signals change at every 1 second: **a)** melt temperature, and **b)** melt pressure.

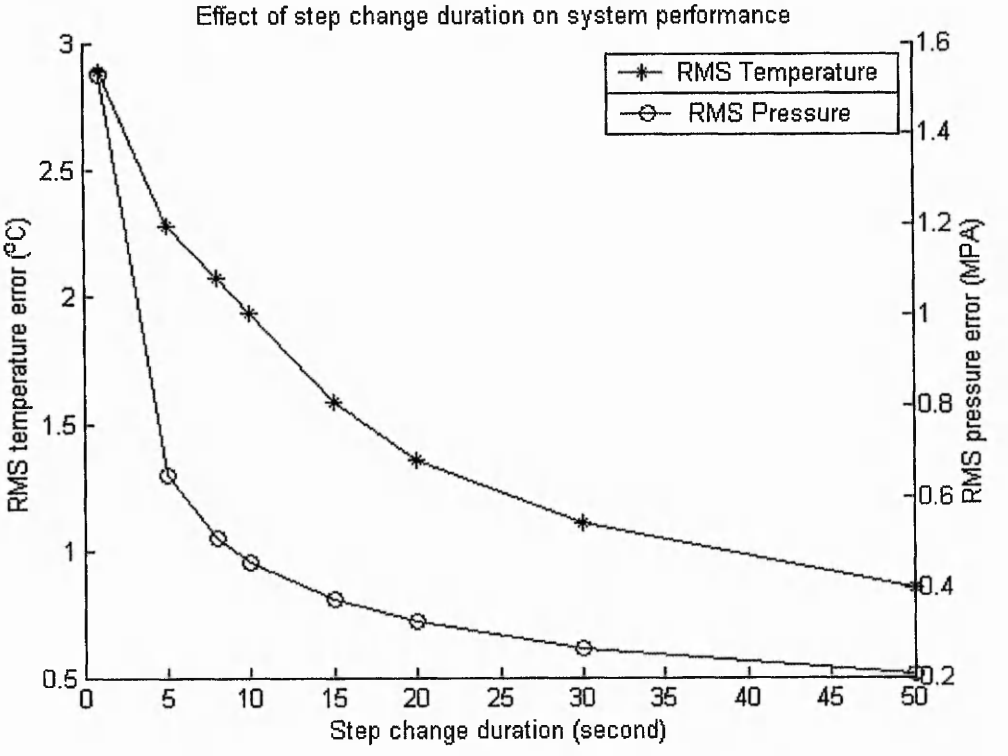

Fig. 6-7: System performance in response to frequency of changes of reference signals.

6.3.4 The best possible controller

The best possible controller of the FsiLPC system is determined by several factors. These include the initial Euclidean distances, the settings on deadzone radii, model adaptation, learning rates and prediction horizons. The definitions of these factors are detailed in Appendix 6. The system performance in response to the variations in each factor is examined here.

Initial Euclidean distances

Initial Euclidean distance is a difference between the parameter vectors of the best possible and the current fuzzy supervisory unit, which is abstractive and not measurable. However, the Euclidean distance affects the accuracy of the fuzzy supervisory unit in approximating the function of a manipulating parameter. This provides an indirect estimation of the Euclidean distance, where Mean Square Error (MSE) of the approximation is measured.

The relationships between the initial Euclidean distances and the system performance are depicted in Fig. 6-8. The bar graph is scaled with the *y*-axis at the left while the line graph is scaled with *y*-axis at the right. The heights of bar graph represent the initial Euclidean distances of the fuzzy supervisory units. The fuzzy supervisory units of screw speed and barrel temperature are indicated in the legend. The performance of the FsiLPC system is measured by means of standard deviations of the melt temperature and the pressure at the die. The solid and dotted lines signify the melt temperature and the pressure respectively. The standard deviations of both temperature and pressure increase with the initial Euclidean distances.

A case study of the FsiLPC system with a set of poor fuzzy supervisory units (set 3 in Fig. 6-8) is also investigated. The term 'poor' in the context is defined as the fuzzy supervisory unit with a large initial Euclidean distance. The melt temperature at the die shown in Fig. 6-9a deviates very much from the reference temperature at the beginning but eventually the temperature is bounded. The similar behaviour is observed in Fig. 6-9b for the melt pressure. The results suggest that the stability of the control system is less sensitive to the initial Euclidean distance of the parameter vectors, provided that the fuzzy supervisory units are reasonably identified.

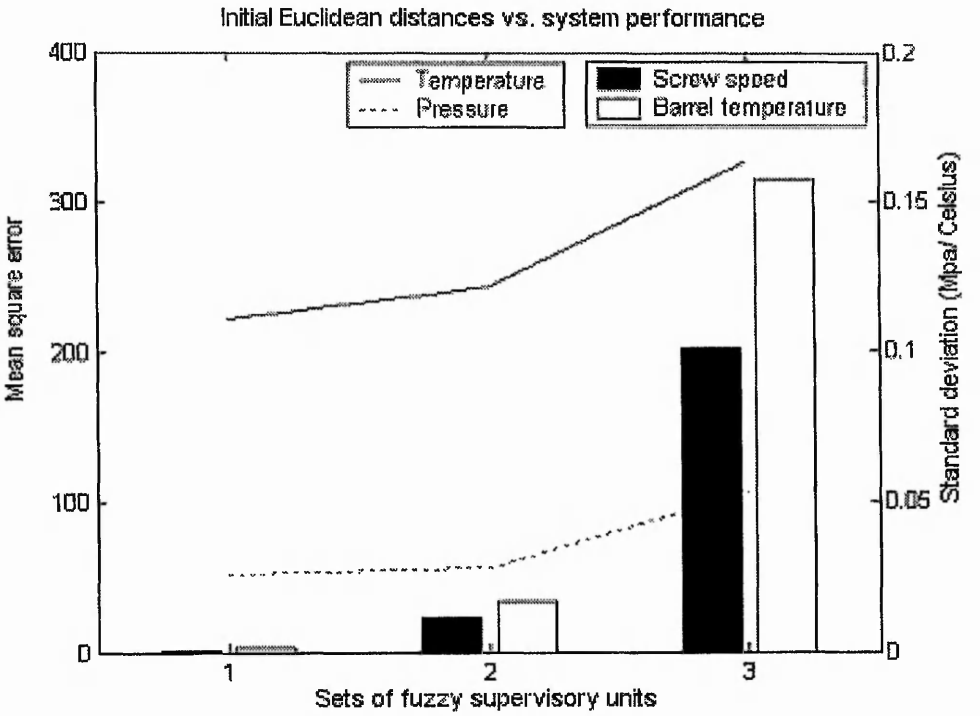

Fig. 6-8: Effect of initial Euclidean distance on system performance.

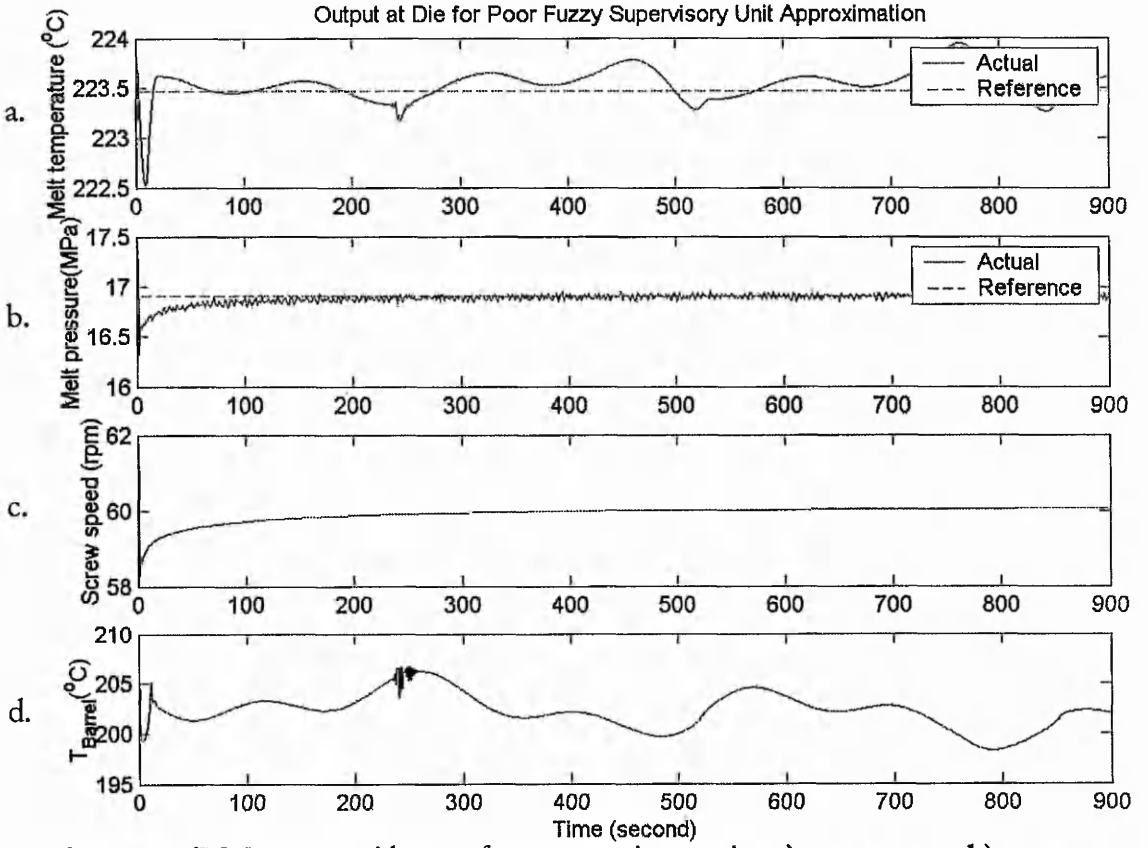

Fig. 6-9: FsiLPC system with poor fuzzy supervisory units: **a)** temperature, **b)** pressure **c)** screw speed, and **d)** barrel temperature.

Deadzone radii

The second factor that determines the best possible controller is the deadzone radius of each fuzzy supervisory unit. The objective of having the deadzone radius is to avoid deterioration of the overall system performance while adapting the controller parameters to the localised system optimum.

The strategy to evaluate the deadzone radii is illustrated in Fig. 6-10. The reference signal vector is step-changed from time to time to measure the overall performance of the system. This is especially useful to identify if the fuzzy supervisory units are over-trained to the localised conditions. The effects of variations in the deadzone radii for the fuzzy supervisory units of screw speed and barrel temperature are presented in Fig. 6-11 and Fig. 6-12 respectively. At the large deadzone radii, the learning of the fuzzy supervisory units is less sensitive and this produces larger standard deviations on the melt temperature and pressure. If the radii are too small, the overall performance also deteriorates ascribed to the over-training of parameters. Though, the effects are relatively trivial if compared with the large deadzone radii. The optimal deadzone radii for the fuzzy supervisory units are difficult to be proven theoretically. However, Fig. 6-11 and Fig. 6-12 could be treated as a reference in setting the radii.

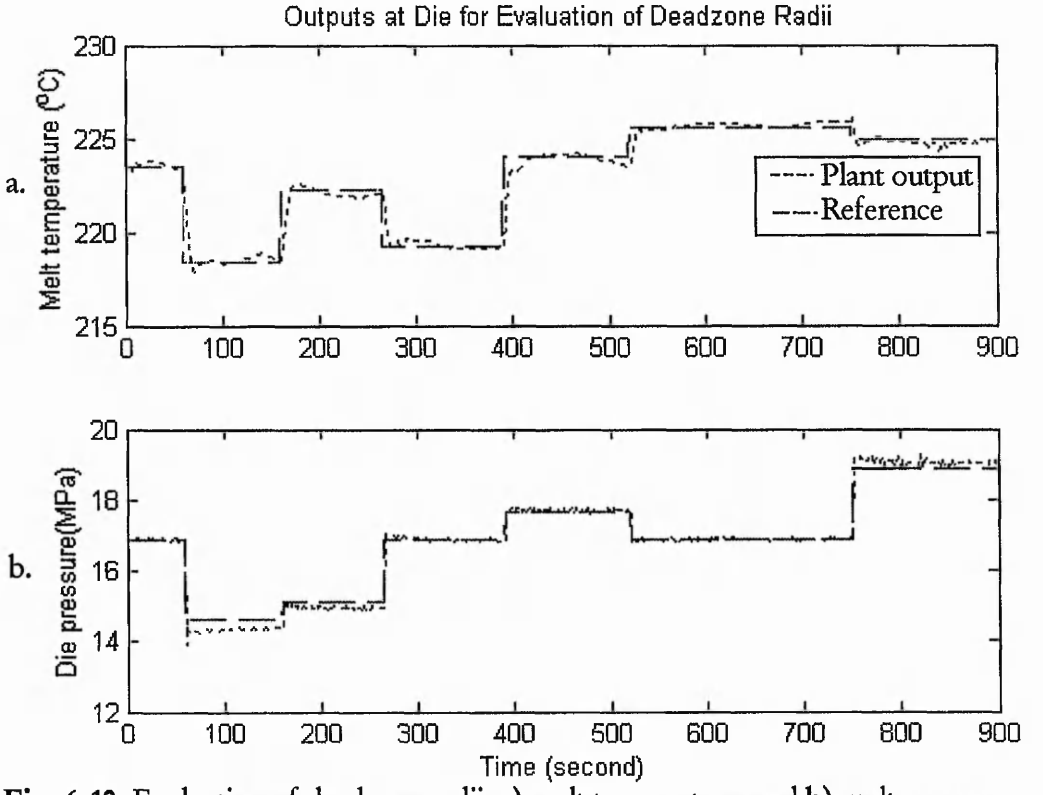

Fig. 6-10: Evaluation of deadzone radii: **a)** melt temperature, and **b)** melt pressure.

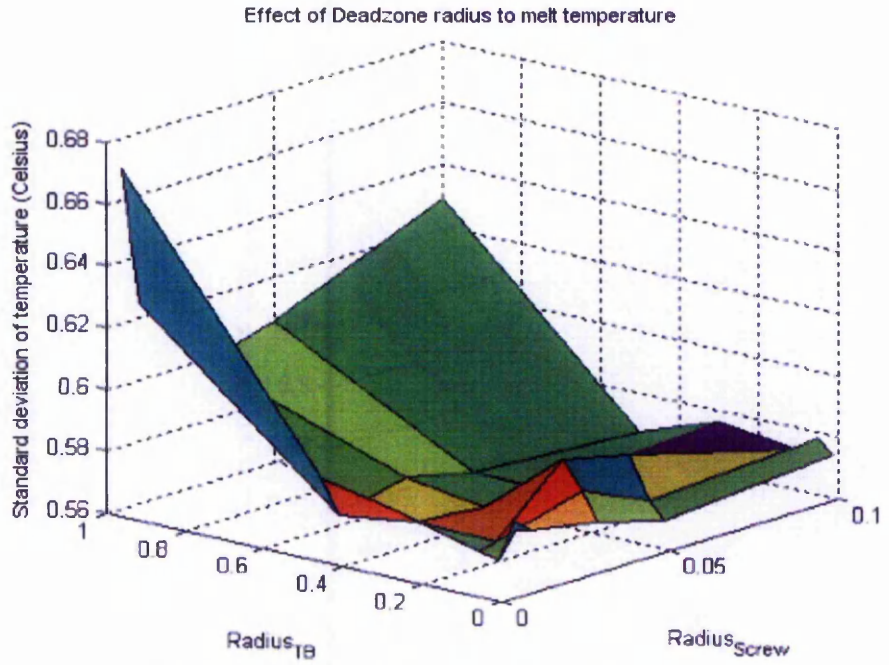

Fig. 6-11: Effect of deadzone radii on melt temperature.

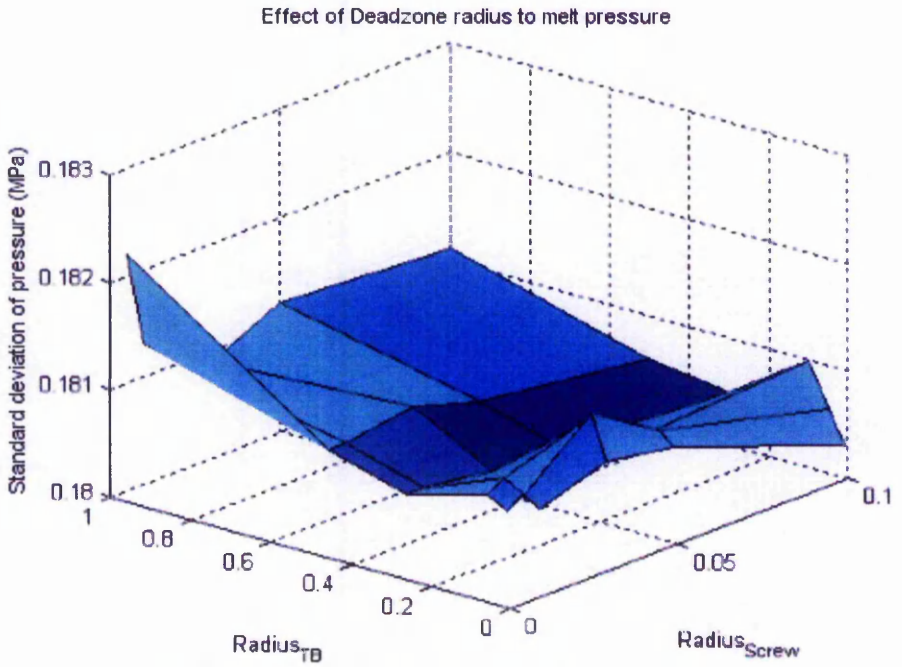

Fig. 6-12: Effect of deadzone radii on melt pressure.

Model adaptation setting

An ideal predictive model is not easy to obtain. The required process knowledge might be incomplete during the model identification and the operating conditions might vary during the operation. This leads to a modelling error, which affects the system performance since the tuning of the fuzzy supervisory unit is reliant upon the model prediction. In this section, the semi-physical dynamic extrusion model with the modelling error is examined.

The response of open loop extrusion system is illustrated in Fig. 6-13. The melt temperature at the die (dotted line in Fig. 6-13a) fluctuates around 223.5 °C while the melt pressure (dotted line in Fig. 6-13b) varies around 16.9 MPa at a higher frequency. When the FsiLPC system is implemented, the modelling error causes the divergences of the controlled signals shown as dotted lines in Fig. 6-14. The dotted lines in Fig. 6-15 represent the controlled signals when the model adaptation phase is activated. In comparison with the outputs of the open loop system (Fig. 6-13), the melt temperature is regulated closer to the desired temperature. The long-term drift in the melt pressure is also eliminated after 100 seconds.

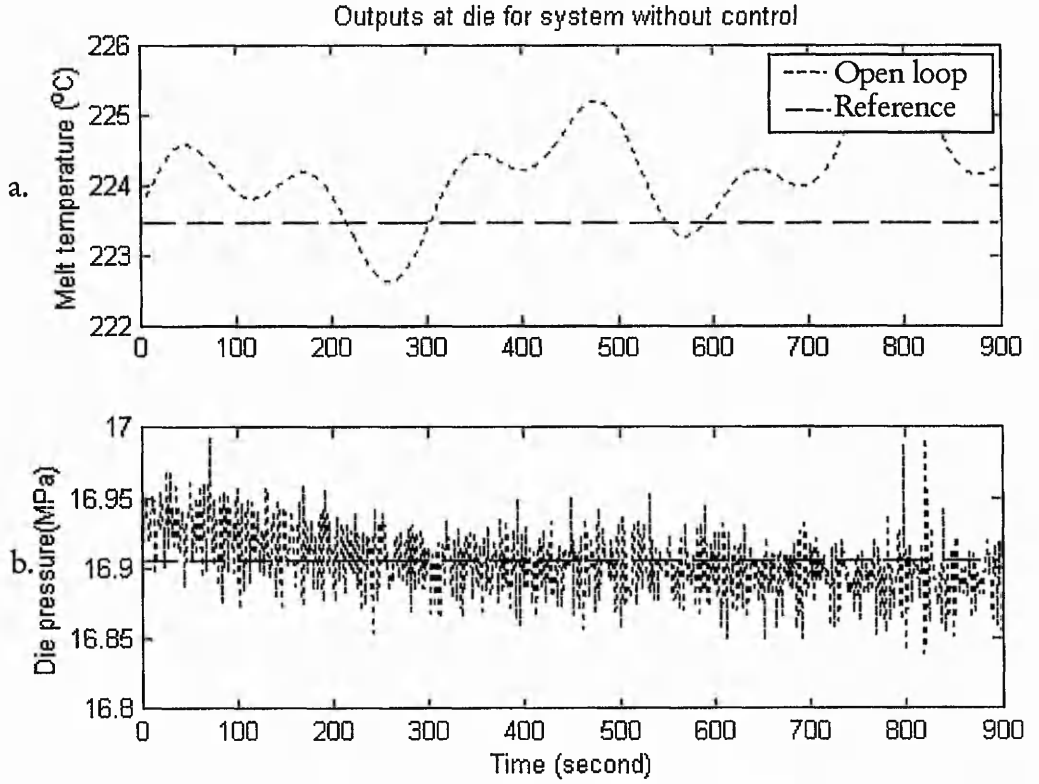

Fig. 6-13: Open loop extrusion system: **a)** melt temperature **b)** melt pressure.

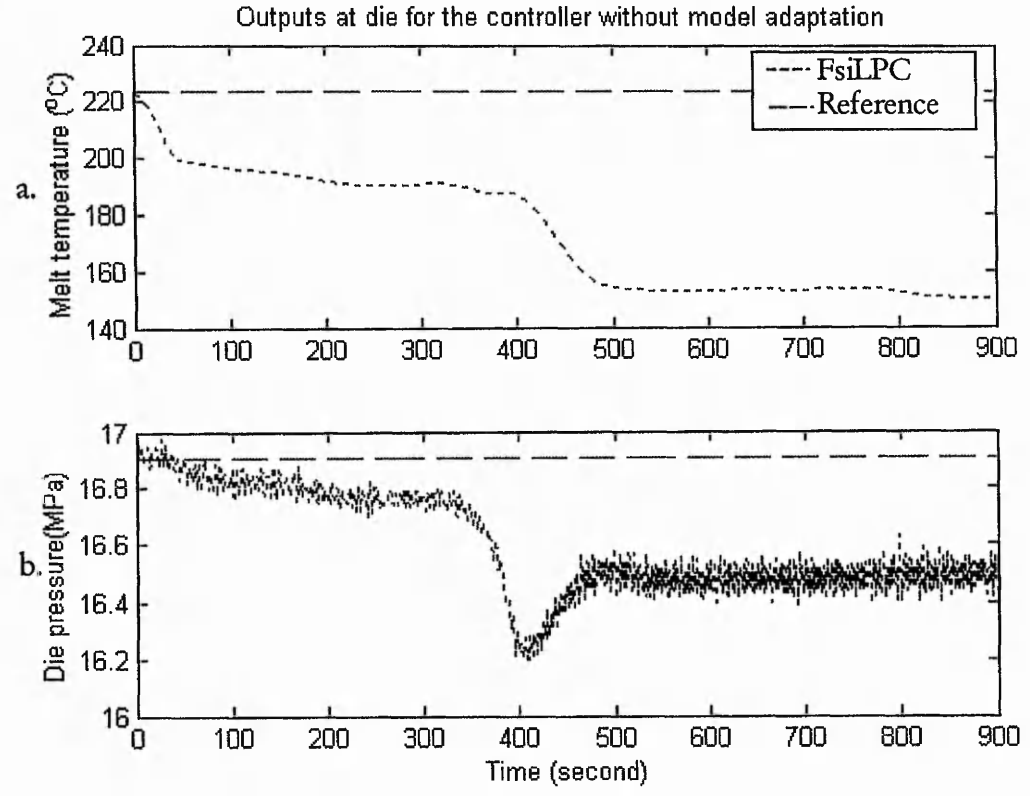

Fig. 6-14: Non-adaptive FsiLPC system: **a)** melt temperature, and **b)** melt pressure.

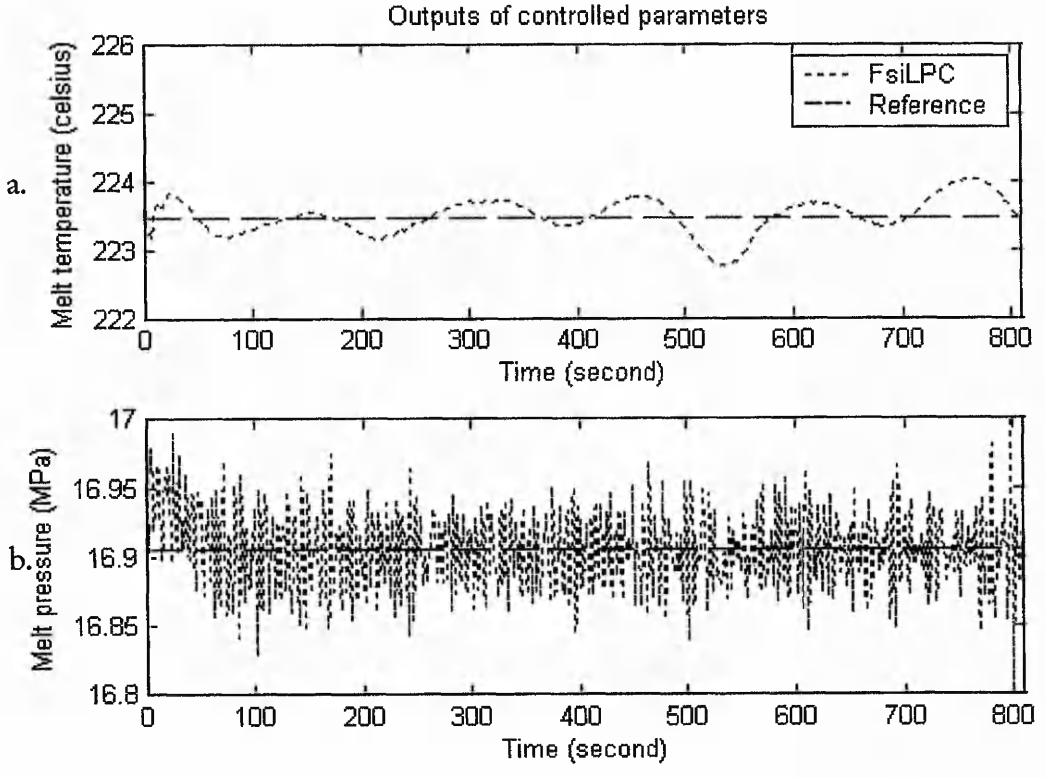

Fig. 6-15: Adaptive FsiLPC system: **a)** melt temperature, and **b)** melt pressure.

The effect of model adaptation settings on the standard deviation of melt temperature is presented in Fig. 6-16. The deviation increases with the adaptation triggered limit and the training epoch. The latter increases especially if the triggered limit is large. Similar behaviour is examined in Fig. 6-17 for the melt pressure. Consequently, to achieve a good performance, the triggered limit and the training epoch for the semi-physical model are desired to be small values within the ranges of investigation.

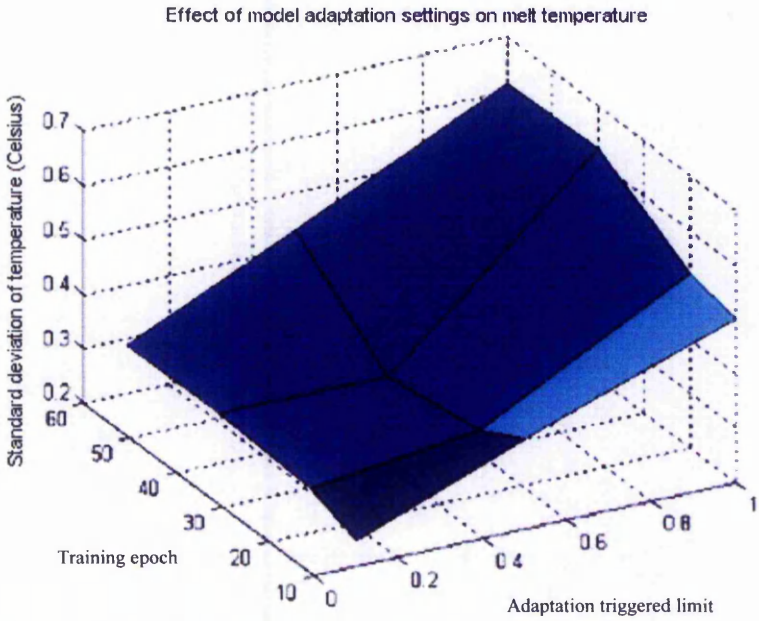

Fig. 6-16: Effect of model adaptation phase settings on melt temperature.

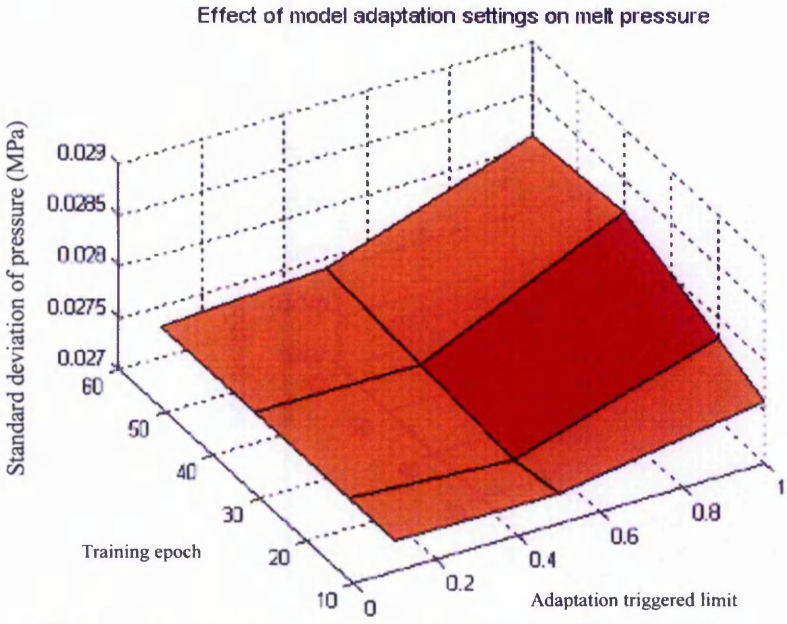

Fig. 6-17: Effect of model adaptation phase settings on melt pressure.

Learning rate

The performance of the FsiLPC system is also determined by the settings on learning rates. There are two types of learning rate, namely the learning rates of fuzzy supervisory units and the learning rate of semi-physical model. The former is required in the manipulating signal optimisation phase, while the latter is needed in the model adaptation phase. It is found that the settings of learning rates of fuzzy supervisory units are critical to avoid divergent of controlled signals. In Fig. 6-18, the unity value at the *z*-axis (standard deviation of the melt temperature) represents the divergent of the melt temperature from the reference signal. In general, it is important that the learning rates of the fuzzy supervisory units are set below 0.5 to avoid the signal divergences. Similar effect of learning rates settings is observed on the melt pressure in Fig. 6-19.

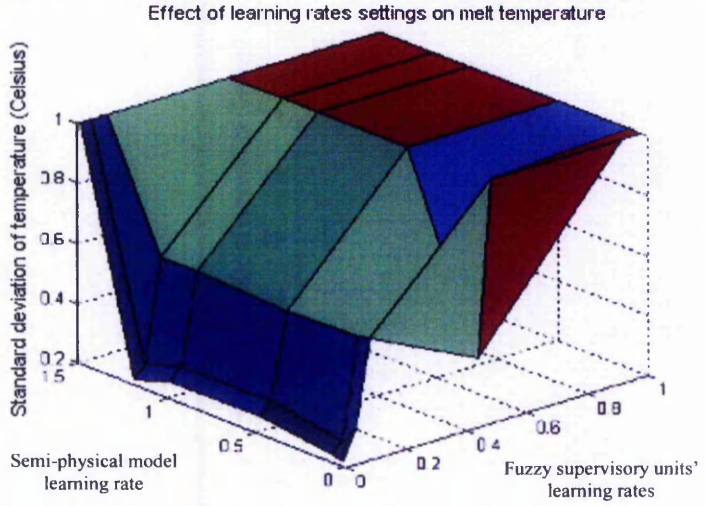

Fig. 6-18: Effect of learning rates settings on melt temperature.

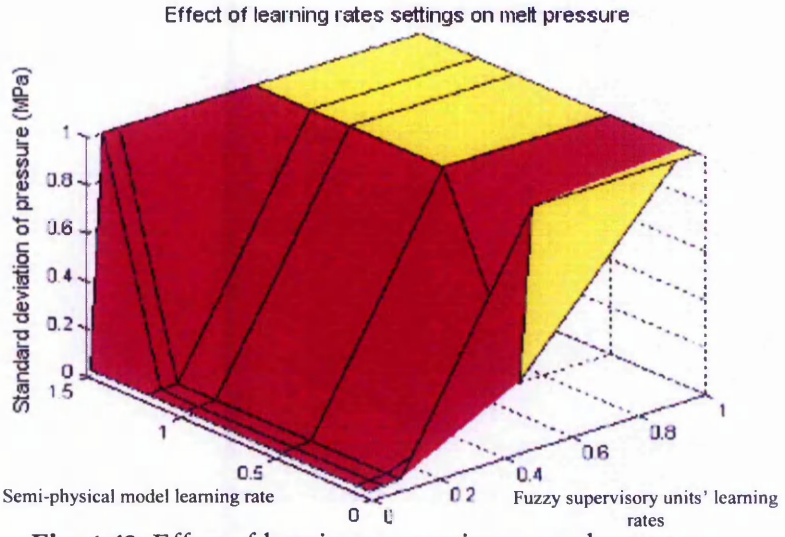

Fig. 6-19: Effect of learning rates settings on melt pressure.

Prediction horizon

The last factor to be considered is the length of prediction horizon. The length determines the time interval allowable for the predicted process output to converge to the desired value. This indirectly determines the necessary changes in the manipulating signals and affects the tuning of the fuzzy supervisory units.

When the FsiLPC system is set to one-step ahead of prediction horizon, the melt temperature and the melt pressure as shown in Fig. 6-20 are obtained. The melt temperature (Fig. 6-20a) overshoots greatly at the beginning and slowly decays to the desired temperature. A significant steady state error on the melt pressure is observed in Fig. 6-20b. The corresponding screw speed and barrel temperature are shown by solid lines in Fig. 6-22. Comparatively, the short prediction horizon causes a large overshoot of the barrel temperature when the reference signal vector is newly changed. The overshooting response requires drastic parameter tunings of the fuzzy supervisory units, which in turn results in the divergence of the melt pressure. This implies that the original functions of the fuzzy supervisory units have been corrupted due to the radical parameter tunings.

A satisfactory performance is attained when the prediction horizon is set to five-steps ahead. The melt temperature raises with slightly overshoot (Fig. 6-21a) and the melt pressure also converges to the reference value (Fig. 6-21b). Table 6-1 presents the simulation results for various prediction horizon lengths. The five-steps ahead prediction horizon provides the best result. It is noticed that the FsiLPC system performs similarly when the prediction horizon is set over ten-steps ahead. When the prediction horizon is approaching infinity, the FsiLPC system would resemble a static gain control system. Effectively, this means that the parameters of the fuzzy supervisory units remain constant providing only static gains in response to the changes in the reference signals.

Table 6-1: Performance of FsiLPC system with various prediction horizons.

Standard deviation of:	1 step	2 steps	3 steps	**5 steps**	10 steps	20 step	50 steps	100 steps	200 steps
Temperature (°C)	0.423	0.298	0.262	**0.259**	0.275	0.282	0.284	0.281	0.281
Pressure (MPa)	0.090	0.088	0.089	**0.089**	0.089	0.090	0.094	0.094	0.094

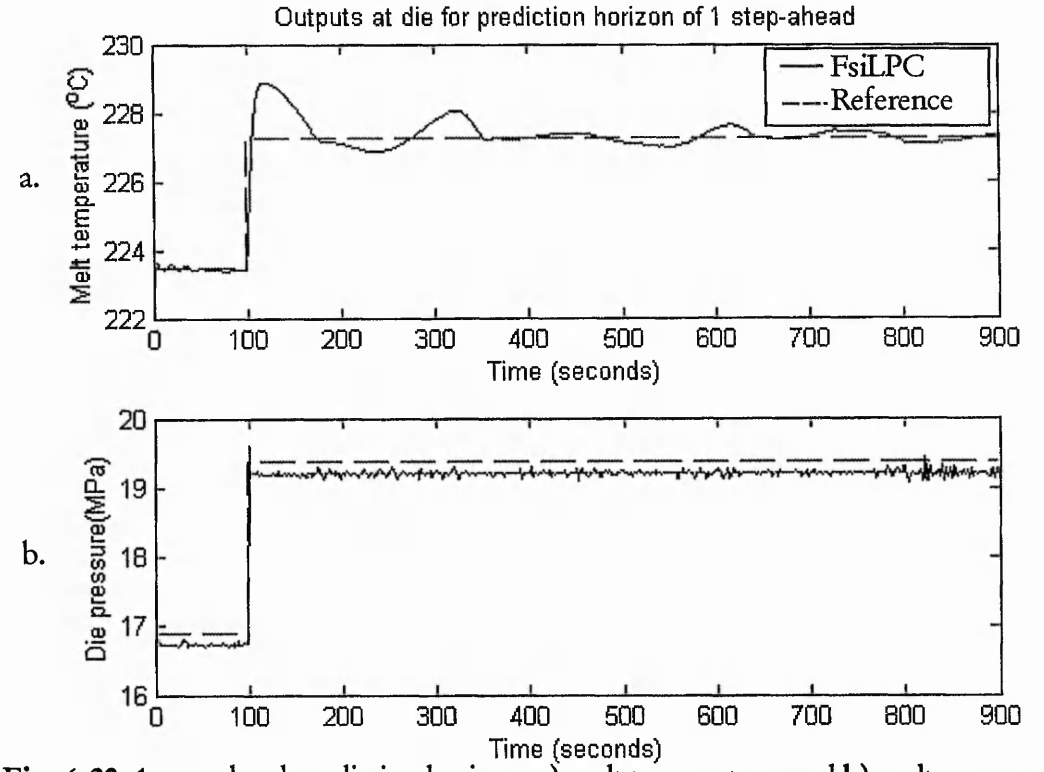

a.

b.

Fig. 6-20: 1-step ahead prediction horizon: **a)** melt temperature, and **b)** melt pressure.

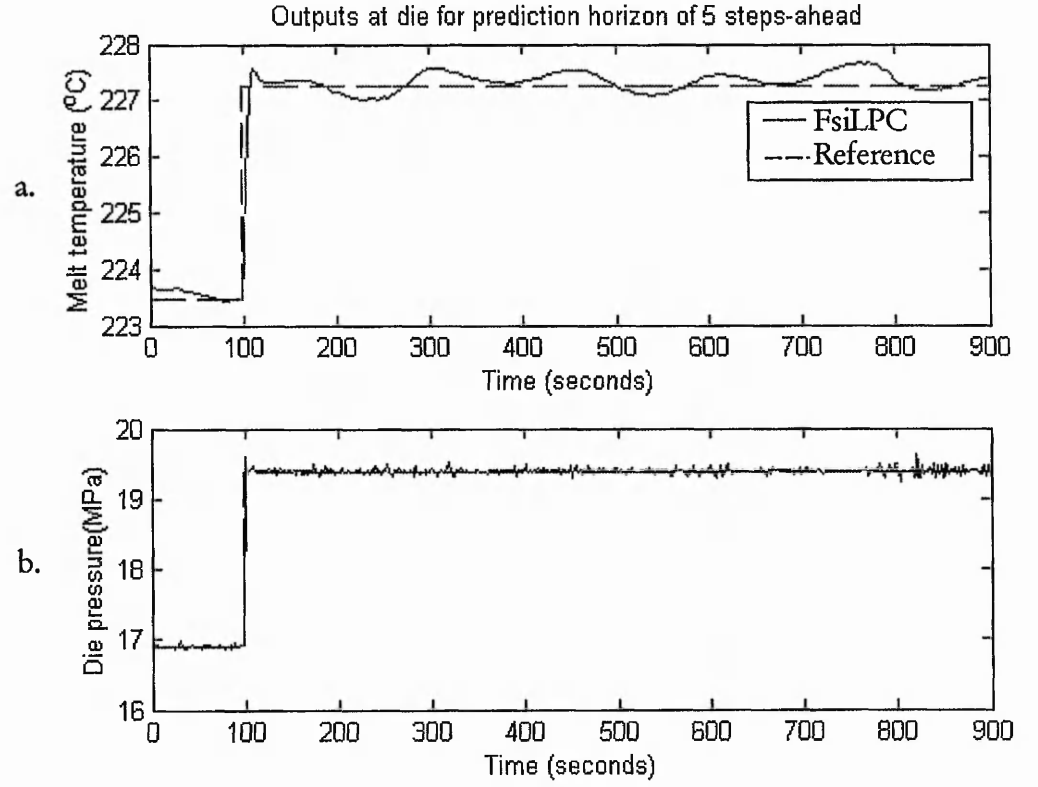

a.

b.

Fig. 6-21: 5-steps ahead prediction horizon: **a)** melt temperature, and **b)** melt pressure.

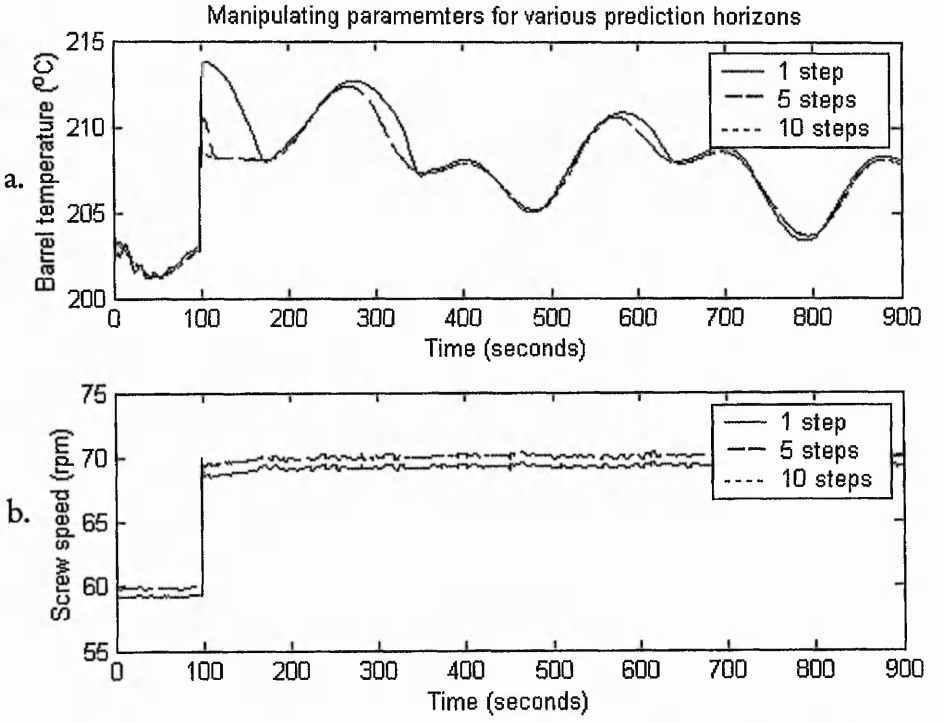

Fig. 6-22: Effect of prediction horizons on: a) barrel temperature, and b) screw speed.

6.3.5 Process disturbances

Even with the suitable settings, the system performance is also affected by the process disturbances. Therefore, it is useful to identify the boundary within which the behaviour of the system is stable. The impact of the process disturbances on the melt pressure and the melt temperature has been examined in Chapter 3. The high frequency disturbances are identified as the signal distortions and should be filtered. This sub-section investigates the system robustness in response to the variations in the intermediate and low frequency disturbances, and the disturbances caused by sensors faulty readings.

The process disturbances in the case studies are simulated with a relative proportion to the original process disturbances as observed in Fig. 6-13. The effects of variations in the temperature and pressure disturbances on the system performance are depicted in Fig. 6-23 and Fig. 6-24 respectively. The *z*-axis in both figures represents the performance comparison with the open loop system. The flat mesh planes represent cases when the performance of the FsiLPC system is identical to the open loop system. In Fig. 6-23, a poor performance on regulating the melt temperature is observed when a large amplitude of temperature disturbance occurring at a high frequency (near to the origin). When the frequency of disturbance decreases (further from the origin), a good

performance is obtained independent of the amplitude. Roughly, an improved performance is obtained in regulating the melt temperature disturbances when the frequencies are above 0.2 fraction ($1/_{0.2}$) of the original. For the melt pressure disturbances, it is observed in Fig. 6-24 that the system performance is less affected by the amplitude of the process disturbance. However, an improved performance is achieved when the frequency of the disturbance becomes lower (further from the origin) as this provides more time for the corrective control action to become effective. Roughly, an improved performance is observed when the pressure disturbance frequencies are above 3 fraction ($1/_{3}$) of original.

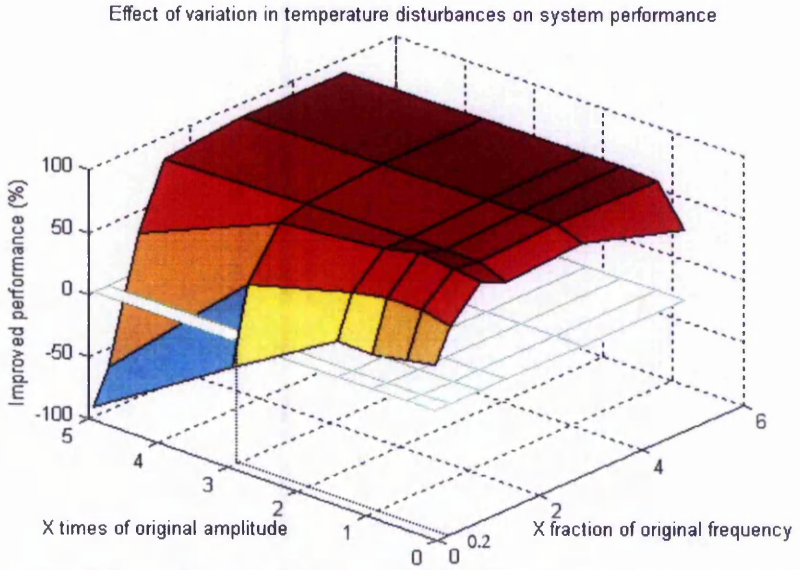

Fig. 6-23: Effect of variation in temperature disturbances on system performance.

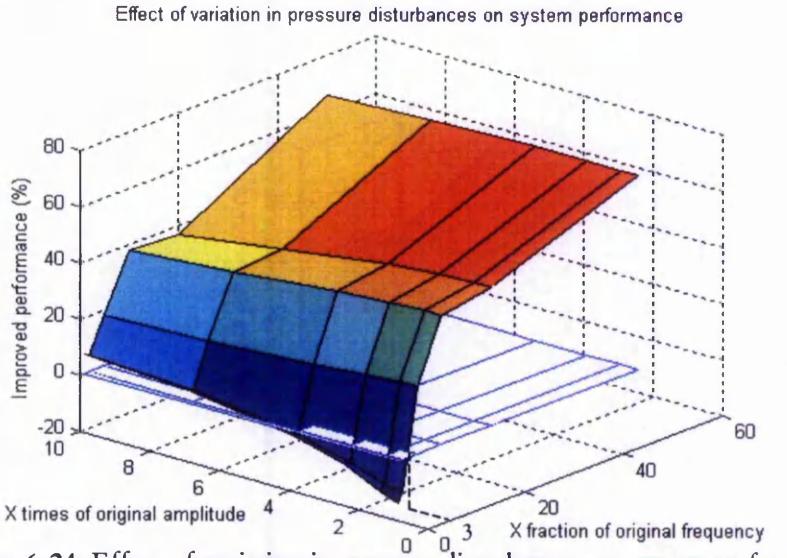

Fig. 6-24: Effect of variation in pressure disturbances on system performance.

Another source of process disturbances is due to the faulty readings from the sensors. A faulty reading is normally identified when the measurement changes radically without any purposely imposed operating conditions. Examples of the faulty readings were found in Fig. 3-11 of Chapter 3 for the melt pressure at the time around 500 seconds. The reasons that may explain the faulty readings of the sensors include:

- the wire connection of the sensors to the data acquisition system is loose;
- the interference of electromagnetic field in the vicinity of the signal transmitting cables;
- the casings of the sensors are cracked due to the excessive pressure.

The FsiLPC system in response to faulty readings from the thermocouple alone, the pressure transducer alone and both the sensors are shown in Fig. 6-25, Fig. 6-26 and Fig. 6-27 respectively. The solid lines in all cases signify the performance of FsiLPC system while the dotted lines indicate the outputs of the uncontrolled system with faulty readings.

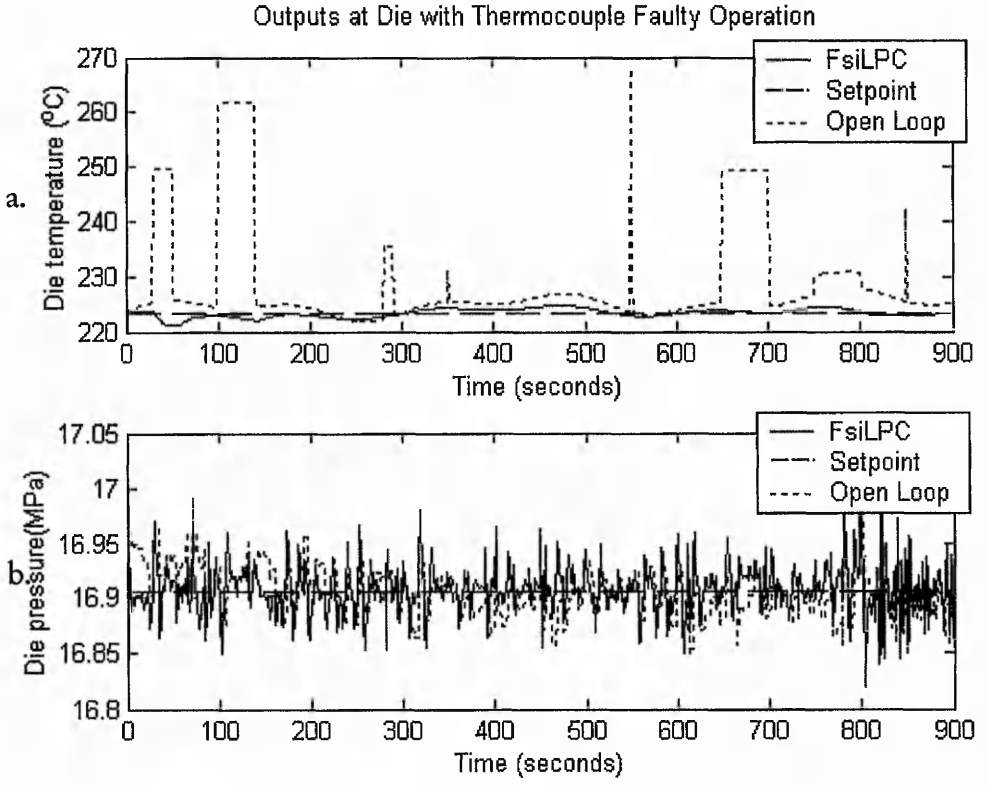

Fig. 6-25: Thermocouple faulty readings: **a)** melt temperature, and **b)** pressure.

Comparing Fig. 6-25 and Fig. 6-26, it is noticed that the FsiLPC system is less sensitive to the thermocouple faulty reading. The thermocouple faulty reading in Fig. 6-25a can be considered as the fast changing reference signal as discussed in Section 6.3.3. The melt temperature responds slowly and the faulty reading returns normal before any substantial change in the melt temperature occurs. In Fig. 6-27, the performance of the FsiLPC system when both pressure transducer and thermocouple provide faulty readings is shown. A stable control on the melt temperature and the melt pressure could still be achieved.

The three case studies show that the FsiLPC system is stable if the faulty readings are within tolerances. The tolerances are taken from Fig. 6-25 and Fig. 6-26 to be 20% for the melt temperature and 15% for the melt pressure. These percentages are relatively larger than the actual faulty readings on the melt pressure of 6% found in Fig. 4-8. An example of an unstable system is presented in Fig. 6-28, when the faulty reading on the melt pressure is beyond the tolerance. Both melt temperature and pressure diverge when the system parameters are over-tuned to cope with the faulty readings.

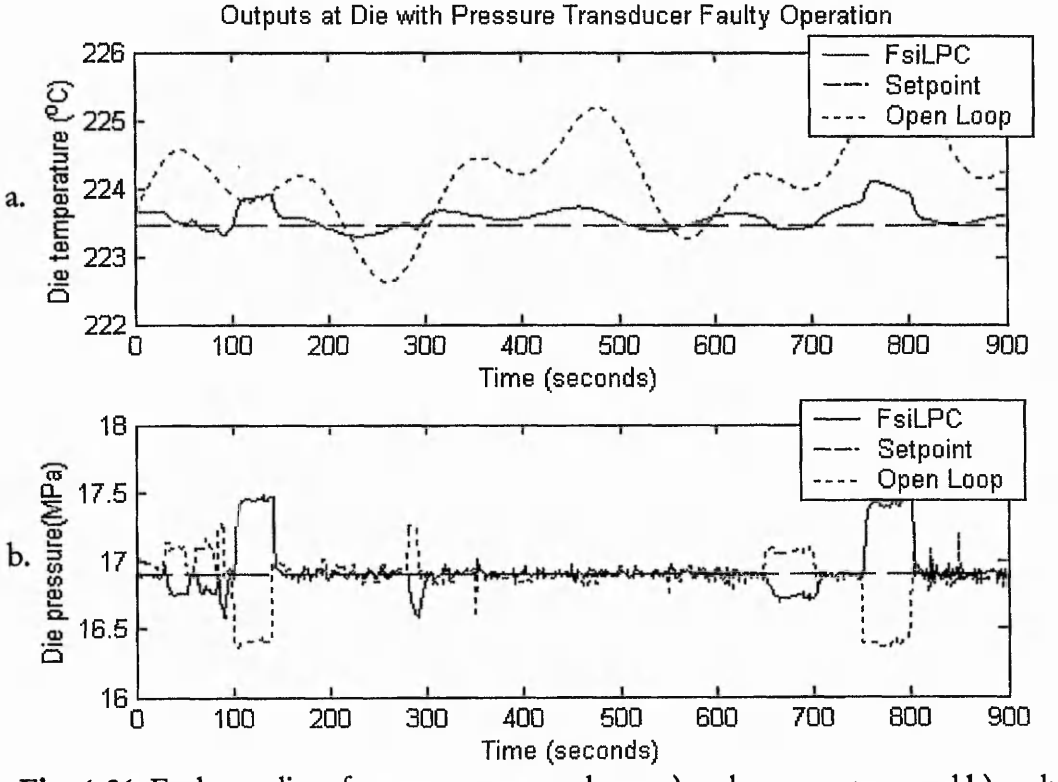

Fig. 6-26: Faulty readings from pressure transducer: **a)** melt temperature, and **b)** melt pressure.

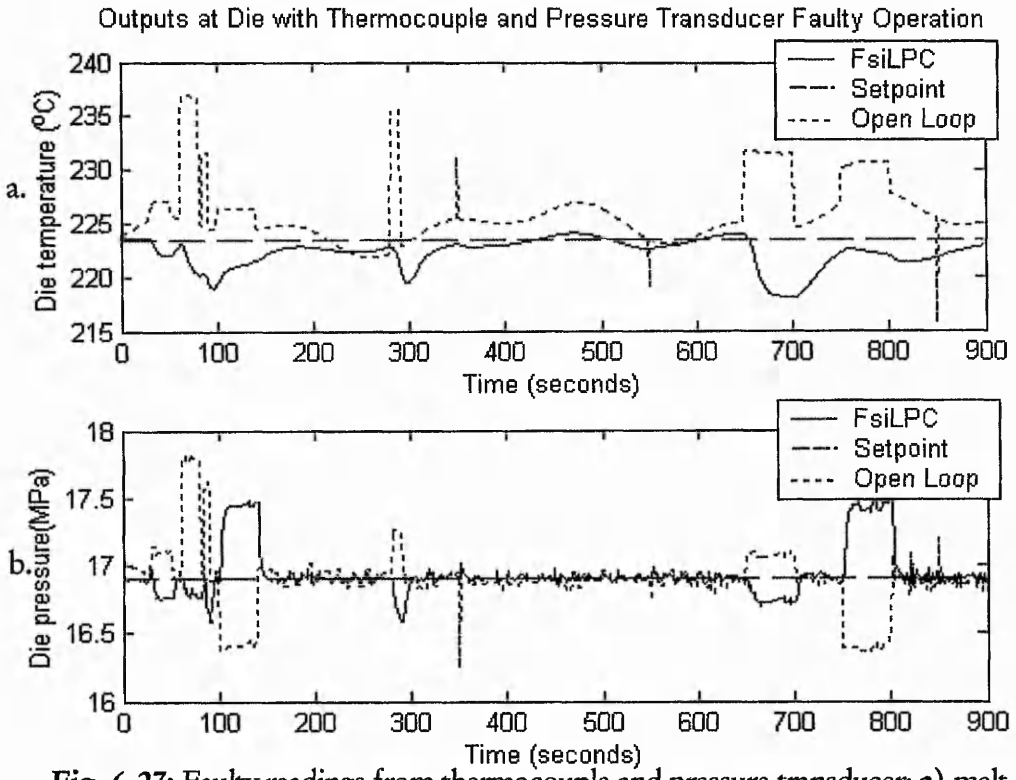

Fig. 6-27: Faulty readings from thermocouple and pressure transducer: **a)** melt temperature, and **b)** melt pressure.

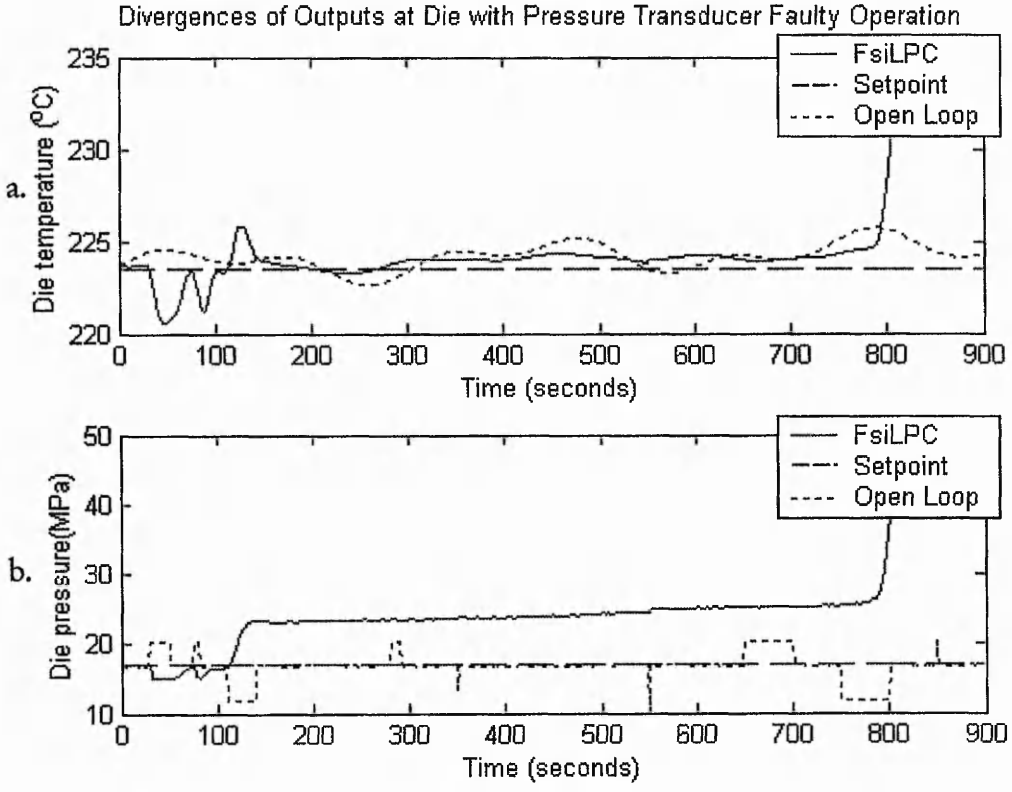

Fig. 6-28: Divergences of controlled signals at die with a large pressure faulty readings: **a)** melt temperature, and **b)** melt pressure.

6.4 A Comparative Study

In this section, the FsiLPC system is compared with PI and STR control systems with respect to the performance in tracking step-changes in reference signals and rejecting process disturbances. To make the chapter self-contained, the developments of the PI and STR controllers are presented. The responses of the systems are shown on graphes with fixed scales of axes to assist the visual comparisons.

6.4.1 Development of Proportional-Integral controllers

The PI controllers are widely applied in the polymer processing industries to control the extrusion process. A discrete function of a PI controller is given below:

$$u(k) = u(k\text{-}1) + K_p\left[\left(e(k) - e(k-1)\right) + \frac{t_s}{\tau_i}e(k)\right] \qquad (6\text{-}3)$$

where k is the discrete time, u is the manipulating signal, K_p is the proportional gain, t_s is the sampling interval, and τ_i is the integral constant. The error term, $e(k)$, is calculated by comparing either the melt pressure, $P(k)$, or the melt temperature, $T(k)$, depending on the design of PI controllers. The expression is:

$$e(k) = P_r(k) - P(k) \quad or \quad e(k) = T_r(k) - T(k)$$

where subscript r represents reference signal. Industrial PI extrusion controllers are generally in a Single-Input-Single-Output (SISO) structure. Therefore, different units of SISO PI controllers are designed to couple different manipulating parameters (screw speed and barrel temperature) with different controlled parameters (melt temperature and melt pressure) for the evaluations. Ziegler-Nichols closed loop tuning method is employed to determine the parameters of PI controllers. It is remarked that this tuning method would be sufficient only for the basic operation of the controllers. More advance tuning methods could be employed to improve the controller performance as more time could be spent (Astrom *et al.*, 1993). The Ziegler-Nichols tuning procedure is listed below:

1. Disable the integral control.
2. Increase the proportional gain, K_p, and observe the response of the system.
3. Repeat Step 2 until the system reaches a point of critical stability where sustained oscillations are observed.
4. Record the gain as the critical gain, K_c, and the interval between two consequent peaks of the oscillations is measured as the critical time, T_c.

5. Calculate the PI parameters using the specifications in Table 6-2.

Five different settings of controller parameters for five different couplings between the manipulating and controlled parameters are indicated in Table 6-2. Settings 1 and 2 are applied when the screw speed is used to regulate the melt temperature and the pressure respectively. The screw speed is assumed to respond instantly to the changes in the controlled signals. Setting 3 is employed for a case study with the barrel temperature responds slowly to the changes in the melt temperature. The slow response barrel temperature is assumed to have a time constant of 2000 seconds plus 70 seconds transport delay (Rauwendaal, 1986). The response of the barrel temperature is approximated by a first order system with the following transfer function:

$$G_{Tb}(z) = z^{-70}\left[\frac{0.0005z^{-1}}{1-0.9995z^{-1}}\right] \tag{6-4}$$

In Settings 4 and 5, the barrel temperature is assumed to respond rapidly without any transport delay when a control signal is applied. This ideal behaviour is impossible to achieve in practice but is simulated solely for the comparative study. The ideal response barrel temperature is expressed in a transfer function given below:

$$G_{Tb}(z) = \frac{0.6321z^{-1}}{1-0.3679z^{-1}} \tag{6-5}$$

The barrel temperature with the slow response behaviour and the ideal response behaviour defined in Equation (6-4) and Equation (6-5) respectively will be referred in the rest of the chapter. The couplings of the manipulating parameters and the controlled parameters with respect to their settings in Table 6-2 are summarised as follows:

- **Setting 1:** Coupling of the screw speed and the melt temperature.
- **Setting 2:** Coupling of the screw speed and the melt pressure.
- **Setting 3:** Coupling of the slow response barrel temperature and melt temperature.
- **Setting 4:** Coupling of the ideal response barrel temperature and melt temperature.
- **Setting 5:** Coupling of the ideal response barrel temperature and the melt pressure.

Table 6-2: Parameter settings of PI controllers for different parameter couplings.

Parameters	Setting 1	Setting 2	Setting 3	Setting 4	Setting 5
Critical gain, K_c	23.5	3.3	90	22	6200
Critical time, T_c	2	4	320	7.5	13
Proportional gain, K_p	0.45× K_c	0.45× K_c	0.45× K_c	0.45× K_c	0.45× K_c
Integral constant, τ_I	0.83× T_c	0.83× T_c	0.83× T_c	0.83× T_c	0.83× T_c

6.4.2 Development of Self-Tuning-Regulators

A STR appears to be a popular alternative solution for the extrusion control due to its adaptive ability. In Fig. 6-29, it is shown that the operation of the STR includes process parameter estimation and controller parameter optimisation. To facilitate the operation, it is required to initialise the STR with a model structure and a cost function.

The process models in the case studies are identified in the Autoregressive Exogenous Input (ARX) structure. An attempt to develop a MIMO ARX model was unsuccessful due to the difficulty in establishing the relationship of the process parameters empirically. The responses of the screw speed and the barrel temperature are in different orders of magnitude. In particular, the screw speed responds within seconds while the barrel temperature takes minutes to respond. The different orders of magnitude were also observed on the responses of the melt temperature and the pressure. Having this difficulty, three SISO ARX models are identified separately. The transfer functions of the models are given in Table 6-3 with respect to the STR settings as follows:

- transfer function for coupling of the screw speed and the melt temperature is given under the column of Setting 1;
- transfer function for coupling of the screw speed and the melt pressure is given under the column of Setting 2;
- transfer function for coupling of the ideal response barrel temperature and the melt temperature is given under the column of Setting 3.

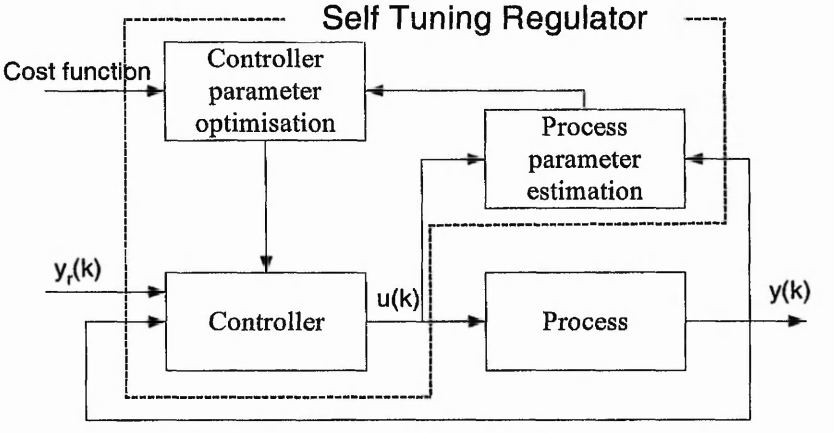

Fig. 6-29: Block diagram of Self Tuning Regulator.

The coefficients of the ARX models shown in Table 6-3 represent only the initial estimation of the system. During the operation, these coefficients are expected to change when the STR systems adapt the models accordingly to the operating conditions. The parameters of the process models are updated based on the recursive least square algorithm using the following equation (Ljung, 1999):

$$\theta(k+1) = \theta(k) + M(k+1)\, a\, (y(k) - a^T\theta(k)) \qquad (6\text{-}6)$$

where θ is the parameter set of a model, M is the matrix of old data pairs and $(a^T; y)$ is the newly measured data pair. The matrix M is updated as follows:

$$M(k+1) = \frac{1}{\alpha}\left(M(k) - \frac{M(k)aa^T M(k)}{\alpha + a^T M(k)a} \right) \qquad (6\text{-}7)$$

where α is the forgetting factor, which is employed to constraint the magnitude of changes in the model parameters during the adaptation operation.

After estimating the model parameters, a control function could be formulated by minimising a cost function. The cost function in the study is given below:

$$J = \tfrac{1}{2} Q[\hat{y}(k+1) - y_r(k+1)]^2 + \tfrac{1}{2} R\Delta\hat{u}(k)^2 \qquad (6\text{-}8)$$

where $\hat{u}$ is the predicted manipulating signal, $\hat{y}$ is the estimated controlled signal and y_r is the reference signal. Q and R are the weight parameters in the cost function for the controlled and the manipulating parameters respectively. The settings emphasize on the consistency of the controlled signal with the reference signal, while the changes of the manipulating signal are slightly confined.

Table 6-3: Parameter settings and process models for different parameter couplings.

Parameters	Setting 1	Setting 2	Setting 3
Forgetting factor, α	0.8	0.8	0.8
Weight, Q	1	1	1
Weight, R	0.5	0.5	0.1
Process model, $\hat{G}$	$\frac{0.0369z^{-1} + 0.0310z^{-2}}{1 - 1.523z^{-1} + 0.5905z^{-2}}$	$\frac{-0.0822z^{-1} + 0.7806z^{-2} - 0.1431z^{-3} + 0.3069z^{-4}}{1 - 0.0530z^{-1} - 0.2956z^{-2} - 0.2947z^{-3} - 0.3468z^{-4}}$	$\frac{0.6321z^{-1}}{1 - 0.3679z^{-1}}$

6.4.3 Tracking step-changes

In this evaluation, step-changes in the reference signals are imposed. The control systems are required to track the changes rapidly in a stable manner. The performance of the PI control systems is first investigated, to be followed by the STR systems and the FsiLPC system.

The tracking performance of PI control systems is shown as solid lines in Fig. 6-30 to Fig. 6-33. The dashed lines represent the reference signals in the stated figures and also the figures in the rest of the chapter. The result of the first coupling between the screw speed and the melt temperature is depicted in Fig. 6-30. It is observed in Fig. 6-30a that the melt temperature responds to the changes in the reference signals reasonably well. A major shortcoming of the SISO controller to control the MIMO process is seen in Fig. 6-30b. The melt pressure fluctuates significantly when tuning the screw speed to track the melt temperature. Similar shortcoming is also found for the second coupling between the screw speed and the melt pressure. In Fig. 6-31, the melt temperature is controlled but the melt pressure deviates. These results indicate that the process parameters have a strong nonlinear relationship. Hence the implementation of a SISO control system is insufficient.

The result of the third coupling between the ideal response barrel temperature and the melt temperature is demonstrated in Fig. 6-32. The melt temperature in Fig. 6-32a oscillates more than the melt temperature in Fig. 6-30a. The melt pressure in Fig. 6-32b signifies that the barrel temperature has little influence on the melt pressure. The result of last coupling in Fig. 6-33 shows that the barrel temperature is unable to regulate the melt pressure (Fig. 6-33b). In fact, the control system is unstable. It has been observed in Fig. 6-3 that the barrel temperature has negligible impact on the melt pressure. Therefore, a significant change in the barrel temperature is required to result an effective change in the melt pressure (Fig. 6-33d). The large change in the barrel temperature, in turn, would have deviated the melt temperature as shown in Fig. 6-33a. Subsequently, the control system becomes unstable as all the process parameters are interrelated.

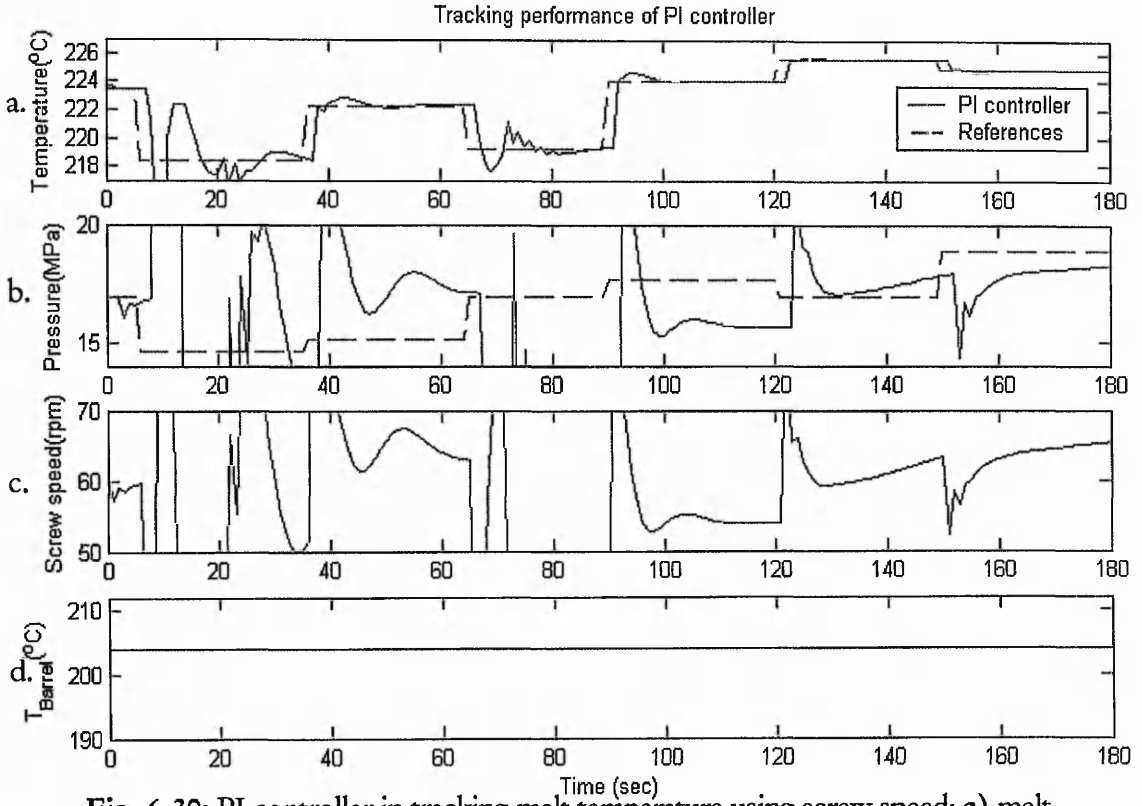

Fig. 6-30: PI controller in tracking melt temperature using screw speed: **a)** melt temperature, **b)** melt pressure, **c)** screw speed, and **d)** barrel temperature.

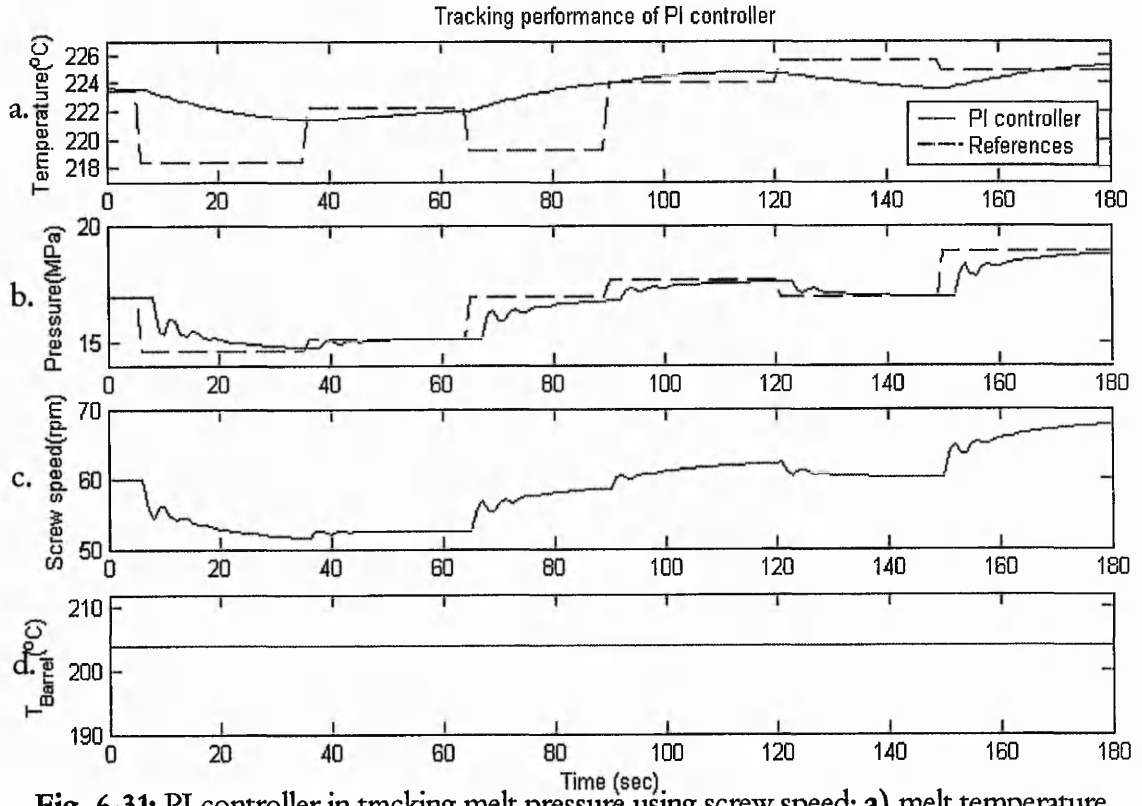

Fig. 6-31: PI controller in tracking melt pressure using screw speed: **a)** melt temperature, **b)** melt pressure, **c)** screw speed, and **d)** barrel temperature.

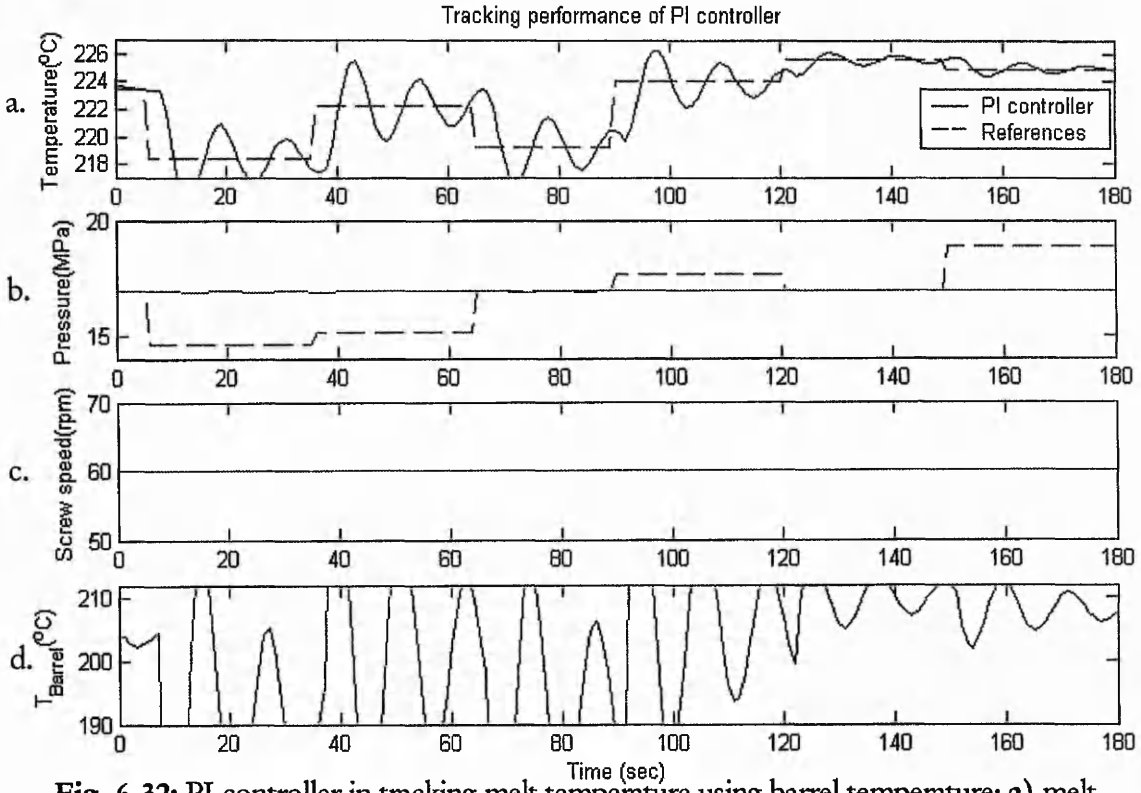

Fig. 6-32: PI controller in tracking melt temperature using barrel temperature: **a)** melt temperature, **b)** pressure, **c)** screw speed, **d)** barrel temperature.

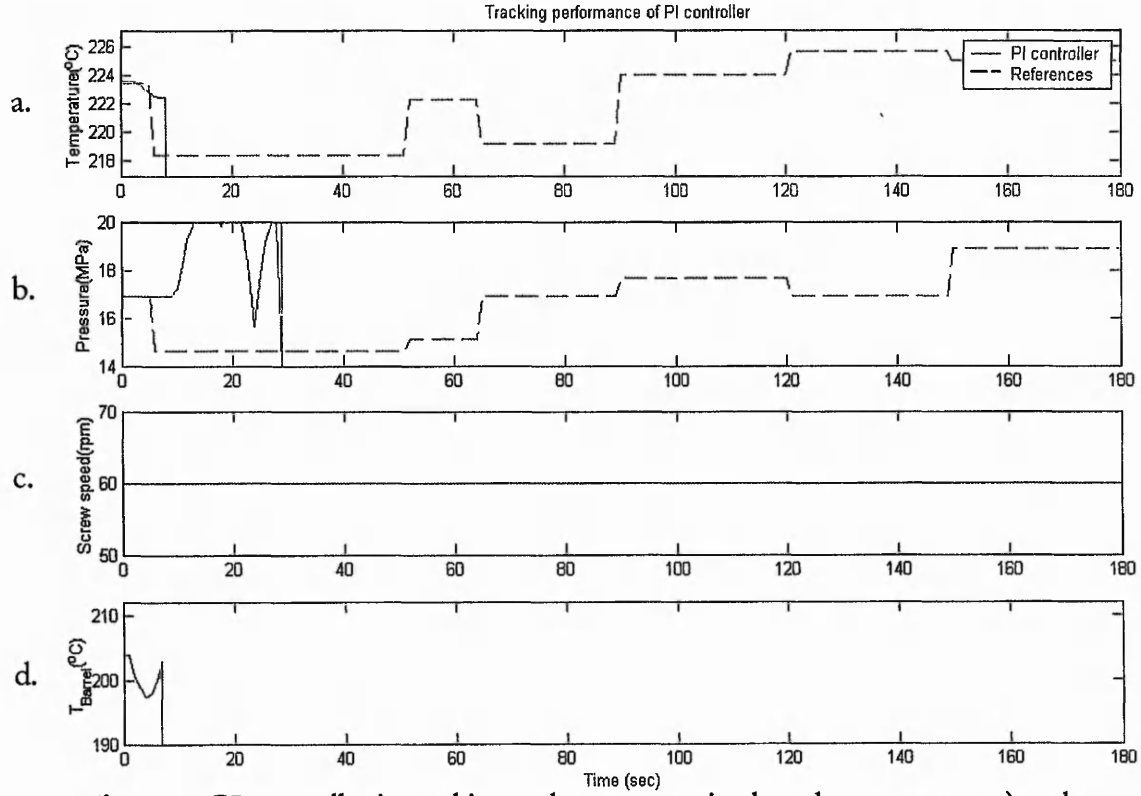

Fig. 6-33: PI controller in tracking melt pressure using barrel temperature: **a)** melt temperature, **b)** pressure, **c)** screw speed, **d)** barrel temperature.

The performance of the STR systems in tracking the melt temperature and the melt pressure using the screw speed is plotted in Fig. 6-34 and Fig. 6-35 respectively. The solid lines show that the controlled signals of the STR systems are more stable if compared with the results of PI control systems illustrated earlier. The changes in the manipulating signals are less abrupt, in line with the criteria specified in the cost function. However, the SISO STR systems are also experiencing the difficulty to control both melt temperature and melt pressure simultaneously. For instance, while the melt temperature in Fig. 6-34a is controlled satisfactory, the melt pressure in Fig. 6-34b diverges very much from the reference. The result in Fig. 6-36 indicates a case where the ideal response barrel temperature is manipulated to drive the melt temperature towards the reference value. Although the result (Fig. 6-36a) is more stable if compared with the result of the PI control system (Fig. 6-32a), the tracking performance is rather poor. Both results suggest that barrel temperature alone is not an effective manipulating parameter.

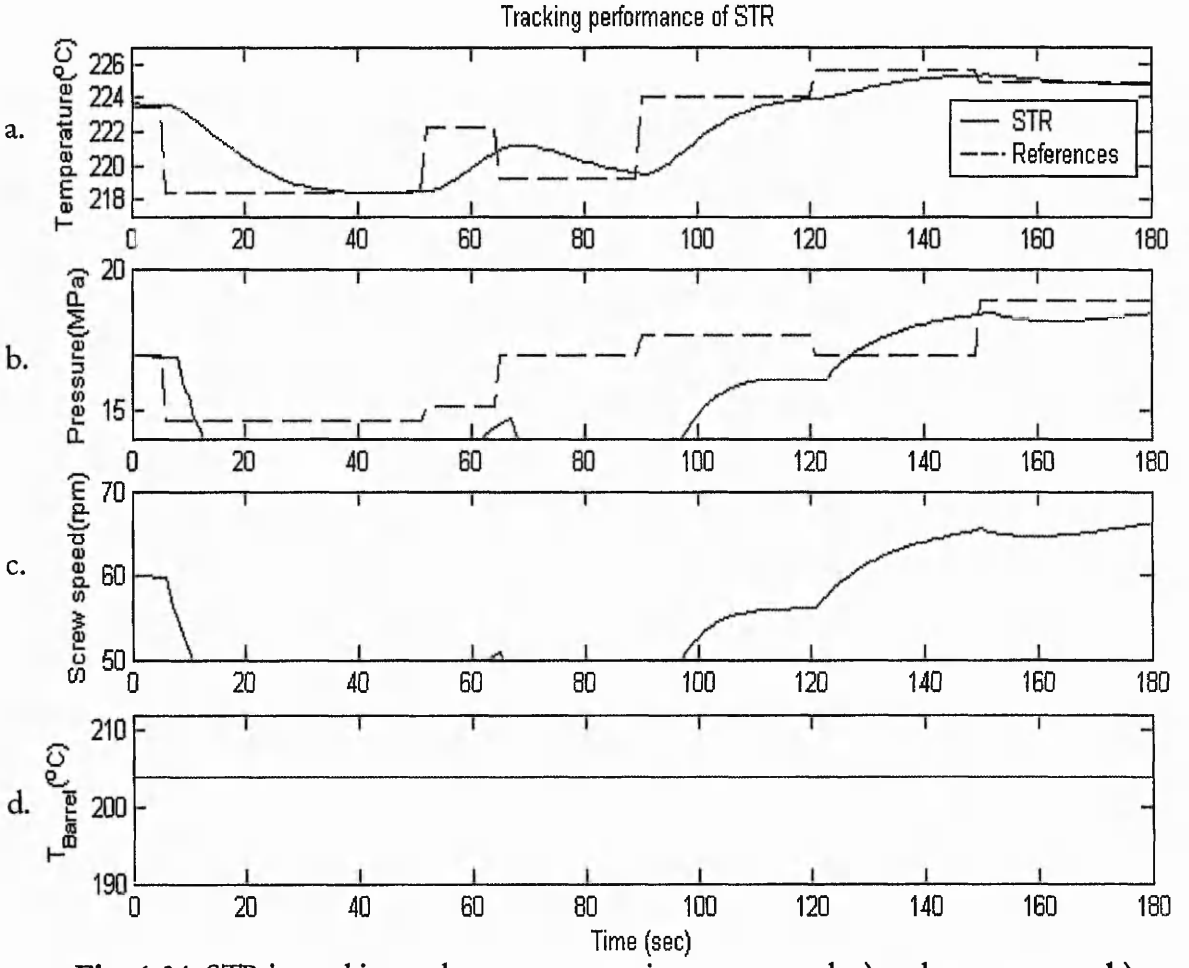

Fig. 6-34: STR in tracking melt temperature using screw speed: **a)** melt temperature, **b)** melt pressure, **c)** screw speed, and **d)** barrel temperature.

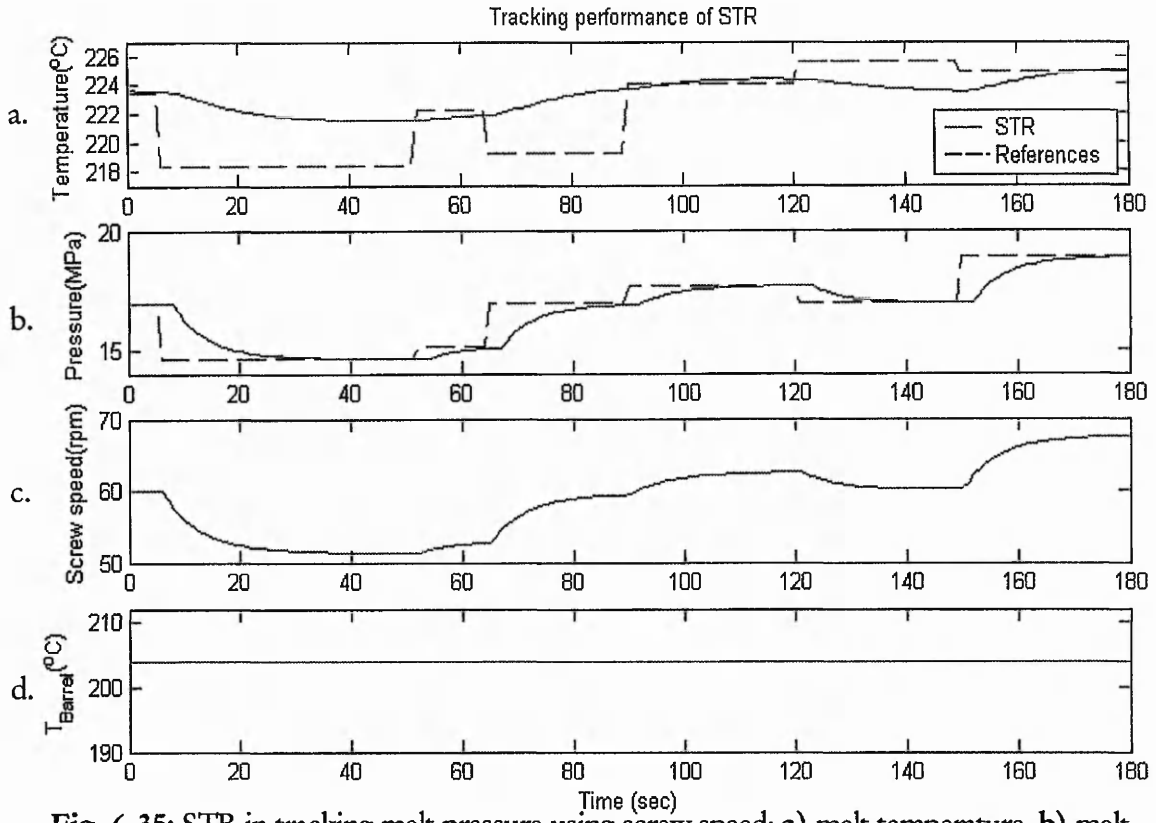

Fig. 6-35: STR in tracking melt pressure using screw speed: **a)** melt temperature, **b)** melt pressure, **c)** screw speed, and **d)** barrel temperature.

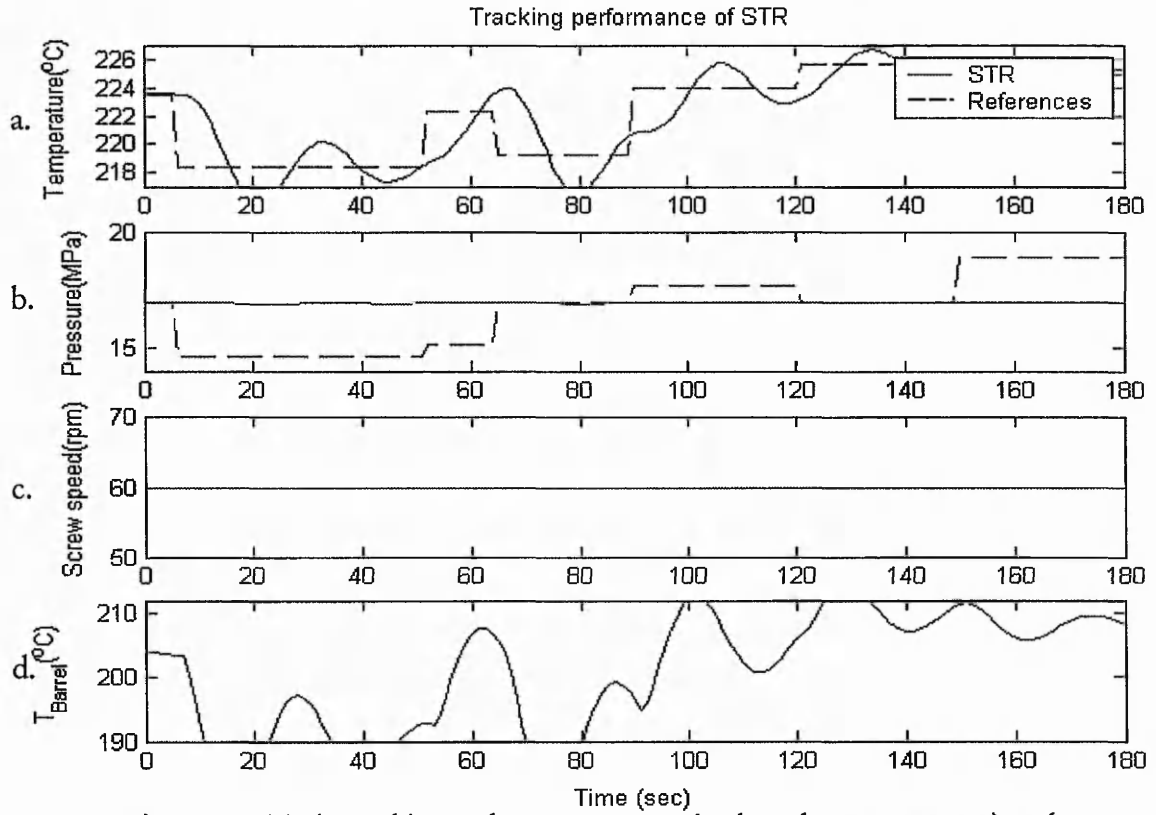

Fig. 6-36: STR in tracking melt temperature using barrel temperature: **a)** melt temperature, **b)** pressure, **c)** screw speed, **d)** barrel temperature.

In Fig. 6-37, the performance of the FsiLPC system with unlearnt fuzzy supervisory units is shown. The melt temperature and the melt pressure represented by dotted lines in Fig. 6-37a and Fig. 6-37b respectively have generated some steady state errors. When the fuzzy supervisory units are learning, the solid lines indicate that the melt temperature and the melt pressure converge to the reference values. The results are relatively outstanding if compared with the results obtained by the PI control systems and the STR control systems. The MIMO control ability of the FsiLPC system is regarded effective for the tracking the changes in the reference signals.

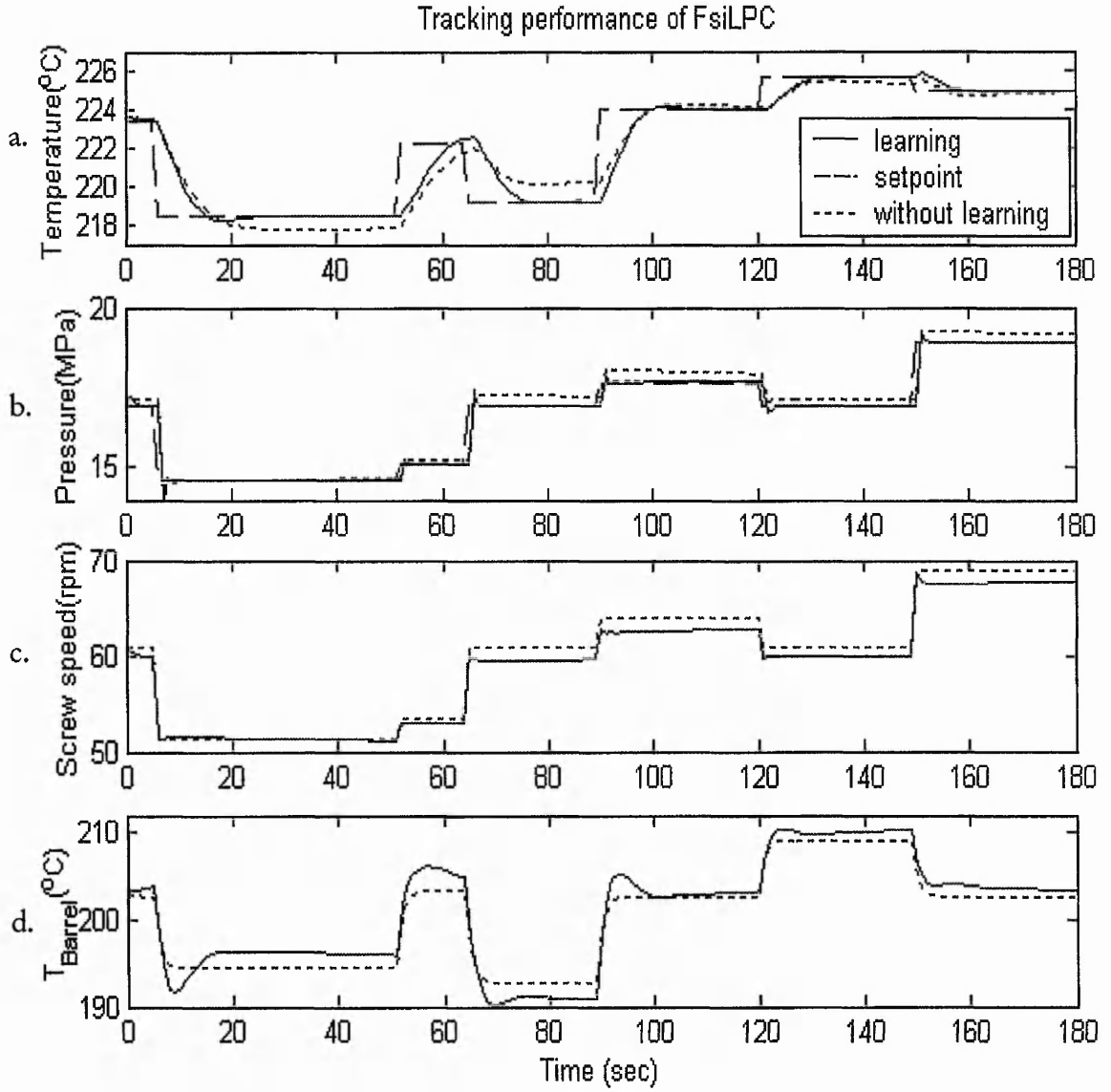

Fig. 6-37: FsiLPC system in tracking reference extrusion outputs: **a)** melt temperature, **b)** melt pressure, **c)** screw speed, **d)** barrel temperature.

6.4.4 Rejecting disturbances

The performance of three control systems is further evaluated in present of process disturbances during the operation. An example of the open loop response of the extrusion process is shown in Fig. 6-13. The signals represented by the dotted lines have been filtered to eliminate the impact of high frequency disturbances (flight noises).

To improve the reality of the case studies, the intermediate and low frequencies disturbances on the melt pressure are simulated using the normalised disturbances reported in (Qiu, 1998). Table 3-1 in Chapter 3 indicates that the amplitude of pressure disturbances is affected by the screw speed. A maximum pressure fluctuation of ±2% is observed when the screw is rotating at 90 rpm to process the MDPE polymer. This effect of the screw speed is also included while generating the pressure disturbances for the case studies. The temperature disturbances are simulated according to the experimental analysis in Tadmor and Klein (1970). The temperature was reported to fluctuate at ±1.25°C for the melt temperature of 201 °C. Various sinusoidal waves are integrated to approximate the temperature disturbances described in the literature.

The performance of the PI control systems and the STR systems in regulating the melt temperature and pressure is shown from Fig. 6-38 to Fig. 6-46. The dotted lines represent the controlled signals and the dashed lines are the reference signals. The observations from the results are similar to those of the previous evaluation, which are stated as follows:

1. The SISO control systems are insufficient to control the MIMO extrusion process. For example, the melt pressure deviates greatly (Fig. 6-38b) while regulating the melt temperature (Fig. 6-38a).
2. The slow response barrel temperature with the transfer function given in Equation (6-4) is not a sensible manipulating parameter. The controlled signals depicted in Fig. 6-40 and Fig. 6-45 fluctuate more than the open loop system.
3. The barrel temperature with ideal response behaviour could be used to regulate the melt temperature (Fig. 6-41 and Fig. 6-46). However, it is not suitable to regulate the melt pressure and the results are illustrated in Fig. 6-42. The radical change in the barrel temperature shown in Fig. 6-42c is practically unrealisable.

The performance of the MIMO FsiLPC system for the extrusion process is given in Fig. 6-47 and Fig. 6-48. In Fig. 6-47, the performance of the FsiLPC is good when the screw speed and the ideal response barrel temperature are employed as the manipulating parameters. In comparison to the response in the open loop system depicted in Fig. 6-13, the variations in the melt temperature and the melt pressure are reduced. The encouraging result implies that the extrusion behaviour with strong parameter interactions has been captured in the function of the FsiLPC system. In Fig. 6-48, the performance of the FsiLPC system is relatively poor when the slow response barrel temperature is employed as the manipulating parameter. The variation in the melt temperature is similar to the response in the open loop system but the long-term drift in the melt pressure is eliminated.

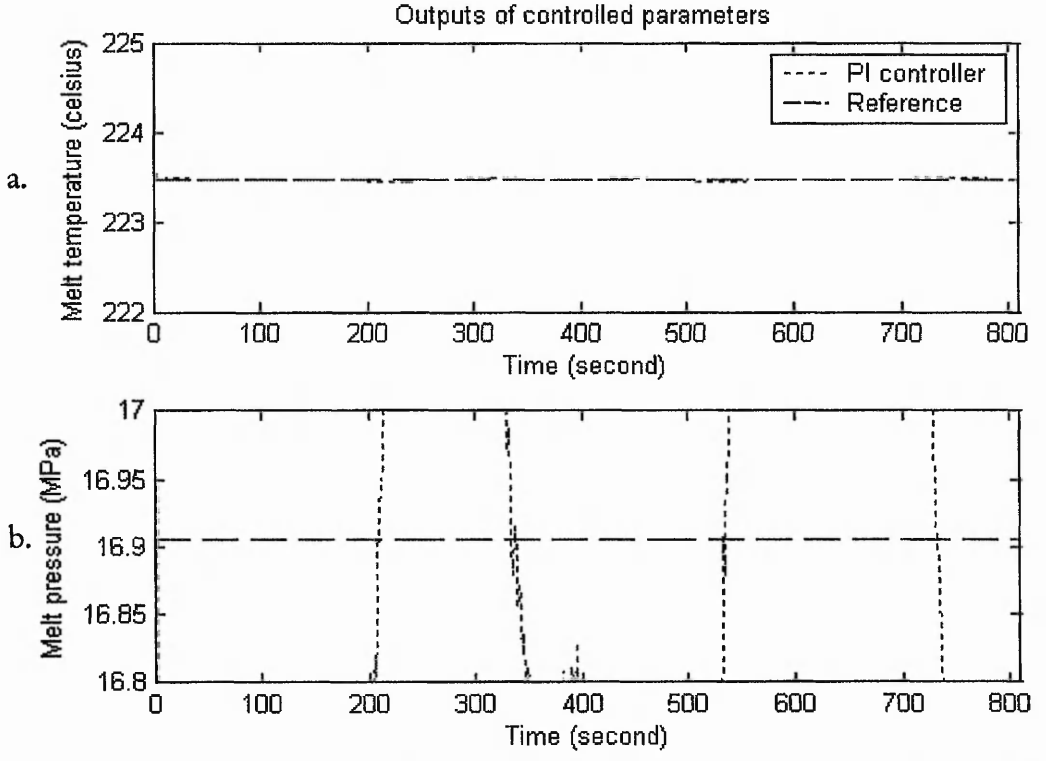

Fig. 6-38: PI controller rejects temperature disturbances using screw speed: **a)** melt temperature, and **b)** melt pressure.

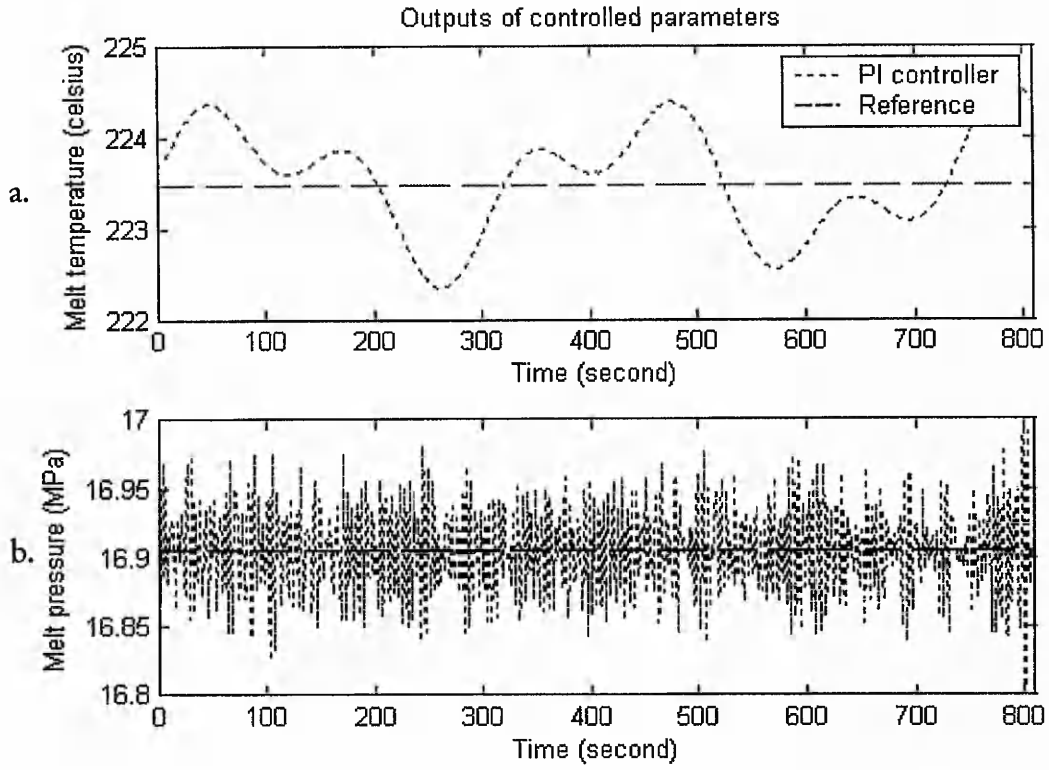

Fig. 6-39: PI controller rejects pressure disturbances using screw speed: **a)** melt temperature, and **b)** melt pressure.

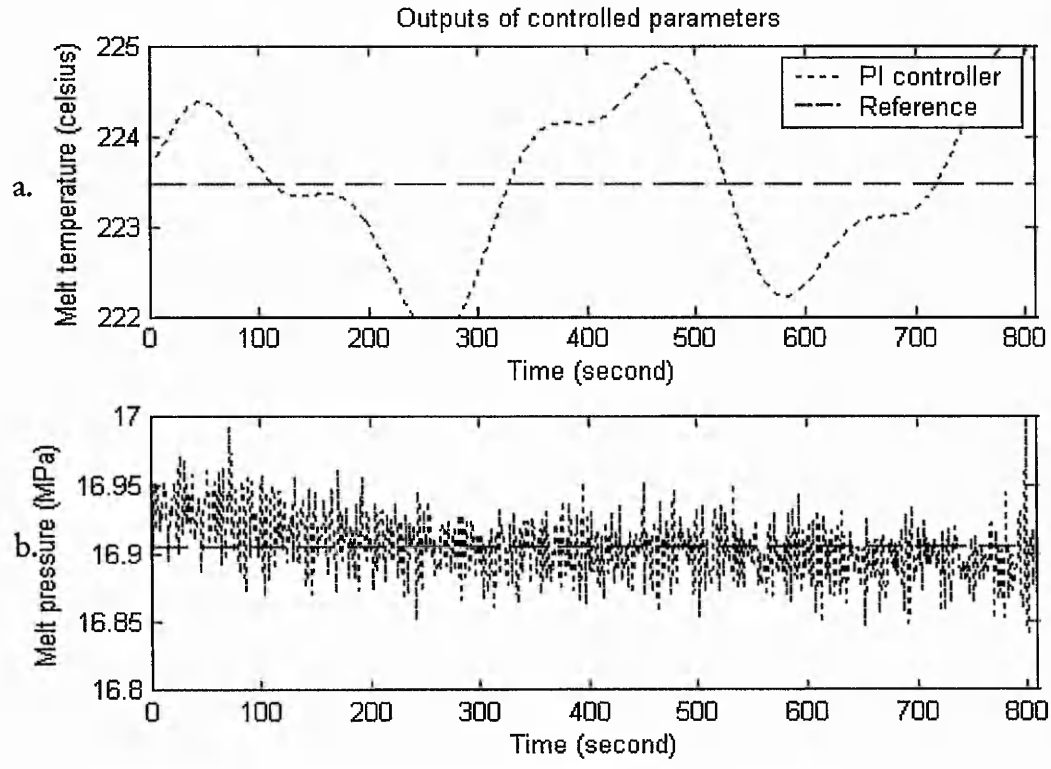

Fig. 6-40: PI controller rejects temperature disturbances using slow response barrel temperature: **a)** melt temperature, and **b)** melt pressure.

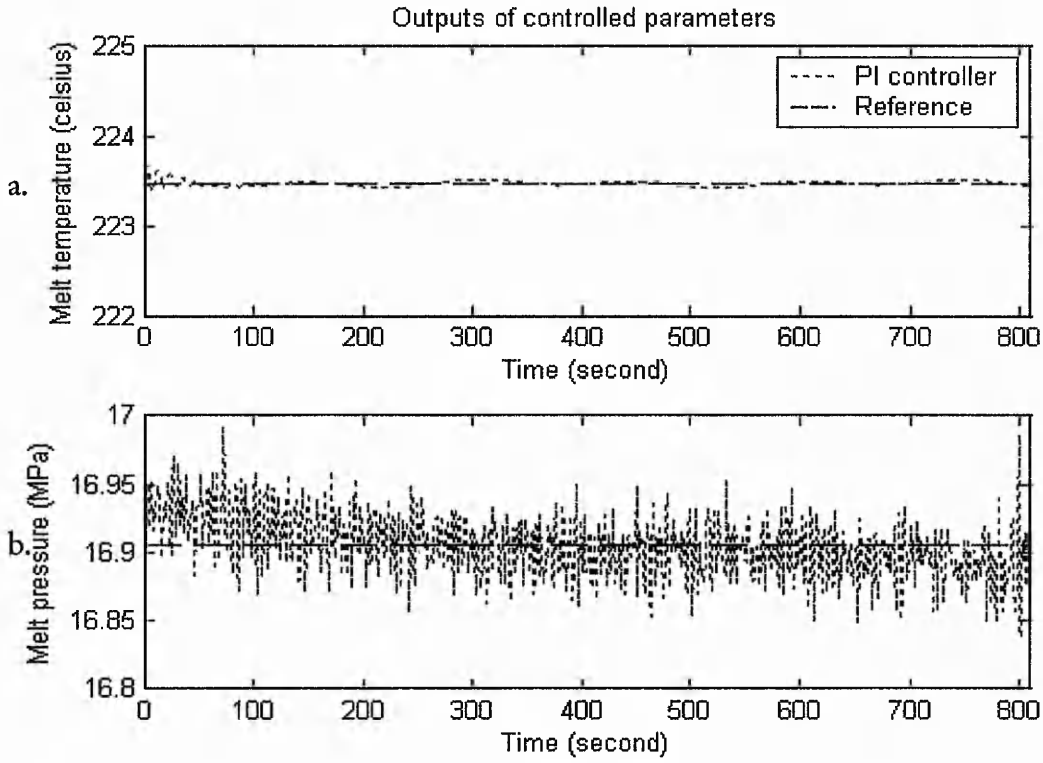

Fig. 6-41: PI controller rejects temperature disturbances using ideal response barrel temperature: **a)** melt temperature, and **b)** melt pressure.

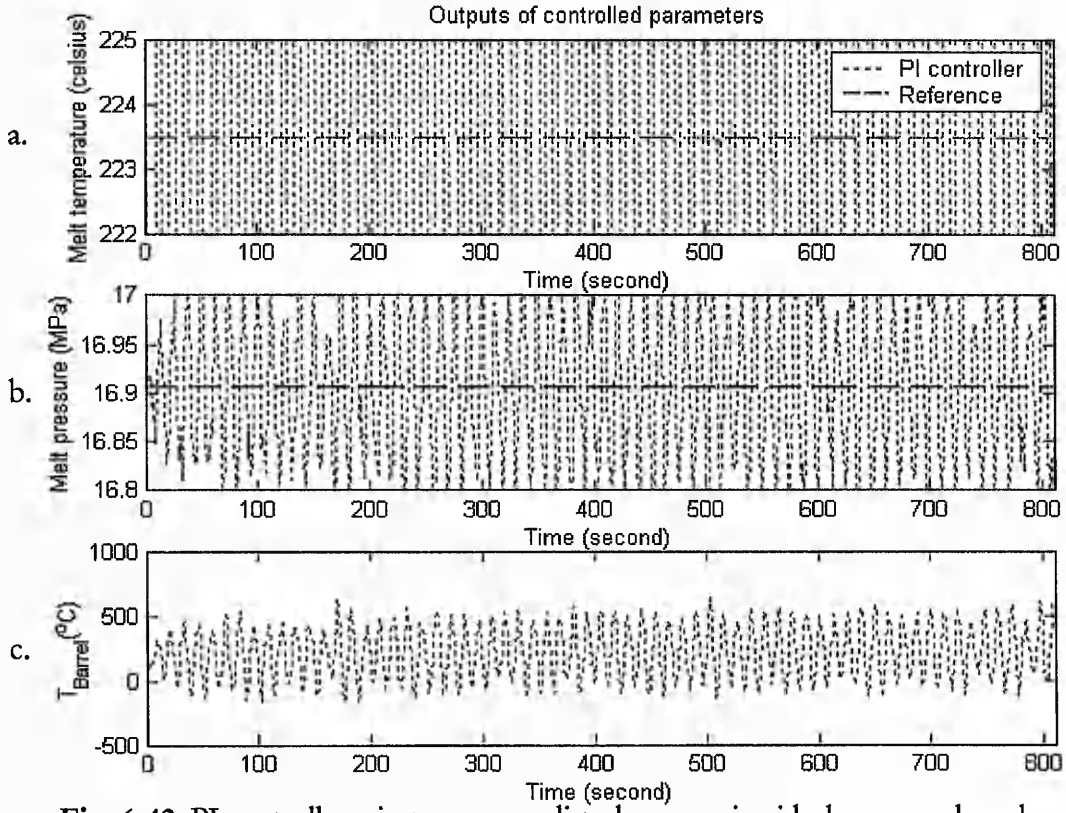

Fig. 6-42: PI controller rejects pressure disturbances using ideal response barrel temperature: **a)** melt temperature, **b)** melt pressure, and **c)** barrel temperature.

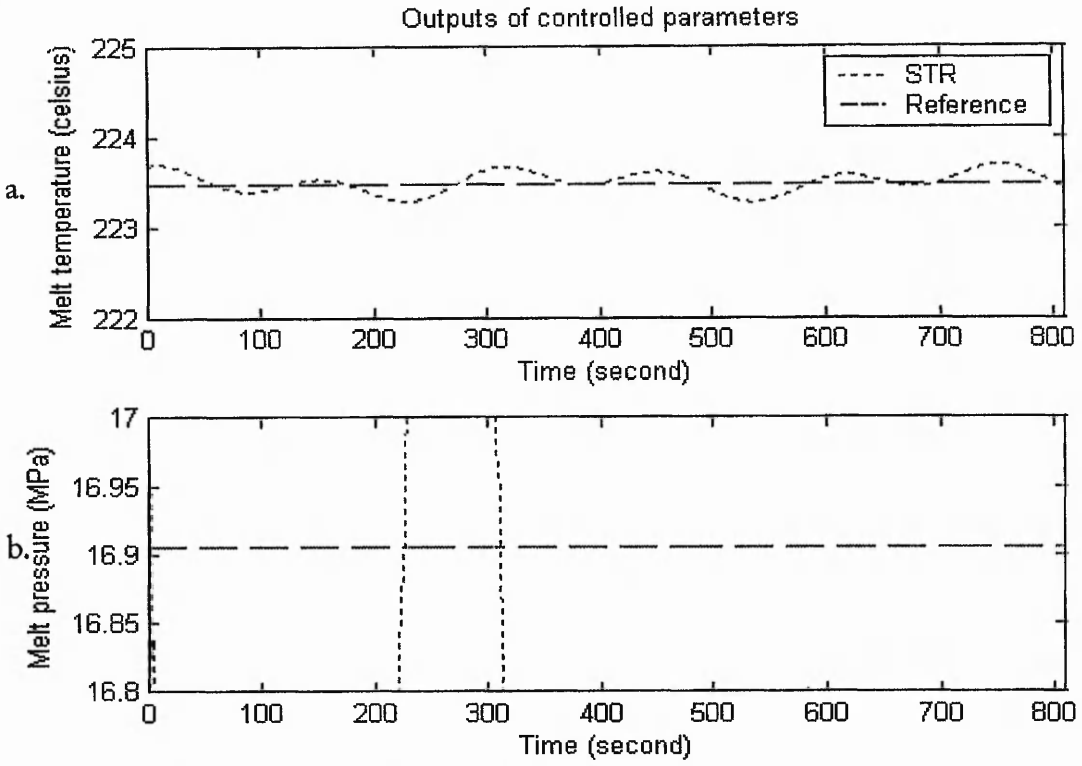

Fig. 6-43: STR rejects temperature disturbances using screw speed: **a)** melt temperature, and **b)** melt pressure.

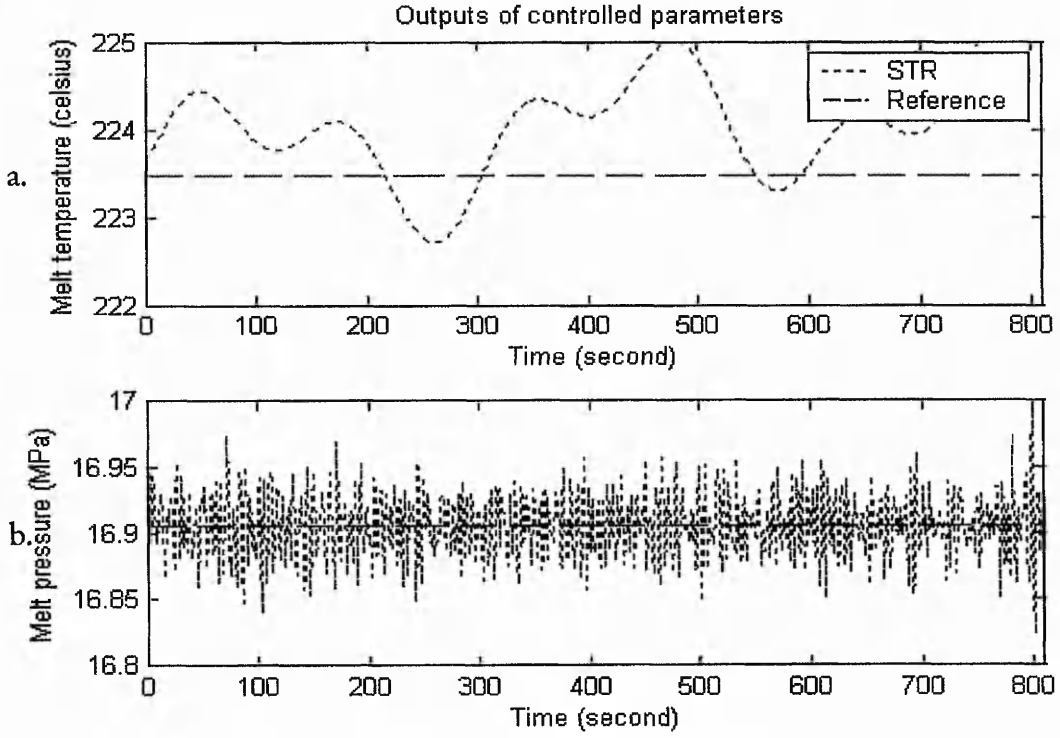

Fig. 6-44: STR rejects pressure disturbances using screw speed: **a)** melt temperature, and **b)** melt pressure.

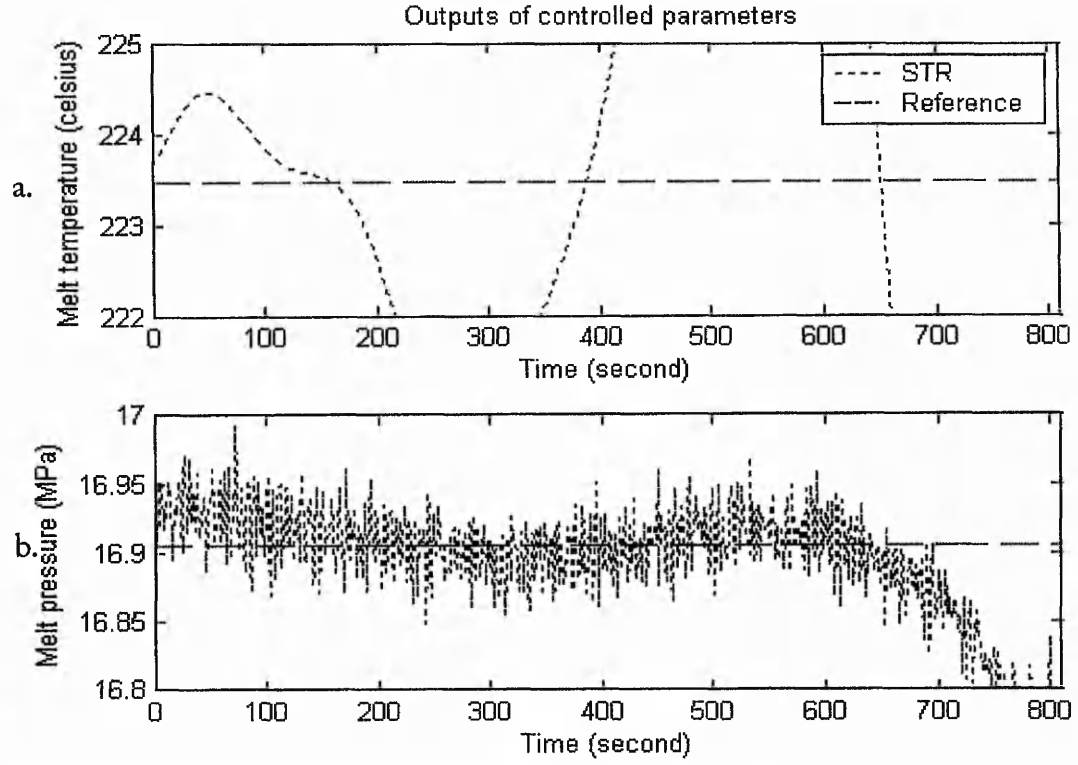

Fig. 6-45: STR rejects temperature disturbances using slow response barrel temperature: **a)** melt temperature, and **b)** melt pressure.

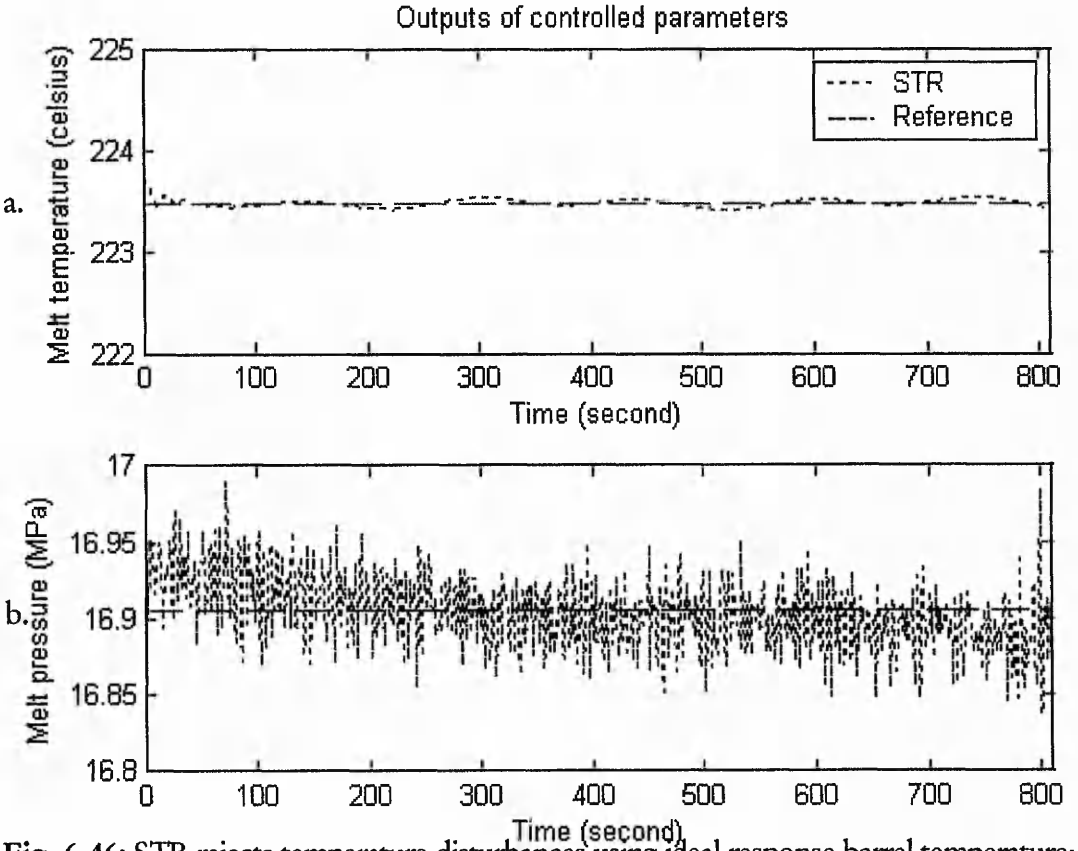

Fig. 6-46: STR rejects temperature disturbances using ideal response barrel temperature: **a)** melt temperature, and **b)** melt pressure.

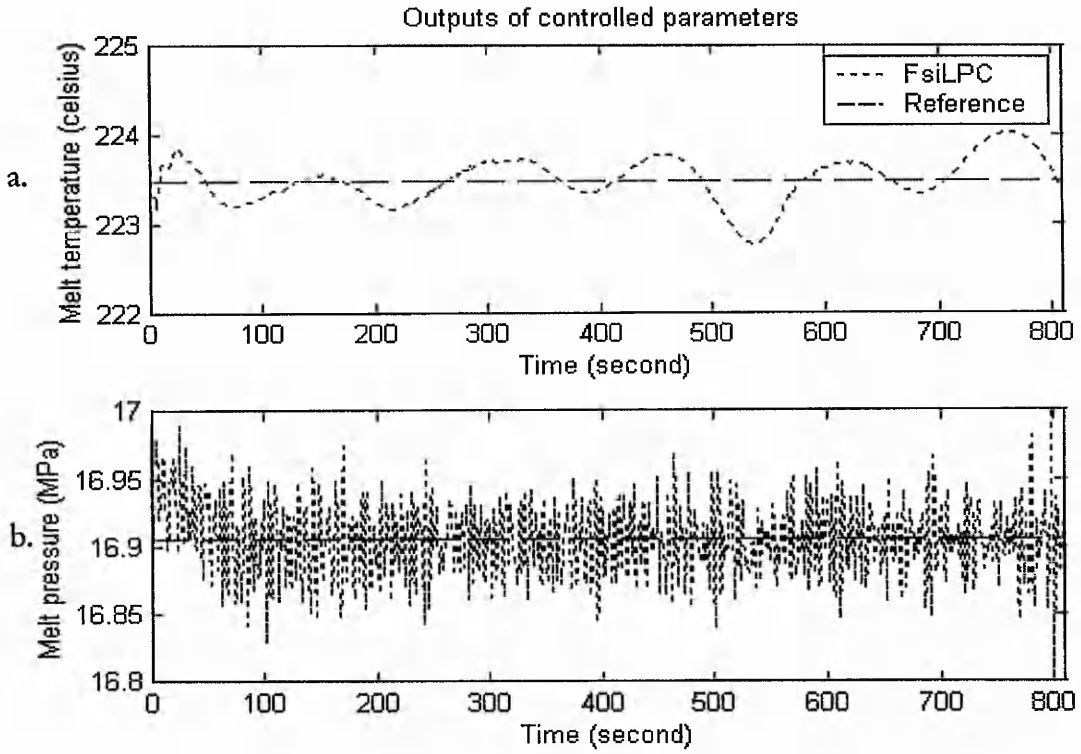

Fig. 6-47: FsiLPC for both temperature and pressure disturbances rejection using screw speed and ideal response barrel temperature: **a)** melt temperature, and **b)** melt pressure.

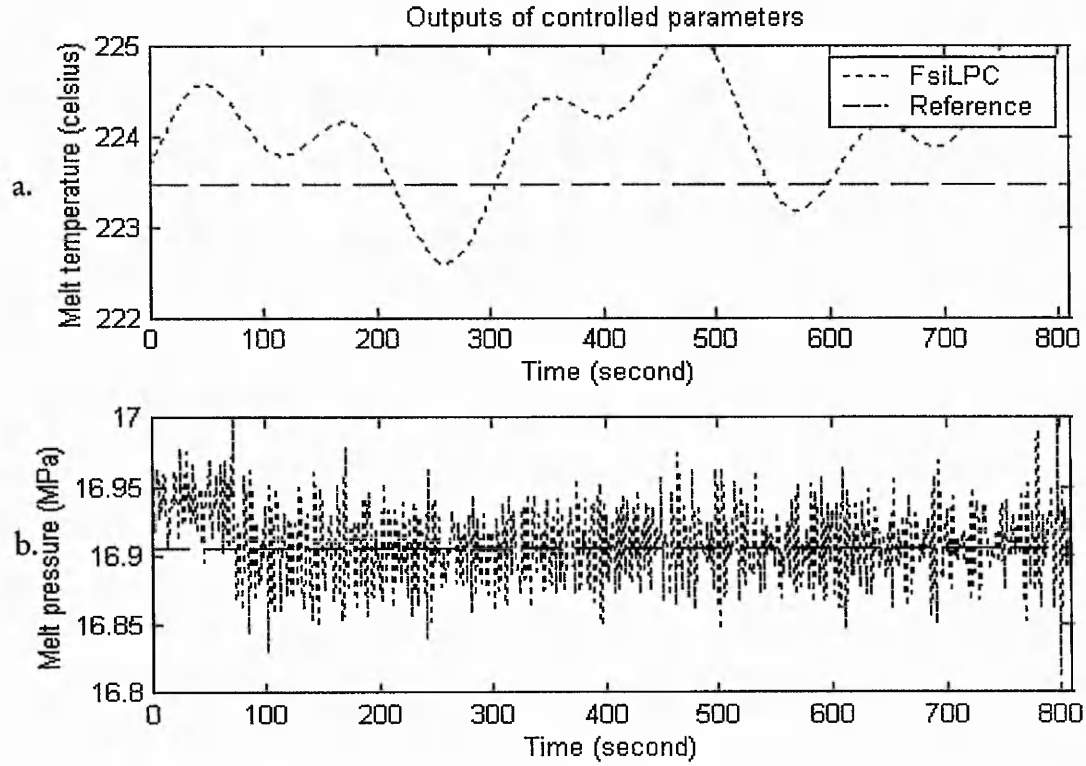

Fig. 6-48: FsiLPC for both temperature and pressure disturbances rejection using screw speed and slow response barrel temperature: **a)** melt temperature, and **b)** melt pressure.

6.5 Summary Remarks

The performance of the FsiLPC system for the extrusion control has been evaluated through simulation studies including a parametric study and a comparative study. The parametric study has investigated the characteristics of the FsiLPC system with respect to changes in the system parameters and variations in the process disturbances. The results of the parametric study indicate that the screw speed and the barrel temperature have different degrees of impact on the melt temperature and the melt pressure. The screw speed is relatively a more effective manipulating parameter. The characteristics of the FsiLPC system are also observed to be depending on the settings of its parameters. These parameters include the initial Euclidean distances, the deadzone radii, the model adaptation settings, the learning rates and the prediction horizon. The operation of the FsiLPC system in response to the variations in the process disturbances is also investigated. Within a specific range of the process disturbances in terms of amplitude and frequency, a stable operation could be ascertained.

In the comparative study, the performance of the FsiLPC system has also been compared with those of the PI and STR control systems. For practical reasons, the designs of the PI and STR control systems are limited to the SISO structures. The implementations of the PI and STR control systems have exhibited a major shortcoming that only one controlled parameter could be regulated at a time. This is insufficient to assure a product of good quality. The FsiLPC system has demonstrated its MIMO ability to control the melt temperature and the melt pressure simultaneously. The predictions of the semi-physical dynamic model in the FsiLPC system have been efficiently used to calculate the suitable control solution.

Chapter 7
Discussion

Single screw extruders remain as a favourite choice of polymer processing device in the plastics industries. This is because the extruders often offer a cost effective approach to produce a product of high quality. The performance of a single screw extruder is determined by the screw geometry and the control system. The design of screw geometry has been extensively researched to meet different requirements of processing conditions. Nevertheless, screw designs alone are not sufficient in practice to produce a product of high quality, especially when it is of a high throughput operation. The need for a good quality and quantity productivity makes an effective control system essential.

There are several process parameters that are important for the design of an extrusion control system. The parameters can be classified into two groups, namely manipulating parameters and controlled parameters. Screw speed, backpressure and barrel temperature are among the popular manipulating parameters. These parameters are the process input parameters. The usefulness of a manipulating parameter is depending on its ability to change the melt condition. In particular, the screw speed is used in nearly all of the extrusion control systems reported in the literature. This is because the heat generated by viscous dissipation attributed to the rotating screw is the most efficient energy to melt polymers inside the extruder. Melt pressure, melt temperature and thickness of the extrudate are examples of the controlled parameters. These parameters are the process output parameters that indicate the melt condition. One of the considerations for selecting the controlled parameters is depending on the accessibility. The melt pressure and the melt temperature are used in most of the extrusion control systems because these two parameters can be measured easily by installing pressure transducers and thermocouples at appropriate locations along the extruder.

To identify the objective of the extrusion control, the dataset of the melt temperature and the melt pressure is reviewed. Variations in these two parameters suggest that the high, intermediate and low frequency disturbances occurred during the extrusion process. The high frequency disturbance occurred at the same frequency as the screw speed. This is the

result of measurement being distorted by the screw flight periodically. To prevent the control performance being affected by this measurement distortion, a low pass filter can be employed for signal conditioning purpose. The impacts of the intermediate and low frequency disturbances on the melt temperature and the melt pressure in general are found to be non-periodical. Their occurrences are attributed to the inconsistency of the operating conditions such as variations in the feed polymer properties. Therefore, minimising the impact of these two disturbances becomes the objective of the extrusion control system.

A Fuzzy supervisory indirect Learning Predictive Control (FsiLPC) system is developed to control the extrusion process. The screw speed and the barrel temperature are employed as the manipulating parameters while the melt temperature and the melt pressure are regarded as the controlled parameters. The performance of the FsiLPC system depends on its ability to predict the controlled signals and to produce the suitable manipulating signals. To predict the controlled signals, a semi-physical dynamic extrusion model is developed.

The semi-physical dynamic extrusion model is governed by conservation laws with the operational-sensitive parameters approximated by FRBS sub-models. The conservation laws are expressed in terms of partial differential equations and solved using the Finite Volume Method. In the present investigation, a converged solution is achieved when the spatial domain of the equations is discretised into 250 discrete volumes with the temporal domain of 0.1 second discrete time. The operational-sensitive parameters of the extrusion process include the melt viscosity, the heat transfer rate, the viscous dissipation rate and the melting rate. These parameters exhibit several characteristics that favour the fuzzy representations in a form of FRBS sub-models. For example, the melt viscosity may change due to the variation in the feed polymer properties, and the viscous dissipation rate is not measurable during the operation hence could not be validated. In a case study, it was found that the prediction of the semi-physical model is improved as the FRBS sub-models adapt to the variation in the feed polymer properties.

The FRBS sub-models in the semi-physical model are identified automatically from the dataset using a GA-Fuzzy algorithm. The identified FRBS sub-models are considered optimal because they contain only a sufficient number of rules and membership functions,

while the accuracy of the approximations is maintained. This helps in aspects of linguistic interpretability, faster computation and less tendency of localised optimality as confronted by the over-parameterised sub-models. The GA-Fuzzy identification process requires a compromise between the sub-model performance and the identification time. This depends very much on the chromosome length and the setting of convergent criteria. The length of a chromosome is defined in Chapter 4 as: $L = s \times r\ (2 \times m + n)$. This signifies that the length increases when the sub-model contains more inputs, outputs, rules, or a higher coding resolution is set during the identification process. A lengthy chromosome induces a larger space of sub-model exploration. This increases the possibility of obtaining a better performance sub-model but the identification might be time consuming.

One of the convergent criteria used in the GA-fuzzy algorithm is the desired fitness level of a sub-model. When a higher fitness level is set as the convergent criterion, a sub-model with higher performance can be expected but the identification time is relatively long. The other commonly used convergent criterion is the desired number of identification iterations. This criterion can determine the time required for the sub-model identification process but cannot assure the sub-model performance.

An alternative approach for automatic identification of the sub-models is by using an Adaptive Neuro Fuzzy Inference System (ANFIS) algorithm (Jang, 1993). To identify a sub-model, the number of membership functions (MFs) for each input of the sub-model is needed to specify. This will determine the number of rules, as the rules in the ANFIS algorithm are obtained by cross-combining the MFs of each input. For example, if the sub-model possesses two inputs and three MFs for each input, then the number of rules would be nine (3^2). The sub-model is then optimised using a hybrid of gradient descent and least-square method. In a preliminary investigation, it was found that the sub-models identified by the ANFIS algorithm produce comparable approximations with those of the sub-models identified by the GA-Fuzzy algorithm. However, the ANFIS sub-models contain redundant rules and this is especially true for the sub-models with more input parameters.

In the FsiLPC system, fuzzy supervisory units are developed to generate appropriate signals for the screw speed and the barrel temperature. Similarly to the FRBS sub-models,

the fuzzy supervisory units could also be identified through various methods including the discussed GA-Fuzzy algorithm and ANFIS algorithm. In the present study, the ANFIS algorithm is employed because each fuzzy supervisory unit has only two input parameters. By assigning three MFs for each input, nine rules are created to define the fuzzy function of each fuzzy supervisory unit. This moderate structure of the fuzzy supervisory unit is a compromise between the flexibility and the sensitivity of the parameter tuning operation. In general, a fuzzy system with more rules and MFs is more flexible to be trained because it has more parameters, but a change in an individual parameter would have less impact on the overall performance of the system.

In comparison with a Model Based Predictive Control (MBPC) system, the FsiLPC system exhibits the similar ability of using a process model effectively to deal with the complicated process control situation. In fact, the FsiLPC system has the capability to use a process model of any structure. The concept of the receding horizon is also applied in the FsiLPC system to promote the efficiency of calculating a suitable control solution. The closed loop control solution is acquired by repeatedly optimising an open loop control performance with every initial condition updated at each time instant. However, the FsiLPC system lacks the ability to explicitly limit the changes of manipulating signals. The simple error back-propagation technique used in the indirect learning method to tune the fuzzy supervisory units prohibits the inclusion of constraints in the cost function. Nevertheless, this limitation is not critical for the extrusion process control because the operation is rather steady. Therefore, demanding changes in the manipulating signals are unlikely to occur.

The performance of the FsiLPC system to control the extrusion process has been evaluated by means of simulation studies, namely a parametric study and a comparative study. The characteristics of the FsiLPC system are examined in the parametric study with respect to changes in the process parameters, settings of system parameters and also variations in the process disturbances. The screw speed is found to have an impact on both the melt temperature and the melt pressure, but the barrel temperature affects only the melt temperature. However, using the screw speed alone as the manipulating parameter is not a wise strategy. A desirable control performance could be obtained only if the system has the flexibility to adjust the impacts of its manipulating parameters. This

is realisable only when both the screw speed and the barrel temperature are employed as the manipulating parameters.

The performance of the FsiLPC system also depends on the settings of system parameters. These parameters include the deadzone radii, training epoch of model adaptation, learning rates and prediction horizon. It is remarked that the setting of prediction horizon has similar effect as assigning constraint to limit the changes of controlled signal in the MBPC system. When the prediction horizon is set to a longer period, a smaller change in the controlled signal occurs at every control cycle.

In a comparative study, the FsiLPC system has demonstrated an encouraging performance in simultaneous control of the melt temperature and the melt pressure. The impacts of process disturbances on both the melt temperature and the melt pressure are reduced. However, the implementation of the FsiLPC system is relatively more computational demanding attributed to the need of simulating the semi-physical model in each control cycle to obtain the predictions. This implies a possible direction for future work to be described in the next chapter.

Chapter 8
Conclusion and Future Work

8.1 Work Achievements

The present research works on modelling and control of a single screw extrusion process. All the research aims have been fulfilled. A new control system, namely Fuzzy supervisory indirect Learning Predictive Control (FsiLPC) system is designed and a semi-physical dynamic extrusion model is developed.

The design of the FsiLPC system has demonstrated the usefulness of soft computing technique to implement the concept of Model Based Predictive Control (MBPC) using a model of any structure. The operating mechanism of the FsiLPC system is similar to that of a MBPC system, but a distinctive strategy is employed that control actions are generated using fuzzy supervisory units. To optimise the control actions, the parameters of the fuzzy supervisory units are adjusted continuously using an indirect learning technique. One of the crucial requirements for a successful operation of the FsiLPC system is the accuracy of model predictions. To meet the requirement, the semi-physical dynamic extrusion model is incorporated in the FsiLPC system as the predictive model. The semi-physical model is developed using hybrid of theoretical and empirical modelling techniques. The model is governed by conservation laws while some process parameters, that ought to be operational-sensitive, are approximated by FRBS sub-models. Model evaluations indicated that the semi-physical model is capable of predicting the complicated behaviour of process parameters, which are distributed, interrelated and varying with the operating conditions.

The performance of the FsiLPC system to control the extrusion process has been evaluated through simulation studies including a parametric study and a comparative study. The parametric study has shown the system performance in response to variations in several system parameters and the process disturbances. As a conclusion, the conditions for the FsiLPC system to achieve a good performance are listed as follows:

- both the screw speed and the barrel temperature are employed as the manipulating parameters;
- the time constant and the pure delay on the response of barrel temperature are below 100 seconds and 40 seconds respectively;
- the parameters of the control system are adequately initialised. An example of the settings is given in Table 8-1;
- the process disturbances are bounded. In general, the disturbances with smaller amplitude and lower frequency are easier to be regulated;
- in cases of faulty readings from the sensors, the tolerances for a stable operation are 20% of the melt temperature and 15% of the melt pressure.

The performance of the FsiLPC system has been then compared with the PI control systems and the self-tuning regulator systems. Encouraging results are obtained by the FsiLPC system in tracking the step-changes of reference signals and minimising the impacts of the process disturbances. The FsiLPC system has demonstrated its ability for simultaneous control of the melt temperature and the melt pressure using both the screw speed and the barrel temperature effectively.

8.2 Suggestions for Future Work

The thesis has demonstrated a combination of different methods in designing the FsiLPC system for the extrusion process. The results of the case studies indicate that the FsiLPC system would help to improve the consistency of the polymer melt conditions. However, the system is by no means perfect and challenges in actual implementation are yet to be investigated. These provide several directions for the future work.

Table 8-1: An example of parameter setting of the FsiLPC extrusion system.

Parameters	Deadzone radii		Model adaptation		Learning rates		Prediction horizon
	*Screw	*Barrel	Epoch	Limit	MSOP	MAP	
Settings	0.02	0.2	10	0.1	0.01	0.1	5

*Screw = Fuzzy supervisory unit of screw speed.

*Barrel = Fuzzy supervisory unit of barrel temperature.

The FsiLPC system for the extrusion control has been extensively evaluated by means of case studies through simulations. Although the result is encouraging, it indicates only the system performance under the known operating conditions. To explore its robustness to unknown conditions, a physical implementation of the FsiLPC system is essential. The realisation of the system needs further considerations including sampling rate selection, filter design, and signal quantisation (Phillips and Nagle, 1990; Chen, 2001; Kavanagh, 2002). Auxiliary systems shall be designed for monitoring and alarming purposes in an event of system operation failure.

The descriptions in Chapter 5 represent the underlying operating concept of the FsiLPC system. Many ideas for further refinements of the system are acquired during the writing-up. Some of these are:

- The present study approximates each manipulating parameter such as the screw speed by using a Multi-Input-Single-Output (MISO) fuzzy supervisory unit. Therefore, several MISO fuzzy supervisory units are identified to generate a vector of manipulating signals in the MIMO system. The design is valid under the assumption that the manipulating parameters have little or negligible interactions with each other. A more general FsiLPC system could be obtained if a MIMO fuzzy supervisory unit is identified using the method as shown in Nefti and Djouani (2002).

- The learning rate, the deadzone radius, and the prediction horizon of the present system are set and remaining constant during the operation. The performance of the FsiLPC system might be improved if the values of these parameters could be varying (Yu, 2003; Gazi *et al*, 2001; Cannon and Kouvaritakis, 2003).

- The tuning of the fuzzy supervisory unit and the FRBS sub-models may eventually lead to the lost of linguistic interpretability. It might be interesting to investigate the effect on the system performance, if constraining methods are applied to conserve the interpretability (Lotfi *et al*, 1996; Antonio, 2000).

The execution speed of the FsiLPC system during the operation is limited by the simulation speed of the semi-physical dynamic model. This is because the calculation of the PDEs-based semi-physical dynamic extrusion model is complicated. A direct solution is by having a simpler dynamic model. Lai and Yu (2000) proposed a steady state model

for the purposes of extrusion process analysis and extruder screw design. The model is governed by algebraic equations and has shown tremendous improvement for the speed of model simulation. In addition, the accuracy of the model predictions is comparable with the results of complex three-dimensional models. These may provide a motivation to extend the algebraic steady state model to a dynamic model.

The present design of the FsiLPC system regards the screw speed and the barrel temperature as the manipulating parameters, while the melt pressure and the melt temperature are the controlled parameters. This MIMO coupling of the process parameters is found difficult due to the large difference between the responses of the manipulating parameters. Therefore, possible couplings of other process parameters could be investigated. The effectiveness of new parameter coupling needs evaluation in terms of model identification and control system design.

References

Abonyi J. *et al*, (1997), Takagi-Sugeno fuzzy control of batch polymerization reactors, *Proc. of IEEE International Conference on Intelligent Engineering Systems*, 251-255.

Albus J.S., (1975), A new approach to manipulator control: The Cerebellar Model Articulate Controller (CMAC), *Trans. of ASME, Journal of Dynamic Systems, Measurement, and Control*, 220-227.

Amellal K. and Lafleur P.G., (1993), Computer simulation of conventional and barrier screw extruder, *Plastics, Rubber and Composites Processing and Applications*, **19**(2), 227-239.

Andersen H.C., (1998), *The Controller Output Error Method*, Ph.D. Thesis, University of Queensland, Australia.

Andersen H.C. *et al*, (1997), A new approach to adaptive fuzzy control: the controller output error method, *IEEE Trans. on Systems, Man and Cybernetics Part B*, **27**(4), 686-691.

Angelov P.P., (2002), An approach to on-line design of fuzzy controllers with evolving structure, *Proc. of International Conference on Recent Advance in Soft Computing*, 164-169.

Antonio F., (2000), Constrained Takagi-Sugeno fuzzy system that allows for better interpretation and analysis, *Fuzzy Sets and Systems*, **118**(2), 307-318.

APME, (2001), *Plastics – At work for a sustainable future- Overview* [Online]. Association of Plastics Manufacturers in Europe. Available from: www.apme.org [Accessed 03 Jun 2004].

Astrom K.J. *et al.*, (1993), Automatic tuning and adaptation for PID controllers – A Survey, *Control Eng. Pract.*, **1**, 699-714.

Astrom K.J. and Hagglund T., (1995), New tuning methods for PID controllers, *Proc. of 3rd European Control Conference*, **3**, 2456-2462.

Astrom K.J. and Wittenmark B., (1995), A survey of adaptive control applications, *Proc. of IEEE Conference on Decision and Control*, 1, 649 –654.

Astrom, K.J., (1996), Adaptive control around 1960, *IEEE Control Systems Magazine*, **16**(3), 44-49.

Babuska R. *et al*, (1998), Identification of MIMO systems by input-output TS fuzzy models, *Proc. of IEEE International Conference on Fuzzy Systems*, **1**, 657-662.

Baez-Lopez D. *et al*, (2001), A package for filter design based on MATLAB, *ASEE/IEEE Frontiers in Education Conference*, **3**, F4D-12-16.

Banks, H.T., (1990), Inverse problems for distributed parameter systems, *Proc. of IEEE Conference on Decision and Control*, **1**, 13-16.

Banks H.T. *et al*, (1994), Noise control in a 3-D structural acoustic system: numerical and experimental implementation of a PDE-based methodology, *Proc. of IEEE Conference on Decision and Control*, **1**, 305-310.

Banks H.T. *et al*, (1997), Experimental confirmation of a PDE-based approach to design of feedback controls, SIAM Journal on Control and Optimization, **35**(4), 1263-1296.

Bezanson L.W. and Harris S.L., (1986), Identification and control of an extruder using multivariable algorithms, *Proc. of IEE*, **133**(D), 145-152.

Bogdan B.P. and Stefan D, (1994), Computer model for optimisation of extruder control system, *Mathematical Models in Automation and Robotics*, 209-214.

Braake H.A.B. Te *et al.*, (1998), Semi-physical modelling of chemical processes with neural networks. *Engineering Applications of Artificial Intelligence*, 11(4) 507-515.

Braake H.A.B. Te *et al.*, (1999) Semi-mechanistic modeling and its application to biochemical processes. In H.B. Verbruggen and R. Babuska, editors, *Fuzzy Control: Advances in Applications*, World Scientific, Singapore, 205-226.

Brauner N. *et al*, (1977), Control of plasticating extruder. *IFAC Conf. on Instrumentation and Automation in the Paper, Rubber and Plastics Industries*, **3**, 353-360.

Breiman L. *et al*, (1984), *Classification and Regression Trees*. Belmont, CA: Wadsworth.

Brukek I. and Balch G.S., (1989), Melting mechanism in single screw extrusion, *Polymer Engineering and Science*, **29**(4), 258-267.

Cannon M. and Kouvaritakis B., (2003), Efficient constrained model predictive control with asymptotic optimality, *SIAM Journal on Control and Optimization*, **41**(1), 60-82.

Carr D.M., (1985), Advantages of cascaded temperature controllers as used on plastics extruders. *IEEE Conf. of Electrical Engineering Problems in the Rubber and Plastics Industries*, 21-28.

Chan D. *et al*, (1986), Dynamic behaviour of a single screw plasticating extruder Part II: Dynamic Modelling, *Polymer Engineering and Science*, **26**(2), 152-161.

Chan G.S.H. and Hon K.K.B., (1990), Integration of computing techniques for plastics extrusion die design, *Journal of Computer-Aided Engineering*, **7**(2), 37-42.

Chan, L.C.Y. and Asokanthan, S.F., (2001), CMAC based controller for hydro-mechanical systems, *Proc. of the American Control Conference*, **6**, 4496-4501.

Chen C.T., (2001), *Digital Signal Processing: Spectral Computation and Filter Design*, Oxford University Press, Oxford.

Chen F.C. and Khalil H.K., (1992), Adaptive control of a class of nonlinear discrete-time systems using neural networks, *IEEE Transactions on Automatic Control*, **40**(5), 791-801.

Chen Z.L. *et al*, (2003), Proposal of an empirical viscosity model for quality control in the polymer extrusion process, *Polymer Testing*, **22**(5), 601-607.

Chiruvella R.V. *et al.*, (1995), Numerical simulation of fluid flow and heat transfer in a single-screw extruder with different dies, *Polymer Engineering and Science*, **35**(3), 261-273

Chiu S.H. and Pong S.H., (1999), In-line viscosity control in an extrusion process with a fuzzy gain scheduled PID controller, *Journal of Applied Polymer Science*, **74**, 541-555.

Chiu S.H. and Pong S.H., (2001), In-line viscosity fuzzy control, *Journal of Applied Polymer Science*, **79**, 1249-1255.

Chodavarapu P. and Spong M., (1996), On non-collocated control of a single flexible link, *Proc. of IEEE International Conference on Robotics and Automation*, 1101-1106.

Coates P.D. *et-al*, (2003), In-process vibrational spectroscopy and ultrasound measurements in polymer melt extrusion, *Polymer*, **44**(19), 5937-5949.

Cordón O. *et al*, (2001), *Genetic Fuzzy Systems: Evolutionary Tuning and Learning of Fuzzy Knowledge Base*, World Scientific Publishing Co., Singapore.

Corporation, R. (1986), *Plastics Processing - Technology and Health Effects*. Noyes Data Corporation, USA.

Costin M.H. *et al*, (1982a), A critical review of dynamic modeling and control of plasticating extruders, *Polymer Engineering and Science*, **22**(7), 393-401.

Costin M.H. *et al*, (1982b), On the dynamics and control of a plasticating extruder, *Polymer Engineering and Science*, **22**(17), 1095-1106.

Dahlin E.B., (1968), Designing and tuning digital controllers, *Instruments and Control Systems*, **41**(6), 77-83.

Denbigh P., (1998), *System Analysis and Signal Processing: with emphasis on the user of MATLAB*, Harlow:Addison-Wesley, England.

Diamond H. Controls Ltd, (1971), Three-term process control system, UK Patent No. 1256500.

Donovan R.C. *et al*, (1971), Pressure profiles model for plasticating extruders, *Polymer Engineering and Science*, **11**(6), 484-491.

Dormeier S., (1979), Digital temperature control: A way to improve the extrusion process, *American Society of Mechanical Engineers, Applied Mechanics Division*, 216-219.

Dormeier S., (1994), Temperature control algorithms for plastics processing units, *Mathematical Models in Automation and Robotics*, 7-15.

Dubois D. and Prade H., (1998), Soft computing, fuzzy logic, and artificial intelligence, *Soft Computing*, **2**(1), 7-11.

Dumitrescu S. and Wu X., (2004), Algorithms for optimal multi-resolution quantization, *Journal of Algorithms*, **50**(1), 1-22.

Espinosa J. and Vandewalle J., (1998), Predictive control using fuzzy models applied to a steam generating unit, *Proc. of the 3rd International FLINS Workshop*, Antwerp, 151-160.

Fassihi F.T., (1993), *Computer Aided Design and Manufacture of Plasticating Extruder Screws for Polymer Processing*, PhD Thesis, The Nottingham Trent University.

Fenner R.T., (1970), *Extruder Screw Design: Solutions to Polymer Melt Flow in Extrusion Equipment, including Wire-coating Dies*. ILIFFE Books: Published for the Plastics Institute, London.

Fenner R.T., (1978), Computer-aided design of extruder screws, *Plastics and Rubber: International*, **3**(1), 27-30.

Forssell U. and Lindskog P., (1997), Combining semi-physical and neural network modeling: an example of its usefulness, *SYSID*, 795-798.

Francis Shaw, (1971), *Maintenance Manual – for the ShawDavis standard 2.5" MK3 thermatic extruder & ancillaries*, Francis Shaw & Co. (Manchester) Limited.

Gawthrop P.J. *et al*, (1990), Adaptive temperature control of industrial processes: a comparative study, *IEE Proc. of Control Theory and Applications*, **137**(3), 137-144.

Gawthrop P.J. *et al*, (1998), Multivariable continuous-time generalised predictive control: A state-space approach to linear and non-linear systems. *IEE Proc. Of Control Theory and Applications*, **145**(3), 241-250.

Gazi V. *et al*, (2001), Adaptive control of discrete time nonlinear systems using dynamic structure approximators, *Proc. of American Control Conference*, **4**, 3091-3096.

Gen M. and Cheng R., (1996), Optimal design of system reliability using interval programming and genetic algorithms. *Computer and Industrial Engineering*, **31**(1/2), 237-240.

Guo P. *et al*, (1993), Polymer extrusion production control using active recognition and adaptive control system, *IEEE International Conference on Fuzzy Systems*, 779-784.

Halasz L., (1993), *Control Methods in Polymer Processing*. Elsevier Science Publishers, The Netherlands and Akademiai Kiado, Budapest, Hungary.

Hannequart J.P. (2004), Good Practices Guide on Waste Plastics Recycling: a guide by and for local and regional authorities [online]. Association of Plastics Manufacturers in Europe. Available from: www.apme.org [Accessed 25 Apr 2004].

Holland J., (1975), *Adaptation in Natural and Artificial Systems*. University of Michigan Press.

Hsia T.C., (1977), *System Identification: Least-Squares Methods*. D. C. Heath and Company.

Huang Y., (1999), *Extrusion Die Design using Finite Element Method for Sheet and Pipe Dies*, Ph.D. thesis, Department of Mechanical & Manufacturing Engineering, The Nottingham Trent University.

Jang J.S., (1993), ANFIS: Adaptive-Network-based Fuzzy Inference Systems, *IEEE Trans. on Systems, Man, and Cybernetics*, **23**(3), 665-685.

Jang J.S., (1994), Structure determination in fuzzy modeling: a fuzzy CART approach. *IEEE International Conference on Fuzzy Systems*, **1**(1), 480 - 485.

Jang J.S. and Sun C.T., (1995), Neuro-Fuzzy modeling and control, *Proc. of IEEE*, **83**(3), 378-406.

Jang J.S. *et al*, (1997), *Neuro-Fuzzy and Soft Computing: A Computational Approach to Learning and Machine Intelligence*, Prentice Hall.

Jha R. and He C., (2002), Neural-network-based adaptive predictive control for vibration suppression of smart structures, *Smart Material and Structures*, **11**(6), 909-916.

Karaboga D. and Kahnh A., (1996), Tuning PID controller parameters using tabu search algorithm, *IEEE International Conference on Systems, Man and Cybernetics. Information Intelligence and System*, 1, 134-6.

Kavanagh R.C., (2002), Improved quantization error characteristics in FIR differentiators using irregular sampling, *IEEE Signal Processing Letters*, 9(10), 326-328.

Kaya A. and Rice L.S., (1985), Measurement and control problems for extrusion processes, *Proc. of the American Control Conference*, 1149-1154

Kiszka J.B. *et al*, (1985), Energetistic stability of fuzzy dynamic systems, *IEEE Transactions on Systems, Man and Cybernetics*, 15(6), 783-792.

Kochhar A.K. and Parnaby J., (1977), Dynamical modelling and control of plastics extrusion processes, *Automica*, 13, 177-183.

Koo K.M. and Kim J.H., (1996), CMAC based control of nonlinear mechanical system, *IEEE Proc. of International Conference on Industrial Electronics, Control, and Instrumentation*, 3, 1954-1959.

Kuo B.C., (1992), *Digital Control Systems*. Saunders College Pub., Tex., USA.

Kwag D.S. *et al*, (2002), A 3D numerical study of fluid flow and heat transfer in a single screw extruder, *International Polymer Processing*, 17(2), 95-101.

Lai E. and Yu D.W., (2000), Modelling of the plasticating process in a single-screw extruder: a fast track approach, *Polymer Engineering and Science*, 40(5), pp. 1074-1084.

Lang, U. and Michaeli, W., (1998), Development of a mathematical model for the calculation of the pressure drop in extrusion dies, *Journal of Reinforced Plastics and Composites*, 17(12), 1110-1118.

Leffew K.W. *et al*, (1987), Application of digital control techniques to a laboratory extrusion process, *Proc. of the American Control Conference*, 1002-1007.

Levy, S., (1981), *Plastics Extrusion Technology Handbook*, Industrial Press, New York.

Lindskog, P. and Sjoberg J. (1995), A comparison between semi-physical and black-box neural net modeling: a case study. *Proc. Int. Conf. Eng. App. Artificial Neural Networks*, 235 - 238.

Lindskog P. and Ljung L., (1994), Tools for semi-physical modeling. *Proc. IFAC SYSID*, **3**, 237-242.

Lindt J.T., (1976), A dynamic melting model for a single screw extruder, *Polymer Engineering and Science*, **16**(4), 284-291.

Lindt J.T., (1985), Mathematical modeling of melting of polymers in a single-screw extruder: A critical review, *Polymer Engineering and Science*, **25**(10), 585-588.

Linko P. *et al*, (1992), Neural networks in fuzzy extrusion control, *ICHEME Symposium*, **126**, 401-410.

Ljung L., (1999), *System Identification: Theory for the User*. Prentice-Hall, Inc., New Jersey.

Lobocki E.J., (1977), An analogue model for the transient behaviour of the melting process in a plasticating extruder, *Proc. Of The AICA Congress*, 1025-1031.

Lopez M.J. and Rubio F.R., (1992), LQG/LTR control of ship steering autopilots, *Proc. of IEEE International Symposium on Intelligent Control*, 447-450.

Lotfi A. *et al*, (1996), Interpretation preservation of adaptive fuzzy inference systems, *Journal of Approximating Reasoning*, **15**, 379-393.

Lotfi A. and Howarth M., (1998), *An Intelligent Closed-Loop Control of Solder Paste Stencil Printing Stage Of Surface Mount Technology.* Technical Report, Nottingham Trent University.

Lu C.H. and Tsai C.C., (2001), Adaptive decoupling predictive temperature control for an extrusion barrel in a plastic injection moulding process, *IEEE Transactions on Industrial Electronics*, **48**(5), 968-975.

Maddock B.H., (1959), A visual analysis of flow and mixing in extruder screw, *SPE Journal*, **15**(5), 383-394.

Maeda M. *et al*, (1995), Predictive fuzzy control of an autonomous mobile robot with forecast learning function, *Fuzzy Sets and Systems*, **72**(1), 51-60.

Mahfouf M. *et al*, (1999), Fuzzy Takagi-Sugeno Kang model predictive control for process engineering, *IEE Two-Day Workshop on Model Predictive Control: Techniques and Applications - Day 2 (Ref. No. 1999/096)*, 4/1 -4/4.

Mahfouf M. *et al*, (2002a), Fuzzy model-based predictive control using an ARX structure with feedforward, *Fuzzy Sets and Systems*, **125**(1), 39-59.

Mahfouf M. *et al*, (2002b), On-line elicitation of Mamdani-type fuzzy rules via TSK-based generalised predictive control (GPC) and self-organising fuzzy logic control (SOFLC) for anaesthesia, *Proc. of European Symposium on Intelligent Technologies*, 26-31.

Marion M. *et al*, (2003), Design of a soft sensor for polymer extrusion, *Proc. of ANTEC*, **1**, 2003, 207-212.

McCulloch W.S. and Pitts W.H., (1943), A Logical Calculus of the Ideas Immanent in Nervous Activity, *Bulletin of Mathematical Biophysics*, **5**, 115-137.

McKay B. *et al*, (1996), Extruder modelling: A comparison of two paradigms, *UKACC International Conference on Control*, **427**, 734 -739.

Medora, N.K. and Kusko, A., (1995), Power harmonic problems at a plastics extrusion plant, *IEEE Industry Applications Conference*, **3**, 8-12.

Menges G. and Giegerich V., (1972), Melt quality control in extrusion processes, *SPE ANTEC*, 793-795.

Menon P.K. and Yousefpor M., (1996) Design of nonlinear autopilots for high angle of attack missiles, *AIAA Guidance Navigation and Control Conference*, 3896-3913.

Miller W.T. III *et al*, (1987), Real-time dynamic control of an industrial manipulator using a neural network-based learning controller, *IEEE Trans. Robotics and Automation*, **6**(1), 1-9.

Minorsky, N., (1922), Directional stability and automatically steered bodies, *J. Am Soc Nav Eng*, **34**, 280.

Moore J.B, (1989), Modern controls for plastics and rubber extrusion, *IEEE Conference on Electrical Engineering Problems in the Rubber and Plastics Industries*, 1-4.

Morari M. and Lee J.H., 1999, Model Predictive Control: Past, Present and Future, *Computers and Chemical Engineering*, **23**, 667-682.

Nefti S. and Djouani K., (2002), Fuzzy modeling of MIMO non linear system: Complexity reduction, *Proc. of the IEEE International Conference on Systems, Man and Cybernetics*, 2, 185-189.

Nelson R.W. *et al*, (1986), Dynamic behaviour of a single screw plasticating extruder Part I: Experimental study, *Polymer Engineering and Science*, **26**(2), 144-151.

Nise N.S., (2000), *Control Systems Engineering*. John Wiley & Sons Inc., New York.

Patankar S.V., (1980), *Numerical heat transfer and fluid flow*, Hemisphere Pub. Co., Washington.

Potente H. and Hanhart W., (1994), Design and processing optimisation of extruder screws, *Polymer Engineering and Science*, **34**(11), 937-945.

Pennington J.N., (1994), Infrared sensor monitors extrusion temperature, *Modern Metals*, **50**(6), 34B-34G.

Phillips C.L. and Nagle H.T., (1990), *Digital Control System Analysis and Design*. Prentice-Hall, London.

Pomares H. *et al*, (2001), Fine tuning of fuzzy controllers using a two-stage algorithm, *Proc. of IEEE International Conference on Fuzzy Systems*, **3**, 1479-1482.

Prentice P., (1995), Improved productivity through extruder screw design, *Proc. in Screws for Polymer Processing – the way to better productivity*, RAPRA Technology Ltd., paper 2, England.

Psaltis D. *et al*, (1988), A multilayered neural network controller, *IEEE Control Systems Magazine*, **8**(2), 17-21.

Qiu D.Q., (1998), *Experimental Study and Simulation of Single Screw Extrusion induding The Effect of Grooved Feed Section*, Ph.D. thesis, Department of Mechanical & Manufacturing Engineering, The Nottingham Trent University.

Raman V. *et al*, (1995), Numerical simulation of fluid flow and heat transfer in a single-screw extruder with different dies, *Polymer Engineering and Science*, **35**(3), 261-273.

Rauwendaal C., (1986), *Polymer Extrusion*. Hanser Publishers, Macmillan Publishing Company Inc., New York.

Reay D.S., (1999), Comments on a new approach to adaptive fuzzy control: the controller output error method, *IEEE Trans. on Systems, Man and Cybernetics Part B*, **29** (4), 545-546.

Reber D.H. *et al*, (1973), A mathematical model for predicting dynamic behavior of a plasticating extruder, *Polymer Engineering and Science*, **13**(5), 346-356.

Rosato D., (1997), *Plastic Processing Data Handbook (2nd ed.)*, Chapman & Hall, London.

Roubos J.A. *et al*, (1999), Fuzzy model-based predictive control using Takagi-Sugeno models, *International Journal of Approximate Reasoning*, **22**(1-2), 3-30.

Sabota K.D. *et al*, (1995), Advanced temperature measurements in polymer extrusion, *Conference Proc. of ANTEC*, **2**, 2832-2842.

Sanchez J.M.M., (1976), *Adaptive Predictive Control System*, USA Patent No. 4, 197, 576.

Sanchez J.M.M. and Rodellar J., (1996), *Adaptive Predictive Control: from the concepts to plant optimisation*, London, Prentice hall.

Spalding M.A. *et-al*, (2003), Temperature gradients in the channels of a single screw extruder, *Proc. of ANTEC*, **1**, 202-206.

Strong, A.B., (1996), *Plastics: materials and processing*, London, Prentice hall.

Surmann H. and Selenschtschikow A., (2002), Automatic generation of fuzzy logic rule bases: Examples I, *Proc. of NF*, 75-81.

Syrjala S., (1999), On the analysis of fluid flow and heat transfer in the melt conveying section of a single-screw extruder, *Numerical Heat Transfer*, **35**(A), 25-47.

Syrjala S., (2000), Numerical simulation of nonisothermal flow of polymer melt in a single-screw extruder: A validation study, *Numerical Heat Transfer*, **37**(A), 897-915.

Tadmor Z., (1966), Fundamentals of plasticating extrusion: part I: A theoretical model for melting, *Polymer Engineering and Science*, **6**(3), 185-190.

Tadmor Z. and Klein I., (1970), *Engineering Principles of Plasticating Extrusion.* Van Nostrand and Reinhold Co., New York.

Tadmor Z. *et al*, (1974), Dynamic model of a plasticating extruder, *Polymer Engineering and Science*, **14**(2), 112-119.

Takagi T. and Sugeno M., (1985), Fuzzy identification of systems and its applications to modelling and control, *IEEE Trans. on Systems, Man and Cybernetics Part B*, **15**, 116-132.

Tan K.C. and Li Y., (1997), Evolutionary system identification in the time-domain, *Proc. I. Mech. E., Part I, Special Issue on Applications of Genetic Algorithms to Eng. Systems*, **211**(4), 319-323.

Temes G.C. and Mitra S.K., (1973), *Modern Filter Theory and Design.* Wiley-Interscience, New York.

Thomas L.H., (1949), *Elliptic Problems in Linear Differential Equations over a Network*, Watson Sci. Comput. Lab. Report, Columbia University, New York.

Todd D.B, (1998), *Plastics compounding: equipment and processing*, Hanser/Gardner Publications, Cincinnati.

Tomlin C. *et al*, (1995), Output tracking for a non-minimum phase dynamic CTOL aircraft model, *Proc. of IEEE Conference on Decision and Control*, 1867-1872.

Tsai C.C. and Lu C.H., (1998a), Multivariable self-tuning temperature control for plastic injection molding process, *IEEE Transactions on Industry Applications*, **34**(2), 310-318.

Tsai C.C. and Lu C.H., (1998b), Fuzzy supervisory predictive PID control of a plastics extruder barrel, *Journal of the Chinese Institute of Engineers*, **21**(5), 619-624.

Turnbull G.F., (1972), Cascade control of melt temperature for extruding and injection moulding machine, *IFAC Conf. on Instrumentation and Automation in the Paper, Rubber and Plastics Industries*, 8.5/1-8.5/13.

Whelan A. and Dunning D.J., (1982), *Development in plastics technology – 1*, Applied Science Publishers, London, UK.

Versteeg H.K. and Malalasekera W., (1995), *An introduction to computational fluid dynamics: The finite volume method*, Longman Scientific & Technical, England.

Viriyayuthakorn M. and Kassahun B., (1984), Three-dimensional model for plasticating extrusion screw design, *SPE ANTEC*, 81-84.

Wagner M.G. *et al*, (1997), Neural networks for steady state modelling of an extruder, *Artificial Intelligence in Engineering*, **11**(4), 375-382.

Weisbrod, S.P., (1969), Time proportioning temperature control system, USA Patent No. 3443121.

White D.H. and Schott N.R., (1972), Dynamic testing of plastics extrusion system, *SPE ANTEC*, 793-795.

White J.L., (1991), *Twin-screw extrusion: technology and principles*, Hanser Publishers, New York.

Whitley D., (1993), *A Genetic Algorithm Tutorial*. Technical Report, Colorado State University.

Wilczynski K., (1989), Evaluating screw performance in a single-screw extrusion process, *Polymer-Plastics. Technological Engineering*, **28**(7&8), 671-690.

Wilczynski, K., (2001), SSEM: A computer model for a polymer single-screw extrusion, *Journal of Materials Processing Technology*, **109**(3), 308-313.

Wilde D.J. and Beightler J.A., (1967), *Foundations of Optimization*, Prentice Hall, Englewood Cliffs, N. J.

Wong A.C.Y. *et al*, (1998), Breakup of solid bed in melting zone of single screw extruder. Part I – Mathematical model, *Inst. of Plastic*, **26**, 336-342.

Yamamoto and Hashimoto, (1991), Present status and future needs: The view from Japanese industry, *Proc. 4th International Conference on Chemical Process Control*, 1-28.

Yang B. and Lee L.J., (1986a), Process control of polymer extrusion. Part I: Feedback control, *Polymer Engineering and Science*, **26**(3), 197-204.

Yang B. and Lee L.J., (1986b), Process control of polymer extrusion. Part II: Feedforward control, *Polymer Engineering and Science*, **26**(3), 205-213.

Yu D.W., (2000), *Development of Intelligent Design Tool of Polymer Screw Extruder*, Ph.D. thesis, Department of Mechanical & Manufacturing Engineering, The Nottingham Trent University.

Yu W. and Li. X., (2003), Fuzzy Neural Modeling Using Stable Learning Algorithm, *Proc. of the American Control Conference*, 5, 4542-4547.

Z. Fuhua *et al*, (1998), Studies on theory of single screw plasticating extrusion: Part I, Physical model of extrusion, *SPE ANTEC*, 90-92.

Zadeh L.A., (1965), Fuzzy sets, *Information and Control*, **8**, 338-352.

Zhang, X *et al*, (2002), PDE modeling and control of a flexible two-link manipulator, *Proc. of American Control Conference*, **5**, 3796-3801.

Ziegler J.G. and Nichols N. B., (1942), Optimum Settings for Automatic Controllers. *Transaction on American Society of Mechanical Engineers*, **65**, 433-444.

Appendix 1

Properties of Various Polyethylene Polymers (Qiu, 1998)

Table 1: Polymer properties:

Polymer properties	LLDPE[1]	MDPE[2]	HDPE[3]
Density of solid polymer, ρ_s (kg/m^3)	920	940	960
Density of melt polymer, ρ_m (kg/m^3)	750	770	770
Heat capacity of solid, C_s (J/kg°C)	2190	2498	2480
Heat capacity of melt, C_m (J/kg°C)	2240	2426	2572
Heat fusion, λ (J/kg)	106500	166350	141100
Melting point, T_m (°C)	124	124	126
Solid thermal conductivity, K_s (W/m°C)	0.21	0.21	0.21
Melt thermal conductivity, K_m (W/m°C)	0.23	0.22	0.22

[1] Grade LLN1004YB, manufactured by EXXON, France.

[2] Grade NCPE 2420, manufactured by NESTE, Sweden.

[3] Grade 3802 YCF, manufactured by FINA, EEC.

NOTTINGHAM TRENTNIVERSITY
DEPARTMENT OF MECHANICAL AND MANUFACTURING ENGINEERING

Appendix 2

A Running Procedure for the Francis Shaw Extruder

J Kipling and N Mullen
Polymer Engineering Centre
March 1998

THE EXTRUDER SHOULD ONLY BE USED BY AUTHORISED PERSONNEL.

WHEN THE MACHINE IS BEING RUN 3 PEOPLE WILL BE REQUIRED

1. Starting up and Running

Warming up the machine

1. The screw requires installing into the barrel. Check that there are no polymer beads in the barrel or in the section where the screw locates into the machine. Screw the screw adapter into the screw to push the screw into the extruder barrel. Ensure that the screw is properly located into the keyway, which is located in the section of the machine adjacent to the barrel end feed hopper. Ensure that the screw rotates freely. Remove the screw adapter and screw in the screw nose, using the screw nose holder (Figure 1).

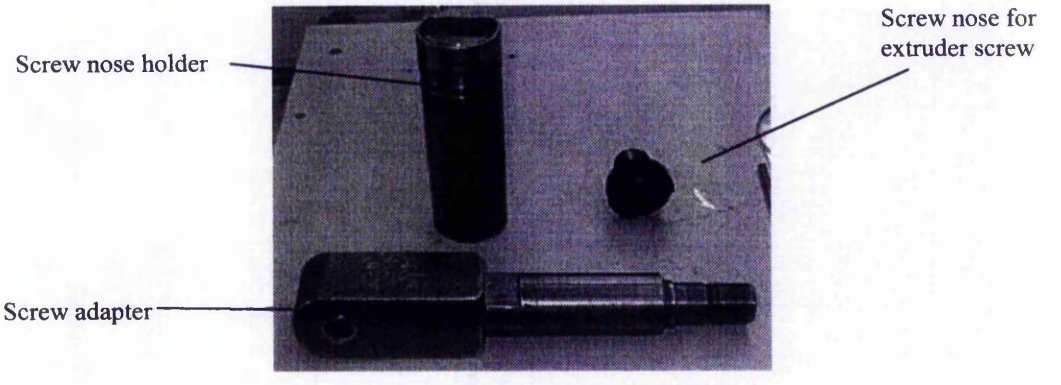

Figure 1 The screw adapter and nose screw

2. Fit the breaker plate, die and the adapter zone heater. Bolt the die holder into position. **THE DIE AND BREAKER PLATE MUST BE CLEAN**.

3. Connect the adapter heater plug on the front end of the machine to the die and the metal sheathed thermocouple to the die head zone. (The adapter heater heats the die and the temperature for this is set on the main control panel with the other heaters (Figure 2).)

J Kipling and N Mullen
Polymer Engineering Centre
March 1998

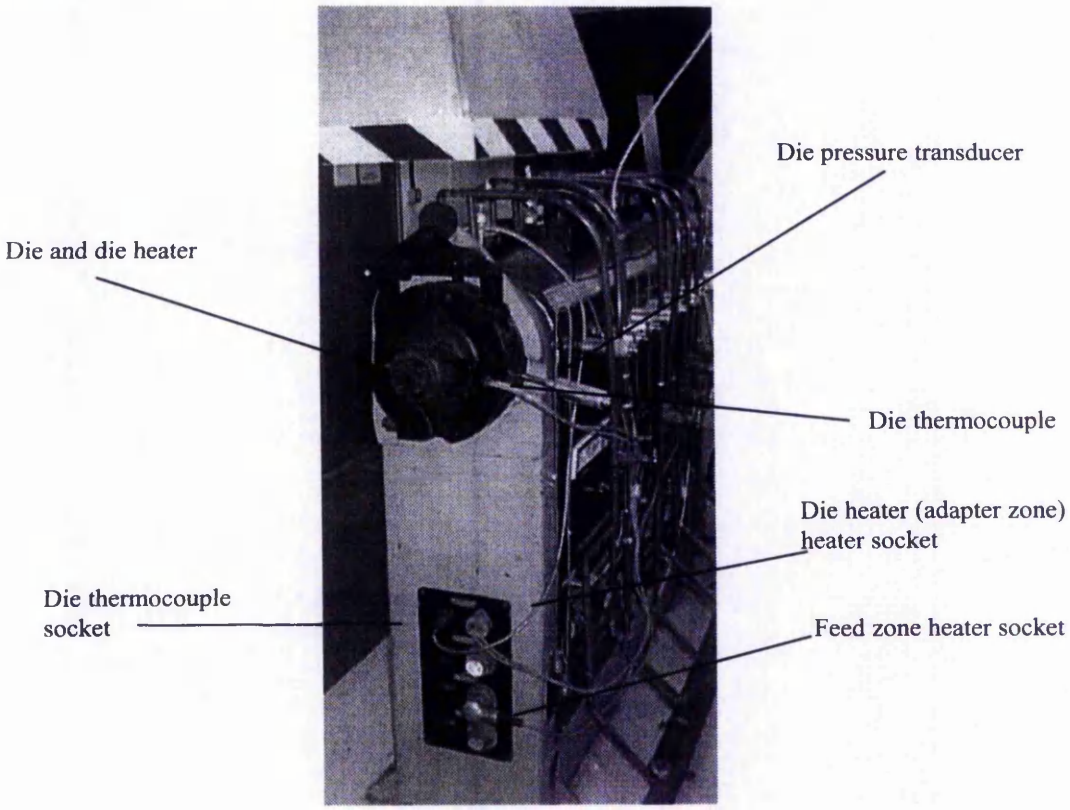

Figure 2 Extruder and the thermocouple and die heater sockets

4. The heater band for the feed zone heater is plugged in the head zone 2 socket at the front of the machine. (The temperature setting is controlled on the main control panel with the rest of the heaters.) The thermocouple wires from the head zone should be plugged into thermocouple socket 3, which is located on the right hand side of the machine (transducer side) near its base. Readings from this transducer are recorded on the Head zone 3 meters on the main control panel (Figure 4).

5. Open wall water lever ball valve. This is located on the wall near the drive motor.

6. Open red floor screw water valve. This is located directly behind the PC, near driving motor.

7. Set the red screw water valve on the gearbox at the entrance pipe for cooling hopper throat so that the ball in the sight glass floats. (This is next to the feed hopper (Figure 3).)

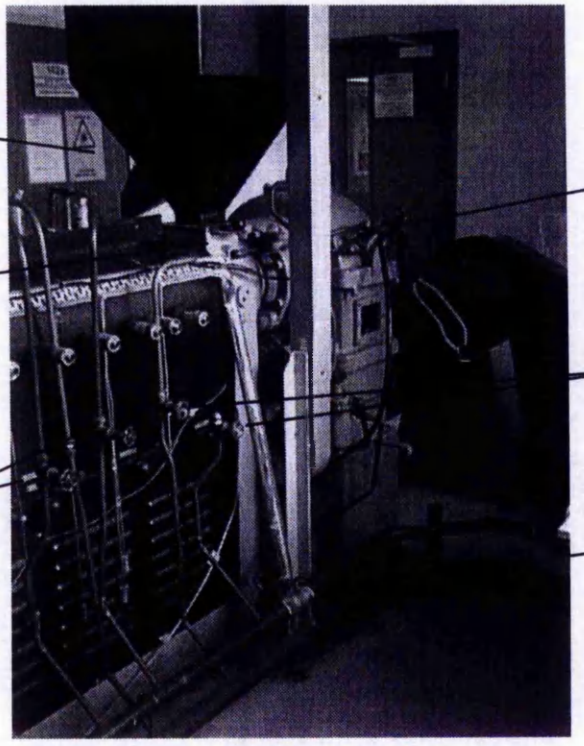

Figure 3 Cooling water taps for extruder

8. For running the extruder with the grooved feed only - Switch on the water lever valve of the main pipe at the base of the machine and the screw water valve on the entrance pipe for the cooling feed section respectively.(These taps are painted red.) (Figure 3)

9. Switch off all the screw water valves which cool the barrel of the extruder (Figure 3).

10. Turn on the main isolator on the heater and control panel. (The switch is on the bottom left side of the main control panel as you face it.)

11. Each heater zone has a set of meters and switches on the control panel. This comprises of an ammeter, a meter to set the temperature and an on/off switch (rocker switch). Set the zone heaters to the process temperatures. For a particular run all the heater should be set to the same temperature (Figure 4).

12. Switch on the heaters using the rocker switches beneath the meter, which switches on the heaters (Figure 4).

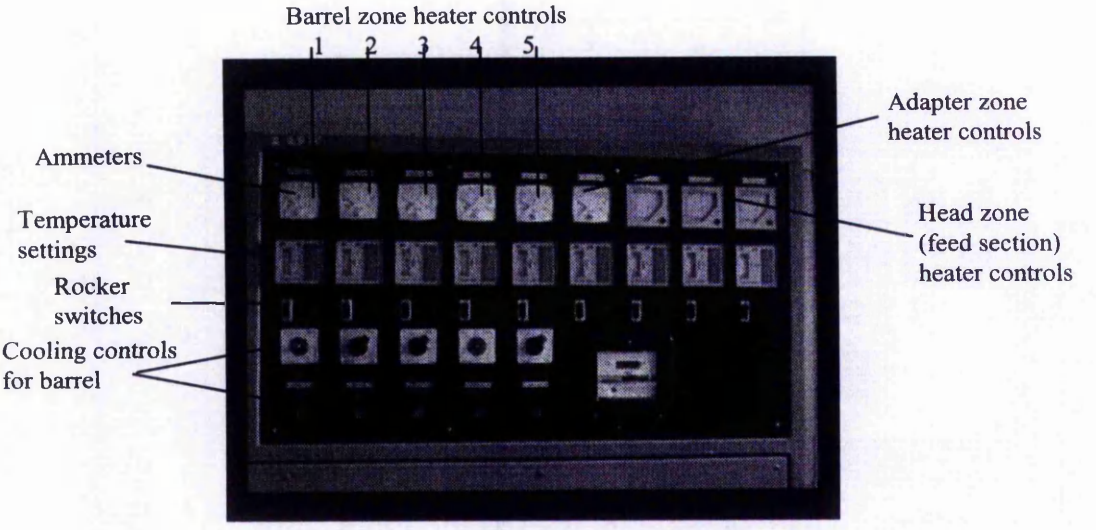

Figure 4 Heater control panel

Zone Positions

Head Zone 2	Head zone 2 at hopper end of machine
Barrel Zone 1	Barrel zone 1 next to head zone 2
Barrel Zone 2	Barrel zone 2 next to barrel zone 1
Barrel Zone 3	Barrel zone 3 next to barrel zone 2
Barrel Zone 4	Barrel zone 4 next to barrel zone 3
Barrel Zone 5	Barrel zone 5 next to barrel zone 4
Adapter Zone	Adapter zone at the die

13. Wait for the heaters to come up to temperature (1.5 - 2 hours). During this period the machine should not be left unattended.

14. Slide and plug in the screw thermocouple unit onto the end of the screw. Connect the unit to the COMACK thermometer via a multiple channel box. Plug the barrel thermocouples into the multiple channel box. If barrel thermocouples have been removed they should be inserted with high temperature grease on their threads when the machine is warm. Note if they are not tightened and/or the thermocouple is damaged molten polymer may be forced through the junction (Figure 5). (The thermocouples for the barrel are mounted in old pressure transducer casings.)

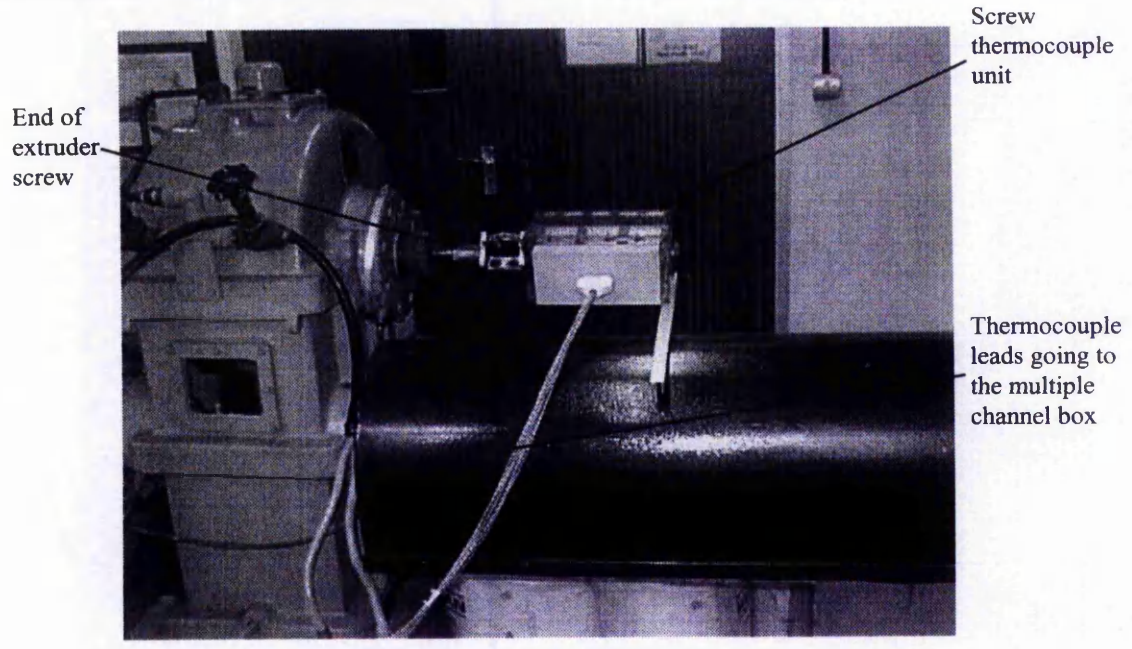

Figure 5 screw thermocouple unit

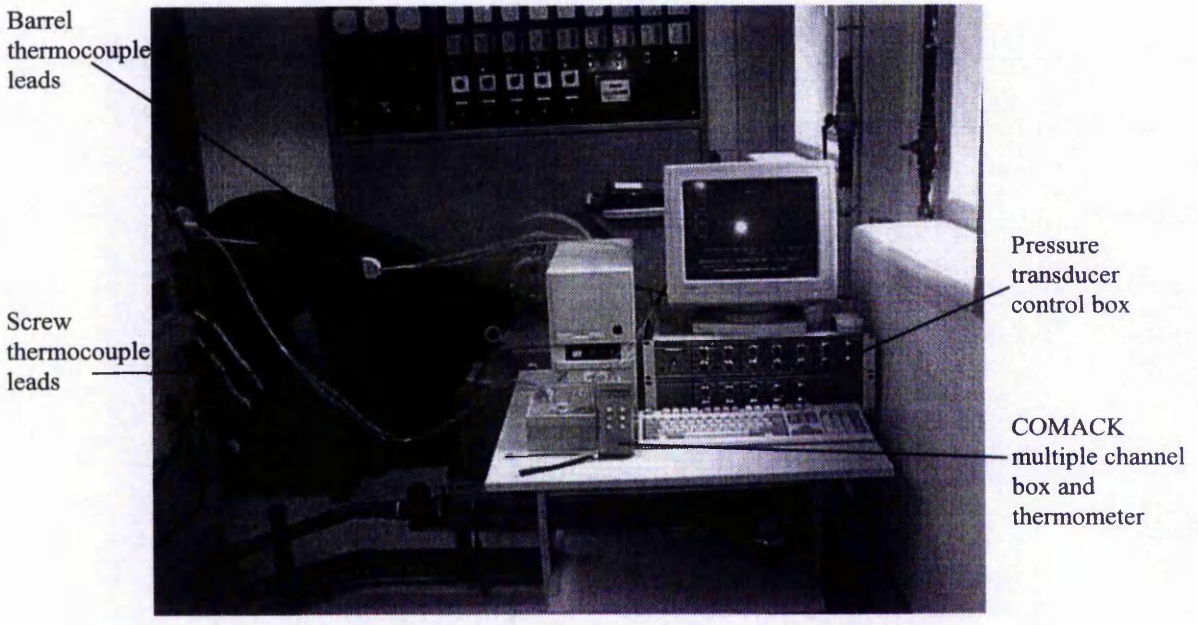

Figure 6 Thermocouples connections to COMACK multiple channel box

The barrel thermocouples are numbered 1-5 on the extruder, 1 at the die end 5 at the feed end. On the multiple channel box 10 is the die end thermocouple and 14 the feed end.

The screw thermocouples are 1-9, 1 at the die end and 9 at the feed end. They are the same numbers on the multiple channel box (Figure 6).

15. During the heating period regularly monitor the temperature of each junction of the barrel, screw and adapter using the temperature controller instrumentation on the heater and control panel and the COMACK thermometer by the multiple channel box.

16. **AUTHORISED PERSONNEL ONLY**. Screw in the pressure transducers - initially hand tight. Tighten as heating progresses as when the temperature rises they transducers will loosen. Make sure they are hand tight at the run temperature before the run commences. Over tightening the transducers may result in damage to their diaphragms. When the temperature is above 140°C tighten a quarter turn. (If they have been removed high temperature grease should be applied to their threads when they are inserted into the machine).

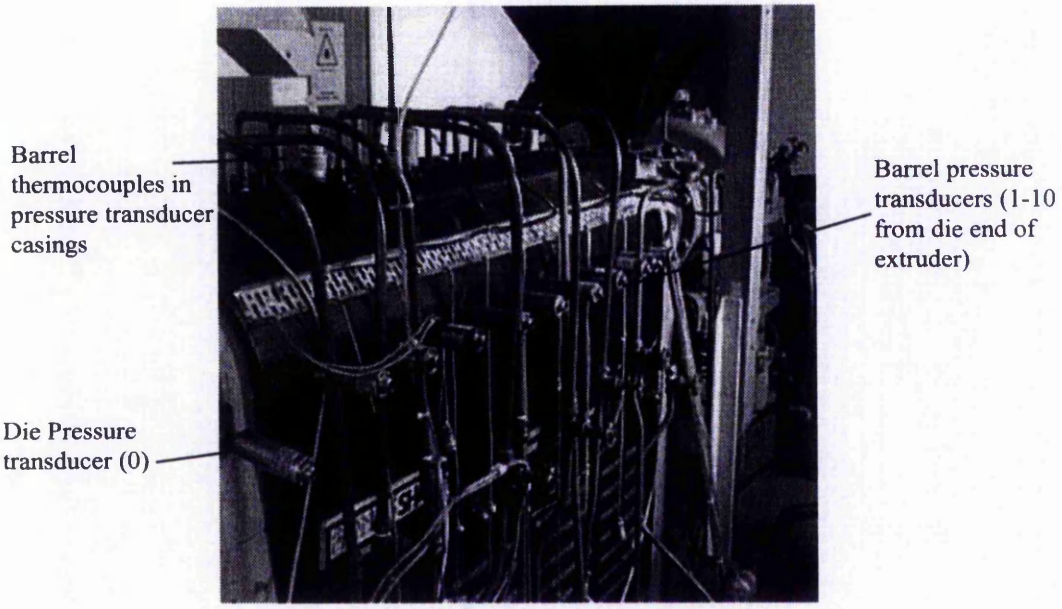

Figure 7 Barrel pressure transducers and thermocouples

17. Connect wires to pressure transducers (Figure 8).(Transducer 0 is near the die and 10 is next to the feed section.)

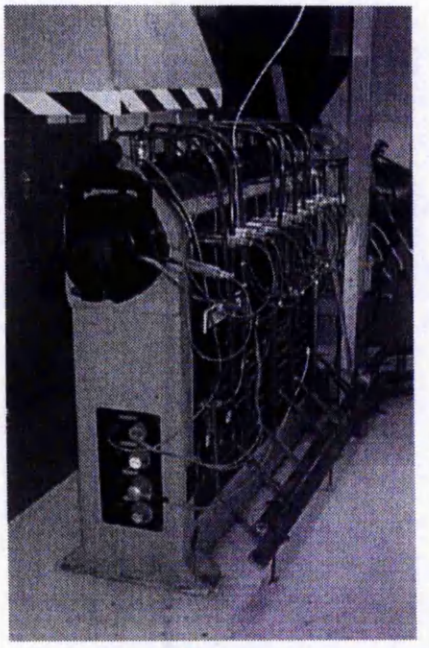

Figure 8 Extrude with transducers connected up

18. Start computer and open *Unimas 2* data collection program (at least 20 minutes before running the machine). The plugs for the computer and amplifiers are on the wall behind the PC.

START THE COMPUTER BEFORE SWITCHING ON THE AMPLIFIERS

19. Switch on the amplifiers and balance the melt transducer amplifiers using then coarse gain dial on the amplifiers (bottom dial)(variation approximately 27psi/100°C.) The zero reading should about 4 psi.

2. Running the extruder

20. Check that the barrel, adapter and head temperatures are at the setting temperatures on the control panel and on the COMACK thermometer.

21. Check the balance point of the individual amplifiers (~4psi).

22. Turn on the main isolator on the control panel (near the PC) (Figure 9).

Figure 9 Main power switch for running the machine

23. On the heater control panel, check that the screw sped adjuster is at zero value (silver dial) (Figure 10).

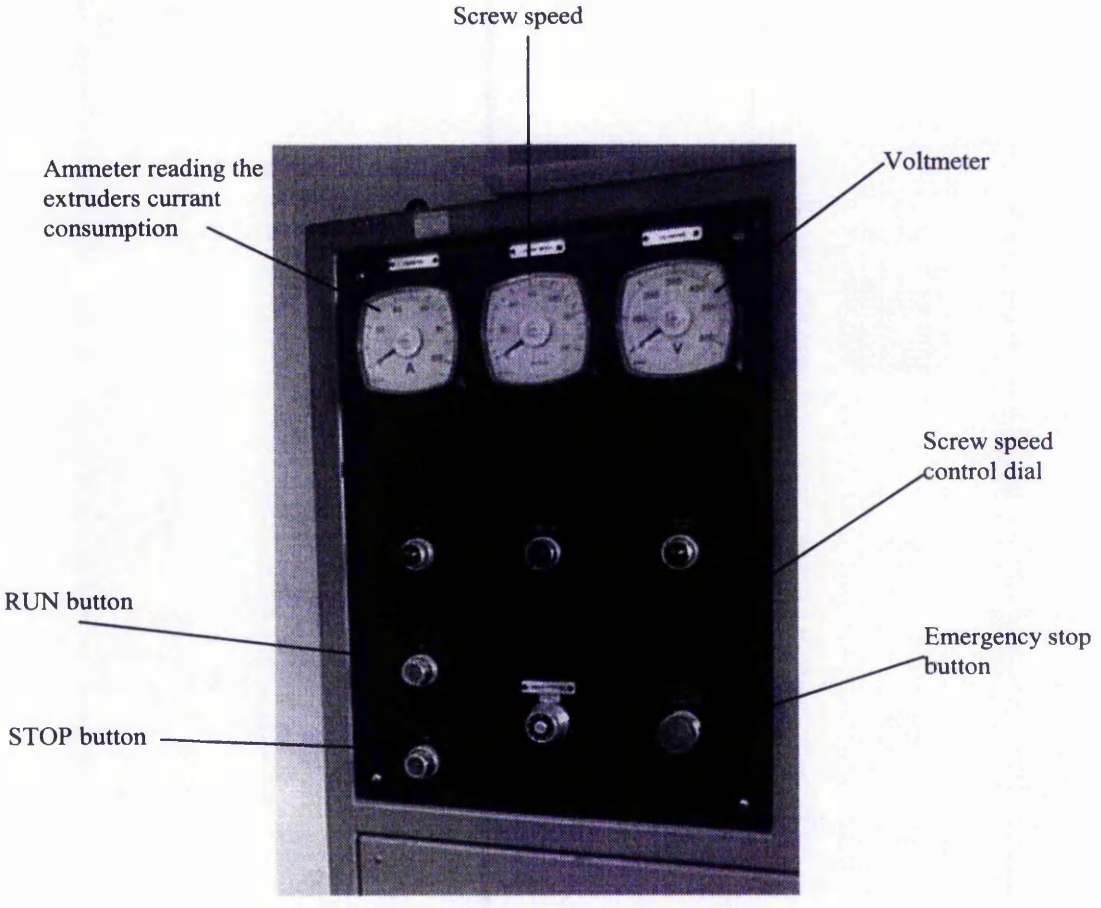

Figure 10 Running control panel

24 Press 'ENTER' on the computer keyboard to start the *Unimas 2* programme.

25. Press green button marked 'RUN'. This turns on the screw.

26. Open the hopper. (The hopper should be opened at this point particularly if a grooved feed is being used as running without polymer could damage the screw and the grooved feed section)

27. Slowly increase the speed of the screw (the silver dial). Listen and watch the ammeter (At 30 rpm the ammeter should read approximately 10A with no material.) If the currant reading goes too high (Note a red mark on the ammeter at 72A) or there are any unexpected noises switch off the extruder.

STOP INCREASING THE SCREW SPEED IF THE CURRENT VALUE INDICATED ON THE AMMETER REACHES 72A AS THE DRIVER MOTOR CURRENT OF 77A MUST NOT BE EXCEEDED. SWITCH OF THE MACHINE IF NECESSARY. IF ANY UNUSUAL NOISE OCCURS DURING THE SETTING OF THE SCREW SWITCH OFF THE MACHINE.

(Whether the machine will require stopping may depend on circumstances, for example if the amount of current is very high when the machine is started at very low rotational speeds the extruder will not be able to be run. However in the case where runs at slow speeds are possible but when the screw speed is increases and the current requirement is too high, the screw speed may be decreased to a suitable level and the machine run.)

With regards to unusual noise, locate where the noise is from. If it is inside the barrel the machine will require stopping to prevent damage to the barrel and screw. If there is some slight noise near the entrance to the feed zone this may be stopped with a little oil. If the noise persists the machine will have to be stopped.

28. Slowly keep increasing the speed until the speed required is reached. Make sure their are no unusual noises while the speed is being increased or the current reading is too high.

29. The machine needs to be run for approximately 30 minutes to reach an equilibrium state. Polymer which has been extruded should be cut off the die at frequent intervals. The small heaps should be put aside until cold when they can be disposed of. **DO NOT LEAVE, WHILE HOT, IN A LARGE HEAP IN A CONFINED SPACE AS THEY MAY CATCH FIRE**

30. During the running period the pressure in the extruder barrel is automatically recorded. Temperature readings along the screw and barrel need to be recorded manually (approximately every 5 minutes - eg take first reading 2 minutes after molten polymer begins to flow out of the extruder, the next reading 5minutes after the molten polymer has begun to flow and subsequent readings every 5 minutes. Note on the computer the time is recorded and starts when the return button is pressed, but the temperature readings begin from when polymer begins to flow out of the extruder.)

Problems encountered with the thermocouples:-

1. A screw thermocouple gives no reading. There can be various reasons for this:

(i) The thermocouple connection with the multiple channel box is loose - this can sometimes be fixed be moving the plugs and wires.

(ii) The thermocouple stops functioning, one may stop and then another - this occurs when the cement around the thermocouple wire in the screw breaks and in the worst cases molten polymer flows into the centre of the screw where all the thermocouple wires are. When this happens cement is often seen in the extrudate.

2. A barrel thermocouple gives no reading. Similarly there can be various reasons:

(i) The connection is loose to the multiple channel box - this may be fixed by adjusting the wires.

(ii) The thermocouple which is housed in a pressure transducer casing stops working and the pressure drops in the extruder - the thermocouple casing may have failed and molten polymer is pushing through the casing.

31. The pressure transducer pressures should be monitored on the computer while the extruder is running. This can be done by pressing the arrow keys up and down which will allow all the pressure transducers to be read during the run. The pressure transducers being used only take pressures up to 5000psi. If the pressures rise above these levels the diaphragms may be damaged.

Problems encountered with pressure transducers during a run:-

(i) No pressure reading on a transducer after the pressure transducer has shown good readings may mean the pressure transducer has failed. During a run no action can be taken.

(ii) No pressure readings when the run starts after the transducer has calibrated correctly - this may be because some polymers under prescribed conditions do not develop very high pressure profiles.
In these cases no action needs to be taken during the run.

(iii) High pressure readings. Careful note of pressure readings needs to be taken as if the pressure readings rise to 5000psi and above the transducers may be damaged. The run should be stopped.

32. The mass flow of the extruder should be measured by taking three samples of polymer which have been extruded for the same length of time after the extruder has stabilised, for 30 rpm the sampling time should be one minute and for 60 and 90 rpm sampling should be for half a minute. Once sampling has been completed a set of temperature readings should be made.

3 Crash Cooling and Removing the Screw

33. Press Control 'S' on the computer keyboard to save the pressure data. Exit *Unimas2* program and switch off the amplifiers and the computer.

34. Press the red button marked 'STOP' on the heater and control panel to stop the screw and close the hopper. Turn the screw speed dial (silver dial) to zero(anti clockwise).

35. Switch off barrel adapter and head zone heaters and main switch located on the main control panel.

36. Switch the extruder's main isolator off on the control panel near the computer.

37. Open main inlet valve at the base of the machine (if not already open for cooling the feed section). Open individual heater block water pipe valves.

38. Remove the die and breaker plate and clean them while the polymer is hot. Clear any polymer from around the tip of the screw and remove the end on the screw tip.

THE METAL PARTS AND POLYMER WILL BE HOT SO SAFETY GLOVES MUST BE WORN.

39. Disconnect the wires to the pressure transducers. Loosen the pressure transducers. This must be done before the polymer cools. If the transducers require removing to it now and clean their tips.

THE PRESSURE TRANSDUCERS MUST BE UNSCREWED WHILE THE POLYMER IS MOLTEN

THE PRESSURE TRANSDUCERS MUST BE REMOVED ONLY WHILE THE POLYMER IS HOT,IF THEY REQUIRE TO BE REMOVED. Removing the transducer from a cold mounting will cause damage to the tip due to cold polymer adhering to the diaphragm which is very sensitive.

40. Disconnect the thermocouples from the COMACK multiple channel box and unplug and remove the thermocouple unit from the screw.

41. Remove the screw nose (Left hand thread) with a special tool. Align hydraulic extractor unit with extruder barrel. Fit the chain connector to the screw; attach the extractor chain to the connector using shear pin. (Check the pin is not bent).

42. Position the hydraulic extractor in a strait line with the extruder barrel and attach the barrel of the extractor to the die holder. (The height of the extractor unit may be adjusted by altering the heights of the wheels of the extractor.)

43. Check that the temperature of the extruder barrel is around ambient. The time to crash cool the barrel is around 30 - 40 minutes.

ALL PERSONNEL IN THE AREA MUST WEAR SAFETY GLASSES WHEN THE SCREW IS PULLED OUT OF THE EXTRUDER.

44. Put the clutches into position and switch on the hydraulic pulling unit.

45. Slowly extract the screw. **MAKE SURE THAT THE PRESSURE READING ON THE MANAOMETER DOES NOT EXCEED APPROXIMATERLY 800 PSI (900PSI OR 6.2Mpa) AS THE SHEAR PIN WILL BREAK AT 1000PSI**

If the screw does not move after a few tries and /or the shear pin has broken, the extruder needs to be warmed up to about 60°C so that the polymer will have softened. This will take about 30 minutes. Slow extraction of the screw should be tried again. If the screw moves slightly but not enough try raise the temperature again and try pulling the screw out. If this is unsuccessful and the screw has not moved at all, disconnect the extractor unit and fasten the screw nose to the end of the screw. Heat up the extruder so that the polymer will melt and then run the extruder, at low speed, to remove as much of the polymer in the barrel as possible. Cool the extruder down to ambient temperature, reconnect the screw to the extractor unit and remove the screw slowly.

46. Once the screw has been extracted from the extruder, disconnect the clutches and pull the screw out of the extractor barrel. Unbolt the shear pin, and remove the screw.

47. Switch of the water supply to the extruder.

48. Empty the polymer hopper and clean the barrel and feeder zone of loose polymer beads.

Computer operation and data capture.

The computer records the pressure readings of the transducers during the run.

Computer operation

1. Switch on the computer and the pressure transducer amplifier on the wall behid the computer.

2. Type :-

   cd *Unimas* ↵
   Unimas2 ↵

3. Menu comes up

J Kipling and N Mullen
Polymer Engineering Centre
March 1998

1. Name — Name the run
2. No. of scans — 10
3. No. of thermocouples — 1(really no. is 0 but PC needs a no.)
4. No. of pressure transducers — 11
5. Y axis range — 0-5000

Press F10

4. The screen which comes up relates to one of the pressure transducers. The arrow keys up and down can be used to look at the pressure profile of the different pressure transducers located along the extruders barrel.

5. In the right hand corner of the screen the actual pressure reading at any time can be seen. When the pressure transducers are being calibrated when a run is being set up, the individual readings can be adjusted to zero using the coarse adjustment knobs (the lower ones on the amplifier beneath the computer screen).

Recovering data

1. Go into *Unimas*

2. Dir will give you the directory of files if you need to find the name of the file.

3. Type:-

CONVERT FILE NAME (rtn)

4. Test time - ie the time of the whole test comes up on the screen.
Output file NAME.CSV (put is the file name and CSV)

The test time is the time over which the whole run has taken place, from the time you type 'ENTER' on the computer to the time you type CTL 'S'. The computer saves all the data from the start of the test to the end. The data you are interested in is the time when the flow of the polymer has stabilised in the extruder - at least 30 minutes after the run has begun. Thus the pressure data you require is that which is collected when you are testing the throughput of the extruder.

If the for example:

Test time 42 minutes,
Output file PPPPPP.CSV
Start time 40 minutes
Stop time 41 minutes ↵

The data extracted will be the data for one minute between 40 -41 minutes, and will be saved in the output file PPPPPP.CSV

5. DIR will show output file.

6. Go to Microsoft Office, and go into Xcel.

7. Open 'C' drive and go into *Unimas* and transfer data into Xcel..

8. Data will come up

Time Temp PG1 PG2 .....PG11

This requires adjusting:-

(i) Delete column for time - the time is from the start of he run not the sampling time required.
(ii) Delete temperature column - no temperatures were recorded by the computer.
(iii) Insert a new time column with times 0,0.1,0.2..... seconds intervals.
(iv) Alter the pressure reading headings, as the extruder transducer numbers go from PG0 to PG10.

9. Average the pressure readings for each pressure transducer.

Other information for running of extruder.

1. Polymer requirements, these are based on the temperatures listed later in this section. If higher temperatures are used more polymer will be required. They are also based on the time to reach a steady throughput. Polymer normally comes in 25kg bags.

Table of polymer requirements for normal runs

EXTRUDER SCREW SPEED (RPM)	NUMBER OF BAGS OF POLYMER	TIME TO STEADY FLOW (MINUTES)
30	>1/2 BAG	30
60	<1 BAG	25
90	1-1/2 BAGS	20-22

Three speeds for a polymer at a particular temperature may be carried out in the same run. In this case about 2 ½ bags of polymer will be needed.

2. If carrying out a run for a company ask for 3 bags of polymer (75kg) for one run. This figure is only a guide amount a lot will depend on temperature.

3. Usual temperature settings:-

Table of usual extruder temperatures for polymers

POLYMER	TEMPERATURE (°C)
Low density polyethylene	190
Linear low density polyethylene	190
High density polyethylene	210
Polypropylene	210
Polystyrene	210

J Kipling and N Mullen
Polymer Engineering Centre
March 1998

Appendix 3

Correction of the Dynamic Melt Temperature Governing Equation

During the model evaluation, the melt temperature governing equation was found erroneous. The original equation is shown below. The symbols used are defined in the Nomenclature of Chapter 4.

$$\frac{\partial T}{\partial t} + v_{mz}\frac{\partial T}{\partial z} = \frac{\phi X^{1/2}(T_f - T)}{\rho_m H(W-X)} + \frac{q_{tr} + q_{vc}}{C_m G_m H(W-X)}$$

The circled parameter should be the melt density, ρ_m, instead of the mass flow rate of the melt, G_m. The correction has been confirmed by deriving the equation from the energy conservation law as stated in the literature.

From the energy conservation law:

$$\begin{bmatrix}\textit{Accumulation of}\\ \textit{heat in melt}\end{bmatrix} + \begin{bmatrix}\textit{Net convection of heat}\\ \textit{in direction of flow}\end{bmatrix} =$$

$$\begin{bmatrix}\textit{Heat convection}\\ \textit{from melt film}\end{bmatrix} + \begin{bmatrix}\textit{Net heat transfer}\\ \textit{through the wall}\end{bmatrix} + \begin{bmatrix}\textit{Heat generated by}\\ \textit{viscous dissipation}\end{bmatrix}$$

$$\rho_m C_m \frac{\partial}{\partial t}\left[H(W-X)(T-T_r)\right] + C_m \frac{\partial}{\partial z}\left[G_m(T-T_r)\right] = C_m \phi X^{1/2}(T_f - T_r) + q_{tr} + q_{vc} \qquad \text{Eq. C-1}$$

$$\begin{bmatrix}\textit{Accumulation of}\\ \textit{heat in melt}\end{bmatrix} = \rho_m C_m \frac{\partial}{\partial t}\left[H(W-X)(T-T_r)\right]$$

$$= \rho_m C_m \left[\frac{\partial H}{\partial t}(W-X)(T-T_r) + \frac{\partial (W-X)}{\partial t} H(T-T_r) + \frac{\partial (T-T_r)}{\partial t}(W-X)H\right]$$

As the channel depth, H, channel width, W, and reference temperature, T_r, are time invariant, the *Accumulation of heat in melt* can be simplified to:

$$\rho_m C_m \frac{\partial}{\partial t}\left[H(W-X)(T-T_r)\right] = \rho_m C_m H\left[\frac{\partial T}{\partial t}(W-X) - \frac{\partial X}{\partial t}(T-T_r)\right] \quad \text{Eq. C-2}$$

$$\begin{bmatrix} \textit{Net convection of heat} \\ \textit{in direction of flow} \end{bmatrix} = C_m \frac{\partial}{\partial z}\left[G_m(T-T_r)\right]$$

$$= C_m\left[\frac{\partial Gm}{\partial z}(T-T_r) + \frac{\partial (T-T_r)}{\partial z} G_m\right]$$

From the paper, the gradient of the melt flow rate can be expressed as:

$$\frac{\partial G_m}{\partial z} = \phi X^{1/2} + \rho_m \frac{\partial X}{\partial t} H$$

Assuming the reference temperature, T_r is constant in down channel direction. Equation for *Net convection of heat in direction of flow* can be simplified as:

$$C_m \frac{\partial}{\partial z}\left[G_m(T-T_r)\right] = C_m\left(\phi X^{1/2} + \rho_m \frac{\partial X}{\partial t} H\right)(T-T_r) + \frac{\partial T}{\partial z} C_m G_m \quad \text{Eq. C-3}$$

Substitute Eq C-2 and Eq. C-3 into the Eq. C-1 for conservation law of energy:

$$\rho_m C_m H\left[\frac{\partial T}{\partial t}(W-X) - \frac{\partial X}{\partial t}(T-T_r)\right] + C_m\left(\phi X^{1/2} + \rho_m \frac{\partial X}{\partial t} H\right)(T-T_r) + \frac{\partial T}{\partial z} C_m G_m$$

$$= C_m \phi X^{1/2}(T_f - T_r) + q_{tr} + q_{vc}$$

$$\rho_m H \frac{\partial T}{\partial t}(W-X) - \cancel{\rho_m H \frac{\partial X}{\partial t}(T-T_r)} + \phi X^{1/2}(T-T_r) + \cancel{\rho_m H \frac{\partial X}{\partial t}(T-T_r)} + \frac{\partial T}{\partial z} G_m$$

$$= \phi X^{1/2}(T_f - T_r) + \frac{q_{tr} + q_{vc}}{C_m}$$

$$\rho_m H \frac{\partial T}{\partial t}(W-X) + \frac{\partial T}{\partial z} G_m = \phi X^{1/2}\left[(T_f - T_r) - (T-T_r)\right] + \frac{q_{tr} + q_{vc}}{C_m}$$

$$= \phi X^{1/2}(T_f - T) + \frac{q_{tr} + q_{vc}}{C_m}$$

The equation can be rearranged to obtain the dynamic melt temperature equation:

$$\frac{\partial T}{\partial t} + v_{mz}\frac{\partial T}{\partial z} = \frac{\phi X^{1/2}(T_f - T)}{\rho_m H(W-X)} + \frac{q_{tr} + q_{vc}}{C_m \rho_m H(W-X)}$$

where,

$$v_{mz} = \frac{G_m}{\rho_m H(w-x)}$$

Appendix 4

Simulator Construction

A simulator is constructed based on a published dynamic theoretical model developed by Tadmor *et al* (1974). It simulates the transient responses of Solid Bed Profile (SBP), Melt Temperature Profile (MTP), Pressure Profile (PP) and mass flow rate at die with respect to step changes in the screw speed.

Verification of Simulator

Simulations were undertaken with the input data as shown in Table 1. Figure 1(a, b, c) show the outputs at die (solid lines) when the system was subjected to a step change in the screw speed from 60 rpm to 100 rpm with Low Density Polyethylene as the processing material. Figure 1a shows the melt temperature at die increased gradually and slightly overshot before achieving a new steady state temperature. Figure 1b and Figure 1c show the pressure and flow rate at die responded instantly to the changes in screw speed. Both responses overshot before decaying to the new steady state values. The transient responses at various locations along the extruder for the step change are shown as the SBP, the MTP and the PP in Figure 2.

Table 1: Material physical properties (Low Density Polyethylene, LDPE)

Heat capacity of melt, C_m	0.620 cal/g°C
Heat capacity of solid, C_s	0.660 cal/g°C
Melt density, ρ_m	0.798 g/cm^3
Solid density, ρ_s	0.915 g/cm^3
Melt thermal conductivity, K_m	0.434x10^{-3} cal/cms°C
Solid thermal conductivity, K_s	0.827x10^{-3} cal/cm s °C
Heat fusion, λ	31 cal/g
Melting point, T_m	110.560 °C
Initial solid temperature, T_s	26.677 °C

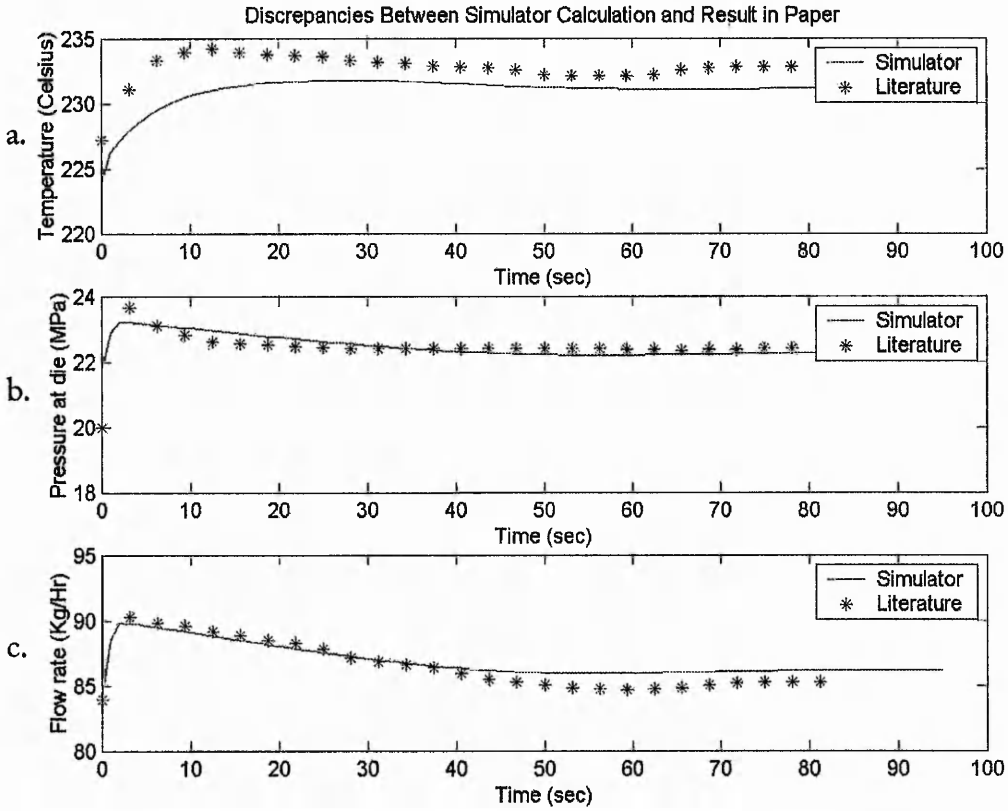

Figure 1: Outputs at die and discrepancies of the calculation: **a)** temperature, **b)** pressure, and **c)** flow rate at die.

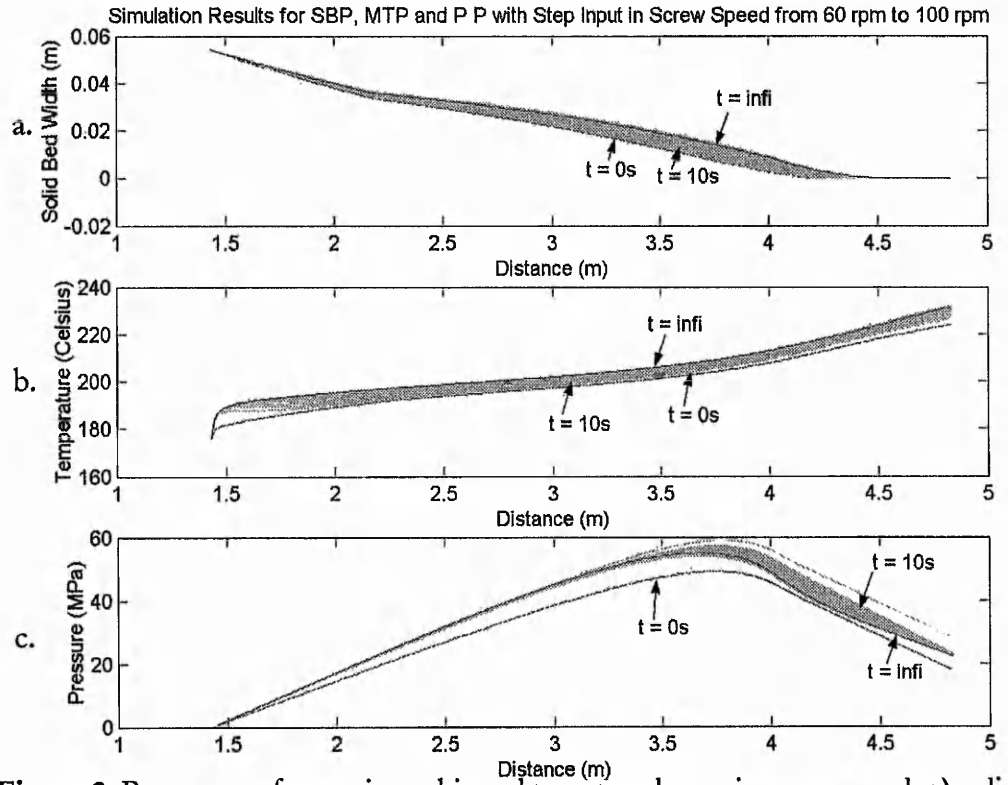

Figure 2: Responses of extrusion subjected to a step change in screw speed: **a)** solid bed profile, **b)** melt temperature profile, and **c)** pressure profile.

The simulator outputs are compared with the published results (marked as '*') under the same operating conditions (Tadmor *et al*, 1974). The discrepancies of the flow rate, the pressure and the temperature at die are recorded in Table 2. The simulator predicted a lower temperature compared to the published temperature with a maximum error of 3.193 °C and a root-mean-square error of 1.498 °C. The predictions of the pressure and the flow rate at die were more accurate with the RMS errors of 0.287 MPa and 0.751 kg/hr respectively. The simulator in general provided reasonably accurate predictions.

The discrepancies might due to the incompleteness of information necessary to construct the simulator. For example, the assumptions for the steady state governing equations of the heat transfer rate, the viscous dissipation rate and the pressure were not indicated. The simulator was developed based on the assumptions that the melt flow was Newtonian and isothermal. The equations used in the simulator might therefore different from the equations used in the literature.

The selection of the discretisation technique, the space step and the time step in the numerical calculation might have also contributed to the discrepancies. The simulator adopted the FVM to solve the PDEs, while the technique of solution in the paper was not specified. The time step in the simulator was set to one second while the space step was set to 1.3603 cm. A total of a thousand discrete nodes were distributed on the effective down channel distance of 340.0706 cm.

Table 2: Comparisons between the simulator predictions and the results in the literature.

	Temperature (°C)	Pressure (MPa)	Flow rate (kg/hr)
Maximum error	3.193	1.689	1.358
RMS error	1.498	0.287	0.751

Appendix 5

Discretisation of the Partial Differential Governing Equations

The partial differential equations of the extrusion model needed to be transformed into a set of algebraic equations for computation. The Finite Volume Method has been employed for this purpose. The symbols used are defined in the Nomenclature of Chapter 4. The procedures of equation discretisation are demonstrated as below:

Discretisation of the SBP Governing Equation

The Solid Bed Profile (SBP) is governed by the equation below:

$$\frac{\partial X}{\partial t} + v_{sz}\frac{\partial X}{\partial z} = -\frac{\phi X^{1/2}}{\rho_s H} + \frac{A v_{sz}}{H} X$$

The equation can be rearranged as:

$$\rho_s \frac{\partial X}{\partial t} + \rho_s v_{sz} \frac{\partial X}{\partial z} = -\frac{\phi}{H}\sqrt{X} + \frac{A\rho_s v_{sz}}{H} X \qquad \text{Eq. E-1}$$

Discretise the partial differential terms at the left hand side of Eq. E-1. Apply implicit scheme for temporal integral, where $X_p = X_p^1$, $X_w = X_w^1$.

$$\rho_s \int_w^e \int_t^{t+\Delta t} \frac{\partial X}{\partial t} dt dz = \rho_s (X_p - X_p^o)\Delta z \qquad \text{Eq. E-1a}$$

Apply upwind scheme for spatial integral, where $X_e = X_p$, $X_w = X_w$

$$\rho_s v_{sz} \int_t^{t+\Delta t} \int_w^e \frac{\partial X}{\partial z} dz dt = \rho_s v_{sz} (X_p - X_w)\Delta t \qquad \text{Eq. E-1b}$$

Discretise the source term at the right hand side of Eq. E-1.

$$s = \frac{A\rho_s v_{sz}}{H} X - \frac{\phi}{H}\sqrt{X}$$

Before discretisation, the source term needed to be linearised, where

$$\sqrt{X_P} = \frac{1}{\sqrt{X_P^0}} X_p$$

Therefore, the linearised source term can be written as:

$$s = \frac{A\rho_s v_{sz}}{H} X_p^o - \frac{\phi}{H\sqrt{X_1^0}} X_p \qquad \text{Eq. E-1c}$$

Discretise the first source term at the right hand side of Eq. E-1c,

$$\frac{A\rho_s v_{sz}}{H} \int_t^{t+\Delta t}\int_w^e X_p^o dzdt = \frac{A\rho_s v_{sz}}{H} X_p^o \Delta z \Delta t \qquad \text{Eq. E-1d}$$

Discretise the second source term at the right hand side of Eq. E-1c,

$$\frac{\phi}{H\sqrt{X_P^0}} \int_t^{t+\Delta t}\int_w^e X_P dzdt = \frac{\phi}{H\sqrt{X_P^0}} X_p \Delta z \Delta t \qquad \text{Eq. E-1e}$$

Rearrange Eq. E-1a, Eq.E-1b, Eq E-1d and Eq E-1e, into Eq. E-1,

$$\rho_s (X_p - X_p^o)\Delta z + \rho_s v_{sz}(X_p - X_w)\Delta t = \frac{A\rho_s v_{sz}}{H} X_p^o \Delta z \Delta t - \frac{\phi}{H\sqrt{X_P^0}} X_p \Delta z \Delta t$$

Let $\Delta z = h$ and $\Delta t = k$,

$$\rho_s (X_p - X_p^o)h + \rho_s v_{sz}(X_p - X_w)k = \frac{A\rho_s v_{sz}}{H} X_p^o hk - \frac{\phi}{H\sqrt{X_P^0}} X_p hk$$

Hence the representative algebraic equation of solid bed for each discrete point is obtained as below:

$$(\rho_s h + \frac{\phi}{H\sqrt{X_p^o}} hk + \rho_s v_{sz} k)X_p = \rho_s v_{sz} k X_w + (\rho_s h + \frac{A\rho_s v_{sz}}{H} hk)X_p{}^0$$

Discretisation of the MTP Governing Equation

The Melt Temperature Profile (MTP) is governed by the equation below:

$$\frac{\partial T}{\partial t} + v_{mz}\frac{\partial T}{\partial z} = \frac{\phi X^{1/2}(T_f - T)}{\rho_m H(W-X)} + \frac{q_{tr} + q_{vc}}{C_m \rho_m H(W-X)}$$

The equation can be rearranged as below:

$$\rho_m \frac{\partial T}{\partial t} + \rho_m v_{mz}\frac{\partial T}{\partial z} = \frac{\phi\sqrt{X}T_f}{H(W-X)} - \frac{\phi\sqrt{X}}{H(W-X)}T + \frac{q_{tr} + q_{vc}}{C_m H(W-X)} \qquad \text{Eq. E-2}$$

$$Let\ \rho_m v_{mz} = F,\ \frac{\phi\sqrt{X}T_f}{H(W-X)} = L,\ \frac{\phi\sqrt{X}}{H(W-X)} = M,\ \frac{q_{tr} + q_{vc}}{C_m H(W-X)} = N$$

$$\therefore \rho_m \frac{\partial T}{\partial t} + F\frac{\partial T}{\partial z} = L - MT + N$$

Discretise the partial differential terms at the left hand side of Eq. E-2 using implicit and upwind schemes as described in the earlier section.

$$\rho_m \int_w^e \int_t^{t+\Delta t} \frac{\partial T}{\partial t} dt dz = \rho_m (T_p - T_P^o)\,\Delta z \qquad \text{Eq. E-2a}$$

$$F\int_t^{t+\Delta t} \int_w^e \frac{\partial T}{\partial z} dz dt = F(T_p - T_w)\,\Delta t \qquad \text{Eq. E-2b}$$

Discretise the source terms at the right hand side of Eq. E-2

$$S = L + N - MT$$

$$\int_t^{t+\Delta t} \int_w^e s dz dt = (L + N - MT_p)\,\Delta z\,\Delta t \qquad \text{Eq. E-2c}$$

Rearrange Eq. E-2a, Eq. E-2b and Eq E-2c into Eq. E-2,

$$\rho_m (T_p - T_P^o)\Delta z + F(T_p - T_w)\Delta t = (L + N - MT_p)\,\Delta z\,\Delta t$$

Let $\Delta z = h, \Delta t = k$

$$\rho_m h T_p - \rho_m h T_p^o + FkT - FkT_w = (L+N)hk - MhkT_p$$

Rearrange the equation,

$$(\rho_m h + Fk + Mhk)T_p = FkT_w + \rho_m h T_p^o + (L+N)hk$$

Hence the representative algebraic equation for each discrete point is obtained as below:

$$(\rho_m h + \rho_m v_{mz} k + \frac{\phi\sqrt{X}}{H(W-X)}hk)T_p = k\rho_m v_{mz} T_w + (\frac{\phi\sqrt{X}T_f}{H(W-X)} + \frac{q_{vc} + q_{tr}}{C_m H(W-X)})hk + \rho_m h T_p^o$$

Appendix 6

Theoretical Stability Analysis of FsiLPC for Linear Processes

This section elaborates the stability of the FsiLPC system under deadzone assumption for linear processes theoretically. Parts of the descriptions are obtained from (Andersen, 1998; Sanchez and Rodellar, 1996). All the symbols used are defined in the Nomenclature of Chapter 5 or stated otherwise.

1 Stability of FsiLPC system on Prediction Horizon Selection

Assuming a linear system with the process dynamics which can be described as:

$$y(k+1) = \sum_{i=1}^{n} a_i Y(k+1-i) + \sum_{i=1}^{m} b_i u(k+1-i) \qquad \text{Eq F-1}$$

Transforming Eq F-1 into z-domain,

$$y(z) = \frac{B(z^{-1})}{A(z^{-1})} u(z) \qquad \text{Eq F-2}$$

where $B(z^{-1})$ and $A(z^{-1})$ are the polynomials given as:

$$B(z^{-1}) = b_1 z^{-1} + b_2 z^{-2} + \ldots + b_m z^{-m}$$
$$A(z^{-1}) = 1 - a_1 z^{-1} - a_2 z^{-2} - \ldots - a_n z^{-n} \qquad \text{Eq F-3}$$

To approximate the dynamics of the system, a predictive model is derived, where:

$$\hat{y}(k+1) = \sum_{i=1}^{\hat{n}} \hat{a}_i y(k+1-i) + \sum_{i=1}^{\hat{m}} \hat{b}_i u(k+1-i) \qquad \text{Eq F-4}$$

Extending Eq F-4 to predict λ-steps ahead system output. It has been shown in Section 5.2.2 of Chapter 5 that the λ-steps ahead prediction, $\hat{y}(k+\lambda)$, can be calculated efficiently when a step manipulating signal sequence is imposed. The following expression is resulted.

$$\hat{y}(k+\lambda) = \sum_{i=1}^{\hat{n}} \hat{e}_i^{(\lambda)} y(k+1-i) + \sum_{i=2}^{\hat{m}} \hat{g}_i^{(\lambda)} u(k+1-i) + \hat{h}^{(\lambda)} \hat{u}(k) \qquad \text{Eq F-5}$$

It is noted that the predicted manipulating signal, $\hat{u}(k)$, is to be applied as actual manipulating signal, $u(k)$, under the step manipulating signal strategy. Therefore, Eq F-5 also can be written as:

$$\hat{y}(k+\lambda) = \sum_{i=1}^{\hat{n}} \hat{e}_i^{(\lambda)} y(k+1-i) + \sum_{i=2}^{\hat{m}} \hat{g}_i^{(\lambda)} u(k+1-i) + \hat{h}^{(\lambda)} u(k) \qquad \text{Eq F-6}$$

Assuming that the reference output, $y_r(k+\lambda)$, remains constant within the prediction horizon. The function of the trajectory planner can be simplified as:

$$y_d(k) = y_r(k) = y_r(k+1) = \ldots = y_r(k+\lambda) \qquad \text{Eq F-7}$$

The objective of the controller is to equating the λ-steps ahead predictive output, $\hat{y}(k+\lambda)$, to the reference of plant output, $y_r(k+\lambda)$, such that:

$$y_r(k+\lambda) = \sum_{i=1}^{\hat{n}} \hat{e}_i^{(\lambda)} y(k+1-i) + \sum_{i=2}^{\hat{m}} \hat{g}_i^{(\lambda)} u(k+1-i) + \hat{h}^{(\lambda)} u(k) \qquad \text{Eq F-8}$$

Applying the z-transformation to Eq F-8:

$$y_r(z) = \hat{E}_\lambda(z^{-1}) y(z) + \hat{G}_\lambda(z^{-1}) u(z) \qquad \text{Eq F-9}$$

with polynomials

$$\hat{E}_\lambda(z^{-1}) = \hat{e}_1^{(\lambda)} z^{-1} + \hat{e}_2^{(\lambda)} z^{-2} + \ldots + \hat{e}_{\hat{n}}^{(\lambda)} z^{-\hat{n}+1} \qquad \text{Eq F-9a}$$

$$\hat{G}_\lambda(z^{-1}) = \hat{h}^{(\lambda)} + \hat{g}_2^{(\lambda)} z^{-1} + \ldots + \hat{g}_{\hat{m}}^{(\lambda)} z^{-\hat{m}+1}$$

Solving for manipulating signal, $u(z)$, in Eq F-9 and substituting into Eq F-2:

$$u(z) = \frac{y_r(z) - \hat{E}_\lambda(z^{-1}) y(z)}{\hat{G}_\lambda(z^{-1})}$$

$$y(z) = \frac{B(z^{-1})}{A(z^{-1})} \frac{y_r(z) - \hat{E}_\lambda(z^{-1}) y(z)}{\hat{G}_\lambda(z^{-1})}$$

$$= \frac{B(z^{-1}) y_r(z) - B(z^{-1}) \hat{E}_\lambda(z^{-1}) y(z)}{A(z^{-1}) \hat{G}_\lambda(z^{-1})}$$

$$[\, A(z^{-1}) \hat{G}_\lambda(z^{-1}) + B(z^{-1}) \hat{E}_\lambda(z^{-1}) \,] y(z) = B(z^{-1}) y_r(z)$$

$$y(z) = \frac{B(z^{-1})}{\hat{\theta}_\lambda(z^{-1})} y_r(z) \qquad \text{Eq F-10}$$

where the characteristic polynomial is given as,

$$\hat{\theta}_\lambda(z^{-1}) = \hat{E}_\lambda(z^{-1})\, B(z^{-1}) + \hat{G}_\lambda(z^{-1})\, A(z^{-1}) \qquad \text{Eq F-10a}$$

Eq F-10 defines the closed loop dynamic relationship between the reference and the actual plant output. The transfer function can be also interpreted as the relationship between the predicted output at the end of the prediction horizon and the current plant output as shown in Eq F-8. Direct substituting of Eq F-2 into Eq F-10.

$$u(z) = \frac{A(z^{-1})}{\hat{\theta}_\lambda(z^{-1})} y_r(z) \qquad \text{Eq F-11}$$

Eq F-11 defines the relationship between the manipulating signal and the reference of plant output. In both Eq F-10 and Eq F-11, the denominators of the transfer functions are characterised by the same polynomial $\hat{\theta}_\lambda(z^{-1})$. This signifies that, given a bounded sequence of output reference, the controlled plant output and the manipulating signal will also be bounded. In both cases, the stability condition is that the polynomial $\hat{\theta}_\lambda(z^{-1})$ has its roots in the modulus $|z| < 1$.

To examine the effect of extending the prediction horizon on the system stability, the value of prediction horizon, λ, is taken to the limit of infinity. In this case, since the predictive model is stable and given that the predicted manipulating signal, $\hat{u}(k)$, is remained constant during the prediction horizon. The predicted plant output will reach a steady state as:

$$\lim_{\lambda \to \infty} \hat{y}(k+\lambda) \triangleq \hat{y}(k+\infty) = \hat{G}_s\, \hat{u}(k) \qquad \text{Eq F-12}$$

where $\hat{G}_s$ is the static gain of the predictive model

$$\hat{G}_s = \frac{\hat{b}_1 + \hat{b}_2 + \ldots + \hat{b}_{\hat{m}}}{1 - \hat{a}_1 - \hat{a}_2 - \ldots - \hat{a}_{\hat{n}}} \qquad \text{Eq F-13}$$

On the other hand, assuming the infinite limit of prediction horizon, λ, in Eq F-5:

$$\hat{y}(k+\infty) = \sum_{i=1}^{\hat{n}} \hat{e}_i^{(\infty)} y(k+1-i) + \sum_{i=2}^{\hat{m}} \hat{g}_i^{(\infty)} u(k+1-i) + \hat{h}^{(\infty)} \hat{u}(k) \qquad \text{Eq F-14}$$

where ∞ indicates the limit of λ being extended to infinity. When the Eq F-12 is compared to the Eq F-14, the following limiting properties for the predictive model coefficients can be deduced:

$$\hat{e}_i^{(\infty)} = 0 \qquad i=1,2,\ldots\ \hat{n}$$
$$\hat{g}_i^{(\infty)} = 0 \qquad i=1,2,\ldots\ \hat{m} \qquad \text{Eq F-15}$$
$$\hat{h}^{(\infty)} = \hat{G}_s$$

Consequently, the polynomials defined in Eq F-9a satisfy the following limiting properties:

$$\lim_{\lambda\to\infty} \hat{E}_\lambda(z^{-1}) = 0 \qquad \text{Eq F-16}$$

$$\lim_{\lambda\to\infty} \hat{G}_\lambda(z^{-1}) = \hat{G}_s$$

The characteristic polynomials, $\hat{\theta}_\lambda(z^{-1})$, defined in Eq F-10a will converge in the limit to the expression:

$$\lim_{\lambda\to\infty} \hat{\theta}_\lambda(z^{-1}) = \hat{G}_s A(z^{-1}) \qquad \text{Eq F-17}$$

It can be deduced from Eq F-17 that the roots of the characteristic polynomial tend towards the denominator of the process transfer function $A(z^{-1})$ as prediction horizon λ increases. Since the process is stable, these roots have modulus $|z|<1$.

The above stability analysis for the prediction horizon is based on the assumption that the predictive model is without modelling error. In the present of the error, an adaptive scheme is necessitated for error minimisation by tuning of the model parameters. The convergence of the model parameters is shown as follows.

2 Convergence of Model Parameters

To investigate the convergence of the model parameters, the dynamics of the process expressed in difference equation as shown in Eq F-1 is compacted as:

$$y(k+1) = \theta x(k) \qquad \text{Eq F-18}$$

where

$$\theta = [a_1, a_2, ..., a_n, b_1, b_2, ..., b_m]' \qquad \text{Eq F-18a}$$

$$x(k) = [y(k), y(k-1), ..., y(k+1-n), u(k), u(k-1), ..., u(k+1-m)]'$$

While the compacted expression for the predictive model is given as:

$$\hat{y}(k+1) = \hat{\theta}(k)\, x(k) \qquad \text{Eq F-19}$$

The modelling error, $\hat{\varepsilon}_y(k)$, can be derived as below:

$$\begin{aligned} \hat{\varepsilon}_y(k) &= y(k+1) - \hat{y}(k+1) \\ &= \theta x(k) - \hat{\theta}(k)\, x(k) \\ &= [\theta - \hat{\theta}(k)]\, x(k) \\ &= -\tilde{\theta}(k)\, x(k) \end{aligned} \qquad \text{Eq F-20}$$

where $\tilde{\theta}(k)$ is the Euclidean distance of the parameter vectors between the ideal and current model.

$$\tilde{\theta}(k) = \hat{\theta}(k) - \theta \qquad \text{Eq F-21}$$

During the model adaptation phase, the modelling error can be minimised by the steepest descent algorithm with the expression given as:

$$\hat{\theta}(k+1) = \hat{\theta}(k) - \kappa(k) \frac{\partial J(k)}{\partial \hat{\theta}(k)} \qquad \text{Eq F-22}$$

where $\kappa(k)$ is a positive scaling factor which regulates the size of the steps taken, J is the prediction error.

$$\kappa(k) = \frac{\eta}{1 + j(k)^T j(k)} > 0 \qquad \text{Eq F-23}$$

The η is the learning rate and $j(k)$ is the derivative of the predicted output with respect to the parameters of predictive model.

$$j(k) = \left.\frac{\partial \hat{y}(k)}{\partial \hat{\theta}(k)}\right|_{\hat{\theta}(k)} = x(k)$$ Eq F-24

Therefore, Eq F-22 can be written as:

$$\hat{\theta}(k+1) = \hat{\theta}(k) - \frac{\eta}{1+x(k)^T x(k)} \frac{\partial J(k)}{\partial \hat{\theta}(k)}$$

$$J(k) = \tfrac{1}{2}\, \hat{\varepsilon}_y(k)$$

$$\frac{\partial J(k)}{\partial \hat{\theta}(k)} = \frac{\partial J(k)}{\partial \hat{\varepsilon}_y(k)} \times \frac{\partial \hat{\varepsilon}_y(k)}{\partial \hat{\theta}(k)}$$

$$= -\hat{\varepsilon}_y(k)\, x(k)$$

$$= \tilde{\theta}(k)\, x(k)^T x(k)$$

$$\hat{\theta}(k+1) = \hat{\theta}(k) - \frac{\eta}{1+x(k)^T x(k)}\, \tilde{\theta}(k)\, x(k)^T x(k)$$ Eq F-25

The Eq F-25 can be rearranged as follows:

$$\hat{\theta}(k+1) = \hat{\theta}(k) - \frac{\eta\, \tilde{\theta}(k)\, x(k)^T x(k)}{1+x(k)^T x(k)}$$

Subtract θ from the above expression,

$$\hat{\theta}(k+1) - \theta = \hat{\theta}(k) - \theta - \frac{\eta\, \tilde{\theta}(k)\, x(k)^T x(k)}{1+x(k)^T x(k)}$$

thus obtained,

$$\tilde{\theta}(k+1) = \tilde{\theta}(k) - \frac{\eta\, \tilde{\theta}(k)\, x(k)^T x(k)}{1+x(k)^T x(k)}$$

square both sides of the above expression,

$$\tilde{\theta}(k+1)^{\mathrm{T}} \tilde{\theta}(k+1) = \tilde{\theta}(k)^{\mathrm{T}} \tilde{\theta}(k) - \frac{2\eta\, \tilde{\theta}(k)^T \tilde{\theta}(k)\, x(k)^T x(k)}{1+x(k)^T x(k)} + \left[\frac{\eta\, \tilde{\theta}(k)^T x(k)}{1+x(k)^T x(k)}\right]^2 x(k)^T x(k)$$

use L_2 – norms to obtain,

$$\left|\tilde{\theta}(k+1)\right|^2 - \left|\tilde{\theta}(k)\right|^2 = \left[\frac{\eta\, \tilde{\theta}(k)^T x(k)}{1+x(k)^T x(k)}\right]^2 x(k)^T x(k) - \frac{2\eta\, \tilde{\theta}(k)^T \tilde{\theta}(k)\, x(k)^T x(k)}{1+x(k)^T x(k)}$$

$$= \frac{[\eta\,\tilde{\theta}(k)^T x(k)]^2}{1+x(k)^T x(k)} \times \frac{x(k)^T x(k)}{1+x(k)^T x(k)} \quad -2\eta$$

For any arbitrary constant,

$$\frac{x}{1+x} \leq 1 \quad \text{for } x \geq 0$$

therefore,

$$\left|\tilde{\theta}(k+1)\right|^2 - \left|\tilde{\theta}(k)\right|^2 \leq \frac{[\eta\,\tilde{\theta}(k)^T x(k)]^2}{1+x(k)^T x(k)} - 2\eta \frac{[\tilde{\theta}(k)\,x(k)^T x(k)]^2}{1+x(k)^T x(k)}$$

$$\leq \frac{\eta[\eta\,\tilde{\theta}(k)^T x(k)]^2}{1+x(k)^T x(k)} (\eta\text{-}2)$$

$$\leq \frac{\eta}{1+x(k)^T x(k)} \quad [\tilde{\theta}(k)^T x(k)]^2 (\eta - 2)$$

$$\leq \kappa(k)\ \hat{\varepsilon}_y(k)\ (\eta - 2)$$

The model adaptation phase commences only if $\kappa(k)>0$, and $\hat{\varepsilon}_y(k) \geq 0$ must not be negative. Therefore, if $0 \leq x \leq 2$,

$$\left|\tilde{\theta}(k+1)\right|^2 - \left|\tilde{\theta}(k)\right|^2 \leq \kappa(k)\ \hat{\varepsilon}_y(k)\ (\eta - 2) \leq 0 \qquad \text{Eq F-26}$$

Consequently

$$\left|\tilde{\theta}(k)\right| \geq \left|\tilde{\theta}(k+1)\right|$$

This shows that if the system behaviour is time-invariant and $0 \leq \eta \leq 2$, the Euclidean distance of the parameters between the ideal and current model will always non-increasing. Under the ideal conditions, the parameters will eventually converge.

$$\tilde{\theta}(k) \geq \tilde{\theta}(k+1) \qquad \forall k \geq k_f \geq 0$$
$$\hat{\varepsilon}_y(k) \to 0 \text{ as } k \to \infty$$

3 Lyapunov Stability Theorem for Linear Digital Systems

Lyapunov stability theorem is required in the remaining stability analysis. The theorem is cited from (Kuo, 1992) for comprehensive purpose. Consider a linear time-invariant digital system is described by the difference equation.

$$x(k+1) = A\,x(k) \qquad \text{Eq F-27}$$

where $x(k)$ is $n \times 1$ and A is a $n \times n$ matrix. The equilibrium state $x_e = 0$ is asymptotically stable if and only if, given any positive-definite real symmetric matrix Q, there exists a positive-definite real symmetric matrix P such that:

$$A^T P A - P = -Q \qquad \text{Eq F-28}$$

Then:

$$V(x) = x(k)^T P x(k) \qquad \text{Eq F-29}$$

where $V(x)$ is a Lyapunov function for the system, and further:

$$\Delta V(x) = -x(k)^T Q x(k) \qquad \text{Eq F-30}$$

where $\Delta V(x)$ is defined as:

$$\Delta V[x(k)] = V[x(k+1)] - V[x(k)] \qquad \text{Eq F-31}$$

The difference of the Lyapunov function $\Delta V(x)$ must be non-positive for a stable system.

4 Deadzone Assumption

A particular concern for the adaptive control is that the overall performance of the system is deteriorated during the adaptation of the system to the current operating region. In this situation, the parameters of the controller have been over-trained in the attempts to improve the performance in the current operating region. When the operating region is changed, the controller might lead the system to an unstable condition. The solution to this problem has been introduced and has been referred as *deadzone assumption* (Chen and Khalil, 1992).

The deadzone radius, δ, specifies the absolute lower limit to the activation of the adaptation. During the operation, the calculated supervisory output error, $\bar{\varepsilon}_u(k)$, is

compared to the radius, δ, before the manipulating signal optimisation phase to be taken. The adaptation mechanism commences only if the error is greater than the radius. Therefore, the error with deadzone consideration, $\bar{\varepsilon}_u^{'}(k)$, used for the optimisation phase can be written as:

$$\bar{\varepsilon}_u^{'}(k) = D\left[\hat{\varepsilon}_u(k)\right]$$

$$where,\ D[x] = \begin{cases} x+\delta & if\ x<-\delta \\ 0 & if\ |x|<\delta \\ x-\delta & if\ x>\delta \end{cases}$$

5 Best Possible Fuzzy Supervisory Unit

Given a particular structure of fuzzy supervisory unit and a certain region of operation, there will be at least one set of parameters, which yield the best possible supervisory output for the plant to reach the reference output, $y_r(k)$. The fuzzy supervisory unit with the best possible set of parameters, $w(k)$, is called the best possible fuzzy supervisory unit with the expression as shown in Eq F-32:

$$\tilde{u}(k) = \hat{g}_c(y_r(k),\ w(k)) \qquad \text{Eq F-32}$$

$\tilde{u}(k)$ distinguishes from the output of actual inverse of model, $\bar{u}(k)$, that has been referred to as the ideal manipulating signal generated through the ideal function, $g_c(.)$. The maximum absolute difference between the best possible supervisory signal, $\tilde{u}(k)$, and the ideal control signal, $\bar{u}(k)$, in the entire region of operation is described by a constant, α, which is given in Eq F-33:

$$|g_c[y_r(k)] - \hat{g}_c[y_r(k), w(k)]| < \alpha \qquad r \in R \qquad \text{Eq F-33}$$

where R is the region of operation.

6 Boundedness and Convergence of Parameters of Fuzzy Supervisory Unit

The section shows the Euclidean distance between the parameters of best possible and current fuzzy supervisory unit will decrease monotonically as k increases under certain conditions. It should be noted that the function of the fuzzy supervisory unit is non-linear, as it is developed based on FRBS. The Controller Output Error Method (COEM) is applied to optimise the manipulating signal (Andersen *et al*, 1997). The FsiLPC system employs adaptation scheme with deadzone assumption.

The cost function required for COEM is developed on the supervisory output error rather than the plant output, which can be written as:

$$J_u(k) = \tfrac{1}{2} D[\,\hat{\varepsilon}_u(k)\,]^2 \qquad \text{Eq F-34}$$

$$\hat{\varepsilon}_u(k) = u(k) - u'(k)$$

where $u(k)$ is the applied manipulating signal while $u'(k)$ is the manipulating signal generated by imaginary fuzzy supervisory unit during the manipulating signal optimisation phase as below:

$$u(k) = \hat{g}_c[y_r(k), \hat{w}(k)] \qquad \text{Eq F-35}$$

$$u'(k) = \hat{g}_c[\hat{y}(k+\lambda), \hat{w}(k)] \qquad \text{Eq F-36}$$

and $D[.]$ is the function under the deadzone assumption such that:

$$D[x] = \begin{cases} x+\delta & \text{if } x < -\delta \\ 0 & \text{if } |x| < \delta \\ x-\delta & \text{if } x > \delta \end{cases}$$

where δ is the deadzone radius. The applied manipulating signal $u(k)$ can be reconstructed using the actual inverse of process model $g_c[.]$.

$$u(k) = g_c[\hat{y}(k+\lambda)] \qquad \text{Eq F-37}$$

The 'reconstruction' warrants some explanations. The original calculation of manipulating signal was performed using Eq F-35. After λ-steps ahead simulation, assuming the predictive model is perfect, the predicted plant output $\hat{y}(k+\lambda)$ is generated. Although the objective was to make the predicted plant output, $\hat{y}(k+\lambda)$, equal to the reference, $y_r(k)$, this

was not achieved because of inaccuracies in the functions $\hat{g}_c[.] \neq g_c[.]$. If the desired response of plant had been the predicted output, $\hat{y}(k+\lambda)$, instead of reference, $y_r(k)$, then the exact function of the fuzzy supervisory unit had been known. The manipulating signal had been calculated by Eq F-37. Therefore, the supervisory output error can be written as:

$$\hat{\varepsilon}_u(k) = u(k) - u'(k) \qquad \text{Eq F-38}$$

$$= g_c[\hat{y}(k+\lambda)] - \hat{g}_c[\hat{y}(k+\lambda), \hat{w}(k)]$$

From Eq F-33, it can be deduced that

$$|g_c[\hat{y}(k+\lambda)] - \hat{g}_c[\hat{y}(k+\lambda), w(k)]| < \alpha \qquad r \in R \qquad \text{Eq F-39}$$

Therefore, Eq F-38 can be again rewritten as:

$$\hat{\varepsilon}_u(k) = u(k) - u'(k) \qquad \text{Eq F-40}$$

$$= g_c[\hat{y}(k+\lambda)] - \hat{g}_c[\hat{y}(k+\lambda), \hat{w}(k)]$$

$$= \hat{g}_c[\hat{y}(k+\lambda), w(k)] + \alpha(k) - \hat{g}_c[\hat{y}(k+\lambda), \hat{w}(k)]$$

where $|\alpha(k)| < \alpha$

With the first order Taylor-series approximation on the function $\hat{g}_c[.]$ around $[\hat{y}(k+\lambda), w(k)]$,

$$\hat{\varepsilon}_u(k) = \tilde{w}(k)^T \left.\frac{\partial \hat{g}_c[\hat{y}(k+\lambda), \hat{w}(k)]}{\partial \hat{w}(k)}\right|_{\hat{w}(k)} + \alpha(k) + \beta(k) \qquad \text{Eq F-41}$$

$$\hat{\varepsilon}_u(k) = \tilde{w}(k)^T j(k) + \alpha(k) + \beta(k)$$

where,

$$j(k) = \left.\frac{\partial \hat{g}_c[\hat{y}(k+\lambda), \hat{w}(k)]}{\partial \hat{w}(k)}\right|_{\hat{w}(k)}, \quad \tilde{w}(k) = w(k) - \hat{w}(k)$$

$\beta(k)$ is the remainder of the expansion which is the sum of the terms of order 2 and higher. Assuming the deadzone radius, δ, is greater than or equal to the sum of $\alpha(k)$ and $\beta(k)$ which can be expressed as:

$$\delta \geq |\alpha(k) + \beta(k)| \qquad \text{Eq F-42}$$

Using this assumption, which has been referred to as the deadzone assumption, a bound on $D[\ \hat{\varepsilon}_u(k)\ ]$ maybe calculated as follows:

- *if* $|\ \hat{\varepsilon}_u(k)\ | \le \delta$ *then* $D[\ \hat{\varepsilon}_u(k)\ ] = 0$
- *if* $\hat{\varepsilon}_u(k)\ > \delta$ *then since*
    - $D[\ \hat{\varepsilon}_u(k)\ ] = \tilde{w}(k)^T j(k) + \alpha(k) + \beta(k) - \delta$ *and* $|\alpha(k) + \beta(k)| < \delta$ *implying that:* $D[\ \hat{\varepsilon}_u(k)\ ] < \tilde{w}(k)^T j(k)$
    - $\tilde{w}(k)^T j(k) + \alpha(k) + \beta(k) > \delta$ *implying that:* $\tilde{w}(k)^T j(k) > 0$
    - $D[\ \hat{\varepsilon}_u(k)\ ] > 0$

    We can infer that $0 < D[\ \hat{\varepsilon}_u(k)\ ] < \tilde{w}(k)^T j(k)$
- *if* $|\ \hat{\varepsilon}_u(k)\ | < -\delta$ *then since*
    - $D[\ \hat{\varepsilon}_u(k)\ ] = \tilde{w}(k)^T j(k) + \alpha(k) + \beta(k) - \delta$ *and* $|\alpha(k) + \beta(k)| < \delta$ *implying that:* $D[\ \hat{\varepsilon}_u(k)\ ] > \tilde{w}(k)^T j(k)$
    - $\tilde{w}(k)^T j(k) + \alpha(k) + \beta(k) < -\delta$ *implying that:* $\tilde{w}(k)^T j(k) < 0$
    - $D[\ \hat{\varepsilon}_u(k)\ ] < 0$

    We can infer that $\tilde{w}(k)^T j(k) < D[\ \hat{\varepsilon}_u(k)\ ] < 0$

This implies that:

$$D[\ \hat{\varepsilon}_u(k)\ ] = \gamma(k)\ \tilde{w}(k)^T j(k)$$

where $\gamma(k)$ is some value bounded by $0 \le \gamma(k) < 1$

Hence the update rule can be written as: $\hat{w}(k+1) = \hat{w}(k) - \dfrac{\eta}{1 + j(k)^T j(k)}\ D[\ \hat{\varepsilon}_u(k)\ ]\ j(k)$

$$= \hat{w}(k) - \frac{\eta}{1 + j(k)^T j(k)}\ [\gamma(k)\ \tilde{w}(k)^T j(k)]\ j(k)$$

The expression can be processed as:

$$\hat{w}(k+1) = \hat{w}(k) - \frac{\eta\ \gamma(k)\ \tilde{w}(k)^T\ j(k)}{1 + j(k)^T\ j(k)}\ j(k)$$

$$\hat{w}(k+1) - w(k+1) = \hat{w}(k) - w(k) - \frac{\eta\ \gamma(k)\ \tilde{w}(k)^T\ j(k)}{1 + j(k)^T\ j(k)}\ j(k)$$

$$\tilde{w}(k+1) = \tilde{w}(k) - \frac{\eta\ \gamma(k)\ \tilde{w}(k)^T\ j(k)}{1 + j(k)^T\ j(k)}\ j(k)$$

$$\tilde{w}(k+1)^T\tilde{w}(k+1) = \tilde{w}(k)^T\tilde{w}(k) - 2\frac{\eta\,\gamma(k)\,\tilde{w}(k)^T j(k)}{1+j(k)^T j(k)}\,\tilde{w}(k)^T j(k) +$$

$$\left[\frac{\eta\,\gamma(k)\,\tilde{w}(k)^T j(k)}{1+j(k)^T j(k)}\right]^2 j(k)^T j(k)$$

$$|\tilde{w}(k+1)|^2 - |\tilde{w}(k)|^2 = \left[\frac{\eta\,\gamma(k)\,\tilde{w}(k)^T j(k)}{1+j(k)^T j(k)}\right]^2 j(k)^T j(k) - 2\frac{\eta\,\gamma(k)\left[\tilde{w}(k)^T j(k)\right]^2}{1+j(k)^T j(k)}$$

$$= \frac{\left[\eta\,\gamma(k)\,\tilde{w}(k)^T j(k)\right]^2}{1+j(k)^T j(k)} \times \frac{j(k)^T j(k)}{1+j(k)^T j(k)} - 2\frac{\eta\,\gamma(k)\left[\tilde{w}(k)^T j(k)\right]^2}{1+j(k)^T j(k)}$$

$$\le \frac{\left[\eta\,\gamma(k)\,\tilde{w}(k)^T j(k)\right]^2}{1+j(k)^T j(k)} - 2\frac{\eta\,\gamma(k)\left[\tilde{w}(k)^T j(k)\right]^2}{1+j(k)^T j(k)}$$

$$\le \frac{\eta\,\gamma(k)\left[\tilde{w}(k)^T j(k)\right]^2}{1+j(k)^T j(k)}\,[\eta\,\gamma(k)-2]$$

It is known that $|[\,\tilde{w}(k)^T j(k)]| > |\delta|$, , therefore $j(k)^T j(k)$ must be always positive.

If $0 \le \eta\,\gamma(k) < 2$, the difference between $|\tilde{w}(k+1)|^2$ and $|\tilde{w}(k)|^2$ must be non-positive.

$$|\tilde{w}(k+1)|^2 - |\tilde{w}(k)|^2 \le \frac{\eta\,\gamma(k)\left[\tilde{w}(k)^T j(k)\right]^2}{1+j(k)^T j(k)}\,[\eta\,\gamma(k)-2] < 0 \qquad \text{Eq F-43}$$

Thus, it can be concluded that the difference between the best and current function of fuzzy supervisory unit must always decrease if the conditions that $\delta \ge |\alpha(k)+\beta(k)|$ and $0 < [\eta\,\gamma(k)-2] \le 2$ are satisfied. Since the magnitude of $|w(k)-\hat{w}(k)|$ is always decreasing, its value at any instant, k, represents an upper bound for $k > k'$. This upper bound is described by the constant, ω. For the sake of convenient, ω is defined as the initial distance between the two parameter vectors:

$$|w(k)-\hat{w}(k)| = |\tilde{w}(k)| < \omega = \tilde{w}(0) \qquad \text{Eq F-44}$$

Although it has been theoretically proven the parameter will converge, the adaptation will not have a chance to converge if the plant becomes unstable. The convergence of the input and output of the plant will be investigated in the following sections.

7 Boundedness of States

The section shows that the states of system converge to within a calculable distance of the reference signal as time approaches infinity. The assumptions on which the proof is based are:

1. The plant function is monotonic with respect to the manipulating signal, *u(k)*.
2. The deadzone assumption holds.

States representation

In the analysis of boundedness of the states, a state space model in terms of supervisory output error and plant output error is utilised. The vectors of these errors are defined as:

$$e_y(k) = [\, \varepsilon_y(k),\ \varepsilon_y(k-1),\ \ldots,\ \varepsilon_y(k-n)\,]^T$$

$$e_u(k) = [\bar{\varepsilon}_u(k), \bar{\varepsilon}_u(k-1), \ldots, \bar{\varepsilon}_u(k-m)]^T$$

where

$$\varepsilon_y(k) = y_r(k) - y(k+1)$$

$$\bar{\varepsilon}_u(k) = \bar{u}(k) - u(k)$$

$$= g_c[y_r(k)] - \hat{g}_c[y_r(k), \hat{w}(k)]$$

The state space model in term of error vectors $e_y(k)$ and $e_u(k)$ may be expressed as:

$$e_y(k+1) = A\, e_y(k) + b\, \varepsilon_y(k)$$

$$e_u(k+1) = A\, e_u(k) + b\, \bar{\varepsilon}_u(k)$$

where $A = \begin{bmatrix} 0 & \cdots & \cdots & \cdots & 0 \\ 1 & 0 & \cdots & \cdots & \vdots \\ 0 & 1 & \ddots & \cdots & \vdots \\ \vdots & & \ddots & \ddots & \vdots \\ 0 & \cdots & \cdots & 1 & 0 \end{bmatrix}$ $b = \begin{bmatrix} 1 \\ 0 \\ \vdots \\ \vdots \\ 0 \end{bmatrix}$

The state vector of the system, *e(k)*, is defined as:

$$e(k) = \begin{bmatrix} e_y(k) \\ e_u(k) \end{bmatrix}$$

8 Boundedness of manipulating signal

A Lyapunov function, $V_u[e_u(k)]$, for the error state space is introduced:

$$V_u[e_u(k)] = e_u(k)^T P e_u(k)$$

where P is a symmetric positive-definite matrix

From the second method of Lyapunov, it is known that if the value of the Lyapunov function is always non-increasing with time, then the system which the Lyapunov function describes is bounded. The sign of $\Delta V_u[e_u(k)]$ must therefore be investigated.

$$\begin{aligned}
\Delta V_u[e_u(k)] &= V_u[e_u(k+1)] - V_u[e_u(k)] \\
&= e_u(k+1)^T P e_u(k+1) - e_u(k)^T P e_u(k) \\
&= [A\, e_u(k) + b\, \bar{\varepsilon}_u(k)]^T P [A\, e_u(k) + b\, \bar{\varepsilon}_u(k)] - e_u(k)^T P e_u(k) \\
&= e_u(k)^T A^T P A e_u(k) + e_u(k)^T A^T P\, b\, \bar{\varepsilon}_u(k) + b^T \bar{\varepsilon}_u(k)\, P A e_u(k) \\
&\quad + b^T \bar{\varepsilon}_u(k)\, P b\, \bar{\varepsilon}_u(k) - e_u(k)^T P e_u(k)
\end{aligned}$$

Since $a^T B c = c^T B^T a$ for arbitrary vectors of a and c, and a matrix B of appropriate size, with P given as symmetric matrix, we have:

$$\Delta V_u[e_u(k)] = e_u(k)^T A^T P A e_u(k) + 2\, e_u(k)^T A^T P\, b\, \bar{\varepsilon}_u(k) + b^T P b\, \bar{\varepsilon}_u(k)^2 - e_u(k)^T P e_u(k)$$

The matrix A is a stable matrix since all of its eigenvalues are at the origin. It is well known that it is possible to select P and a symmetric positive-definite matrix Q such that $A^T P A - P = -Q$. Thus:

$$\begin{aligned}
\Delta V_u[e_u(k)] &= e_u(k)^T A^T P A e_u(k) + 2\, e_u(k)^T A^T P\, b\, \bar{\varepsilon}_u(k) + b^T P\, b\, \bar{\varepsilon}_u(k)^2 - e_u(k)^T P e_u(k) \\
&= e_u(k)^T [A^T P A - P] e_u(k) + 2\, e_u(k)^T A^T P\, b\, \bar{\varepsilon}_u(k) + b^T P\, b\, \bar{\varepsilon}_u(k)^2 \\
&= -\, e_u(k)^T Q\, e_u(k) + 2\, e_u(k)^T A^T P\, b\, \bar{\varepsilon}_u(k) + b^T P\, b\, \bar{\varepsilon}_u(k)^2
\end{aligned}$$

Since for an arbitrary vector a and an arbitrary positive-definite matrix B, $a^T B a \le \lambda_{max}(B) |a|^2$ (where $\lambda_{max}(B)$ signifies the maximum eigenvalue of matrix B) and like-wise $-a^T B a \le -\lambda_{min}(B) |a|^2$, it may be deduced that:

$$\Delta V_u[e_u(k)] = -\lambda_{min}(Q) |e_u(k)|^2 + 2\, e_u(k)^T A^T P\, b\, \bar{\varepsilon}_u(k) + \lambda_{max}(P) |b|^2\, \bar{\varepsilon}_u(k)^2$$

Since for any scalar a, it is know that $a \leq |a|$, this becomes:

$$\Delta V_u[e_u(k)] \leq -\lambda_{min}(Q)|e_u(k)|^2 + 2|e_u(k)^T A^T P b\, \bar{\varepsilon}_u(k)| + \lambda_{max}(P)|b|^2\, \bar{\varepsilon}_u(k)^2$$

The magnitude of b is 1, therefore:

$$\Delta V_u[e_u(k)] \leq -\lambda_{min}(Q)|e_u(k)|^2 + 2|e_u(k)^T A^T P\, \bar{\varepsilon}_u(k)| + \lambda_{max}(P)\, \bar{\varepsilon}_u(k)^2$$

There exists a constant, $\Phi_1 > 0$ such that:

$$\Phi_1 |e_u(k)|\, |\bar{\varepsilon}_u(k)| \geq 2|e_u(k)^T A^T P\, \bar{\varepsilon}_u(k)|$$

Hence the inequality becomes:

$$\Delta V_u[e_u(k)] \leq -\lambda_{min}(Q)|e_u(k)|^2 + \Phi_1 |e_u(k)|\, |\bar{\varepsilon}_u(k)| + \lambda_{max}(P)\, \bar{\varepsilon}_u(k)^2$$

Introducing two constants, $0 < \Phi_2 < 1$ and $\Phi_3 > 1$, the first and third term of the expression can be broken up as follows:

$$\begin{aligned}\Delta V_u[e_u(k)] \leq\ & -\Phi_2\lambda_{min}(Q)|e_u(k)|^2 - (1-\Phi_2)\lambda_{min}(Q)|e_u(k)|^2 + \Phi_1 |e_u(k)|\, |\bar{\varepsilon}_u(k)| \\ & - (\Phi_3 - 1)\lambda_{max}(P)\, \bar{\varepsilon}_u(k)^2 + \Phi_3\, \lambda_{max}(P)\, \bar{\varepsilon}_u(k)^2 \\ \leq\ & -\Phi_2\lambda_{min}(Q)|e_u(k)|^2 + \Phi_3\, \lambda_{max}(P)\, \bar{\varepsilon}_u(k)^2 \\ & - [(1-\Phi_2)\lambda_{min}(Q)|e_u(k)|^2 - \Phi_1 |e_u(k)|\, |\bar{\varepsilon}_u(k)| + (\Phi_3 - 1)\lambda_{max}(P)\, \bar{\varepsilon}_u(k)^2] \end{aligned} \qquad \text{Eq F-45}$$

The expression in the square brackets of the above equation may be factorised as:

$$(1-\Phi_2)\lambda_{min}(Q)|e_u(k)|^2 - \Phi_1 |e_u(k)|\, |\bar{\varepsilon}_u(k)| + (\Phi_3 - 1)\lambda_{max}(P)\, \bar{\varepsilon}_u(k)^2$$

$$= [\sqrt{(1-\phi_2)\lambda_{min}(Q)}\, |e_u(k)| - \sqrt{(\phi_3 - 1)\lambda_{min}(P)}\, \bar{\varepsilon}_u(k)]^2$$

Thus the inequality in Eq F-45 can be written as:

$$\begin{aligned}\Delta V_u[e_u(k)] \leq\ & -\Phi_2\lambda_{min}(Q)|e_u(k)|^2 + \Phi_3\, \lambda_{max}(P)\, \bar{\varepsilon}_u(k)^2 \\ & - [\sqrt{(1-\phi_2)\lambda_{min}(Q)}\, |e_u(k)| - \sqrt{(\phi_3 - 1)\lambda_{min}(P)}\, \bar{\varepsilon}_u(k)]^2\end{aligned}$$

Since the last term is positive, the following must be true:

$$\Delta V_u[e_u(k)] \leq -\Phi_2\lambda_{min}(Q)|e_u(k)|^2 + \Phi_3\, \lambda_{max}(P)\, \bar{\varepsilon}_u(k)^2 \qquad \text{Eq F-46}$$

Since $e_u(k)^T P\, e_u(k) \leq \lambda_{max}(P)\, |e_u(k)|^2$ and $V_u[e_u(k)] = e_u(k)^T P\, e_u(k)$, it is known that:

$$|e_u(k)|^2 = \frac{1}{\lambda_{max}(P)} V_u[e_u(k)]$$

Therefore, Eq F-46 may be written as:

$$\Delta V_u[e_u(k)] \leq -\frac{\phi_2 \lambda_{\min}(Q)}{\lambda_{\max}(P)} V_u[e_u(k)] + \Phi_3 \lambda_{max}(P) \bar{\varepsilon}_u(k)^2$$

The right hand side of the expression will be non-positive if:

$$V_u[e_u(k)] \geq \frac{\phi_3 \lambda_{\max}(P)^2 \bar{\varepsilon}_u(k)^2}{\phi_2 \lambda_{\min}(Q)}$$

$$or\ V_u[e_u(k)] \geq \gamma \bar{\varepsilon}_u(k)^2 \qquad \text{Eq F-47}$$

$$where\ \gamma = \frac{\phi_3 \lambda_{\max}(P)^2}{\phi_2 \lambda_{\min}(Q)}$$

Thus, if this condition is satisfied, then the Lyapunov function will be non-increasing and the manipulating signal will be bounded.

Now, consider a set of state vectors, $e \in E$ for which $|e_y| \leq \mu_y$ and $|e_u| \leq \mu_u$ where μ_y and μ_u are positive constants. Clearly, for any $e(j) \in E$, its components, $\bar{\varepsilon}_u(j-i) : i = 1, \ldots, m$, will satisfy $|\bar{\varepsilon}_u(j-i)| \leq u_u$. It is observed that since:

$$\bar{\varepsilon}_u(j-i) = g_c[y_r(j-i)] - \hat{g}_c[y_r(j-i), \hat{w}(j-i)]$$

If $\hat{w}(j-i) = w(k)$, then $\bar{\varepsilon}_u(j-i) = 0$. Consequently, there exist constants ξ_1 and ξ_2 such that the set $e \in E$ is equivalent to:

$$|\bar{\varepsilon}_u(j-i)| = \omega\xi_1 + \alpha\xi_2$$

where ω is the bound on the initial Euclidean distance between the parameter vectors of the best possible and current fuzzy supervisory unit. α is the function difference between the actual inverse of the plant dynamic and the best possible controller. In particular, if $e(k) \in E$, then:

$$|\bar{\varepsilon}_u(k)| \leq \omega\xi_1 + \alpha\xi_2$$

The condition in Eq F-47 for $\Delta V_u[e_u(k)]$ to be negative and consequently for the manipulating signal to be bounded, then becomes:

$$V_u[e_u(k)] \geq \gamma(\omega\xi_1 + \alpha\xi_2)^2$$

It is apparent that, given any value of $V_u[e_u(k)]$, if ω and α are small enough, then the system is bounded.

9 Boundedness of plant output

The boundedness of the plant output can be inferred from the proven boundedness of the manipulating signal by expression below:

$$\left|\varepsilon_y(k)\right| \leq D_g^{\max}\left|\bar{\varepsilon}_u(k)\right|$$

where $D_g^{\max}$ is the maximum absolute rate of change of the plant output $y(k+1)$ with respect to the plant input $u(k)$ within the region of operation R. The expression can be given as:

$$D_g^{\max} = \max_o \left|\frac{\partial g[y(k),\ldots,y(k-n+1),u(k),\ldots,u(k-m+1)]}{\partial u(k)}\right|$$

This relationship may be derived using the mean value theorem. The mean value theorem states that for a multi-variable function, $g(a_0, b_0, c)$, which is continuous and differentiable at each point in the interval $c \in [c_1, c_2]$, if a_0 and b_0 are constant then there is at least one point $c_3 \in [c_1, c_2]$ for which:

$$\frac{g(a_0,b_0,c_1) - g(a_0,b_0,c_2)}{c_1 - c_2} = \left.\frac{\partial g(a_0,b_0,c_1)}{\partial c}\right|_{c=c_3}$$

The ideal manipulating signal is, by definition, the signal which brings the plant output to the reference in one instant, such that $y(k+1) = y_r(k)$. The reference signal $y_r(k)$, can therefore be expressed as follows:

$$y_r(k)=g[y(k), \ldots, y(k-n+1), \bar{u}(k), u(k-1), \ldots, u(k-m+1)]$$

Thus by the mean value theorem the following is true:

$$\frac{\varepsilon_y(k)}{\bar{\varepsilon}_u(k)} = \frac{y(k)-y(k+1)}{\bar{u}(k)-u(k)}$$

$$= \frac{g[\ldots,\bar{u}(k),\ldots] - g_p[\ldots,u(k),\ldots]}{\bar{u}(k)-u(k)}$$

$$= \left.\frac{\partial g[\ldots,u,\ldots]}{\partial u}\right|_{u=u_0} \qquad \text{for some } u_0 \in [u(k),\bar{u}(k)]$$

Since $D_g^{\max}$ represents the maximal $\left|\frac{\partial g[...,u,...]}{\partial u}\right|$, the following relation exists:

$$\left|\frac{\varepsilon_y(k)}{\bar{\varepsilon}_u(k)}\right| \leq D_g^{\max}$$

$$\Leftrightarrow \left|\varepsilon_y(k)\right| \leq D_g^{\max}\left|\bar{\varepsilon}_u(k)\right|$$

Since $\varepsilon_y(k)$ is bounded by a constant times $\bar{\varepsilon}_u(k)$, and since $\bar{\varepsilon}_u(k)$ has been shown to be bounded under the condition that ω and α are small enough, it may be deduced that $\varepsilon_y(k)$ is also bounded under this condition. Since $\varepsilon_y(k)$ is bounded, and the matrix A has all of its eigenvalues at the origin, it may be concluded that the system is bounded if ω and α are small enough.

10 Convergence of States

The convergence of the states is dependent on the convergence of the controller parameter, which in turn is dependent on the boundedness of the states. The conditions for boundedness of the states and controller parameters are:

- The plant is time-invariant,
- The maximum difference α between the best possible controller and the inverse plant model is small within the region of operation,
- The initial Euclidean distance ω between the parameter vectors of the best possible and current fuzzy supervisory unit is small within the region of operation,
- The deadzone assumption holds, i.e. $\delta \geq \left|\alpha(k)+\beta(k)\right|, \forall k$ where $\alpha(k)$ is the difference between the best possible controller and the actual plant inverse at time k, and $\beta(k)$ is the remainder of a first-order Taylor approximation of $\hat{g}_c$ at time k,
- The learning rate η for both the manipulating signal optimisation and model adaptation is between 0 and 2.

In the following sections, it will be assumed that the above conditions are satisfied and that, by implication, the controller parameters will converge.

11 Convergence of manipulating signal

Since the Euclidean distance ω will not increase when the conditions listed above are fulfilled, it may be inferred that the distance will approach a constant value $C \leq \omega$ which is not necessary to be zero:

$$\left|\tilde{w}(k)\right| \rightarrow C \text{ as } k \rightarrow \infty$$

This implies that:

$$\left|\tilde{w}(k+1)\right|^2 - \left|\tilde{w}(k)\right|^2 \rightarrow 0 \text{ as } k \rightarrow \infty$$

Combining this observation with Eq F-43, it can be seen that:

$$\frac{\eta\,\gamma(k)\left[\tilde{w}(k)^T j(k)\right]^2}{1 + j(k)^T j(k)} \left[\eta\,\gamma(k) - 2\right] \rightarrow 0 \text{ as } k \rightarrow \infty$$

If $\eta < 2$ then, since $0 \leq \gamma(k) < 1$, then $[\eta\,\gamma(k) - 2]$ cannot be approach zero, so:

$$\frac{\eta\,\gamma(k)\left[\tilde{w}(k)^T j(k)\right]^2}{1 + j(k)^T j(k)} \rightarrow 0 \text{ as } k \rightarrow \infty$$

Likewise, η is a constant and will therefore not approach zero which implies:

$$\frac{\gamma(k)\left[\tilde{w}(k)^T j(k)\right]^2}{1 + j(k)^T j(k)} \rightarrow 0 \text{ as } k \rightarrow \infty$$

The denominator will remain bounded if the manipulating signal and the plant output remain bounded if α and ω are small enough, so it will not approach infinity. Therefore:

$$\gamma(k)\left[\tilde{w}(k)^T j(k)\right]^2 \rightarrow 0 \text{ as } k \rightarrow \infty$$

Since $D[\,\hat{\varepsilon}_u(k)\,] = \gamma(k)\,\tilde{w}(k)^T j(k)$, this can be expressed as:

$$\frac{D\left[\hat{\varepsilon}_u(k)\right]}{\gamma(k)} \rightarrow 0 \text{ as } k \rightarrow \infty$$

Since $0 \leq \gamma(k) < 1$, it may therefore be concluded that:

$$D\left|\hat{\varepsilon}_u(k)\right| \rightarrow 0 \text{ as } k \rightarrow \infty$$

Which means that the manipulating signal will converge to within a deadzone radius δ of the ideal manipulating signal as time approaches infinity, that is

$$\hat{\varepsilon}_u(k) \rightarrow \delta \text{ as } k \rightarrow \infty$$

12 Convergence of plant output

The plant output error $\varepsilon_y(k)$ between the reference and the actual plant output is bounded by a constant times the supervisory output error, $\hat{\varepsilon}_u(k)$:

$$\left|\varepsilon_y(k)\right| \le \frac{1}{D_{\hat{g}_c}^{\min}}\left|\hat{\varepsilon}_u(k)\right|$$

where $D_{\hat{g}_c}^{\min}$ is the minimum absolute rate of change of the manipulating signal *u(k)* with respect to the reference plant output $y_r(k)$ within the region of operation *R*:

$$D_{\hat{g}_c}^{\min} = \min_{o}\left|\frac{\partial g_c[y_r(k),\hat{w}(k)]}{\partial y_r(k)}\right|$$

This can be proved using the mean value theorem:

$$\hat{\varepsilon}_u(k) = g_c[y_r(k),\hat{w}(k)] - g_c[\hat{y}(k+n),\hat{w}(k)]$$

$$\Leftrightarrow \hat{\varepsilon}_u(k) = \left.\frac{\partial g_c[y_r(k),\hat{w}(k)]}{\partial y_r(k)}\right|_{y_r=y_{ro}} [y_r(k) - \hat{y}(k+n)]$$

where

$$y_{ro} \in [\hat{y}(k+n), y_r(k)]$$

$$\Leftrightarrow \left|\hat{\varepsilon}_u(k)\right| \ge D_{g_c}^{\min}\left|\varepsilon_y(k)\right|$$

$$\Leftrightarrow \left|\varepsilon_y(k)\right| \le \frac{1}{D_{\hat{g}_c}^{\min}}\left|\hat{\varepsilon}_u(k)\right|$$

Since the supervisory output error $\hat{\varepsilon}_u(k)$ will converge to a value less than or equal to deadzone radius δ, the plant output error $\varepsilon_y(k)$ will converge to a value less than or equal to $\frac{\delta}{D_{\hat{g}_c}^{\min}}$, that is:

$$\left|\varepsilon_y(k)\right| \to \left[-\frac{\delta}{D_{\hat{g}_c}^{\min}}, \frac{\delta}{D_{\hat{g}_c}^{\min}}\right] \text{ as } k \to \infty$$

Appendix 7

List of Publications

Conference publications

Tan L.P., Lotfi A., Lai E., (2002), Distributed Parameter System Identification Through Semi-physical Model Structure, *18th National Conference of Manufacturing Research*, 539-543.

Tan L.P., Lotfi A., Lai E., (2002), Hybrid Soft Computing Methods in Semi-physical Polymer Extrusion Model Identification, *2nd European Symposium on Intelligent Technologies*, 652-656

Tan L.P., Lotfi A. and Lai E., (2002), Hybrid Technique in Dynamic Model Identification of Polymer Extrusion Process, *4th International Conference on Recent Advance in Soft Computing*, pp. 362 – 367.

Tan L.P., Lotfi A., Lai E., Hull J.B., (2003), Development and Application of a Fuzzy Supervisory Indirect Learning Predictive Control, *3rd European Symposium on Intelligent Technologies*, 346-352.

Journal publication

Tan L.P., Lotfi A., Lai E., Hull J.B. (2004), Soft Computing Applications in Dynamic Model Identification of Polymer Extrusion Process, *Applied Soft Computing Journal*, 4(4), 345-355.